

A FINITE ELEMENT PROGRAM FOR THE STATIC ANALYSIS OF

BRANCHED, THIN SHELLS OF REVOLUTION UNDER AXISYMMETRIC LOADING.

A thesis submitted in partial fulfilment
of the requirements for the degree of
Master of Science in Engineering by :

T.B. GRIFFIN

September, 1974.

Department of Civil Engineering
University of Cape Town.

The copyright of this thesis vests in the author. No quotation from it or information derived from it is to be published without full acknowledgement of the source. The thesis is to be used for private study or non-commercial research purposes only.

Published by the University of Cape Town (UCT) in terms of the non-exclusive license granted to UCT by the author.

LIST OF CONTENTS

	Page
Synopsis	i
Acknowledgements	ii
List of Symbols	iii
<u>CHAPTER 1: Introduction</u>	1
<u>CHAPTER 2: Thin Shell Theory</u>	
2.1 Assumptions and Definitions	3
2.2 Deformations	4
2.3 Stress Resultants	6
2.4 Approximate Expressions for the Stress Resultants	9
2.5 A Special Remark	12
<u>CHAPTER 3: Finite Element Theory</u>	
3.1 The Conical Frustrum Element	13
3.1.1 The Element Stiffness Equations	13
3.1.2 Numerical Integration of the Element Stiffness Matrix	21
3.1.3 Derivation of the Element Load Vector	22
3.2 The Circular Plate Closure Element	26
3.2.1 Derivation of the Closure Element Stiffness Matrix and Load Vector	27
3.2.2 The Application of the Closure Element	31
3.3 The Assembled Structure	33
3.3.1 The System Stiffness Matrix	34
3.3.2 The System Load Vector	40
3.3.3 Nodal Boundary Conditions	41
3.3.4 Solution of the System Stiffness Equations	44
3.3.5 Calculation of Stresses and Moments	46
<u>CHAPTER 4: Evaluation and Discussion</u>	
4.1 Introduction and Definition	50
4.2 Circular Cylinders and Plates: the Limiting Shapes of the Conical Frustrum	52
4.2.1 Example 1: An Edge Loaded Circular Cylinder	52
4.2.2 Example 2: A Uniformly Loaded Circular Disc	58

	Page	
4.2.3	Conclusions I	64
4.3	Cylinder-Plate and Cylinder-Cone Shells: The Problem of Shell Junctions	66
4.3.1	Example 3: A Closed Cylindrical Water Tank	66
4.3.2	Example 4: An Open Sludge Digester Tank	74
4.3.3	Conclusions II	80
4.4	Example 5: The Thin Shell Analysis of a Thick Pressure Vessel: Comparison with Experimental Results	81
4.5	Branched Shells of Revolution	87
4.5.1	The Philosophy for Testing the Branched Shell Solution	87
4.5.2	Example 6: The Analysis of a Single-Branch Shell of Revolution	91
4.5.3	Example 7: The Analysis of a Doubly Branched Shell of Revolution	96
4.6	An Example from Practice	98
4.6.1	Example 8: The Analysis of an Elevated Effluent Tank	99
4.7	Computer Time-Cost Analysis	107

CHAPTER 5: Summary and Conclusions 109

Bibliography 115

List of Appendices

A	CONFRU User's Manual	118
B	Integration of Equation (2.10b) for the Stress Resultant N_{θ}^*	205
C	Notes on the Principle of Minimum Total Potential Energy	207
D	Numerical Integration Techniques	210
E	Explicit Expressions for the Equivalent Nodal Surface and Body Forces	213
F	Circular Plate Theory	215
G	The Theory of Cylindrical Water Tanks	220

SYNOPSIS

A finite element computer program which uses the conical frustrum element is presented for the linear elastic, static analysis of variable thickness, branched, thin shells of revolution, composed of straight sections and subject to general axisymmetric mechanical loading. The thin shell theory and finite element theory forming the basis of the analysis are described, with particular attention being given to the closing of the shell at the axis of symmetry, and shell branching. Numerous problems embodying all relevant features of the program are analysed, and their solutions are discussed. A user's manual for the program is appended, and guidelines for the efficient use of the program are given.

Acknowledgements

Acknowledgements and thanks are due to :

My supervisor Mr. W.S. Doyle whose continued interest, guidance and encouragement were the sine qua non of this thesis.

Bob Harrison and Wim Gevers for many fruitful discussions.

Professor J.B. Martin for his valuable criticism of parts of the manuscript.

Mr. Bjorn Watson of Ninham Shand and Partners for providing much of the practical background to this work.

Christiani and Nielsen, and Consani's Engineering for providing further practical problems for analysis.

Miss Bridget Spalding for typing the manuscript.

Charlie Basson for duplicating the thesis.

I would like dedicate this thesis to my parents Mr. and Mrs. K.B. Griffin.

LIST OF SYMBOLSSpecial Meanings

$\textcircled{3}$	node number 3
$\boxed{5}$	element number 5
[]	a matrix
{ }	a vector
[] ⁻¹	the inverse of a matrix
[] ^t	the transpose of a matrix
(i × j)	the dimensions of a matrix
Δ	an incremental increase in
s (subscript)	in the meridional direction
θ (subscript)	in the circumferential direction
∞	infinity
dV	differential volume
dA, dS	differential surface area
i, j (subscripts)	numeric subscripts

Lower Case Characters

a	radius
e	base of the natural logarithms
h	height or depth of cylinder
k^i	(6 × 6) element stiffness matrix for the i th element
$k_{i,j}$	(3 × 3) element stiffness submatrix
p	pressure
r	radius
s	meridional distance
$s' = \frac{ss}{L}$	non-dimensional meridional distance
t	element or shell thickness

u, w	global axial and radial displacements
u_i, w_i	nodal axial and radial displacements
x	general displacement
z	perpendicular distance from middle surface to an arbitrary point in the shell wall.

Upper Case Characters

A_i, B_i, C_i	arbitrary constants of integration
D	extensional rigidity
E	Young's modulus
F	shear force
G	shear modulus
K	flexural rigidity
$K_{i,j}$	(3×3) system stiffness submatrix
L	element length
M_s	meridional bending moment $[Nm/m]$
M_θ	circumferential bending moment $[Nm/m]$
N_s	meridional stress resultant $[N/m]$
N_θ	circumferential stress resultant $[N/m]$
P	general concentrated line load
S	surface area
U	total potential energy
\bar{U}	elastic strain energy density
U_i, W_i, M_i	equivalent nodal loads at node i
V	volume

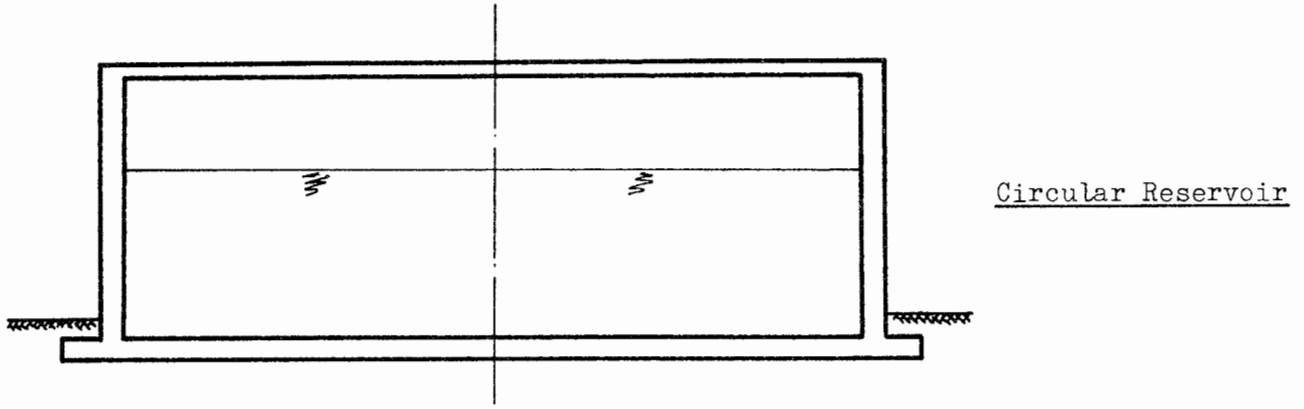
Greek Characters

α	an angle; the coefficient of thermal expansion
β_i	rotation at node i
γ	unit weight
ϵ	strain in the middle surface
ϵ^*	strain at an arbitrary point within the shell wall
$\bar{\epsilon}$	approximation to ϵ^*

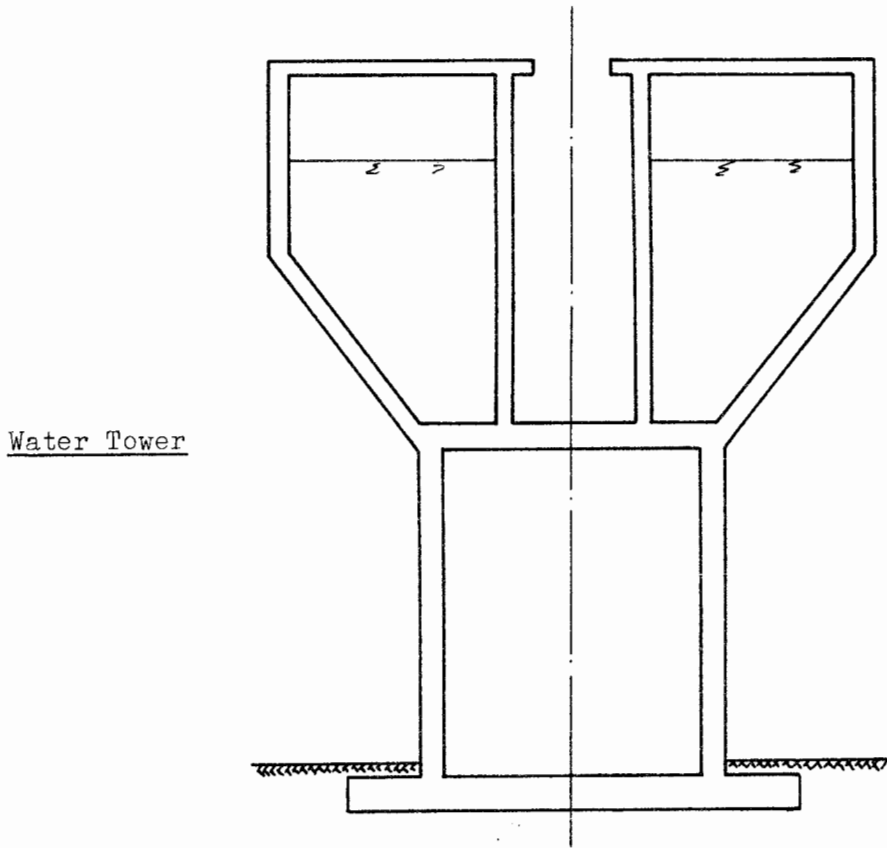
θ	angle; change in temperature
$\sigma, \sigma^*, \bar{\sigma}$	stresses associated through Hooke's law with the strains ϵ, ϵ^* and $\bar{\epsilon}$
ν	Poisson's ratio
ϕ	angle of inclination of a conical frustrum
χ	curvature of the middle surface.

Matrices and Vectors

$\{\alpha\}$	generalised nodal coordinates
$[B]$	strain-displacement matrix
$[D]$	elasticity matrix
$[D^*]$	matrix $[D]$ with the factor $E/(1 - \nu^2)$ removed
$\{\epsilon\}$	strains
$\{\epsilon_0\}$	initial strains
$\{F_e\}$	element load vector
$\{F\}$	system load vector
$[k]$	element stiffness matrix
$[K]$	system stiffness matrix
$[N']$	shape function matrix in local coordinates
$[N]$	shape function matrix in global coordinates
$\{q'_e\}$	local element nodal displacements
$\{q_e\}$	global element nodal displacements
$\{q\}$	global system nodal displacements
$[T]$	element transformation matrix
$\{\sigma\}$	stress resultants
$[S^*]$	stress matrix
$\{\phi\}$	surface forces
$\{X\}$	body forces.

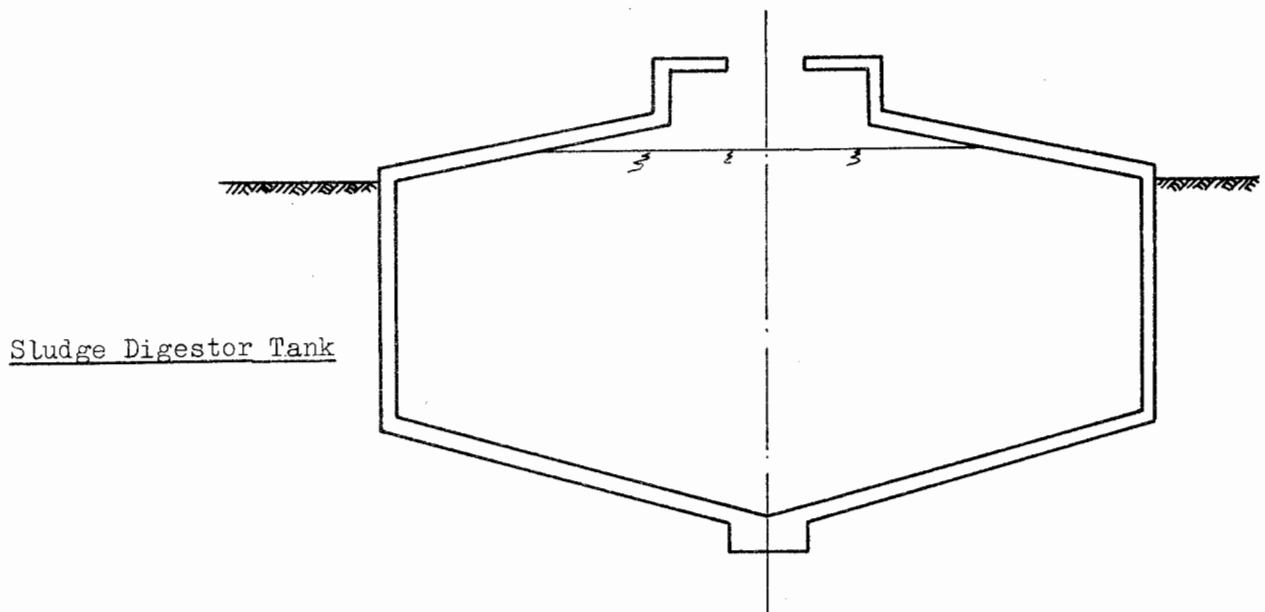


Circular Reservoir



Water Tower

Fig. 1.1



Sludge Digester Tank

CHAPTER 1

INTRODUCTION

There is a wide variety of structures that may be classified as axisymmetric thin shells of revolution, ranging from the parabolic cooling tower to the simple circular water reservoir. An important sub-class of these shells, and the one most often encountered in practice, consists of those shells made up of cylinders conical frustra and circular plates, whose primary function is the storage of some liquid (Fig. 1.1). We will be concerned in the present work with this sub-class of shells.

The structural analysis of thin shells of revolution has by no means suffered from lack of investigation [24, 25, 26, 27]. The computer analysis of these shells was first performed by Galletly^[28] in 1960. This was followed by attempts to analyse arbitrary shaped shells of revolution using flat triangular and quadrilateral elements^[29, 30] which met with little success.

In 1963 Grafton and Strome^[17] made the first use of the direct stiffness finite element method. This marked the beginning of a period of intensive research into the analysis of shells of revolution using the conical frustrum element^[16, 31, 32]. Shortly thereafter the curved meridional element was introduced to provide a more efficient analysis of meridionally curved shells of revolution^[33, 34]. In 1967 the final stage of element sophistication was reached with the development of the doubly curved quadrilateral element^[35, 36, 37]. Since then research has been directed mainly towards the refinement of existing elements for purposes such as elastic-plastic analysis^[38] and analysis of orthotropic shells^[39].

Notwithstanding the fact that the solution to the axisymmetric thin shell problem is within the state of art, there remains the need for readily available computer programs, in particular programs which are capable of taking into account the branching which often occurs in this class of shell.* The present work is concerned with the development of such a program.

*A pertinent assessment of the current capabilities for computer analysis of shells is given by Hartung [42]. It is surprising that neither of the two more widely used general structural analysis programs, viz. STRUDL (V2, M1) [40] and GENESYS [41] contain facilities for the analysis of shells of revolution.

The fundamental scope of the program was decided upon after consultation with engineers who were actively engaged in the design and construction of a number of water towers and sludge digester tanks. In particular it was felt that considerable simplification could be achieved, with no intrinsic loss of generality, by making use of:

- (i) the axial symmetry of both the structure and the principal loading viz., the liquid contained in the structure and the self-weight of the structure itself, and
- (ii) the fact that the large majority of the structures are made up of straight sections, viz., cylinders, conical frustra and circular plates.

In view of this, therefore, the conical frustrum element was chosen as the basic analysis tool.

The present work therefore concerns the development, testing and documentation of a finite element computer program CONFRU (CONical FRUstrum) designed for the linear elastic, static analysis of variable thickness, branched, axisymmetric thin shells of revolution under general axisymmetric mechanical loading. Chapter 2 deals with the thin shell theory leading to the approximate strain-displacement and stress-strain relations for a conical frustrum. The discrete element formulation as well as the assembly and solution of the system stiffness equations are discussed in Chapter 3. In Chapter 4 a large variety of solutions obtained from the program are presented and discussed, together with an analysis of problem solution times and costs. The program and its associated plotting routines are documented in Appendix A, and full listings of all programs are given. The complete data input and printed output for a sample problem are also included.

CHAPTER 2

THIN SHELL THEORY

Of fundamental importance in the derivation of a finite element stiffness matrix are the strain-displacement and stress-strain relationships which describe the mechanical behaviour of the element. These relationships are derived here for an isotropic conical frustrum, subject to axisymmetric deformation only, with both membrane and bending stresses being taken into account.

2.1 Assumptions and Definitions

We consider here only those conical frustra which can be defined as thin shells of revolution, whose meridians are straight lines inclined at an angle ϕ to the axis of symmetry (Fig. 2.1). The middle surface is the surface which lies midway between the two faces of the frustrum.

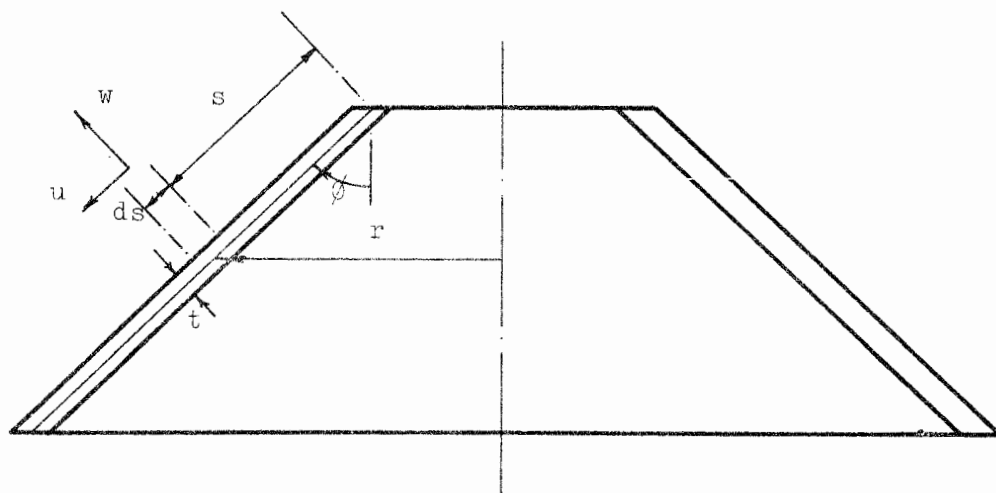
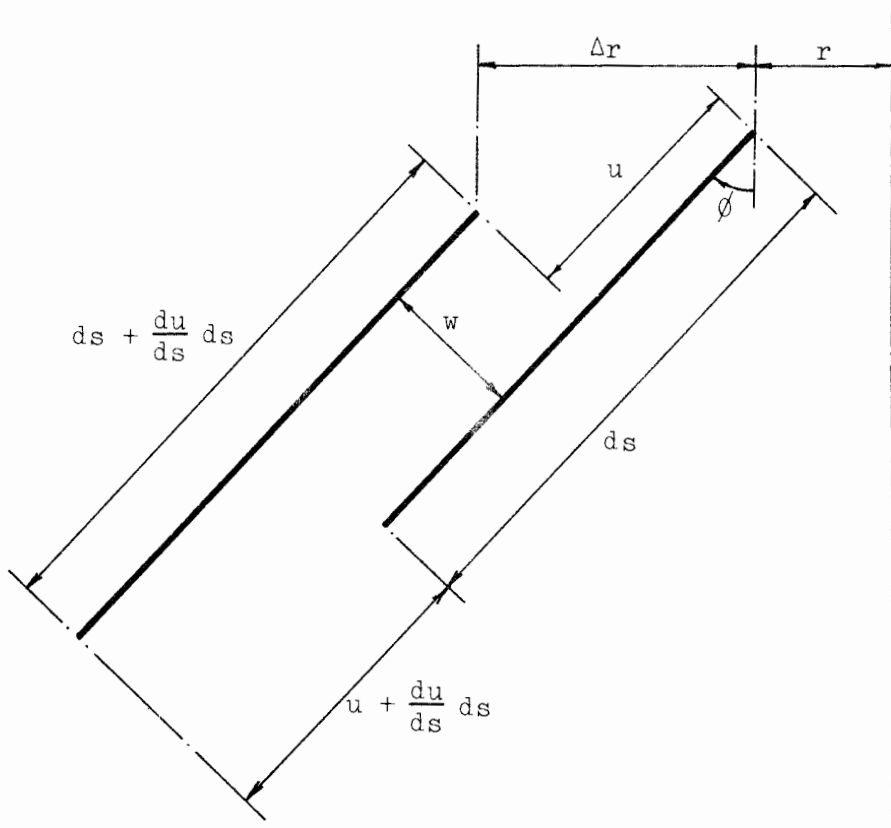
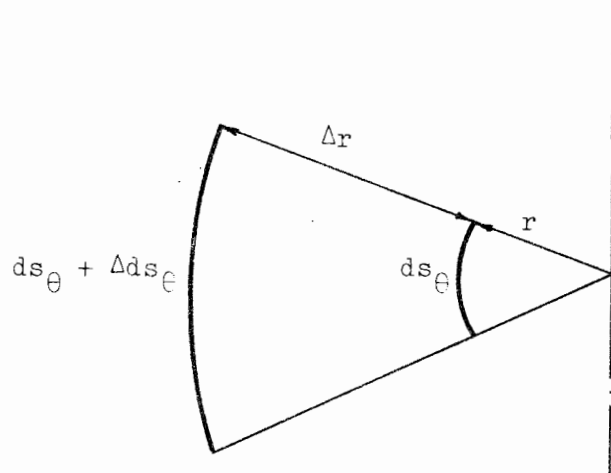


Fig. 2.1

Since the shell is assumed to undergo axisymmetric deformations only, the displacement in the circumferential direction is zero. Hence only two displacements are necessary to describe the kinematic behaviour of the middle surface of an element of length ds ; these are the meridional displacement u , and the normal displacement w . The position of the element may be described either by its distance s from an arbitrary datum point, (usually taken as the upper edge of the frustrum), or by its radius r . The shell has thickness t which may vary as a function of s .



(a) Meridian



(b) Parallel Circle

Fig. 2.2: Middle surface of the line element before and after deformation

The thin shell theory developed here is based on the following assumptions:*

- (i) Points lying on the normal to the middle surface before deformation remain on the normal after deformation. This assumption allows deformation due to transverse shear forces to be neglected.
- (ii) The distance of an arbitrary point from the middle surface remains the same before and after deformation. This assumption allows the stresses and strains in the direction normal to the middle surface to be neglected.
- (iii) All displacements are small compared with the radius of curvature of the middle surface, and the slopes are negligible compared with unity. This assumption maintains the linearity of equations.

Furthermore, we assume that the shell material is elastic according to Hooke's law.

These assumptions may now be used to establish the kinematic relationships for the conical frustrum.

2.2 Deformations

We begin by considering the deformation of the middle surface of a small line element of length ds (Fig. 2.2).

The ends of the element undergo meridional displacements u and $u + \frac{du}{ds} ds$ respectively; hence the elongation of the element is $\frac{du}{ds} ds$. Since the element remains straight in the deformed position, normal displacements do not cause additional elongation of the element, and we define the meridional strain in the middle surface by

$$\epsilon_s = \frac{du}{ds} \quad (2.1)$$

The circumferential strain arises as a result of an increase in the arc length ds_θ of an element of a parallel circle (Fig. 2.2b). The increase in arc length Δds_θ is caused by an increase Δr in the radius r , given by,

$$\begin{aligned} \Delta ds_\theta &= \left(\frac{r + \Delta r}{r} \right) ds_\theta - ds_\theta \\ &= \frac{\Delta r}{r} ds_\theta \end{aligned}$$

* This chapter has its origin in the thin shell theory of Flügge [1]

From the geometry of Fig. 2.2(a),

$$\Delta r = u \sin \phi + w \cos \phi \quad (2.2a)$$

Hence, the circumferential strain in the middle surface is,

$$\begin{aligned} \epsilon_{\theta} &= \frac{\Delta r}{r} \\ &= \frac{u \sin \phi + w \cos \phi}{r} \end{aligned} \quad (2.2b)$$

To take account of bending stresses it is necessary to describe the deformation of the shell in terms of the displacements of an arbitrary point A, a distance z from the middle surface (Fig. 2.3). The point A has components of displacement u_A in the meridional direction, and w_A in the direction normal to the middle surface. These displacements are associated with the displacements u and w of the corresponding point A_0 in the middle surface.

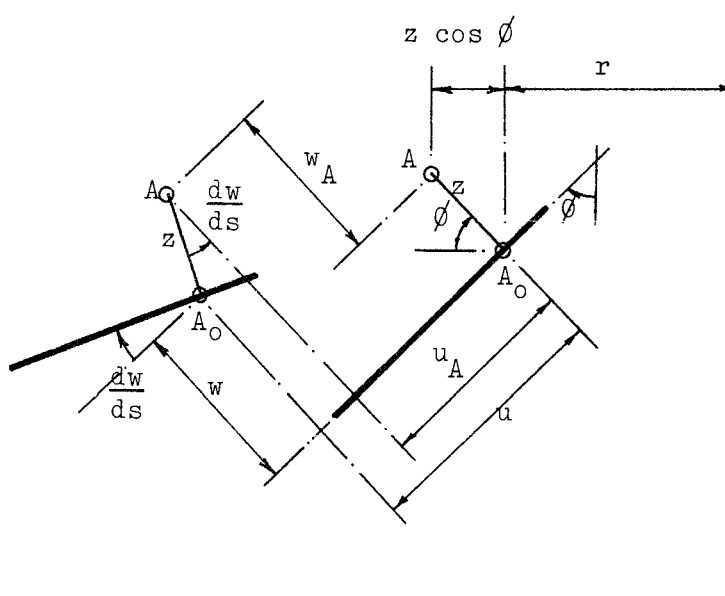


Fig. 2.3

From assumption (ii) the distance z between the points A_0 and A in the original position remains unchanged in the deformed position. Hence, if the slope dw/ds is small, we may write,

$$\frac{dw}{ds} = w' = \frac{u - u_A}{z}$$

$$\text{or, } u_A = u - zw' \quad (2.3)$$

Again, if the slope w' is small, the normal displacements w and w_A are almost equal and we may take

$$w_A = w \quad (2.4)$$

We may now write down expressions for the strains which describe the deformation of a small element of a conical frustrum passing through A . Making use of Eqs. (2.1) and (2.2b) we have,

$$\begin{aligned} \epsilon_s^* &= \frac{du_A}{ds} \\ \epsilon_\theta^* &= \frac{u_A \sin \phi + w_A \cos \phi}{r + z \cos \phi} \end{aligned} \quad (2.5)$$

where the radius r is replaced by the radius $r + z \cos \phi$ of the point A . Introducing Eqs. (2.3) and (2.4), the above expressions may be rewritten in terms of the displacements u and w of the point A_0 in the middle surface:

$$\begin{aligned} \epsilon_s^* &= \frac{du}{ds} - z \frac{d^2 w}{ds^2} \\ \epsilon_\theta^* &= \frac{u \sin \phi + w \cos \phi - zw' \sin \phi}{r + z \cos \phi} \end{aligned} \quad (2.6)$$

Eqs. (2.6) give the in-plane strains at the arbitrary point A in terms of the displacements of the point A_0 in the middle surface.

2.3 Stress Resultants

Associated with the in-plane strains ϵ_s^* and ϵ_θ^* are two normal stresses, the meridional stress σ_s^* , and the circumferential stress σ_θ^* . For a linear elastic material the relationship between these stresses and strains is expressed by Hooke's law as,

$$\begin{aligned} \sigma_s^* &= \frac{E}{1 - \nu^2} [\epsilon_s^* + \nu \epsilon_\theta^*] \\ \sigma_\theta^* &= \frac{E}{1 - \nu^2} [\epsilon_\theta^* + \nu \epsilon_s^*] \end{aligned} \quad (2.7)$$

where Young's modulus E and Poisson's ratio ν are constants of the shell material. Since tensile strains are considered to be positive it follows that the stresses are positive if they cause tension in a small element of the frustrum as shown in Fig. 2.4(a).

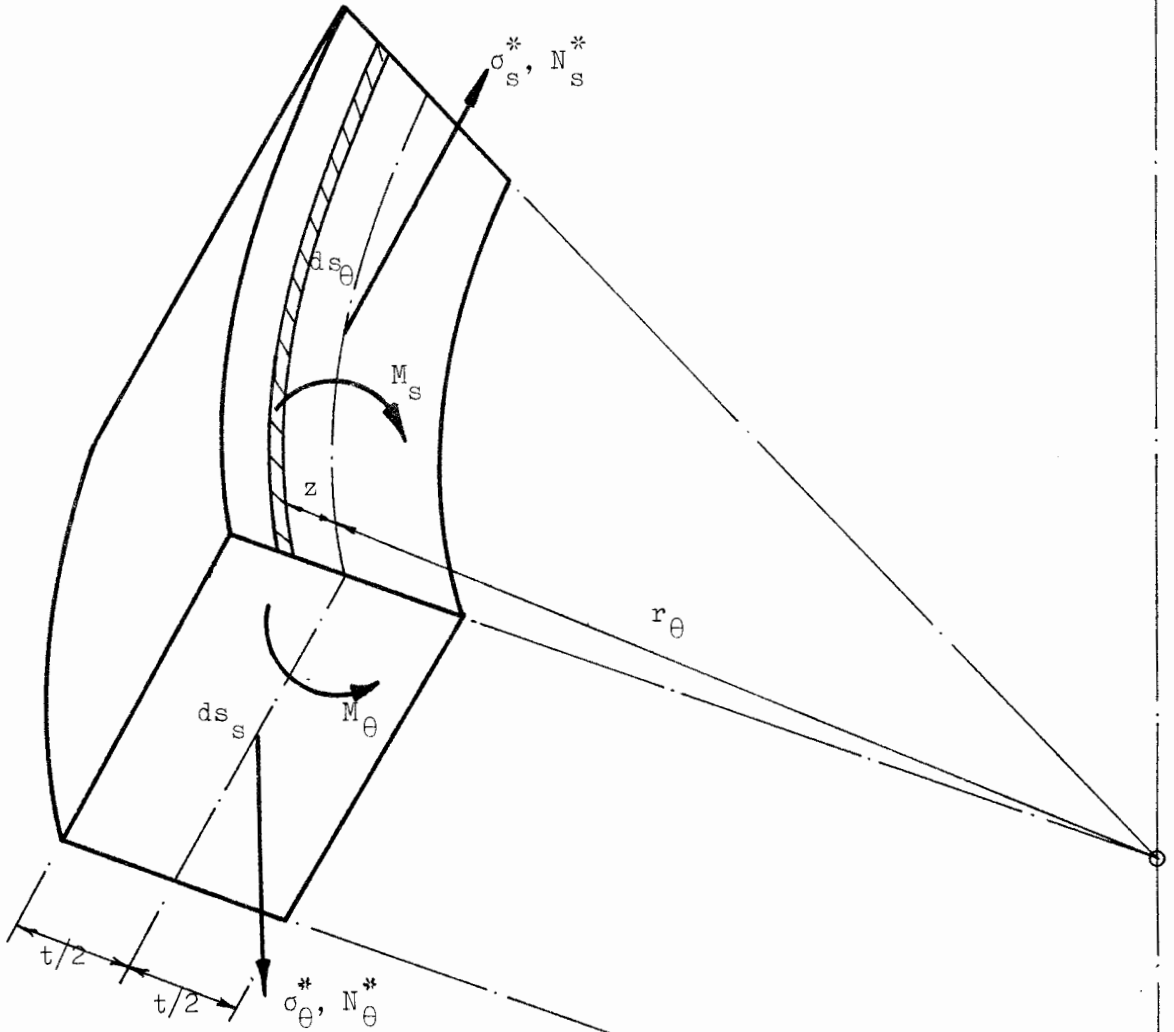


Fig. 2.4(a)

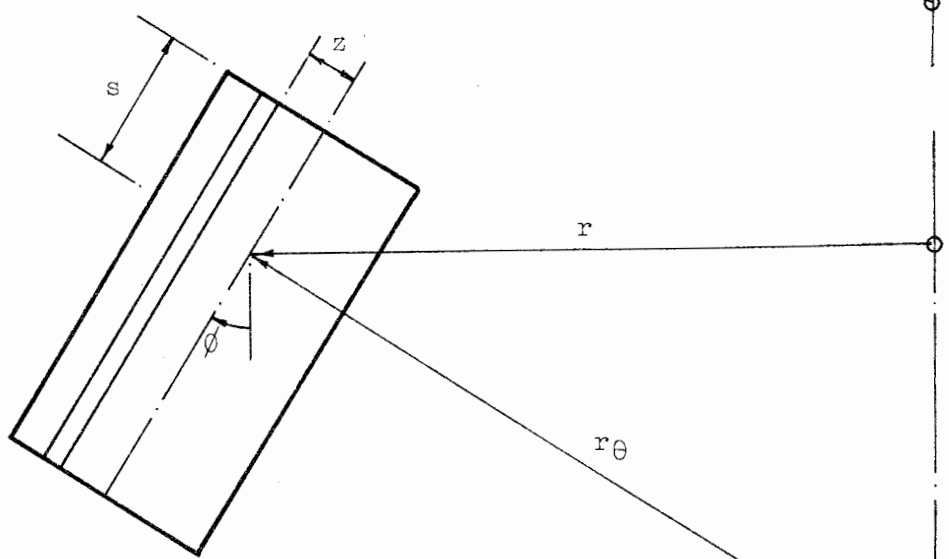


Fig. 2.4(b)

The stresses σ_s^* and σ_θ^* clearly have resultants which depend on the lengths ds_θ and ds_s of the elemental sections. Furthermore, if the stresses are non-uniformly distributed over these sections they will have moments with respect to the centres of the sections. In view of this we introduce the stress resultants N_s , N_θ , M_s and M_θ ; N_s and N_θ are the resultant normal forces per unit length in the meridional and circumferential directions respectively, and M_s and M_θ are the corresponding moments per unit length.

The stress resultants are found by integrating the stresses acting on the elemental sections. In the following derivation of these integrals it will be useful to introduce the notation,

$$D = \frac{Et}{1 - \nu^2} \quad (2.8a)$$

for the extensional rigidity, and

$$K = \frac{Et^3}{12(1 - \nu^2)} \quad (2.8b)$$

for the flexural rigidity of the conical frustrum.

Consider the circumferential section perpendicular to the middle surface, of length ds_θ , and having a radius of curvature r_θ (Fig. 2.4a). The total force acting on this section is

$$N_s^* ds_\theta \quad (2.9a)$$

The shaded element of this section has a length

$$\left(\frac{r_\theta + z}{r_\theta}\right) ds_\theta$$

and hence the total force acting on the shaded element is

$$\sigma_s^* \left(\frac{r_\theta + z}{r_\theta}\right) ds_\theta \cdot dz \quad (2.9b)$$

Equating expressions (2.9a,b) for the whole section and noting from Fig. 2.4(b) that

$$r_\theta = \frac{r}{\cos \phi}$$

we have,

$$N_s^* = \int_{-t/2}^{t/2} \sigma_s^* \left(\frac{r + z \cos \phi}{r} \right) dz \quad (2.10a)$$

Similar reasoning leads to the following expressions for the remaining stress resultants:

$$N_\theta^* = \int_{-t/2}^{t/2} \sigma_\theta^* dz \quad (2.10b)$$

$$M_s^* = \int_{-t/2}^{t/2} \sigma_s^* \left(\frac{r + z \cos \phi}{r} \right) z \cdot dz \quad (2.10c)$$

$$M_\theta^* = \int_{-t/2}^{t/2} \sigma_\theta^* z dz \quad (2.10d)$$

The expressions for the stress resultants N_θ^* and M_θ^* do not contain the radius of curvature r_s of the meridian, since $r_s = \infty$ and

$$\lim_{r_s \rightarrow \infty} \left(\frac{r_s + z}{r_s} \right) = 1$$

It will be noticed that even when the normal stress σ_s^* is uniformly distributed over the section, i.e., $\sigma_s^* = \text{constant}$, there will still be a moment M_s^* . This is because the section is trapezoidal in shape and as such, its centroid does not coincide with the middle surface.

The actual integration of Eqs. (2.10) is a lengthy procedure involving, in the case of N_θ^* and M_θ^* , the Taylor's series expansion of log functions. The detailed integration of the expression for N_θ^* is given in Appendix B by way of illustration, and only the results of the integration are presented here.

The exact expressions for the stress resultants are then as follows:-

$$N_s^* = D \left[\frac{du}{ds} + \nu \left(\frac{u \sin \phi + w \cos \phi}{r} \right) \right] + K \left[- \frac{\cos \phi}{r} \frac{d^2 w}{ds^2} \right] \quad (2.11a)$$

$$N_\theta^* = D \left[\frac{u \sin \phi + w \cos \phi}{r} + \nu \frac{du}{ds} \right] + K \left[\frac{\cos^2 \phi}{r^2} \left(\frac{u \sin \phi + w \cos \phi + r w' \sin \phi}{r} \right) \right] \quad (2.11b)$$

$$M_s^* = K \left[-\frac{d^2 w}{ds^2} - \nu \frac{w' \sin \phi}{r} - \frac{\cos \phi}{r} \frac{du}{ds} \right] \quad (2.11c)$$

$$M_\theta^* = K \left[-\frac{w' \sin \phi}{r} - \nu \frac{d^2 w}{ds^2} - \frac{\cos \phi}{r^2} (u \sin \phi + w \cos \phi) \right] \quad (2.11d)$$

Eqs. (2.11) form the basis of the bending theory for a thin conical frustrum shell; when $K = 0$ the expressions for N_s^* and N_θ^* which remain constitute the membrane theory of a conical shell. However, certain of the terms in these equations are clearly of the second order of magnitude, for example, the third term in Eq. (2.11d). Such terms are unlikely to be of significance in practice, and it would thus appear worthwhile to investigate the possibility of deriving an approximate bending theory.

2.4 Approximate Expressions for the Stress Resultants

There are two sources from which the second order terms in Eqs. (2.11) arise, both of which derive from the fact that the elemental section $s = \text{constant}$ (Fig. 2.4) is trapezoidal in shape. Due to this the hoop fibres vary in length across the section, as expressed by Eq. (2.6) for the circumferential strain,

$$\epsilon_\theta^* = \frac{u \sin \phi + w \cos \phi - zw' \sin \phi}{r + z \cos \phi}$$

If the shell is thin enough we may neglect the distance $z \cos \phi$ in comparison to r and so write an approximate expression for the circumferential strain as,

$$\bar{\epsilon}_\theta = \frac{u \sin \phi + w \cos \phi - zw' \sin \phi}{r} \quad (2.12a)$$

The second source of second order terms derives specifically from the expression for the area of the trapezoidal section, as contained in Eq. (2.9b), viz.,

$$\text{Elemental area} = \left(\frac{r_\theta + z}{r_\theta} \right) ds_\theta \cdot dz$$

Again, for a sufficiently thin shell, the distance z is small compared with the radius of curvature r_θ , and we may take

$$\frac{r_\theta + z}{r_\theta} = \frac{r + z \cos \phi}{r} \doteq 1 \quad (2.12b)$$

The above approximations are incorporated into the original Eqs. (2.10)

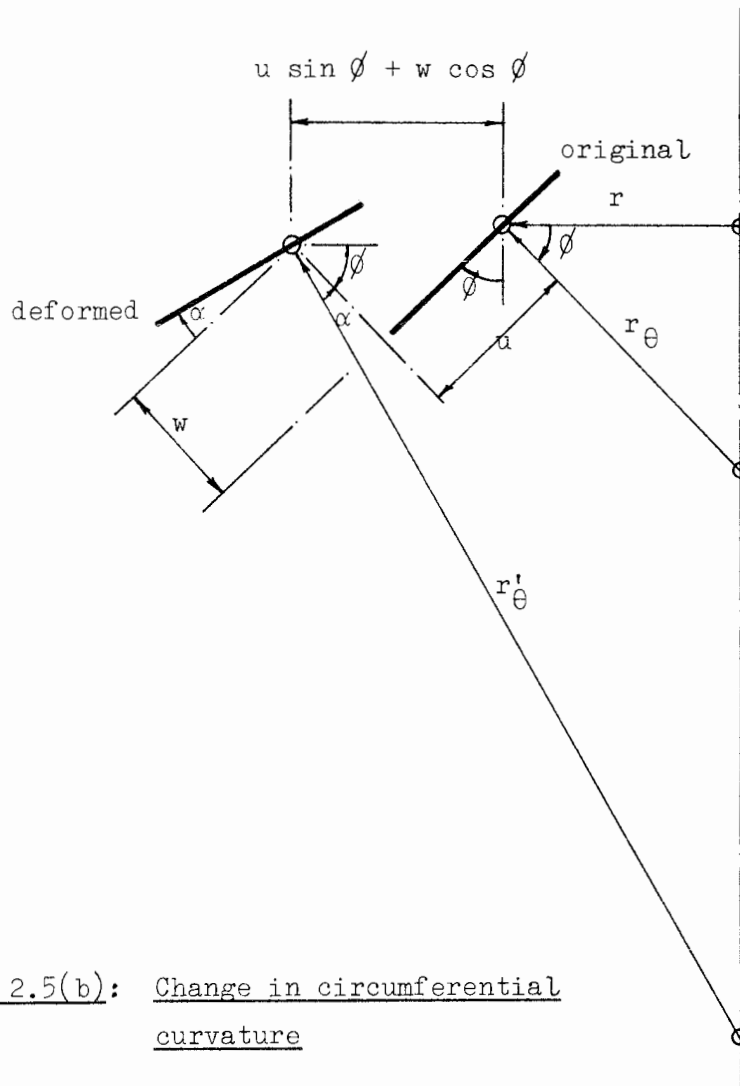


Fig. 2.5(b): Change in circumferential curvature

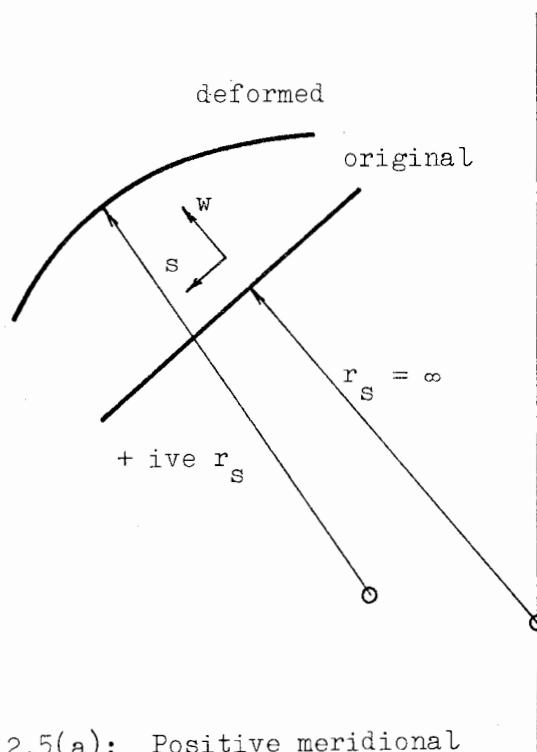


Fig. 2.5(a): Positive meridional curvature

for the stress resultants; integration of the revised equations then yields the following approximate expressions for the stress resultants:-

$$\begin{aligned} N_s &= \int_{-t/2}^{t/2} \bar{\sigma}_s dz \\ &= D \left[\frac{du}{ds} + \nu \left(\frac{u \sin \phi + w \cos \phi}{r} \right) \right] \end{aligned} \quad (2.13a)$$

$$\begin{aligned} N_\theta &= \int_{-t/2}^{t/2} \bar{\sigma}_\theta dz \\ &= D \left[\frac{u \sin \phi + w \cos \phi}{r} + \nu \frac{du}{ds} \right] \end{aligned} \quad (2.13b)$$

$$\begin{aligned} M_s &= \int_{-t/2}^{t/2} \bar{\sigma}_s z dz \\ &= K \left[-\frac{d^2w}{ds^2} - \nu \frac{\sin \phi}{r} \frac{dw}{ds} \right] \end{aligned} \quad (2.13c)$$

$$\begin{aligned} M_\theta &= \int_{-t/2}^{t/2} \bar{\sigma}_\theta z dz \\ &= \left[-\frac{\sin \phi}{r} \frac{dw}{ds} - \nu \frac{d^2w}{ds^2} \right] \end{aligned} \quad (2.13d)$$

Each of the terms in Eqs. (2.13) has a clear physical interpretation, connected with the deformation of the conical frustrum. We immediately recognise the in-plane strains (Eqs. 2.1 and 2.2b),

$$\epsilon_s = \frac{du}{ds}$$

$$\text{and } \epsilon_\theta = \frac{u \sin \phi + w \cos \phi}{r} \quad (2.14a,b)$$

The term d^2w/ds^2 is clearly the change of curvature in the meridional direction, (the original meridional curvature is zero), which we will denote by,

$$\chi_s = \frac{1}{r_\theta} = -\frac{d^2w}{ds^2} \quad (2.14c)$$

The minus sign is necessary since a positive meridional radius of curvature, as indicated in Fig. 2.5(a), has associated with it a negative value d^2w/ds^2 .

The physical meaning of the term $(\sin \phi \cdot w'/r)$ however, requires more detailed explanation.

Consider the original and deformed positions of a small element in the middle surface, as shown in Fig. 2.5(b). The circumferential radii of curvature in these two positions are r_θ and r'_θ respectively. From the geometry of the figure,

$$r_\theta = \frac{r}{\cos \phi}$$

$$\text{and } r'_\theta = \frac{r + u \sin \phi + w \cos \phi}{\cos (\phi + \alpha)}$$

where $\cos(\phi + \alpha) = \cos \phi \cos \alpha - \sin \phi \sin \alpha$.

If α is small,

$$\cos \alpha \doteq 1$$

and $\sin \alpha \doteq \tan \alpha = w'$

Hence, $\cos(\phi + \alpha) \doteq \cos \phi - \sin \phi \cdot w'$.

Making use of this approximation we may write,

$$\frac{1}{r'_\theta} - \frac{1}{r_\theta} = \frac{\cos \phi - \sin \phi \cdot w'}{r + u \sin \phi + w \cos \phi} - \frac{\cos \phi}{r}$$

If the displacements u and w are small, we may neglect the terms $u \sin \phi$ and $w \cos \phi$; we then have

$$\frac{1}{r'_\theta} - \frac{1}{r_\theta} = - \frac{\sin \phi \cdot w'}{r}$$

The above expression is clearly the change in circumferential curvature which we will denote by

$$\chi_\theta = - \frac{\sin \phi \cdot w'}{r} \tag{2.14d}$$

The stress resultants may now be written in terms of the strains and changes of curvature in the middle surface. Combining Eqs. (2.13) and (2.14) we have,

$$N_s = D [\epsilon_s + \nu \epsilon_\theta]$$

$$N_\theta = D [\epsilon_\theta + \nu \epsilon_s]$$

(2.15a,b,c,d)

$$M_s = K [\chi_s + \nu \chi_\theta]$$

$$M_\theta = K [\chi_\theta + \nu \chi_s]$$

The positive sense of the moment stress resultants M_s and M_θ are shown in Fig. 2.4(a).

Eqs. (2.14) and (2.15) will be used to define the mechanical behaviour of the conical frustrum element.

2.5 A Special Remark

We have derived the thin shell bending theory for a conical frustrum, and it is clear that the theory is equally applicable to the special cases of the circular cylinder and the annular plate or disc.

In the chapter following, however, we will come across a particular application of the circular disc, viz., as a closure element, which will require an investigation of equilibrium conditions in a circular disc in pure bending and axial tension. Since the study of equilibrium conditions is required only in a special case, it has been given in Appendix F.

One of the examples used in Chapter 4 to test the program is the cylindrical water tank with a circular disc roof. The theoretical solution of Flügge used for comparison has been rewritten for a different coordinate system, and the revised cylindrical water tank theory is given in Appendix G.

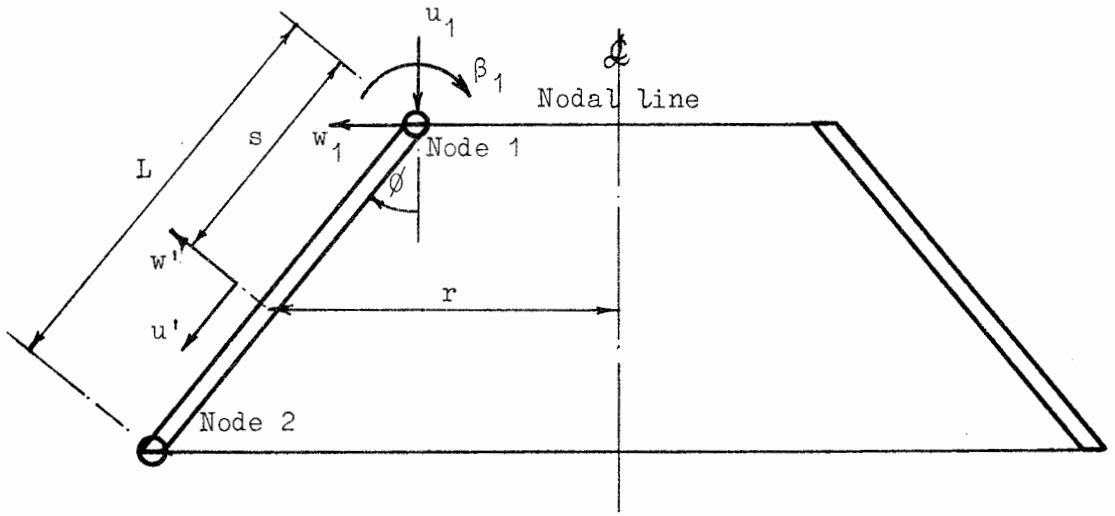


Fig. 3.1(a): The Conical Frustrum Element

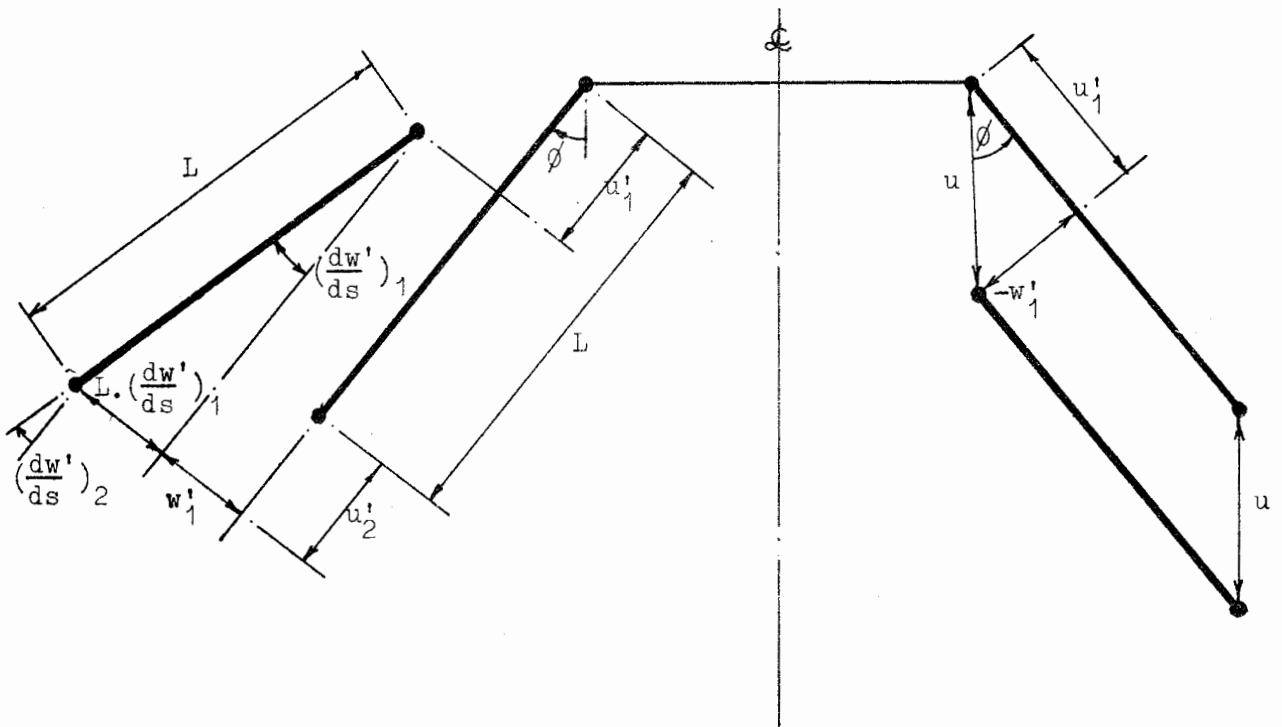


Fig. 3.1(b): Arbitrary Rigid Body Displacement

CHAPTER 3

FINITE ELEMENT THEORY

The finite element method provides the structural analyst with mathematical building blocks in the form of discrete structural elements. In the direct stiffness formulation, the mechanical behaviour of these elements is completely described by a set of stiffness equations relating the known forces acting on the element to the unknown displacements at pre-selected nodes on the element. Once the mechanical behaviour of a typical element is defined, a number of elements can be combined to idealise, and hence analyse, a complete structure.

The first part of this chapter deals with the description of the two elements required for the present analysis. These are the conical frustrum element and the circular disc closure element. The latter part of this chapter then deals with the assembly of these elements to form a complete structure, and a description of the general solution procedure.

3.1 The Conical Frustrum Element

3.1.1 The element stiffness equations

The shell which is to be analysed is divided along nodal lines into a series of conical frustra. Due to axial symmetry the displacements at any point on a nodal line are uniquely described by the displacements at any one node on this line. The element is thus effectively one-dimensional (Fig. 3.1a).

Since both bending and membrane forces are admissible, three degrees of freedom (or nodal displacements) are required at each node. At node 1 these are the translations u_1 and w_1 (in the global coordinate system), and the rotation β_1 . The displacement of an arbitrary point in the middle surface is described by the local displacement components u' and w' . The position of such a point is given by its radius r or its distance s from node 1. The frustrum is inclined at an angle ϕ to the axis of symmetry, the direction of positive increase being clockwise, as shown in the figure.

The displacement functions: The displacement functions suggested by Zienkiewicz [4] are,

$$\begin{aligned}
u' &= \alpha_1 + \alpha_2 s \\
w' &= \alpha_3 + \alpha_4 s + \alpha_5 s^2 + \alpha_6 s^3 \\
\frac{dw'}{ds} &= \alpha_4 + 2\alpha_5 s + 3\alpha_6 s^2
\end{aligned} \tag{3.1}$$

where the six arbitrary constants α_i are functions of the six nodal displacements of the element.

Substituting the nodal coordinates $s = 0$ and $s = L$ into the displacement functions we have

$$\begin{aligned}
u'_1 &= \alpha_1 & u'_2 &= \alpha_1 + \alpha_2 L \\
w'_1 &= \alpha_3 & w'_2 &= \alpha_3 + \alpha_4 L + \alpha_5 L^2 + \alpha_6 L^3 \\
\left(\frac{dw'}{ds}\right)_1 &= \alpha_4 & \left(\frac{dw'}{ds}\right)_2 &= \alpha_4 + 2\alpha_5 L + 3\alpha_6 L^2
\end{aligned} \tag{3.2a}$$

Eqs. (3.2a) can be written concisely in matrix notation as,

$$\{q'_e\} = \underset{(6 \times 6)}{[A]} \{\alpha\} \tag{3.2b}$$

where $\{q'_e\}$ is a column vector of the six element nodal displacements in the local coordinate directions. The constants α_i are found by inverting Eq. (3.2b). These values are then substituted back into Eqs. (3.1) to give the displacements at any point within the element in terms of the nodal displacements. We then have,

$$\begin{aligned}
u' &= u'_1 + s'(u'_2 - u'_1) \\
w' &= w'_1(1 - 3s'^2 + 2s'^3) + w'_2(3s'^2 - 2s'^3) \\
&\quad + \left(\frac{dw'}{ds}\right)_1 L[s' - 2s'^2 + s'^3] + \left(\frac{dw'}{ds}\right)_2 L[-s'^2 + s'^3]
\end{aligned} \tag{3.3a}$$

where $s' = s/L$ is the dimensionless distance measured from node 1. In matrix notation,

$$\{u\} = \left\{ \begin{matrix} u' \\ w' \end{matrix} \right\} = \underset{(2 \times 6)}{[N']} \{q'_e\} \tag{3.3b}$$

The displacement functions given in Eqs. (3.1) satisfy both the conditions of continuity within the element and compatibility between adjacent elements, the latter point being trivial for one-dimensional elements. The conical frustrum element is therefore a conforming one.

The expression for the axial strain in terms of the nodal displacement is

$$\epsilon_s = \frac{du'}{ds} = \frac{u'_2 - u'_1}{L} \quad (3.4a)$$

The axial strain is clearly constant throughout the element; moreover, in the case of a rigid body movement given by $u'_1 = u'_2$, the axial strain vanishes. On the other hand, any local translation or rotation of the element, whether as a rigid body or not, must give rise to circumferential strains. If the element is given an arbitrary rigid body movement (Fig. 3.1b) defined by.

$$u'_1 = u'_2$$

$$w'_2 = w'_1 + L \cdot \left(\frac{dw'}{ds}\right)_1$$

$$\left(\frac{dw'}{ds}\right)_2 = \left(\frac{dw'}{ds}\right)_1$$

then the circumferential strain is,

$$\begin{aligned} \epsilon_\theta &= \frac{u' \sin \phi + w' \cos \phi}{r} \\ &= \frac{u'_1 \sin \phi + \{w'_1 + s \left(\frac{dw'}{ds}\right)_1\} \cos \phi}{r} \end{aligned} \quad (3.4b)$$

For a local rigid body movement then, the circumferential strain does not vanish. In fact, if the element rotates as a rigid body by an amount $\left(\frac{dw'}{ds}\right)_1$ the strain is not even constant, as indicated by the term in s . However, if the conical frustrum undergoes a global rigid body movement as shown in the right hand side of Fig. 3.1(b), and defined by,

$$u'_1 = u \cos \phi$$

$$-w'_1 = u \sin \phi$$

$$\text{and} \quad \left(\frac{dw'}{ds}\right) = 0$$

then the circumferential strain ϵ_θ given by Eq. (3.4b) does in fact vanish. The axial strain ϵ_s clearly also vanishes. Hence, since this is the only rigid body movement of the frustrum as a whole, possible within the limitations of axially symmetric deformations, the conical frustrum element is complete.

Transformation and the shape function: The relationship between the local and global displacements at the n th node is,

$$\begin{bmatrix} u'_n \\ w'_n \\ \left(\frac{dw'}{ds}\right)_n \end{bmatrix} = \begin{bmatrix} \cos \phi & \sin \phi & 0 \\ -\sin \phi & \cos \phi & 0 \\ 0 & 0 & 1 \end{bmatrix} \cdot \begin{bmatrix} u_n \\ w_n \\ \beta_n \end{bmatrix} \quad (3.5a)$$

which may be written as,

$$\{q'_n\} = [T_n] \cdot \{q_n\} \quad (3.5b)$$

For the element as a whole we therefore have,

$$\{q'_e\} = [T] \cdot \{q_e\} \quad (3.5c)$$

where

$$[T] = \begin{bmatrix} T_n & | & 0 \\ 0 & | & T_n \end{bmatrix}$$

Eq. (3.3b) may therefore be rewritten as,

$$\begin{aligned} \{u\} &= [N'] [T] \{q_e\} \\ &= \underset{(2 \times 6)}{[N]} \{q_e\} \end{aligned} \quad (3.6a)$$

The matrix $[N]$ is called the shape function of the element and is given by,

$$[N] = \begin{bmatrix} \frac{(1-s') \cos \phi}{-(1-3s'^2+2s'^3)} & | & \frac{(1-s') \sin \phi}{(1-3s'^2+2s'^3)} & | & 0 \\ \frac{s' \cos \phi}{-(3s'^2-2s'^3)} & | & \frac{s' \sin \phi}{(3s'^2-2s'^3)} & | & L(-s'^2+s'^3) \end{bmatrix} \quad (3.6b)$$

The strain-displacement relationships: The relationship between the strains, curvatures, and displacements of a point in the middle surface is, from Eqs. (2.14),

$$\{\epsilon\} = \begin{bmatrix} \epsilon_s \\ \epsilon_\theta \\ \chi_s \\ \chi_\theta \end{bmatrix} = \begin{bmatrix} \frac{du'}{ds} \\ \frac{u' \sin \phi + w' \cos \phi}{r} \\ -\frac{d^2 w'}{ds^2} \\ -\frac{\sin \phi}{r} \frac{dw'}{ds} \end{bmatrix} \quad (3.7a)$$

We now require a relationship between the strain components and the six nodal displacements of the element, of the form,

$$\{\epsilon\} = \underset{(4 \times 6)}{[B]} \cdot \{q_e\} \quad (3.7b)$$

The matrix $[B]$ can be derived in explicit form by differentiation of the shape function $[N]$.

The stress-strain relationship: Four stress resultants are required to completely define a state of axisymmetric stress in a conical frustrum. These are shown acting on a small element of the frustrum in Fig. 3.2.

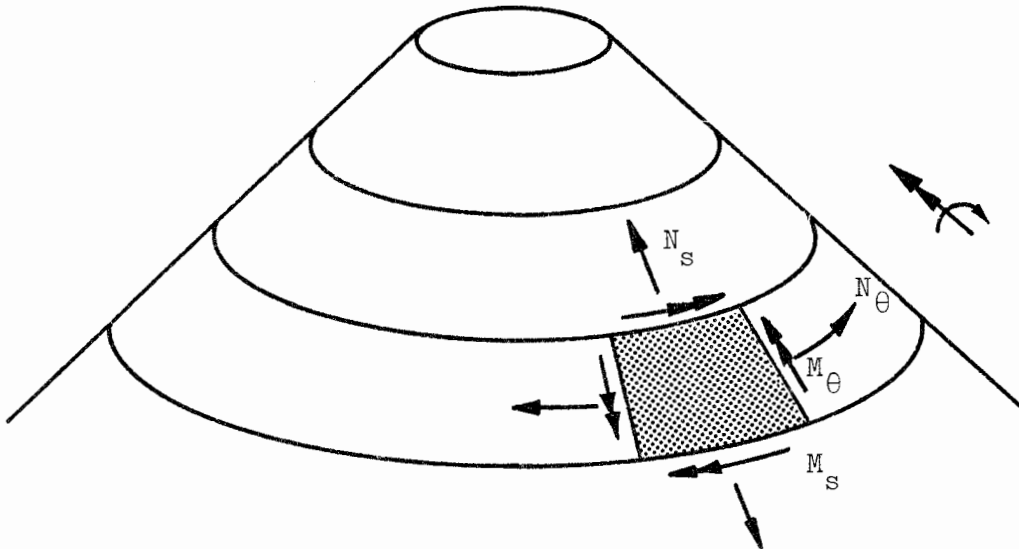


Fig. 3.2

Under certain conditions, for example, changes in temperature, the element may be subject to initial strains $\{\epsilon_0\}$. In such cases the actual stresses are caused by the difference between the actual and initial strains, the relationship being of the form,

$$\{\sigma\} = \begin{bmatrix} N_s \\ N_\theta \\ M_s \\ M_\theta \end{bmatrix} = [D] (\{\epsilon\} - \{\epsilon_0\}) \quad (3.8)$$

where $[D]$ is the elasticity matrix given by,

$$[D] = \frac{E}{1 - \nu^2} \begin{bmatrix} t & \nu t & 0 & 0 \\ \nu t & t & 0 & 0 \\ 0 & 0 & \frac{t^3}{12} & \frac{\nu t^3}{12} \\ 0 & 0 & \frac{\nu t^3}{12} & \frac{t^3}{12} \end{bmatrix} \quad (3.9a)$$

Eq. (3.9a) can be written more concisely in the form,

$$[D] = \frac{E}{1 - \nu^2} [D^*] \quad (3.9b)$$

The element stiffness matrix and load vector: The element stiffness matrix, which expresses the fundamental relationship between the nodal displacements and forces, will be derived here by direct application of the Principle of Minimum Total Potential Energy.*

Let \bar{U} denote the elastic strain energy density of the element, and let $\{X\}$ and $\{\phi\}$ be vectors containing components of the body and surface forces respectively, acting on the element. Then the total potential energy U of the element is,

$$U = \int_V \bar{U} \, dV + \int_V \{u\}^t \{X\} \, dV + \int_S \{u\}^t \{\phi\} \, dS \quad (3.10)$$

where integration is over the volume or surface of the element as required.

The elastic strain energy density is given by,

$$\bar{U} = \frac{1}{2} \{\epsilon\}^t [D] \{\epsilon\} - \{\epsilon\}^t [D] \{\epsilon_0\} + \frac{1}{2} \{\epsilon_0\}^t [D] \{\epsilon_0\} \quad (3.11)$$

*Supplementary notes on the Principle, including the derivation of Eq. (3.11), may be found in Appendix C.

Substituting for the strains $\{\epsilon\}$ from Eq. (3.7b) and for the displacements $\{u\}$ from Eq. (3.6a), the total potential energy may be rewritten in the form,

$$\begin{aligned}
 U = & \frac{1}{2} \int_V \{q_e\}^t [B]^t [D] [B] \{q_e\} dV \\
 & - \int_V \{q_e\}^t [B]^t [D] \{\epsilon_o\} dV \\
 & + \frac{1}{2} \int_V \{\epsilon\}^t [D] \{\epsilon_o\} dV \\
 & - \int_V \{q_e\}^t [N]^t \{X\} dV \\
 & - \int_S \{q_e\}^t [N]^t \{\phi\} dS
 \end{aligned} \tag{3.12}$$

Taking the first variation of U with respect to the nodal displacements $\{q_e\}$ and setting it equal to zero we have,

$$\begin{aligned}
 \delta U = 0 = & \left[\int_V [B]^t [D] [B] \{q_e\} dV \right. \\
 & - \int_V [B]^t [D] \{\epsilon_o\} dV \\
 & - \int_V [N]^t \{X\} dV \\
 & \left. - \int_S [N]^t \{\phi\} dS \right] \delta \{q_e\}
 \end{aligned} \tag{3.13}$$

The variation $\delta \{q_e\}$ is arbitrary, from which it follows that the expression in the square brackets must vanish. We therefore have that,

$$\int_V [B]^t [D] [B] dV \cdot \{q_e\} = \int_V [B]^t [D] \{\epsilon_o\} dV + \int_V [N]^t \{X\} dV + \int_S [N]^t \{\phi\} dS \tag{3.14}$$

The right hand side of Eq. (3.14) contains expressions for the equivalent nodal loads due to initial strains, body forces and surface forces acting on the element. Hence the equation may be written in the form

$$[k] \{q_e\} = \{F_e\} \tag{3.15}$$

where $[k]$ is the element stiffness matrix relating the nodal load vector $\{F_e\}$ to the corresponding nodal displacement vector $\{q_e\}$.

polynomials of degree $2n - 1$, e.g., the formula for $n = 4$ is exact for seventh degree polynomials. However, in the present application the use of Gaussian formulae is limited for the following reasons:-

- (i) The standard formulae are derived for the interval $[-1, 1]$. In our case we require to integrate over the interval $[0, 1]$. Hence we must use half-interval formulae which can be derived only from the formulae for which n is even.
- (ii) We have no quantitative information on the errors involved in using half-interval formulae, i.e. whether the half-interval formulae are capable of the same accuracy as the full interval formulae.
- (iii) Due to the complexity of the derivation of Gaussian formulae we have no composite formulae available. For example, the half-interval formula for $n = 4$ has 3 sub-intervals (or 2 abscissae), but the number of sub-intervals cannot be increased except by using higher order formulae ($n = 6, 8$, etc.); in other words, all the half-interval formulae are limited to $n/2$ abscissae.

There appears, therefore, to be only one way of determining the accuracy of the Gaussian formulae under the present limitations, and that is to use them in an actual analysis. Our intention is therefore to compare results obtained from the Gaussian half-formulae for $n = 4, 6, 8$ and 10 , as well as the Simpson's formulae for 5 and 7 points, with a view to determining which is the most efficient.

We must now illustrate the precise method by which the stiffness matrix is evaluated using the 5-point Simpson's rule. Returning to Eq. (3.17) we let

$$[Z]_i = \left[[B]^t [D^*] [B] r \right]_i \quad (3.18)$$

where the subscript i indicates that the matrices have been evaluated at the point (s'_i, r_i) on the element. In the present illustration the matrix $[Z]_i$ is evaluated at the following points:-

3.1.2 Numerical integration of the element stiffness matrix

The general form of the element stiffness matrix is, from Eq. (3.14),

$$[k] = \int_{\dot{V}} [B]^t [D] [B] dV \quad (3.16)$$

The thickness t of the element has already been included in the elasticity matrix $[D]$, which has the effect of reducing the volume integration to integration over the surface area of the element. Writing the element surface area in the form

$$dA = 2\pi r ds = 2\pi r L ds'$$

and making use of the alternate form of the elasticity matrix $[D^*]$ (Eq. 3.9b), the expression for the element stiffness matrix becomes,

$$[k] = \frac{2\pi L E}{(1 - \nu^2)} \int_0^1 [B]^t [D^*] r ds' \quad (3.17)$$

The integration involved is not simple enough to warrant an explicit formulation of the stiffness matrix. Hence, recourse must be had to numerical methods.

We have a choice of two methods of numerical integration, viz., the Gauss quadrature and Newton-Cotes quadrature formulae.* From the computer programming point both methods are equally simple to apply; hence the choice of method to be used will depend on the expected accuracy of results in relation to the number of abscissae or sub-intervals required to achieve it.

A study of the $[B]$ and $[D^*]$ matrices in Eq. (3.17) suggests that we will need to integrate a sixth degree polynomial in s' . Simpson's rule, which is the Newton-Cotes formula for $n = 2$, is capable of exactly integrating a third degree polynomial. For higher order polynomials the approximation, although not exact, may be maintained at a suitable level of accuracy by using a larger number of sub-intervals than the basic two. Thus we have Simpson's formulae for 4 sub-intervals (5 abscissae, or 5 points), 6 sub-intervals (7 abscissae, or 7 points), and so on.

The Gaussian quadrature formulae are capable of exactly integrating

*A discussion of quadrature theory is given in Appendix D.

$$\begin{aligned}
[Z]_1 &: (0, r_1) \\
[Z]_2 &: (0.25, r_2) \\
[Z]_3 &: (0.50, r_3) \\
[Z]_4 &: (0.75, r_4) \\
[Z]_5 &: (1.00, r_5)
\end{aligned}$$

Applying Simpson's 5-point formula we have,

$$[k] = \frac{2\pi EL}{1-\nu^2} \cdot \frac{0.25}{3} \left[[Z]_1 + 4[Z]_2 + 2[Z]_3 + 4[Z]_4 + [Z]_5 \right] \quad (3.19a)$$

The final result of the matrix manipulation is a symmetrical (6×6) element stiffness matrix of the form,

$$[k]_i = \begin{array}{c} \begin{array}{c} U_1 \\ W_1 \\ M_1 \\ U_2 \\ W_2 \\ M_2 \end{array} \begin{array}{c} \begin{array}{ccc} u_1 & w_1 & \beta_1 \\ \vdots & \vdots & \vdots \end{array} \\ \begin{array}{cc} k_{11}^i & k_{12}^i \\ \vdots & \vdots \\ \vdots & \vdots \\ k_{21}^i & k_{22}^i \\ \vdots & \vdots \\ \vdots & \vdots \end{array} \end{array} \quad (3.19b)
\end{array}$$

Eq. (3.19b) defines the notation to be used subsequently when referring to the stiffness matrix for the i th element.

3.1.3 Derivation of the element load vector

During the initial formulation of the element stiffness equations, allowance was made for three distinct types of loading, viz., loading due to initial strains, loading due to forces distributed over the surface of the element, and loading due to forces distributed over the volume of the element. Each of these types of loading is represented by an integral in Eq. (3.14), from which six equivalent nodal loads (corresponding to the three global degrees of freedom at each node), can be evaluated.

The equivalent nodal loads will be derived here for each of the types of loading in turn.

The initial strain load vector: We will consider only the initial strains caused by uniform changes in temperature. If the element undergoes a relative change in temperature of θ degrees, then the initial strain vector is given by,

$$\{\epsilon\} = \begin{bmatrix} \alpha \theta \\ \alpha \theta \\ 0 \\ 0 \end{bmatrix} \quad (3.20)$$

where α is the coefficient of thermal expansion of the element material. The two non-zero components are the in-plane axial and circumferential strains, and there are no initial changes of curvature. The equivalent nodal load vector for the element is,

$$\begin{aligned} \{F_e\}_i &= \begin{bmatrix} U_1 \\ W_1 \\ M_1 \\ U_2 \\ W_2 \\ M_2 \end{bmatrix}_i = \int_V [B]^t [D] \{\epsilon_o\} dV \\ &= \frac{2\pi L E}{1 - \nu^2} \int_0^1 [B]^t [D]^* \{\epsilon_o\} r ds' \end{aligned} \quad (3.21)$$

The integral in the above equation is very similar to the integral for the element stiffness matrix $[k]$ (Eq. 3.17), so that in both cases precisely the same method of evaluation may be used.

The surface force load vector: The most common type of distributed load is one which acts normal to the surface of the element, and whose magnitude varies linearly from one end of the element to the other (Fig. 3.3).

The positive directions of the six equivalent nodal loads are shown in the figure and their values are given by,

$$\{F_e\}_s = \begin{bmatrix} U_1 \\ W_1 \\ M_1 \\ U_2 \\ W_2 \\ M_2 \end{bmatrix}_s = \int_A [N]^t \{\phi\} dA \quad (3.22)$$

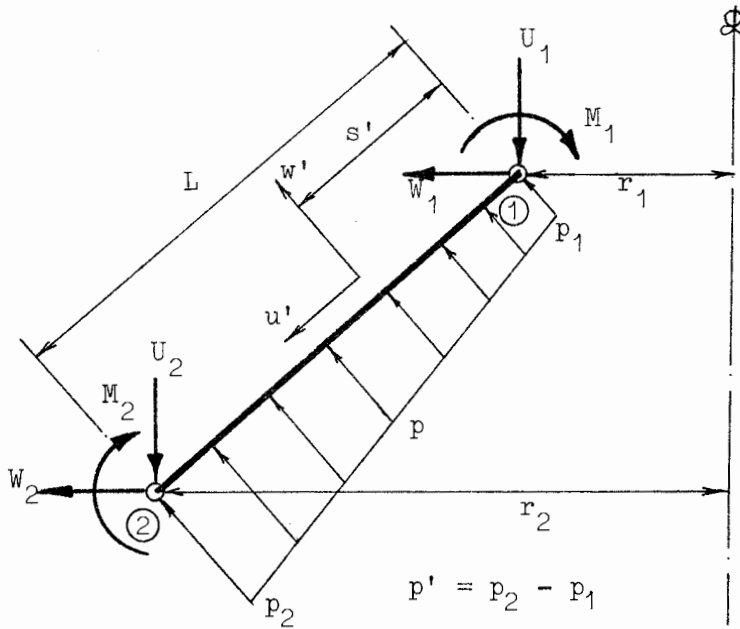


Fig. 3.3

The vector $\{\phi\}$ contains the components, in the local coordinate directions, of the distributed load p , considered positive if acting in the direction of the positive normal to the element w' , i.e.

$$\{\phi\} = \begin{bmatrix} 0 \\ p_1 + s'(p_2 - p_1) \end{bmatrix} \quad (3.23)$$

Explicit evaluation of the surface load vector $\{F_e\}_s$ is a straightforward procedure and the expressions for the components of this vector are given in Appendix E.

The body force load vector: The self-weight of the structure is the only body force likely to occur in a shell structure. The equivalent nodal loads for the self-weight of the structure are,

$$\{F_e\}_b = \begin{bmatrix} U_1 \\ W_1 \\ M_1 \\ U_2 \\ W_2 \\ M_2 \end{bmatrix}_b = \int_V [N]^t \{X\} dV \quad (3.24)$$

The vector $\{X\}$ contains the components of the self-weight of the element, given by,

$$\{X\} = \begin{bmatrix} \gamma \cos \phi \\ -\gamma \sin \phi \end{bmatrix} \quad (3.25a)$$

where γ is the unit weight of the structural material. The minus sign is due to the fact the self-weight acts in a direction opposite to the positive normal to the element.

Again, explicit evaluation of $\{F_e\}_b$ is a straightforward procedure, and expressions for the components of this vector are given in Appendix E.

Clearly, since the shell is thin the body forces may be replaced by equivalent surface forces and vice versa. Hence, the load vector $\{F_e\}_b$ amounts to the equivalent nodal loads due to a uniformly distributed vertical load, say p_v . Distributed vertical loading may therefore be included in the analyses by making the substitution

$$\gamma = \frac{p_v}{t} \quad (3.25b)$$

Although it is not absolutely necessary, there is an advantage in retaining the concept of a body force load vector. If the form of the surface load components (Eq. 3.23) was restricted so as to take account of the self-weight of the structure as an equivalent pressure, then the pressure at each node of the structure would have to be calculated prior to the actual assembly of the load vector (Eq. 3.22). By specifying the self-weight in the form of Eq. (3.25a) however, only the parameter γ is required and no equivalent nodal pressures are calculated. This amounts to a considerable saving in computation as well as data input preparation.

To summarise, the structure may be subject to three different types of loading: loads due to change in temperature, surface loads, and body loads. In addition to these loads, there may be discrete point loads (in actual fact, line loads) applied at the nodes of an element, given by,

$$\{F_e\}_l = \begin{bmatrix} U_1 \\ W_1 \\ \cdot \\ \cdot \\ \cdot \\ \cdot \\ M_2 \end{bmatrix}_l \quad (3.26)$$

These point loads are simply added in as such, so that the total equivalent nodal load vector for a particular element is the sum of the individual load vectors, i.e.,

$$\{F_e\} = \{F_e\}_i + \{F_e\}_s + \{F_e\}_b + \{F_e\}_l \quad (3.27)$$

Care should however be taken not to add point loads to the load vectors of both the elements adjacent to the node at which the point loads are applied; this would be equivalent to adding in twice the actual point loads, since, when the system load vector is assembled, the element load vectors overlap at each node.

3.2 The Circular Plate Closure Element

It has already been mentioned that when an element closes on the axis of symmetry the stiffness of the element becomes infinite. This is because the stiffness matrix of the conical frustrum element contains terms of the form,

$$k' = \int_0^1 \frac{m}{r_1 + s' \sin \phi} \cdot ds \quad (3.28a)$$

where r_1 is the radius at the first node of the element, and m is a constant depending on the geometry of the element. Integration of Eq. (3.28a) yields,

$$k' = [m \log (r_1 + s' \sin \phi)]_0^1 \quad (3.28b)$$

which is indeterminate when the limits $r_1 = 0$ and $s' = 0$ are substituted.

The conical frustrum element may therefore never be allowed to touch the axis of symmetry.* The singularity at the axis of symmetry arises from the strain-displacement relationships (Eq. 2.14), which contain the radius r in the denominator. Greenbaum^[11] has advanced an alternative set of relationships, based on the shell theory of Novozhilov^[12], which do not contain the radius r in the denominator, and hence effectively overcome the singularity problem. These strain-displacement relationships have been used successfully by Percy et al^[13].

An alternative and simpler method of overcoming the singularity problem is to derive a special element having only one node. A circular plate element was chosen since it is mathematically easy to work with and is for practical purposes the most generally applicable closure shape.**

3.2.1 Derivation of the closure element stiffness matrix and load vector

Consider a circular plate element*** of radius a and having three degrees of freedom, or global displacements, u_1 , w_1 and β_1 at its single node. The local coordinate directions are defined by u' and w' (Fig. 3.4).

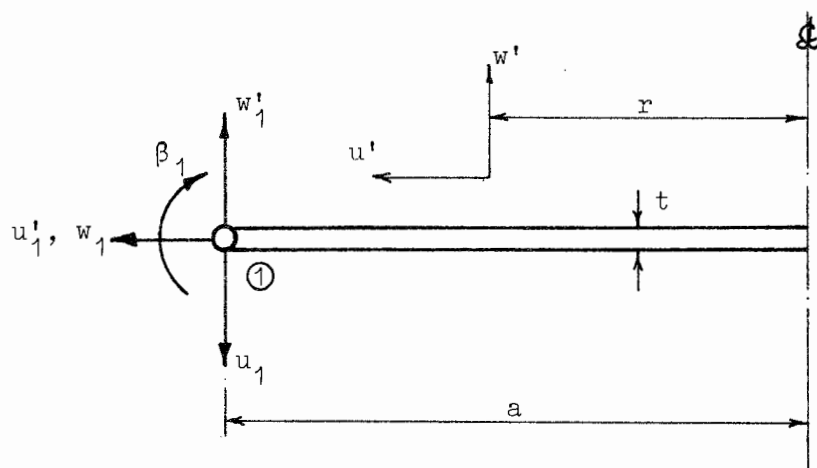


Fig 3.4: The circular disc closure element

* If the element is turned 'upside down' so that r_1 becomes the outer radius ($\neq 0$), $\sin \phi$ becomes negative and the same situation exists, since we then have $r_1 = -s' \sin \phi$.

** Pardoen and Hagen^[14] appear to be the only authors who describe the use of a circular disc as a closure element. The present work is independent of theirs.

*** In the present derivation we make use of the fact that the circular plate is a special case of the conical frustrum when $\phi = 90^\circ$.

The following displacement functions are assumed:

$$\begin{aligned} w' &= \alpha_1 + \alpha_2 (r^2 - a^2) \\ u' &= \alpha_3 r \\ \frac{dw'}{dr} &= 2\alpha_2 r \end{aligned} \quad (3.29a)$$

The reason for such a choice will become apparent as the derivation progresses. Substituting the nodal coordinate $r = a$ into the above functions, we have

$$\begin{aligned} w'_1 &= \alpha_1 \\ u'_1 &= \alpha_3 a \\ \left(\frac{dw'}{dr}\right)_1 &= \beta_1 = 2\alpha_2 a \end{aligned} \quad (3.29b)$$

from which the generalised displacements α_i are solved for in terms of the local nodal displacements. Substituting these values back into Eq. (3.29a) we have,

$$\begin{aligned} w' &= w'_1 + \frac{\beta_1}{2a} (r^2 - a^2) \\ u' &= u'_1 \frac{r}{a} \end{aligned} \quad (3.29c)$$

Transformation from the local coordinate system to the global system is accomplished by means of the transformation matrix Eq. (3.5b) with $\phi = 90^\circ$, i.e.,

$$\begin{bmatrix} u'_1 \\ w'_1 \\ \left(\frac{dw'}{dr}\right)_1 \end{bmatrix} = \begin{bmatrix} 0 & 1 & 0 \\ -1 & 0 & 0 \\ 0 & 0 & 1 \end{bmatrix} \begin{bmatrix} u_1 \\ w_1 \\ \beta_1 \end{bmatrix} \quad (3.30)$$

Making use of this transformation we may rewrite Eq. (3.31a) as,

$$\begin{aligned} \begin{bmatrix} u' \\ w' \end{bmatrix} &= \begin{bmatrix} 0 & \frac{r}{a} & 0 \\ -1 & 0 & \frac{r^2 - a^2}{2a} \end{bmatrix} \begin{bmatrix} u_1 \\ w_1 \\ \beta_1 \end{bmatrix} \\ &= [N] \{q_e\} \end{aligned} \quad (3.31)$$

where $[N]$ is the shape function for the closure element. The strain-displacement relationships (Eq. 3.7a) for the closure element are,

$$\begin{bmatrix} \epsilon_r \\ \epsilon_\theta \\ \chi_r \\ \chi_\theta \end{bmatrix} = \begin{bmatrix} \frac{du'}{dr} \\ \frac{u'}{r} \\ \frac{d^2w'}{dr^2} \\ \frac{dw'}{dr} \cdot \frac{1}{r} \end{bmatrix} = \begin{bmatrix} 0 & \frac{1}{a} & 0 \\ 0 & \frac{1}{a} & 0 \\ 0 & 0 & \frac{1}{a} \\ 0 & 0 & \frac{1}{a} \end{bmatrix} \begin{bmatrix} u_1 \\ w_1 \\ \beta_1 \end{bmatrix} \quad (3.32a)$$

$$\text{or } \{\epsilon\} = [B] \{q_e\} \quad (3.32b)$$

Clearly the choice of displacement functions ensures that the in-plane strains are constant and equal to each other; the same holds for the changes of curvature. Furthermore, the in-plane strains depend only on the radial displacement w_1 , and the changes of curvature only on the rotation β_1 .

The stress-strain relationships are identical to those of the conical frustrum (Eq. 3.8) except that initial strains are not taken into account. The relationship we recall is,

$$\{\sigma\} = \frac{E}{1 - \nu^2} [D^*] \{\epsilon\}$$

The formulation of the element stiffness matrix is again identical to that of the conical frustrum (Eq. 3.17), except that the area dA is taken simply as $dA = 2\pi r dr$; hence we may write,

$$[k]_c = \frac{2\pi E}{(1 - \nu^2)} \int_0^1 [B]^t [D^*] [B] r dr \quad (3.33)$$

The closure element stiffness matrix has only two non-zero elements, an axial stiffness and a bending stiffness, given respectively by,

$$\begin{aligned} k_{22} &= \frac{2\pi E t}{1 - \nu^2} \int_0^a \frac{2(1 + \nu)}{a^2} r dr \\ &= \frac{2\pi E t}{1 - \nu^2} \end{aligned} \quad (3.34a)$$

$$\begin{aligned}
 \text{and } k_{33} &= \frac{2\pi Et}{1-\nu^2} \int_0^a \frac{2t^2(1+\nu)}{12a^2} r \, dr \\
 &= \frac{2\pi Et^3}{12(1-\nu)} \qquad (3.34b)
 \end{aligned}$$

The complete closure element stiffness matrix may therefore be written as,

$$[k]_c = \begin{matrix} & \begin{matrix} u_1 & w_1 & \beta_1 \end{matrix} \\ \begin{matrix} U_1 \\ W_1 \\ M_1 \end{matrix} & \begin{bmatrix} 0 & 0 & 0 \\ 0 & k_{22} & 0 \\ 0 & 0 & k_{33} \end{bmatrix} \end{matrix} \qquad (3.34c)$$

It is interesting to note the following points in connection with the closure element stiffness matrix:-

- (i) The element has no lateral shear stiffness, (i.e., $k_{11} = 0$) due to the fact that it has only a single node. The application of a lateral force to this node causes the element to move as a rigid body.
- (ii) The stiffness k_{22} and k_{33} in Eqs. (3.34) are independent of the length (= radius) of the element. This is because these stiffnesses are the relationship between total force or moment at the circumference of the element, and the corresponding displacements. It is however more meaningful to write the closure element stiffnesses in terms of forces and moments per unit of circumference. Thus, if M^* is the total moment at the circumference such that

$$M^* = 2\pi a M \qquad (3.35a)$$

where M is the moment per unit of circumference, then we may write for the bending stiffness per unit of circumference,

$$k'_{33} = \frac{M}{\theta} = \frac{M^*}{2\pi a \theta} \qquad (3.35b)$$

The bending stiffness therefore clearly depends on the size of the element, becoming larger as the length a of the element decreases. A similar argument exists for the axial stiffness.

(iii) The expressions derived above for k_{22} and k_{33} are identical to those derived from the differential equations of equilibrium of a circular plate in pure bending and pure axial tension. The latter results are derived in Appendix F.

The equivalent nodal loads: The equivalent nodal loads at the single node due to a uniformly distributed pressure p acting on the closure element may be derived from Eq. (3.22), using the surface load vector,

$$\{\phi\} = \begin{bmatrix} 0 \\ p \end{bmatrix} \quad (3.36a)$$

The equivalent nodal loads are then,

$$\begin{aligned} \begin{bmatrix} U_1 \\ W_1 \\ M_1 \end{bmatrix} &= 2\pi \int_0^a [N]^t \begin{bmatrix} 0 \\ p \end{bmatrix} r \, dr \\ &= 2\pi a \begin{bmatrix} -\frac{pa}{2} \\ 0 \\ -\frac{pa^2}{8} \end{bmatrix} \end{aligned} \quad (3.36b)$$

The components of the load vector given above are identical to the fixed-end forces and moments in a circular plate subject to a uniformly distributed pressure p . These results are also derived in Appendix F.

3.2.2 The application of the closure element

The closure element is used to close a shell by forming a special link between the standard conical frustrum elements approaching the axis of symmetry, and the axis itself (Fig. 3.5a).

Part of the system stiffness matrix corresponding to this assemblage of elements is shown in Fig. 3.5(b). Since the closure element has only a single node, and since this node is also common to the first standard element, the only change in the system stiffness matrix is the addition to it of the closure element stiffness matrix $[k]_c$ as follows:

$$[K_{11}] = [k_{11}^1] + [k]_c \quad (3.37)$$

This amounts to an increase in the diagonal stiffness shown shaded in the figure.

If the closure element has a distributed load p acting on it, then the components U_1 , W_1 and M_1 of the system load vector (also shown shaded in the figure) are augmented by the amounts given in Eq. (3.36b). In this case the positive direction of the load p depends on the order in which the adjoining standard elements are numbered, since the positive direction of the normal to an element depends on whether the element is numbered from its lower to its upper edge or vice versa.* It will be noticed however that no such rule applies to the addition of the closure element stiffnesses, since they are independent of element numbering order or orientation.

Once the displacements at the nodes have been obtained it is possible to calculate the displacements at the axis of symmetry by making use of the closure element displacement functions, in the form given in Eq. (3.31). Substituting $r = 0$ at the axis of symmetry we have,

$$\begin{aligned} u'_0 &= 0 \\ w'_0 &= -u_1 - \beta_1 \frac{a}{2} \\ \beta_0 &= 0 \end{aligned} \quad (3.38)$$

which give the displacements at the axis of symmetry in the local coordinate directions in terms of the global displacements at node 1. It is clear from these results that at the axis of symmetry the structure may undergo displacement only in the direction of the axis itself.

It has already been shown that the in-plane strains ϵ_r and ϵ_θ , and the changes of curvature χ_r and χ_θ are constant and equal. Hence the stress resultants N_s and N_θ are constant and equal, and in the case of N_s , given by,

$$\begin{aligned} N_s &= \frac{Et}{1 - \nu^2} [\epsilon_s + \nu \epsilon_\theta] \\ &= \frac{Et}{1 - \nu} \cdot \frac{u'_1}{a} = N_\theta \end{aligned} \quad (3.39a)$$

Similarly, the stress resultants M_s and M_θ are constant and equal,

* See Section 3.3.5, Fig. 3.19.

and in the case of M_2 , given by,

$$\begin{aligned} M_s &= \frac{Et^3}{12(1-\nu^2)} \left[\frac{d^2 w'}{dr^2} + \frac{\nu}{r} \frac{dw'}{dr} \right] \\ &= \frac{Et^3}{12(1-\nu)} \cdot \frac{\beta_1}{a} = M_\theta \end{aligned} \quad (3.39b)$$

A point worth considering before one makes use of the closure element is whether in fact it is worth using at all; in other words, will an analysis which uses the closure element yield results which are significantly different from one in which a small hole is left at the axis of symmetry*. Clearly if the closure element is small its contribution to the system load vector will be insignificant.

The closure element's contribution to the system stiffness matrix is, as we have shown, constant, i.e., independent of the radius a of the element. However, as the radius of the closure element changes, so the value of r_1 in Eq. (3.28b) for the adjacent element changes; hence the stiffness matrix $[k_{11}^1]$ in Eq. (3.37) changes. Thus the radius of the closure element, while not affecting its own contribution to the system stiffness matrix, nevertheless has an effect on the system stiffness matrix via the stiffness of the adjacent element.

A quantitative evaluation of the effect of the size of the closure element is not possible here since we have no explicit version of the conical frustrum element stiffness matrix. We therefore defer further discussion until some numerical results have been examined.

3.3 The Assembled Structure

In turning our attention to the structure as a whole we may describe its behaviour in the same way as that of an element of the structure, viz., by a set of stiffness equations of the form.

$$[K] \{q\} = \{F\} \quad (3.40)$$

where $[K]$ is the system or structural stiffness matrix, relating the displacements $\{q\}$ of the nodes of the structure to the applied loads $\{F\}$ acting at these nodes. The solution of a structural problem rests therefore

*In one case, viz., that of a simply supported circular plate with a central point load, the displacements are unaffected if a very small hole is left at the axis of symmetry. See Ref. [3], p 60.

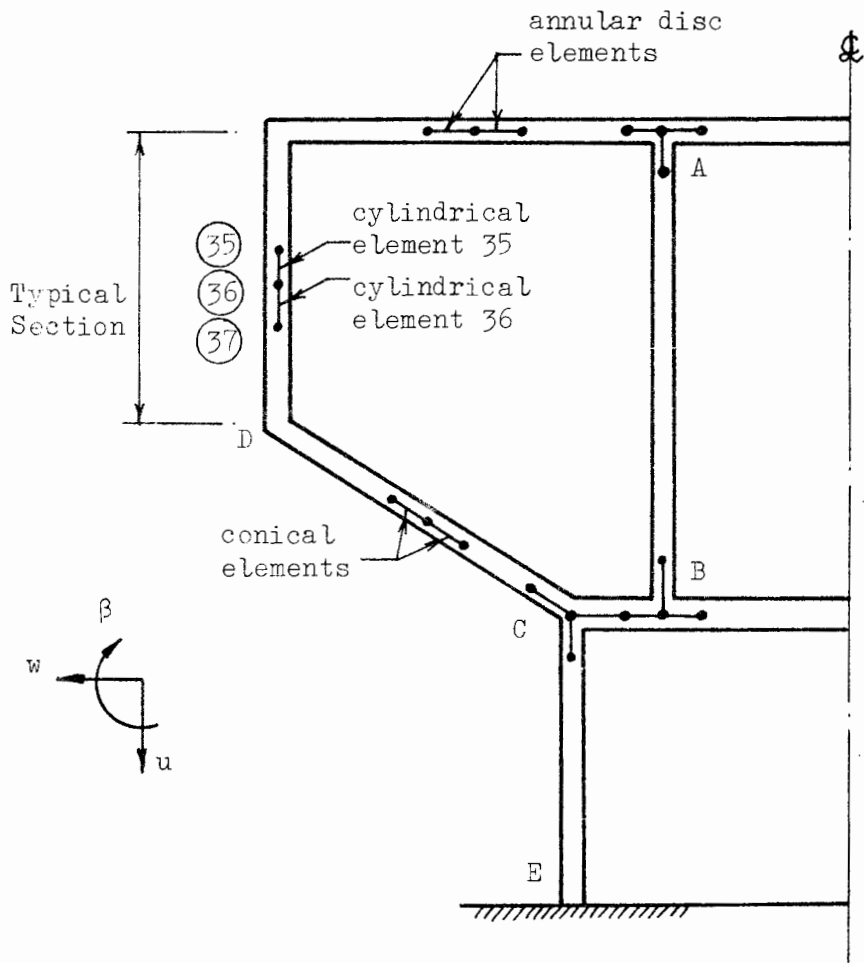


Fig. 3.6: Illustration of a Branched Shell of Revolution

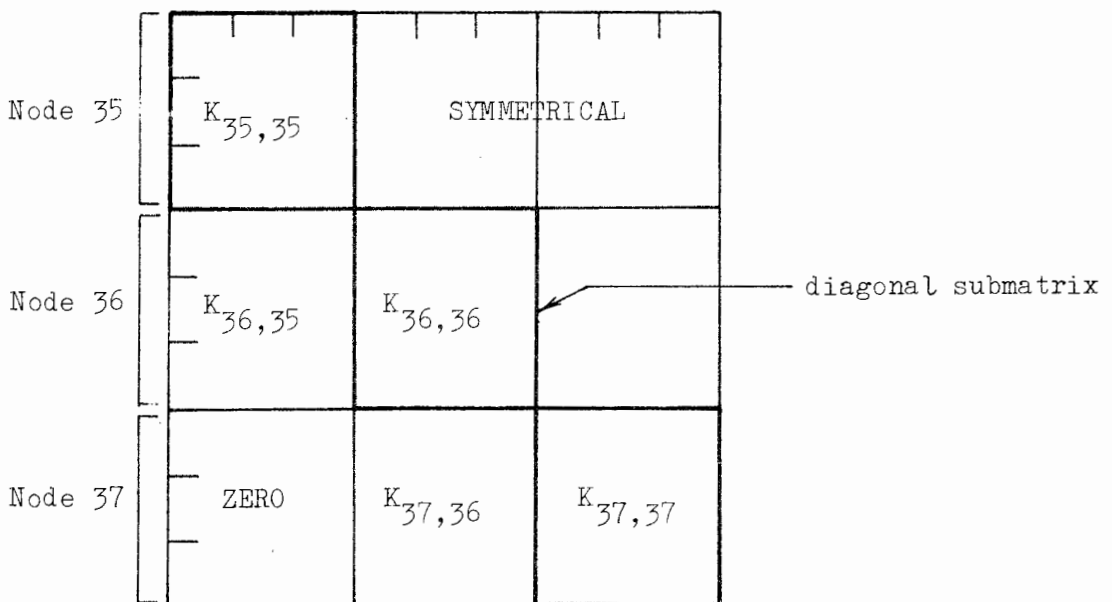


Fig. 3.7: Standard Part of the System Stiffness Matrix

on the setting up and solution of Eq. (3.40). The steps in the procedure are as follows:

- (i) Set up the matrix $[K]$ as an assemblage of element stiffness matrices.
- (ii) Augment this matrix with the appropriate load vector $\{F\}$.
- (iii) Modify the augmented matrix by applying boundary conditions.
- (iv) Solve the resulting set of stiffness equations for the unknown displacements $\{q\}$.
- (v) Calculate the stresses in the structure from these displacements.

In the following sections each of these steps will be dealt with in turn, with special emphasis being given to the problem of shell branching as it effects the setting up and solution of the system stiffness equations.

3.3.1 The system stiffness matrix

The shells of revolution which we will consider here are composed of a number of straight line sections (Fig. 3.6). Each section is idealised by a number of finite elements, (cylindrical, conical or annular disc), which are numbered consecutively from one end of the section to the other. At various points within the structure, such as A, B and C, the shell branches, the branching being defined simply by the fact that three elements instead of two, meet at a single node.

The stiffness matrix for such a structure consists of a basic diagonal band, 9 columns wide, part of which is shown in Fig. 3.7. We will refer to such parts of the stiffness matrix as standard, being formed as follows:

$$\begin{aligned} K_{35,36} &= k_{22}^{35} + k_{11}^{36} \\ K_{36,37} &= k_{21}^{36} \end{aligned} \tag{3.41}$$

At those nodes where branching occurs the standard part of the stiffness matrix is supplemented by an off-diagonal sub-matrix, indicating that a third element (or third node) is joined to the branch node. At this stage then we must distinguish between the main shell and a shell branch, since the off-diagonal

sub-matrix must be associated with the shell branch. We therefore define the main shell at a branch as comprising the two sections over which the elements are numbered consecutively, and the remaining section as the shell branch. For example, if in Fig. 3.6 the elements are numbered consecutively over the composite section * DCE, then sections DC and CE together constitute the main shell at branch point C, and section BC the shell branch; the numbering of the elements in section BC need bear no relation to the numbering of the elements in the main shell.

It is worthwhile emphasising the point that the concepts of main shell and shell branch are relative and apply only with regard to a specific branch point. We cannot in general define an absolute main shell in a structure which is branched. For example, section BC may be a shell branch relative to branch point C, yet form part of the main shell relative to branch point B.

There are two advantages to be gained by making use of this relative concept:

- (i) Any shell configuration may be analysed without the need to rigidly define a specific main shell with attendant branches; any number of branches may be nested within each other.
- (ii) There is a good deal more leniency in the numbering of elements.** Jumps in the sequence of element numbers may occur, (e.g., the elements of section CE may be numbered 20 through 60 and those of section AB numbered 61 through 95), and dummy elements may also be used to break the numbering sequence between sections.

Within the framework thus established we are able to identify five specific cases of branching, each one giving rise to a slightly different variation in the manner in which the system stiffness matrix is set up. Each of these cases will now be illustrated by means of simple examples.

*The word 'section' has limited meaning in the context of shell branching, and refers specifically to a single straight portion of the shell.

**A more detailed discussion of the rules for the numbering of elements is given in Appendix A, "Program data input".

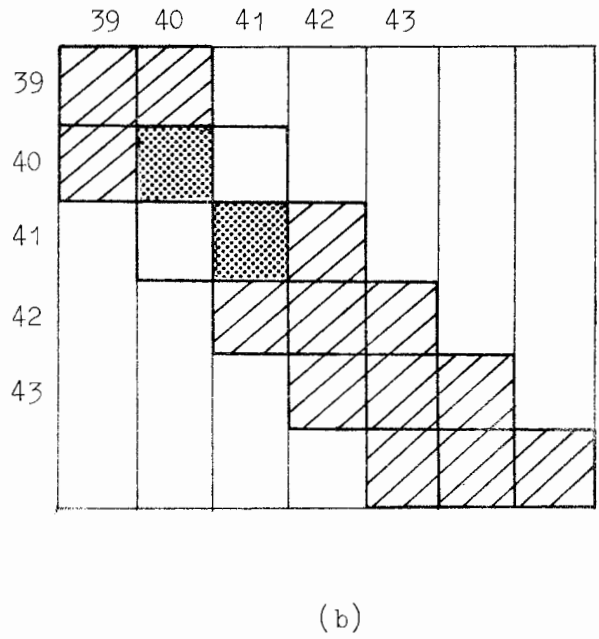
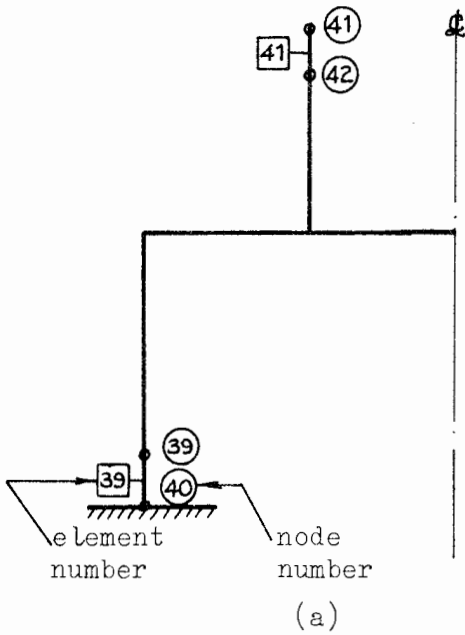


Fig. 3.8: Branch Type 1

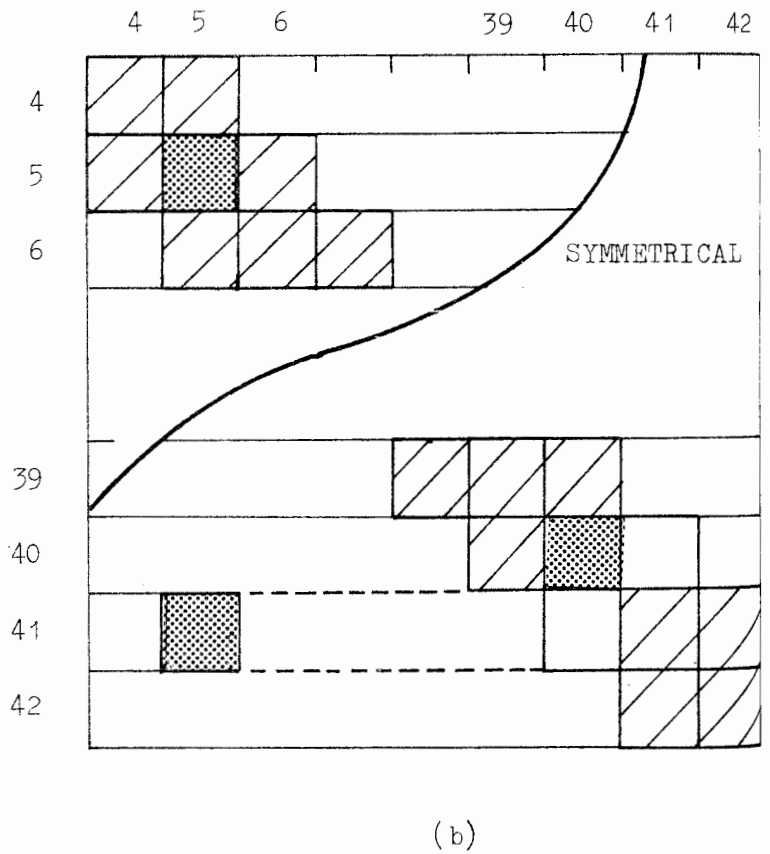
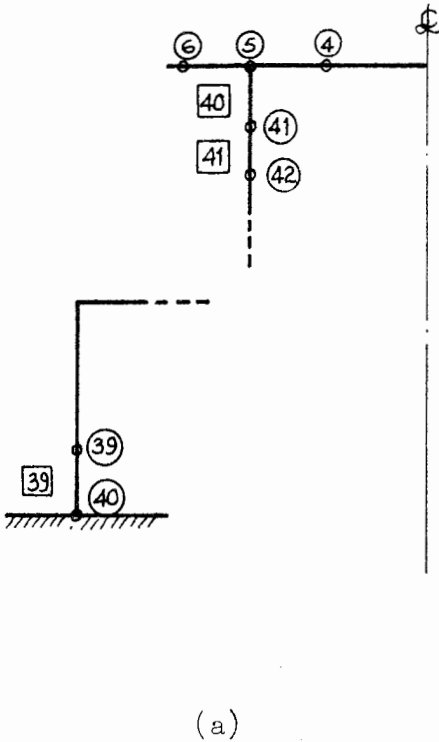


Fig. 3.9: Branch Type 2

Notes on Figs. 3.8(b) through 3.12(b):

- (i) Each 'block' represents a 3×3 submatrix.
- (ii) Standard submatrices, defined by Eqs. (3.41), are shown cross-hatched; non-standard sub-matrices are shaded; all other submatrices are zero.
- (iii) Row and column numbers refer to the relevant node.

Branch Type 1:

The simplest type of branch occurs when the element numbering sequence jumps from one section to another section totally unconnected to the first (Fig. 3.8a).

The stiffness matrix associated with this type of branch remains essentially standard, the principal change being $K_{40,41} = K_{41,40} = 0$, indicating that node 40 is not joined to node 41 (Fig. 3.8b). Before stating the second change however, it is necessary to introduce a fundamental assumption: that each element must follow its corresponding node, i.e. element i must always follow node i .

As a consequence of this assumption it is clear that there can be no element 40. However, far from ignoring element 40, we retain it in name, assign zero geometric properties to it, and call it a dummy element. Since this dummy element has zero stiffness the setting up of the stiffness matrix remains completely standard, the zero stiffness sub-matrices being automatically generated. Similarly, the second change referred to above will be automatically generated by the standard procedure as follows:

$$\begin{aligned} K_{40,40} &= k_{22}^{39} + k_{11}^{40} = k_{22}^{39} \\ K_{41,41} &= k_{22}^{40} + k_{11}^{41} = k_{11}^{41} \end{aligned} \tag{3.42}$$

$$\text{since } k_{11}^{40} = k_{22}^{40} = 0$$

In view of the above definition of a dummy element, branch type 1, may be defined as occurring when two consecutively numbered nodes are not joined, and the element associated with one of the nodes is a dummy element.

Branch Type 2:

The second type of branch is that which occurs at node 5 in Fig. 3.9(a). It is defined by the fact that the main shell with respect to branch node 5 is comprised of elements having lower numbers (3, 4, 5 and 6) than those of the shell branch (40, 41, etc.), and the numbering of the elements in the shell branch is away from the main shell.

The changes to the system stiffness matrix are as follows:

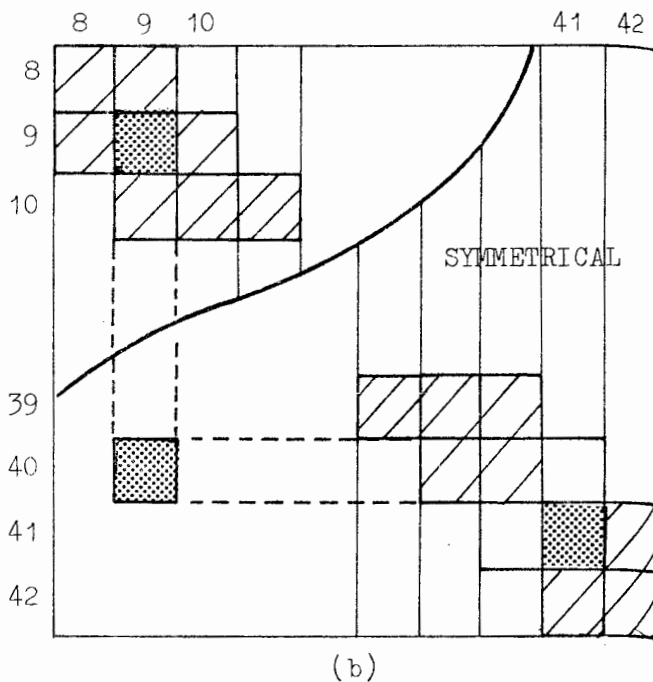
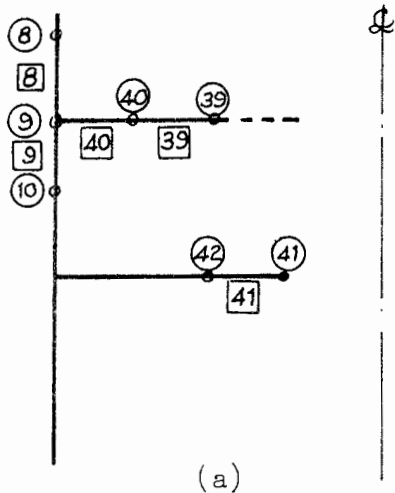


Fig. 3.10: Branch Type 3

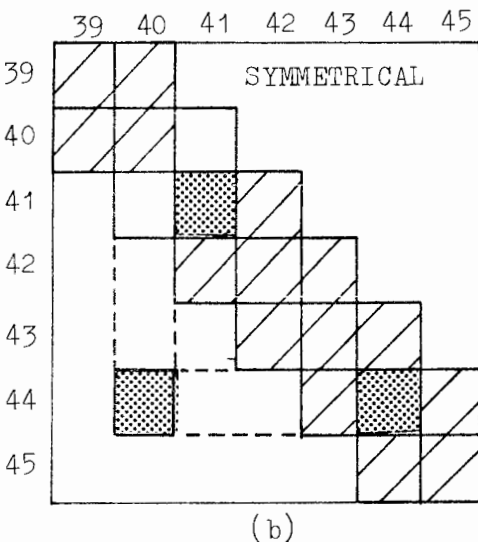
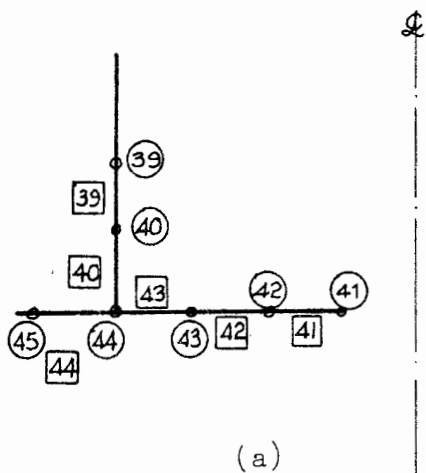


Fig. 3.11: Branch Type 4

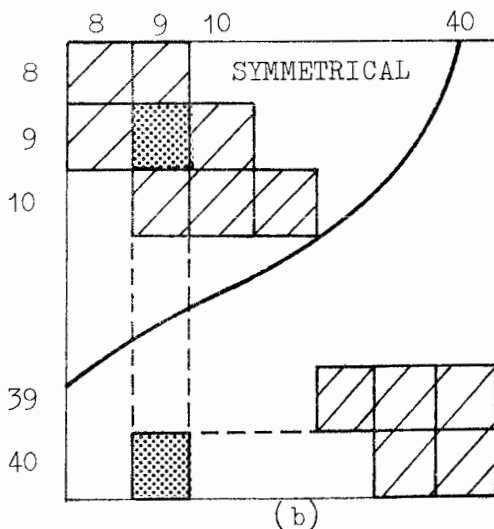
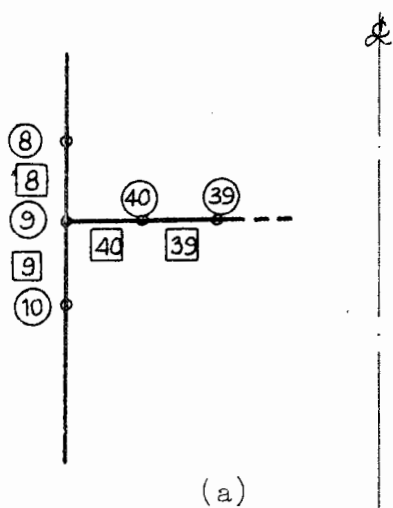


Fig. 3.12: Branch Type 5

- (i) The stiffness of the main shell at node 5 must be augmented by the stiffness of the shell branch, i.e.

$$K_{5,5} = k_{22}^4 + k_{11}^5 + k_{11}^{40} \quad (3.43a)$$

where k_{11}^{40} is the additional stiffness.

- (ii) The connection between nodes 5 and 41 must be effected by linking these two nodes in the system stiffness matrix. This is accomplished by inserting the off-diagonal submatrix,

$$K_{41,5} = k_{21}^{40} \quad (3.43b)$$

as shown in Fig. 3.9(b).

The insertion of this off-diagonal submatrix necessitates the generation of a significant body of zero submatrices, lying between the off-diagonal submatrix and the main diagonal. Special methods are therefore required for the efficient storage and handling of the system stiffness matrix; these methods will be discussed in Section 3.3.4.

It is clear from the definition above that branch type 2 is always accompanied by a type 1 branch, and in fact the two types are treated as one composite branch type in the computer program.

Branch Type 3:

The third type of branch is that which occurs at node 9 in Fig. 3.10(a). It is defined by the fact that the main shell with respect to branch node 9 is comprised of elements having lower numbers (7, 8, 9,) than those of the shell branch (....., 39, 40), and by the fact that the numbering of the elements in the shell branch is towards the main shell. The latter point distinguishes branch type 3 from branch type 2.

The changes to the system stiffness matrix, which are essentially the same as those for branch type 2, are:

- (i) The stiffness of the main shell at branch node 9 is augmented by the stiffness of the shell branch, i.e.

$$K_{9,9} = k_{22}^8 + k_{11}^9 + k_{22}^{40} \quad (3.44a)$$

where k_{22}^{40} is the additional stiffness.

- (ii) The connection between nodes 9 and 40 is accomplished by the insertion of the off-diagonal matrix,

$$K_{40,9} = k_{12}^{40} \quad (3.44b)$$

as shown in Fig. 3.10(b).

In the present case the absence of connection between nodes 40 and 41 does not constitute a type 1 branch, since element 40 is not a dummy element. The lack of connection is effected by simply setting,

$$K_{41,40} = 0$$

and $K_{41,40} = k_{11}^{41}$ (3.44c)

Branch Type 4:

The fourth type of branch is that which occurs at node 44 in Fig. 3.11(a). It is defined by the fact that the main shell relative to branch node 44 consists of elements having higher numbers (41, 42, 43, 44) than those of the shell branch (.... 39, 40). Due to a certain limitation which will be stated later, the numbering of the shell branch is always towards the branch node.

The changes to be made to the system stiffness matrix are illustrated in Fig. 3.11(b), and are as follows:

- (i) The absence of a connecting element between nodes 40 and 41 is effected by setting

$$K_{41,40} = 0$$

and $K_{41,41} = k_{11}^{41}$ (3.45a)

- (ii) The connection between nodes 40 and 44 is accomplished by the insertion of the off-diagonal submatrix,

$$K_{44,40} = k_{21}^{40} \quad (3.45b)$$

(iii) The stiffness of the main shell at node 44 is augmented by the stiffness of the shell branch,

$$K_{44,44} = k_{22}^{43} + k_{11}^{44} + k_{22}^{40} \quad (3.45c)$$

where k_{22}^{40} is the additional stiffness.

Branch Type 5:

The final type of branch is that which occurs at node 9 in Fig. 3.12(a), and is a special case of Branch Type 3. This type of branch is defined in the same way as Branch Type 3, with the additional specification that the element connecting the shell branch to the main shell at the branch node, is the last (or highest numbered) element in the structural idealisation.

This type of branch is classified as a specific branch type for two reasons:

- (i) It is the second of two possible ways in which the element idealisation may be terminated (the first way being for the element idealisation to terminate at a boundary), and as such requires special consideration.
- (ii) From the computer programming point of view this type of element termination cannot be efficiently handled as a type 3 branch, and must be specifically programmed.

The changes to be made to the system stiffness matrix in this case are precisely the same as those of the type 3 branch, with the exception of the submatrices which now lie outside the system. The changes can be seen more clearly by mentally superimposing Figs. 3.10(b) and 3.12(b).

An important irregularity exists in respect of the off-diagonal submatrices of Branch Types 3 and 5, which bears emphasising. In both of these cases the off-diagonal submatrices are given by ,

$$K_{40,9} = [k_{21}^{40}]^t = k_{12}^{40} \quad (3.44b, \text{bis})$$

and not, as we might expect by,

$$K_{40,9} = k_{21}^{40} \quad (3.44c)$$

The reason for this irregular use of the transposed submatrix lies in the relative numbering of the main shell and shell branch at the respective branch points. Further edification on this point may be gained by comparing the definitions of Branch Types 3, 4 and 5.

We have already mentioned that there is a limitation on the manner in which the elements may be numbered. This limitation is that all cylindrical and conical sections must have their elements numbered from top to bottom, and all circular disc sections must have their elements numbered from the axis of symmetry towards the periphery of the disc. This rule applies where branching is concerned, and was introduced in order to limit the number of possible ways in which a branch type could be described to the program. It does not in any way restrict the number or type of actual branches which a structure may have.

The concept of a 'branch type' is thus not altogether a classification of the geometrical shapes which a branch may assume. In fact, four of the five branch types described consist essentially of a three-pronged intersection of elements*, and depending on the relative numbering of the nodes at a branch point, it is possible for an actual branch in a structure to have more than one branch type classification. The object of this apparent duplication of effort is to allow the analyst the maximum amount of freedom in the choice of his element idealisation, consistent with the minimum number of idealisation rules.

3.3.2 The system load vector

The setting up of the system load vector is a relatively simple procedure, since explicit expressions are available for the equivalent nodal loads corresponding to both linearly distributed loading and dead load.

The system load vector is made up of three equivalent nodal loads U , W and M for each node (Fig. 3.13b). Point loads, (or more correctly, line loads), which we will assume are applied only at nodes, are broken up into their global components, and placed directly into the appropriate row of the load vector. It should, however, be emphasised that the value used must be that of the total load over the circumference of the shell at that node.

*In the interest of simplicity, each branch type has been shown as a right-angled intersection. The relative angles of the elements at a branch point do not however affect the setting up of the system stiffness matrix.

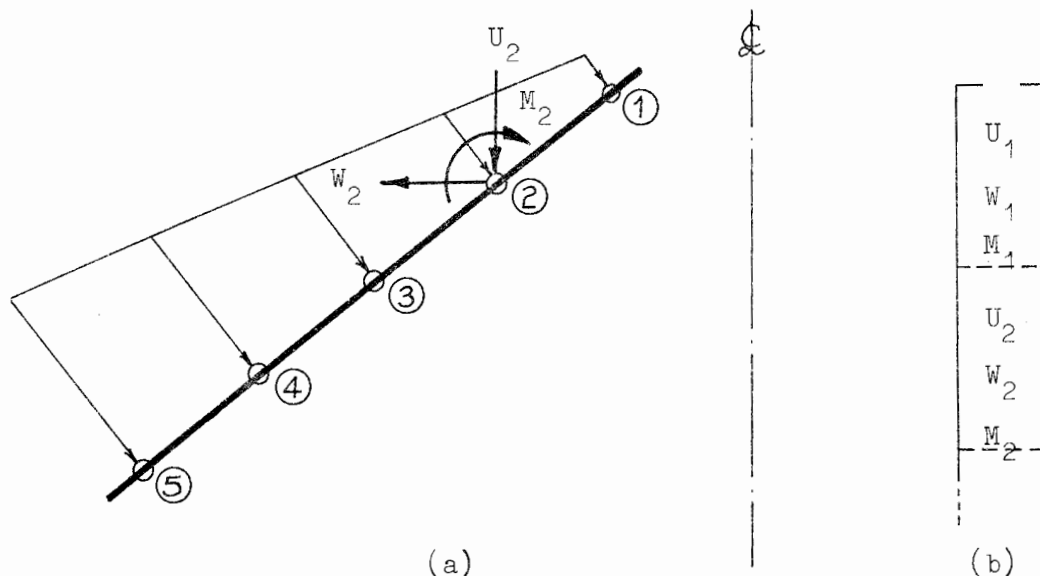


Fig. 3.13

The procedure to be followed in the case of linearly distributed loads (Fig. 3.13a) is as follows:

The total equivalent nodal loads at a typical node 2 are formed from the sum of the equivalent nodal loads from each of the elements adjacent to the node, i.e.,

$$\begin{aligned}
 U_2 &= U_2^1 + U_1^2 \\
 W_2 &= W_2^1 + W_1^2 \\
 M_2 &= M_2^1 + M_1^2
 \end{aligned}
 \tag{3.46}$$

where U_i^j , W_i^j , and M_i^j are the vertical and horizontal loads, and moment respectively at node i of element j . Explicit expressions for the equivalent nodal loads U_i^j , W_i^j and M_i^j at the first and second nodes of a general element, subject to a linearly distributed load, are given in Appendix E. The loads U_2 , W_2 and M_2 are then inserted into the appropriate rows of the system load vector.

The procedure in the case of dead load is precisely the same as that outlined above; explicit expressions for the equivalent nodal dead loads are also given in Appendix E.

3.3.3 Nodal boundary conditions

By nodal boundary conditions is meant the imposition of kinematic

constraints at certain nodes on the structure. Kinematic constraints may in general be divided into two categories:

- (i) Zero-displacement boundary conditions.
- (iii) Elastically restrained boundaries.

The first category is by far the most common type of boundary condition encountered in practice, and is also the easier of the two to implement in a computer program.

Zero displacement boundary conditions:

The system stiffness matrix represents a set of stiffness equations expressing the relationship between known forces and unknown displacements at the nodes. If a particular displacement is known to be zero then it does not contribute to the value of any equation in which it appears; hence, this displacement may be deleted from the system by removing from the system stiffness matrix the column associated with this displacement. Since the stiffness matrix must remain symmetrical, the corresponding row of the stiffness matrix must also be removed.

In practice the row and column corresponding to the known zero-displacement are not removed, but are set to zero. Since this entails having a zero on the leading diagonal, special precautions must be taken when solving the final system of equations. These are discussed in the following section.

Some typical examples of zero-displacement boundary conditions are given in Fig. 3.14. In each example the row and column of the system stiffness matrix corresponding to the zero displacements are set to zero.

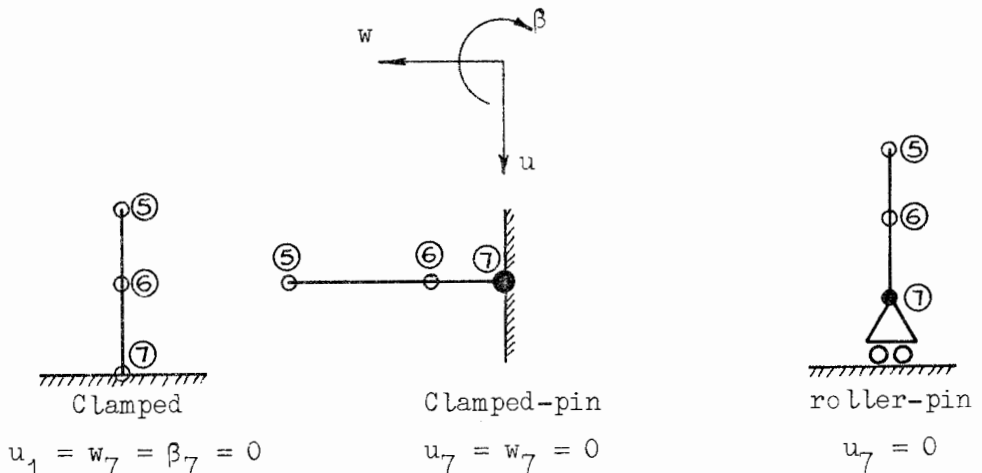


Fig. 3.14

Elastically restrained boundaries:

It is sometimes necessary to be able to specify an elastic support, for example when part of a structure such as the roof of a water tank is supported on rubber bearing pads. We will use this example to illustrate the procedure.

The actual support and its structural idealisation are shown in Fig. 3.15.

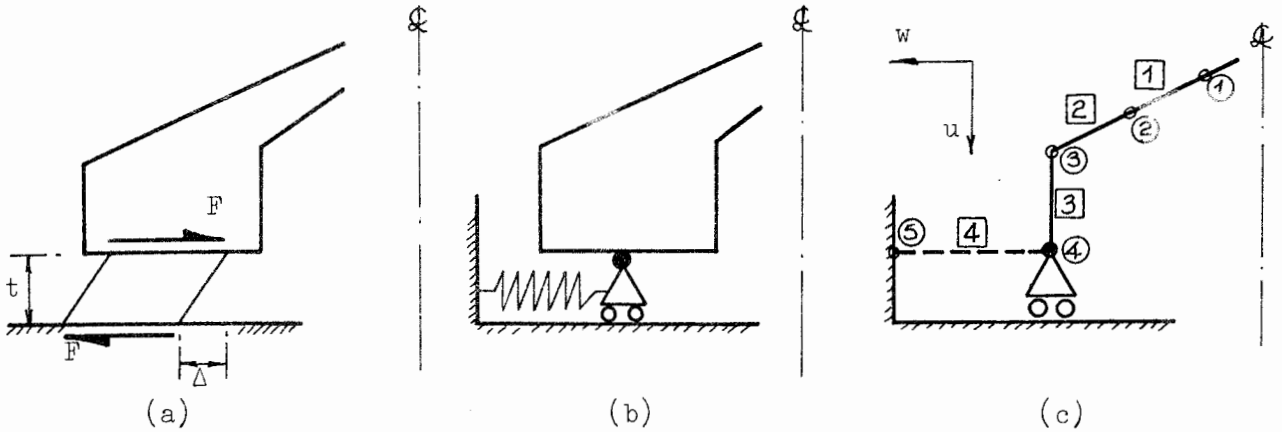


Fig. 3.15

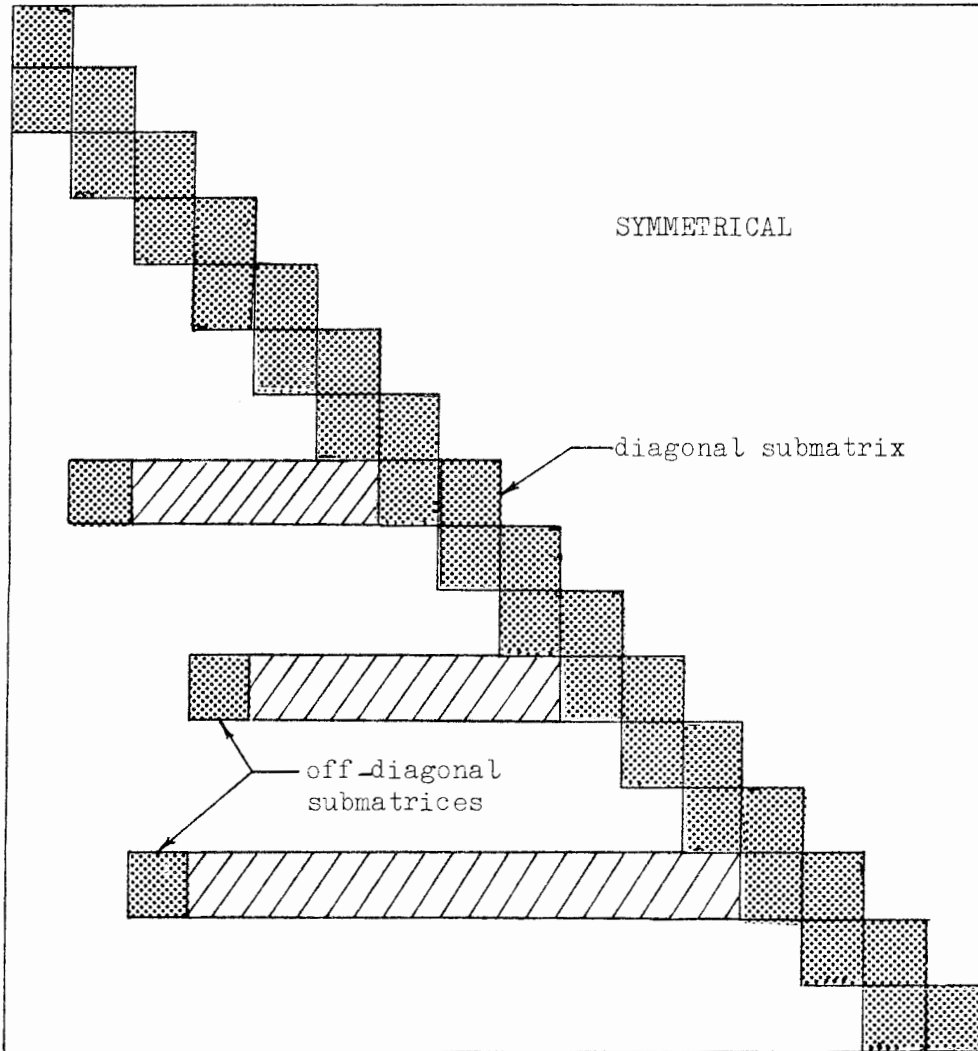
Assuming that the bearing pad is incompressible and allows rotation at its point of contact with the shell, its only effect will be to resist, elastically, the horizontal movement of the structure. We may reason intuitively then that the only change in the stiffness matrix will be an increase in the shear stiffness of element 3 at node 4 (Fig. 3.7c)

To show this we insert a dummy element 4 which has only axial stiffness k given by

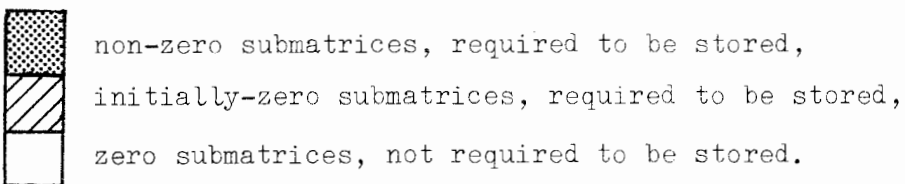
$$\begin{bmatrix} W_4 \\ W_5 \end{bmatrix} = \begin{bmatrix} k & -k \\ -k & k \end{bmatrix} \begin{bmatrix} w_4 \\ w_5 \end{bmatrix} \tag{3.47a}$$

When the dummy element is included in the structural idealisation the stiffness matrix is augmented as follows:

$$\begin{bmatrix} U_4 \\ W_4 \\ M_4 \\ W_5 \end{bmatrix} = \begin{bmatrix} & & & & \\ & & & & \\ & & & & \\ & & & +k & -k \\ & & & -k & +k \end{bmatrix} \begin{bmatrix} u_4 \\ w_4 \\ \beta_4 \\ w_5 \end{bmatrix} \tag{3.47b}$$



Legend:



Notes:

- (i) Each block represents a (3×3) submatrix.
- (ii) Although the diagonal submatrices are shown fully shaded (due to the size of the diagram), only the lower half of each, including the leading diagonal, need be stored.

Fig. 3.16: General Form of the System Stiffness Matrix

However, the last row and column (shown shaded) are deleted, since the displacement $w_5 = 0$. Thus the net effect of the dummy element is to increase the horizontal (shear) stiffness of the structure at node 4, while still allowing the structure to move freely on the roller.

The stiffness k is the shear stiffness of the rubber bearing pad. If the pad allows a displacement Δ under a shear force F , then its shear modulus G may be expressed by

$$G = \frac{F/A}{\Delta/t} \quad (3.48a)$$

where A is the area over which the force F acts. The stiffness k is then

$$k = \frac{F}{\Delta} = \frac{GA}{t} \quad (3.48b)$$

Knowing the shear modulus of rubber,* the contact area of the pad A , and its thickness t , the stiffness k can be calculated and inserted into the system stiffness matrix.

3.3.4 Solution of the system stiffness equations

The system stiffness matrix, the setting up of which is described in Section 3.3.1, consists of a narrow diagonal band, 9 columns wide, and a number, (depending on the number of branch points), of irregularly placed off-diagonal submatrices (Fig. 3.16). Since the matrix is symmetrical only half of it need be stored, and in the present work we have chosen to store the lower half.

The normal method of storing a matrix in a 2-dimensional array will lead in the present case to highly inefficient use of storage space, even if the matrix is stored diagonally, because of the large blocks of unwanted zero submatrices lying above and below the off-diagonal submatrices. The only initially-zero submatrices required are those shown cross-hatched in the figure, and these are required in order to complete the equations containing elements of the off-diagonal submatrices.

The only alternative is therefore to store the system stiffness matrix in a single-dimension array. The method of doing this is illustrated in Fig. 3.17

*The shear modulus of rubber is generally taken to be 0,450 MPa.

a single-dimension array, is required.

It was envisaged that, for large branched structures requiring over 400 finite elements for idealisation, the coefficient matrix would become so sparse as to cause significant deterioration in the accuracy of the solution. For this reason a special back-substitution subroutine BANBAC was developed in order to compare the original load vector with the one obtained through back-substitution, and thereby assess the accuracy of the solution. The back-substitution (working in double precision arithmetic) was assumed to be accurate, since each row of the coefficient matrix contains at most only 15 non-zero coefficients, and thus each back-substitution involves a maximum of 15 multiplications. The accuracy of the solution procedure may be gauged by the fact that in a 435 element analysis involving 3 branch points, correlation between the original and back-substituted load vectors was to 6 significant figures.

A discussion of the technique employed in the subroutine BANDO is given in Appendix A.

3.3.5 Calculation of stresses and moments

The solution of the system stiffness equation yields values for the three global displacements u , w and β at each node. The stress resultants at any point within an element can then be calculated directly from the nodal displacements. Combining Eq. (3.7b) and (3.8) for a given element we have,

$$\{\sigma\} = \begin{bmatrix} N_s \\ N_\theta \\ -M_s \\ -M_\theta \end{bmatrix} = [D] ([B] \{q_e\} - \{\epsilon_o\}) \quad (3.49)$$

To give a concise idea of the parameters involved in the stress calculations we rewrite Eq. (3.49) in the form

$$\{\sigma\} = \frac{E}{1 - \nu^2} \begin{bmatrix} D^* = f(t, \nu) \\ (4 \times 4) \end{bmatrix} \cdot \begin{bmatrix} B = f(s', \theta, r, L) \\ (4 \times 6) \end{bmatrix} \cdot \begin{bmatrix} u_1 \\ w_1 \\ \beta_1 \\ u_2 \\ w_2 \\ \beta_2 \\ (6 \times 1) \end{bmatrix} - [D] \{\epsilon_o\}$$

$$\begin{aligned}
 &= \frac{E}{1 - \nu^2} [D]^* [B] \{q_e\} - [D] \{\epsilon_o\} \\
 &= \frac{E}{1 - \nu^2} [S]^* \{q_e\} - [D] \{\epsilon_o\} \quad (3.50)
 \end{aligned}$$

The matrix $[S]^*$ is called the stress matrix for element i , and is a function of the parameters indicated in the equation. Of these parameters the values of the dimensionless distance s' , the radius r , and the thickness t vary along the length of the element (Fig. 3.18). Hence by specifying a

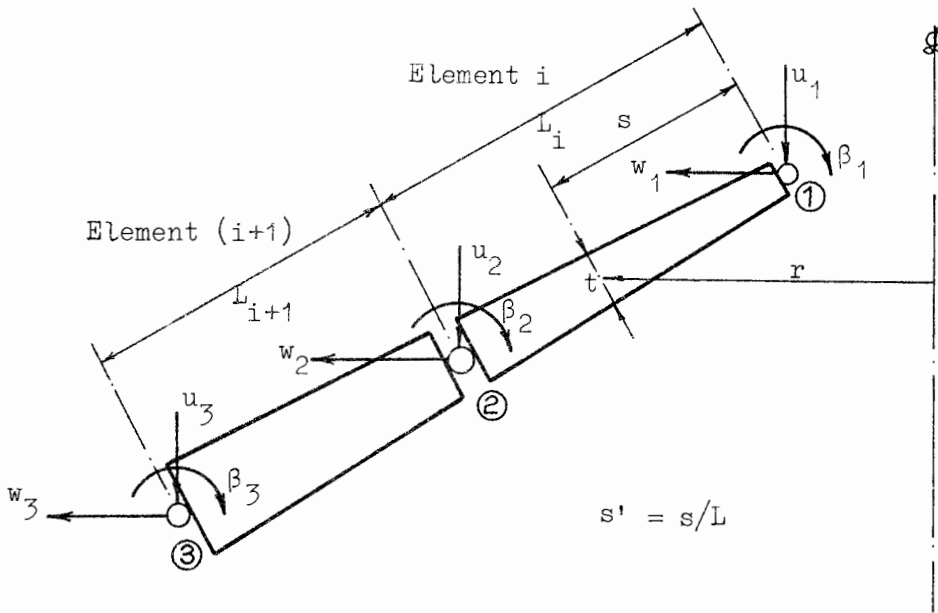


Fig. 3.18

particular value of s' ($0 \leq s' \leq 1$), together with the corresponding values of r and t , the stress resultants at any point within the element can be calculated from the displacements at the element nodes. In practice, however, where we are dealing with large numbers of elements of varying lengths, there is nothing to be gained from calculating the stress resultants at points within the element; the more systematic and meaningful procedure is to calculate the stress resultants at the element nodes.

When two elements are connected by a particular node the stress resultants at this node may be calculated by applying Eq. (3.50) to either of the adjacent elements. However, because of the fundamental numerical approximations involved, the two sets of stress resultants thus obtained will seldom be the same. Hence the best approximation to the stress resultants at a node is obtained by taking the mean of the stress resultants obtained for this node

from each of the adjacent elements. For example, if node 2 in Fig. 3.18 is assumed to link elements i and $i + 1$, then the stress resultants at node 2 are given by,

$$\{\sigma\}_2 = \frac{1}{2} \left[\frac{E}{1 - \nu^2} [S^*]_{s'=1}^i \begin{bmatrix} q_1 \\ q_2 \end{bmatrix} + \frac{E}{1 - \nu^2} [S^*]_{s'=0}^{i+1} \begin{bmatrix} q_2 \\ q_3 \end{bmatrix} \right] \quad (3.51)$$

Eq. (3.51) forms the basis of the stress calculation procedure in the present work.

There are however a number of occasions when Eq. (3.51) cannot be used, (e.g., where three elements meet at a node), and other occasions where it should not be used, (e.g., where there are abrupt or significant changes in the geometry of two adjacent elements. A convenient method of retaining the general applicability of Eq. (3.51) is to divide the structure at such nodes into separate sections. Thus, for the purpose of stress calculations the dividing node is no longer the link between two or more adjacent elements, but forms the boundary node of two or more sections of the structure. The stress resultants at boundary nodes are then calculated from the individual terms in Eq. (3.51). For example, if a boundary node forms the beginning of a section then the stress resultants are given by the second term in Eq. (3.51), without the factor $\frac{1}{2}$. Similarly, if a boundary node forms the end of a section, then the first term is used.

Once the stress resultants have been calculated section by section, it is the prerogative of the analyst to decide whether or not it is meaningful to average them at nodes common to two or more sections

Once the stress resultants are known, the stresses at any point within the shell may be calculated from the following formulae:

$$\begin{aligned} \sigma_s &= \frac{N_s}{t} + \frac{12 M_s \cdot z}{t^3} \\ \sigma_\theta &= \frac{N_\theta}{t} + \frac{12 M_\theta \cdot z}{t^3} \end{aligned} \quad (3.52a,b)$$

The first term in each formulae is the direct stress, and the second term the bending stress. In deriving the bending stress formulae the stresses are assumed to be linearly distributed over a rectangular cross-section, where z is the distance from the neutral axis, positive if in the direction of the positive normal to the element.

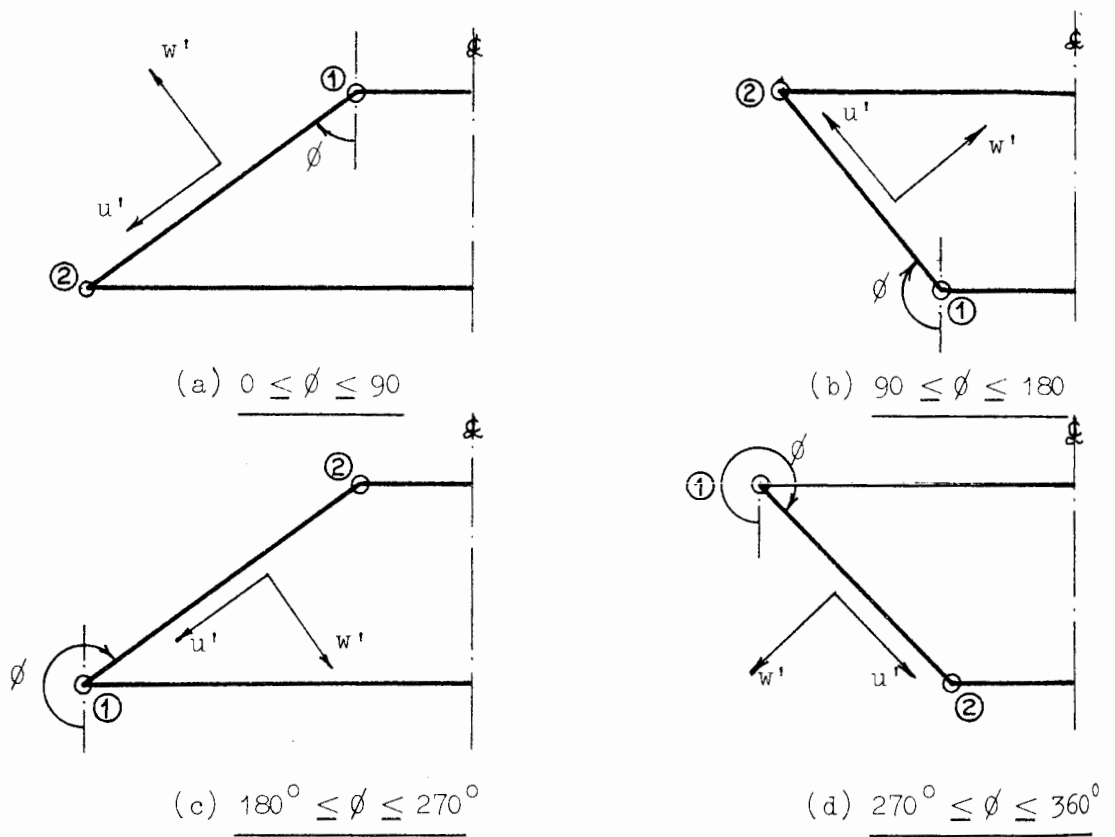


Fig. 3.19

Sign convention:

Eqs. (3.52) are based on a sign convention which was established in Chapter 2, and retained throughout the derivation of the finite element theory. We recall that,

- (i) positive N_s denotes meridional tension, and positive N_θ circumferential tension, and
- (ii) positive M_s and M_θ denote tension on the outer face of the shell.

The convention given above for the moments M_s and M_θ is in fact incomplete: a positive moment causes tension on the side of the positive normal to the element. This follows from the fact that both the curvatures χ_s and χ_θ are functions of the derivatives of the normal displacement w' (see Eq. 3.7a).

The implication can be seen in Fig. 3.19. If the angle ϕ lies between 90° and 270° (a state obtained by numbering the element nodes from bottom to top), then the positive normal points towards the axis of symmetry, and a positive moment will indicate tension on the inside face of the shell.

The interpretation of the moments therefore requires a knowledge of the order in which the nodes are numbered (whether up the shell or down). This could cause confusion in cases where the moments are automatically plotted by computer,* since without a knowledge of the node numbering we could not tell whether a positive moment indicated tension on the inside or outside of the shell. It is thus not advisable to number the nodes from bottom to top. This limitation amounts to no real loss of generality since any shape of shell can still be generated from the cases $0^\circ \leq \phi \leq 90^\circ$ and $270^\circ \leq \phi \leq 360^\circ$.

*The program described in this work has comprehensive automatic plotting facilities.

CHAPTER 4EVALUATION AND DISCUSSION4.1 Introduction and Definitions

The object of this chapter is to evaluate and discuss the solutions to a number of examples of axisymmetric shells of revolution, obtained using the computer program CONFURU. The examples have been chosen for the purpose of checking the various features contained within the program, assessing the accuracy of the results obtained, and to indicate the general range of problems to which the program may be applied. The operation of the program is described in the User's Manual given in Appendix A.

Many more problems than are given here have been solved using CONFURU, including water towers, sludge digester tanks and pressure vessels which are at present in service. As far as comparing results with independent solutions is concerned, only those problems for which exact theoretical solutions are available have been used, (except in the case of branched shells where other methods of checking the program have been devised). In such cases, the theoretical solutions themselves have been programmed so as to provide accurate, reliable and comprehensive sets of comparison results. (This we consider superior to comparison with the results of other programs or methods of solution, and it will be noticed that at no stage are such comparisons attempted.)

The chapter is divided into five sections, each section containing examples of a more advanced nature than the previous section. An attempt has been made to introduce continuity between the sections by making use in each section of conclusions arrived at in the preceding ones.

Among the features discussed are:

- (i) Methods of numerical integration.*
- (ii) Choice of element aspect ratio, and the effects of changes in element aspect ratio between different sections of a shell.

*The reason for devoting considerable attention to this aspect arose from the observation that program SABOR 4 (c.f. Pian et al [20]) allows up to 29 points to be used in the Simpson's formula. We considered it of interest to determine whether such high order integration formulae are really necessary.

- (iii) Circular plates closed at the axis of symmetry.
- (iv) Linearly distributed surface loads, loads due to self-weight of the shell, and line loads.
- (v) The effect of Poisson's ratio ν , particularly with regard to hoop stresses.
- (vi) Variable and/or discontinuous shell thickness.
- (vii) Shell junctions and sharp changes in shell geometry.
- (viii) The validity of a thin shell analysis of a thick shell.
- (ix) The analysis of branched shells.

More detailed descriptions of these features are given at the beginning of the relevant example.

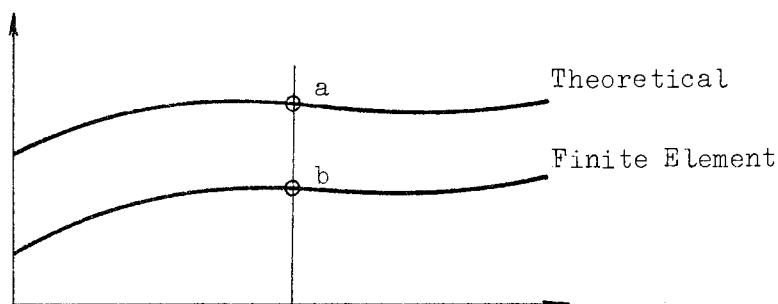
In the final section of the chapter an analysis of the computer time and cost for some of the more important examples is given.

Definitions

- (a) Element aspect ratio (or L/t ratio):

The ratio of element length to its thickness, or in the case of variable thickness elements, its mean thickness. The element aspect ratio is used to define the degree of element subdivision over a given section of the shell. It will be noticed that wherever an existing subdivision is refined, the refined subdivision always contains the original subdivision. This is in fact a necessary condition for meaningful convergence testing (c.f. Ref. [23], p 164).

- (b) Percentage absolute error:



$$\text{Percentage absolute error} = \frac{a - b}{a} \times 100$$

Note in this connection that:

- (i) The word absolute implies comparison with an exact theoretical solution.
- (ii) Percentage errors in general give no indication as to whether the finite element solution is a lower or upper bound one. Hence, unless otherwise stated all finite element displacement solutions may be assumed to be lower bound.
- (iii) Where the theoretical solution is very small or zero the percentage error is meaningless, so that wherever possible, comparisons in such regions have been avoided.

It will be noticed that in the first two sections of the chapter the majority of comparisons have been given in terms of percentage absolute error diagrams. This has been necessary because of the high degree of accuracy of the finite element results obtained, making it impossible to compare the finite element and theoretical solutions directly in graphical form. The same is also often true of individual finite element results where differences in individual solutions are too small for direct graphical comparison. At the same time, however, the variation in accuracy from one section of a shell or plate to another has on occasion been so large that plotting to a logarithmic scale has been necessary.

4.2 Circular Cylinders and Plates: the Limiting Shapes of a Conical Frustrum

In this section we will analyse a circular cylinder under edge loading, and a circular plate under a uniformly distributed load, the two types of loading constituting the most and least severe types of mechanical loads which are likely to occur.

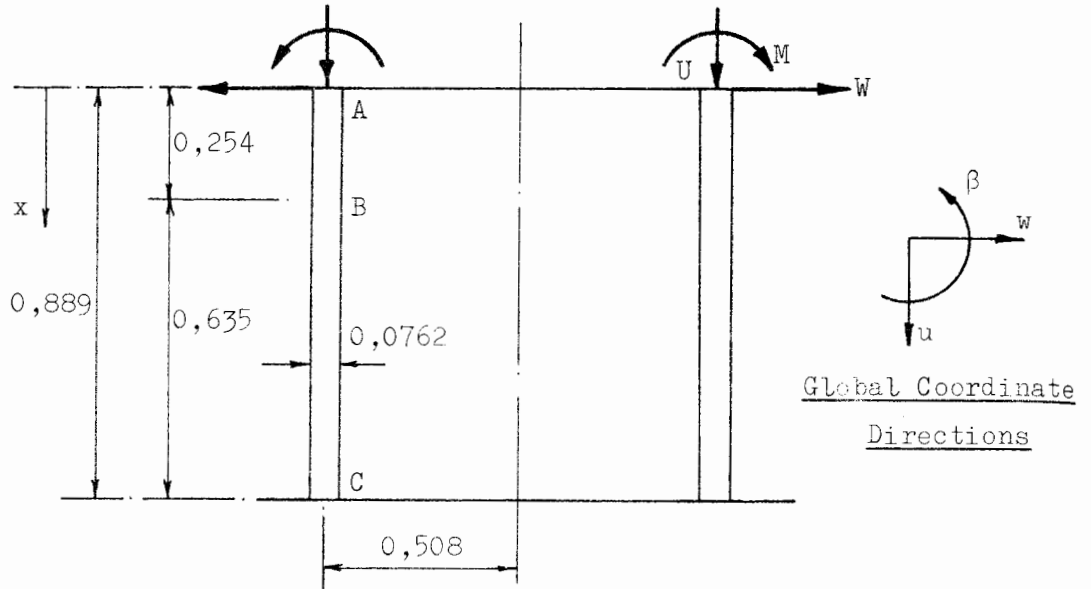
Because of their simple geometrical shapes these examples will be used to test some of the more basic aspects of the program.

4.2.1 Example 1: An edge loaded circular cylinder

Objectives:

- (i) To investigate the accuracy and efficiency of various methods of numerical integration.
- (ii) To determine at what element aspect ratio the displacement solution converges, and to investigate the effects of changes in element aspect ratio from one section of the cylinder to another.

TABLE 4.1



Loadings:

$$U = 250,0 \times 10^3 \text{ N/m}$$

$$W = 264,0 \times 10^3 \text{ N/m}$$

$$M = -4,448 \times 10^3 \text{ Nm/m.}$$

Material Properties:

$$E = 1,0$$

$$\nu = 0$$

Analysis I.D. No.	Quadrature Formula	Element Subdivision*	
		AB	BC
C/N/01	Simpson: n = 5	10 @ 0,0254 (1/3)	5 @ 0,127 (5/3)
C/N/02	" : n = 7	"	"
C/N/03	Gauss : n = 4	"	"
C/N/04	" : n = 6	"	"
C/N/05	" : n = 8	"	"
C/N/06	" : n = 10	"	"
C/C/01	Simpson: n = 5	3 @ 0,1016 (4/3)	5 @ 0,11684 (1,53)
C/C/02	"	5 @ 0,0508 (2/3)	5 @ 0,127 (5/3)
C/C/03	"	10 @ 0,0254 (1/3)	"
C/C/04	"	20 @ 0,0127 (1/6)	"

*Aspect ratios (L/t) given in brackets.

- (iii) To determine the range of element aspect ratios which may be expected to yield reasonably accurate stress solutions.

Description of the Analysis:

The data for the example are given in Table 4.1, together with a description of the element subdivisions and quadrature formulae used in each of the ten analyses.

This example, (without the axial load U), was originally analysed by Klein [16], and has also been used by many authors since [17, 18, 19] to test the performance of shell of revolution elements under edge loading. The axial load is required for when this example is used again as part of Example 6.

The theoretical solutions used here for comparison are obtained from an independent computer program TIMCYL, which is based on the cylindrical shell equations of Timoshenko and Woinowsky-Krieger.*

Discussion of results

Numerical integration: We choose the radial displacement w , being in general the most important displacement component, to assess the relative accuracy of the quadrature formulae given in Table 4.1 for analyses C/N/01 through C/N/06. Each of these analyses is identical except for the method of numerical integration used.

The percentage absolute error in w for the various quadrature formulae is shown in Fig. 4.1, where the region chosen for the comparison includes the edge of the cylinder and hence the maximum radial displacement.**

The results shown are abundantly clear, and we conclude that:

- (i) Results obtained using either of the Simpson's formulae are far more accurate than any of the Gaussian formulae results. This is undoubtedly due to the fact that, for the limits of integration required here, only half-formulae can be used in the Gaussian process (c.f. Appendix D).

* Ref. [3], p 469

**The results for the Gaussian formula, $n = 8$, are not shown due to a suspected error which we suggest must arise in the source of information, Ref. [4], p 147.

Distance x from edge of cylinder

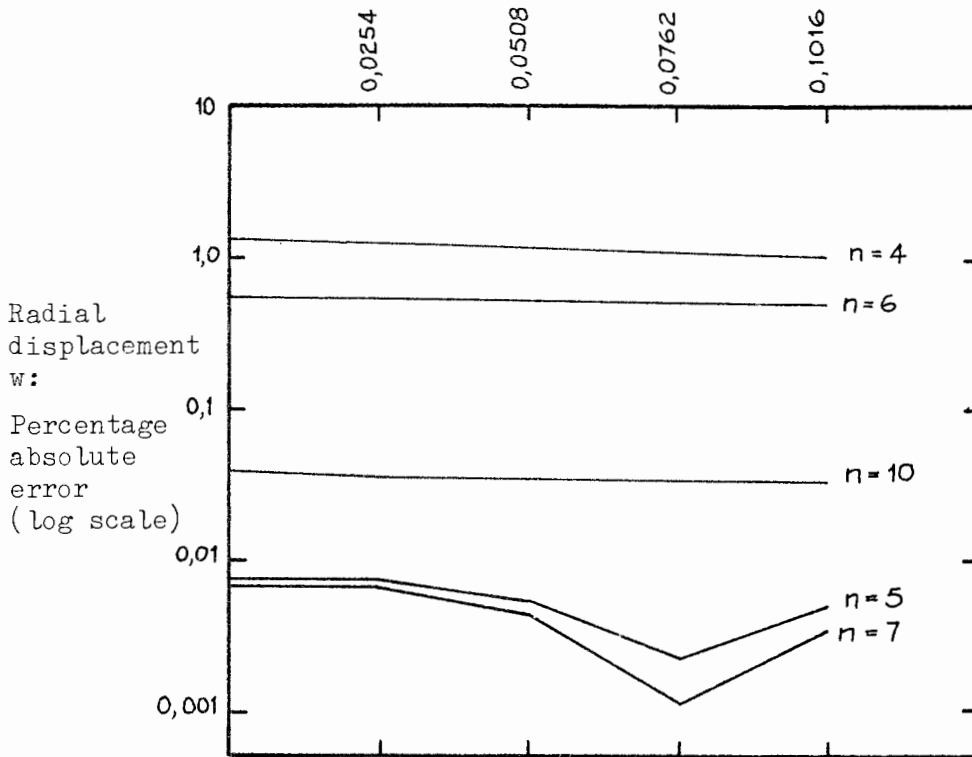


Fig. 4.1

- (ii) There is little difference between the five and seven point Simpson's formulae results, so that further increase in the number of points used appears to be entirely unwarranted. Moreover, even the five point Simpson's formula results are extremely accurate, yielding a maximum error at the loaded edge of only 0,007 %.

Convergence study:

We choose again the radial displacement w to investigate the general question of convergence as stated in objective (ii).

For this purpose four analyses (each using the five-point Simpson's rule) have been carried out. Each of these analyses has a different element aspect ratio for the region $x = 0$ to $x = 0,2032$ (region 1), but all have the same element aspect ratio ($L/t = 5/3$) for $x > 0,2032$ (region 2).

The percentage absolute error in w for each analysis is given in Fig. 4.2.

Distance x from edge of cylinder

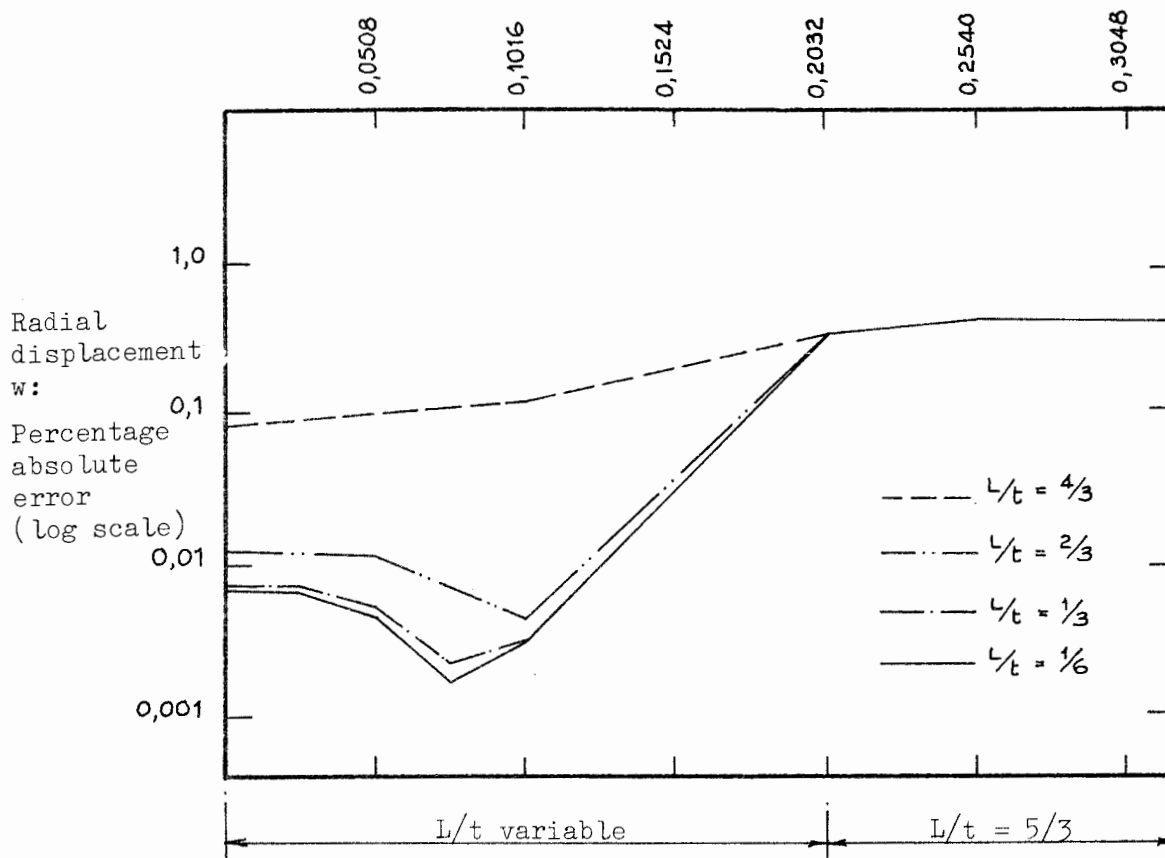


Fig. 4.2

From these results it is clear that,

- (i) Over region 1 each decrease in the L/t ratio gives rise to an improvement in accuracy, up to a point where convergence may be said to have occurred.
- (ii) Over region 2, where each analysis has the same element aspect ratio, the percentage errors are identical.

Of particular interest here is the fact that as region 2 is approached all results tend to the same percentage error, and the point at which this occurs is exactly on the border between the two regions. It appears, therefore that the relative change in the L/t ratio between the two regions does not affect the results for region 2. The effect on the results of region 1, however, is that the larger the relative change in the L/t ratio, the larger the relative percentage error change between the best result of region 1 and those of region 2; the larger this relative change is, the wider the transition region required to effect it. Moreover, it appears that the transition region may occur entirely within (the more important) region 1.

We conclude, therefore, that:

- (i) Convergence of the displacement results occurs for an element aspect ratio of approximately $L/t = 1/6$.
- (ii) Where changes in the element aspect ratio from one section to another are deemed necessary, suitable transition regions should be allowed for.

Accuracy of stresses and moments

The stress and moment of most significance for design purposes are the hoop stress σ_θ and the meridional moment M_s . These quantities are calculated from the displacements according to Eq. 3.51, and in the case of a circular cylinder the expressions are,

$$\sigma_\theta = \frac{E}{1 - \nu^2} \left[\frac{w_2}{r} + \nu \frac{(u_3 - u_1)}{L} \right] \quad (4.1a)$$

$$\text{and } M_s = \frac{Et^3}{12(1 - \nu^2)} \left[\frac{3(w_1 - 2w_2 + w_3)}{L^2} + \frac{(\beta_1 - \beta_3)}{L} \right] \quad (4.1b)$$

where the numerical subscripts refer to the displacements at the general set of nodes shown in Fig. 4.3.

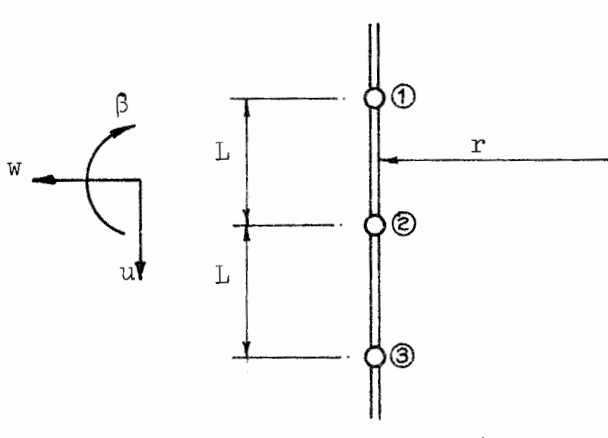


Fig. 4.3

The quantities defined by Eqs. (4.1) are clearly average stresses and moments whose accuracy depends on:

- (i) the accuracy of the displacement components, and
- (ii) the element length L .

Hence, as a result of (ii) and the fact that both σ_θ and M_s depend on more than one displacement component, (e.g., σ_θ depends on both w and u), there can be no direct correlation between the accuracy of the displacements (already investigated) and the accuracy of the stresses and moments.

The theoretical solution for M_s is shown in Fig. 4.4(a). At the upper edge of the cylinder M_s is equal to the applied edge moment M , and at a short distance from the edge the meridional moment reaches a peak after which it dies out to practically zero at the base of the cylinder.

Shown alongside the meridional moments are curves indicating the percentage error in the finite element solution for four values of the L/t ratio. The three lines correspond to three points in the vicinity of the loaded edge, and as it happens, are perfectly linear when plotted to a logarithmic scale. These three lines indicate clearly two rather trivial points, which we mention here for completeness:

- (i) as the L/t ratio is decreased, the percentage error decreases,
- (ii) as we move away from the loaded edge the accuracy of the solution improves.

What we are particularly interested in, however, is the range of L/t ratios which can be expected to give solutions having errors $\leq 1\%$. From the diagram these ranges are:

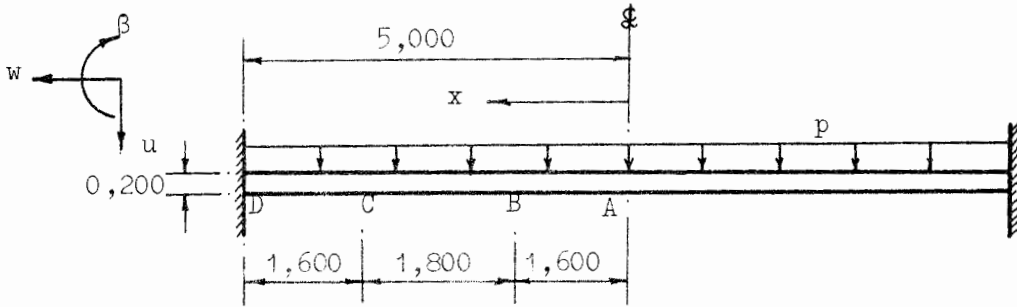
$$\begin{array}{lll} x = 0 & \text{(loaded edge)} & : L/t \leq 1/6 \\ x = 0,1016 & \text{(peak moment)} & : 1/3 \leq L/t \leq 2/3 \\ x = 0,2032 & \text{(normal conditions)} & : 2/3 \leq L/t \leq 4/3. \end{array}$$

Note that the radial displacement w at $x = 0$, $L/t = 1/6$, had an error of only 0,007%, whereas the moment M_s , which depends partly on w , has for the same point an error of just over 1%.

The hoop stress distribution for the cylinder is shown in Fig. 4.4(b), and alongside, the percentage error in the finite element solution for four values of the element aspect ratio. The results shown are again for two points in the vicinity of the loaded edge, but far from being linear, (as was the case with the corresponding M_s results), the curves show a marked trend towards convergence. This is due to the fact that, because $\nu = 0$, σ_θ depends only on a single radial displacement component w_2 , whose pattern of convergence has already been illustrated. For the same reason, the σ_θ results are far more accurate than the corresponding M_s results.

Hence, σ_θ places no additional constraints on the choice of the range of L/t ratios which can be expected to yield reasonably accurate stress and moment solutions.

TABLE 4.2



Loading:

$$p = 100 \text{ N/m}^2$$

Material Properties:

$$E = 20 \times 10^9 \text{ N/m}^2$$

$$\nu = 0,3$$

Analysis I.D. No.	Quadrature formula*	Element Subdivision**		Remarks
		Regions AB, CD	Region BC	
D/2/01	S - 5	16 @ 0,100 (1/2)	6 @ 0,300 (3/2)	
D/2/02	S - 7	"	"	
D/2/03	G - 10	"	"	
D/2/04	S - 5	8 @ 0,200 (1)	"	
D/2/05	"	4 @ 0,400 (2)	"	
D/2/06	"	2 @ 0,800 (4)	"	
D/2/07	"	7 @ 0,200 (1)	"	Hole at centre, of radius 0,200
D/2/08	"	1 @ 0,800 (4)	"	Hole at centre, of radius 0,800

* S - 5: Simpson, 5 point. S - 7: Simpson, 7 point. G - 10: Gauss, n = 10.

**L/t ratios given in brackets.

We therefore conclude with the suggestion of a general range of element aspect ratios, viz.,

$$1/6 \leq L/t \leq 1$$

where, in regions near to concentrated loads or peak stresses, the lower end of the range should be used. Note, finally, that the suggestion does not necessarily apply to regions where the stresses or moments are negligible and where accuracy is thus of little importance.

4.2.2 Example 2: A uniformly loaded circular disc

Objectives

- (i) To investigate further the accuracy of various methods of numerical integration.
- (ii) To test the circular disc closure element.

Description of the analysis

The data for the example are given in Table 4.2 together with a description of the element breakdown and the quadrature formulae used in each of the eight analyses.

This example has been used by Klein ^[16] and Ahmad, Irons and Zienkiewicz ^[19] to test the performance of shell elements in analysing circular plates. The theoretical solutions used here for comparison have been obtained from another independent computer program TIMDISC, which is based on the circular plate equations of Timoshenko and Woinowsky-Krieger.*

For a uniformly distributed lateral load the in-plane stresses in a circular plate are zero, and of the two bending moments present, only the meridional moment is of importance. Since the meridional moment has peak values at the centre and edge of the plate, the latter two regions have finer element subdivisions than the middle region (BC in Table 4.2). The middle region has the same element subdivision for all the analyses.

To limit the number of analyses required for testing the closure element, we have limited the choice of closure elements to those having the same length as the adjacent (standard) elements. Also, where holes have been left at the

*Ref. [3], p 55.

centre of the plate they too have a radius equal to the length of the adjacent element.

Discussion of results

Numerical integration: We choose the lateral displacement u to assess the relative accuracy of the three quadrature formulae given in Table 4.2 for analyses D/2/01 through D/2/03. A comparison of the percentage absolute error in u for each formula is given in Fig. 4.5.

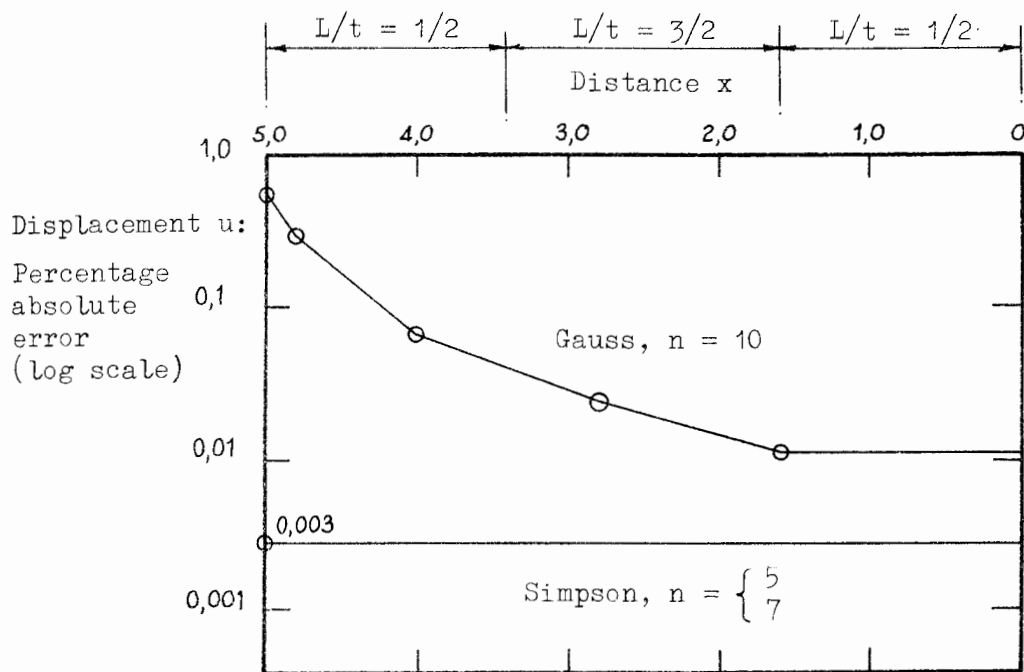


Fig. 4.5

The displacement solutions obtained using the five and seven point Simpson's formulae are essentially identical, yielding extremely low errors of 0,003%; the order of accuracy remains, moreover, constant along the entire radius of the plate.

The Gaussian results on the other hand, although reasonably accurate at the centre of the plate, show a marked increase in error towards the edge of the plate.

We conclude therefore that

- (i) the Simpson's formulae yield far superior results than do the Gaussian formulae;

- (ii) there is nothing to be gained by increasing the number of points used in the Simpson's formula above five.

The closure element: We begin our study of the closure element by investigating the percentage absolute error in the lateral displacement u for three different values of the element aspect ratio (Fig. 4.6).

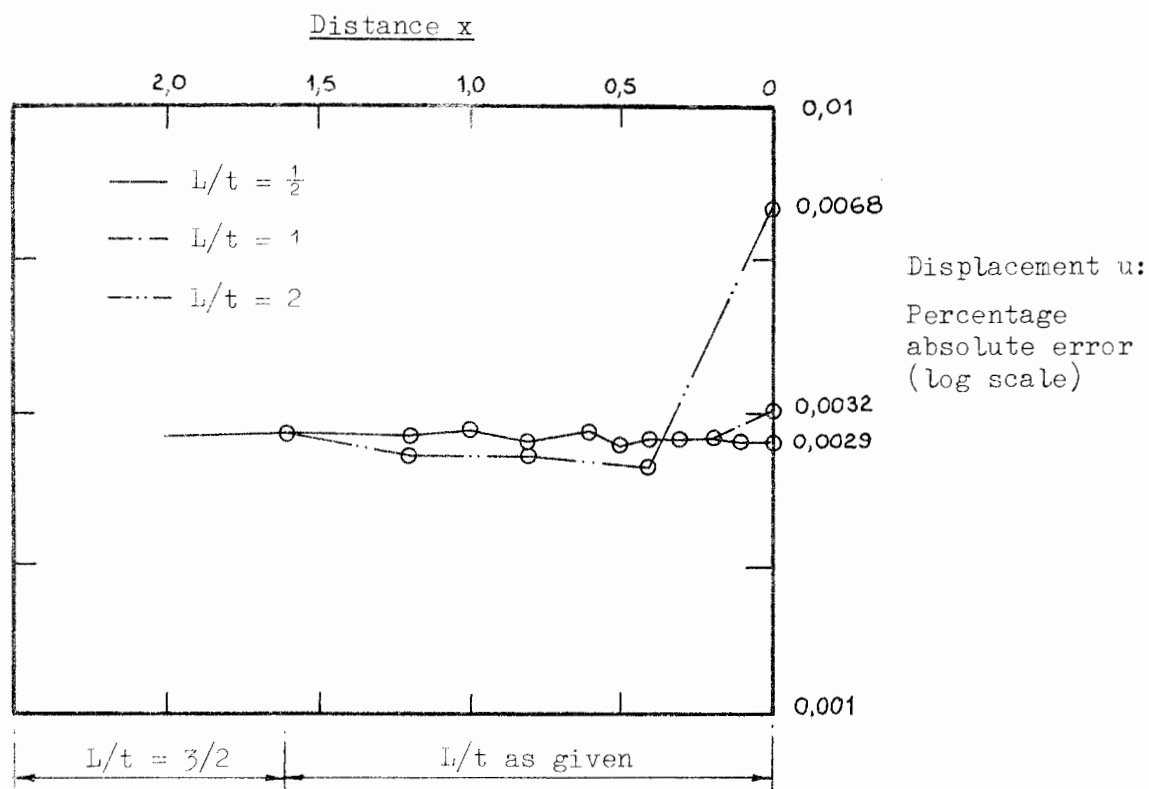


Fig. 4.6

From the figure the following results are apparent:

- (i) The increasing size of the closure element has no adverse effects on the accuracy of the displacements in the rest of the plate. (This is rather strikingly illustrated by the results for $L/t = 2$, and immediately dispels the intuitive notion that the closure element should always be as small as possible.) The fact, however, that the results for $L/t = 2$ are the most accurate of all defies logical explanation, particularly since, for $x > 1,6$ all the analyses exhibit the same percentage error.
- (ii) As the size of the closure element increases there is a general decline in the accuracy of the displacements at the axis of symmetry.

The latter decline is due to the fact that the lateral displacement u_0 at the axis of symmetry is calculated from the expression,

$$u_0 = u_1 + \frac{\beta_1}{a} \quad (3.38, \text{ bis})$$

where u_1 and β_1 are the lateral displacement and rotation at the closure element's single node, and a is the radius of the closure element. Even assuming that the accuracy of u_1 and β_1 are unaffected by the size of the closure element (or alternatively, by the L/t ratio of the adjacent elements), the accuracy of u_0 is bound to decrease as the radius a increases, since Eq. (3.38) assumes a state of pure bending to exist in the closure element. It will be noticed, however, that the percentage error plotting scale is very much exaggerated, and that the error in u_0 at the axis of symmetry for $L/t = 2$ is only 0,0068%. The average error over the rest of the plate is only 0,003%, both errors being extremely small.

The necessity for using a closure element is clearly demonstrated by the results shown in Fig. 4.7. Here the effect of leaving a small hole at the centre of the plate is compared with that of closing the hole with a closure element.

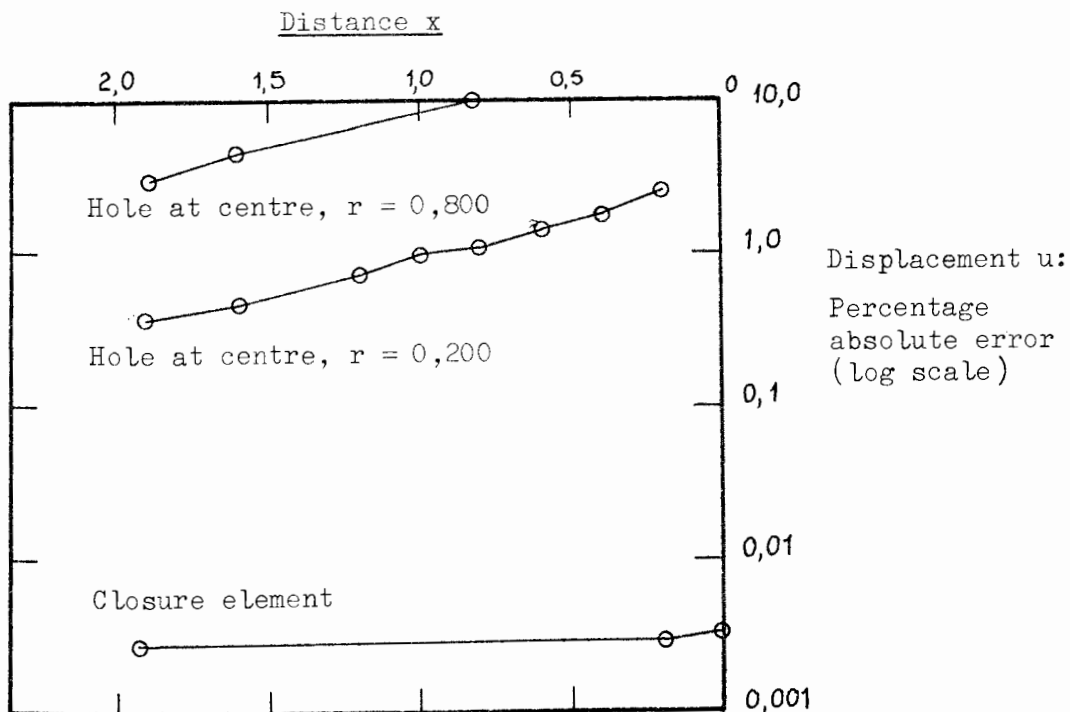


Fig. 4.7

The two sets of results for holes at the centre indicate, as we would expect, that the larger the hole the worse the error in the displacement solution. Of more importance, however, is the very significant improvement in accuracy to be gained by using a closure element.

The necessity for using a closure element is further demonstrated by the results for the meridional moment M_s , shown in Fig. 4.8. The results for the plate with a hole at the centre, while not very accurate, do indicate a tendency to zero moment at the edge of the hole. Hence, in the region of the centre of the plate, the results for a plate with a hole at the centre will always be blatantly incorrect. However, there is a surprisingly rapid convergence of the two bending moment diagrams with the result that over that half of the plate nearest to the fixed end the hole at the centre does not affect the moments at all.

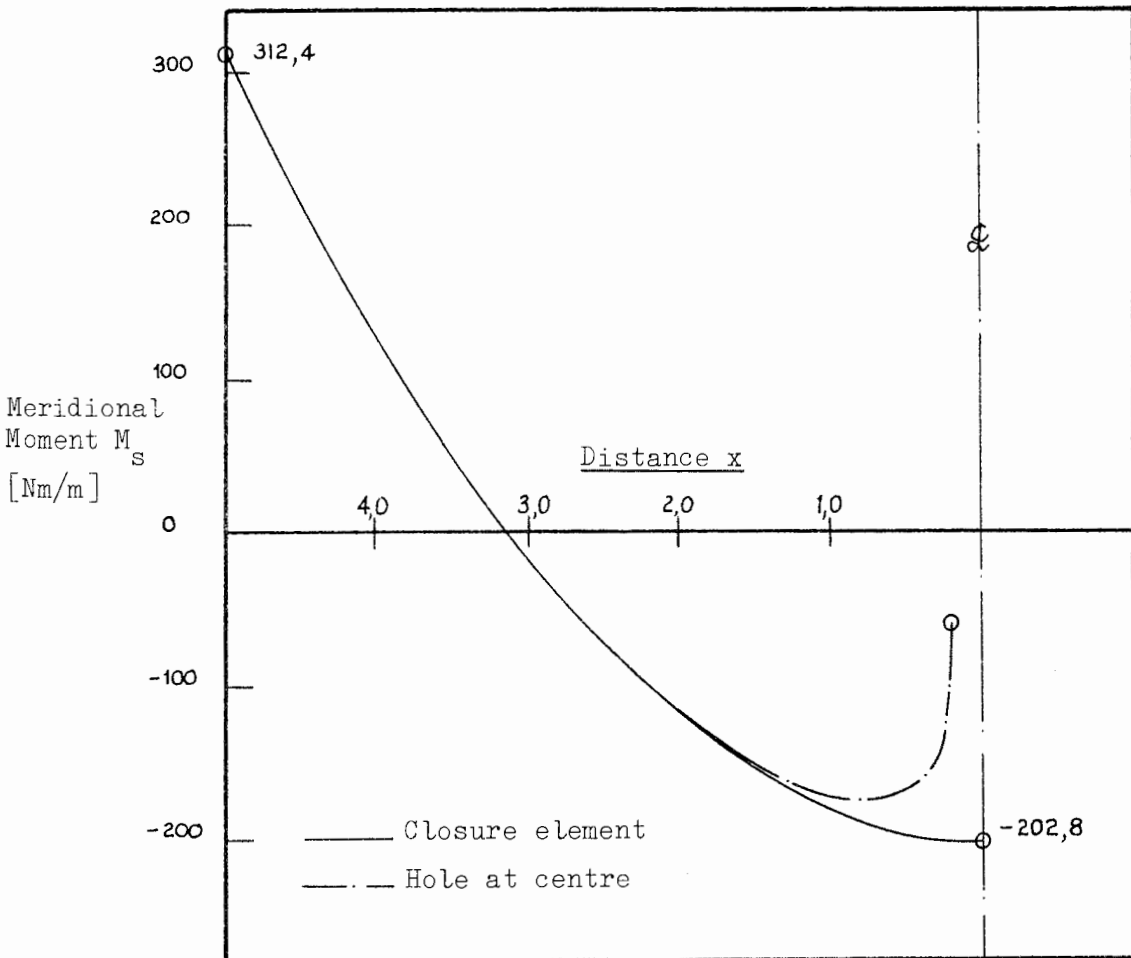


Fig. 4.8

When the closure element is used the meridional moment at the axis of symmetry is calculated from the expression,

$$M_0 = \frac{Et^3}{12(1-\nu)} \cdot \frac{\beta_1}{a} \quad (3.39, \text{ bis})$$

Again, because this expression assumes a state of pure bending in the closure element, the error in M_0 can be expected to increase as the radius a increases.

The extent of the increase in error is, however, negligible, as can be gauged from the fact that if the M_s solutions for $L/t = \frac{1}{2}$ and $L/t = 2$ were also plotted in Fig. 4.8 they would coincide with the curve for $L/t = 1$ already shown there.

The overall accuracy of the meridional moments as a function of various element aspect ratios is shown in Fig. 4.9. The moments at the axis of symmetry ($x = 0$) are, as we might expect, the least accurate. Nevertheless, there appears to be a fairly constant relationship between the accuracy of these moments and the accuracy of those in the rest of the plate (except over the region $\frac{1}{2} \leq L/t \leq 1$), thus indicating the size of the closure element has no special effect on the accuracy of the moments in the rest of the plate.

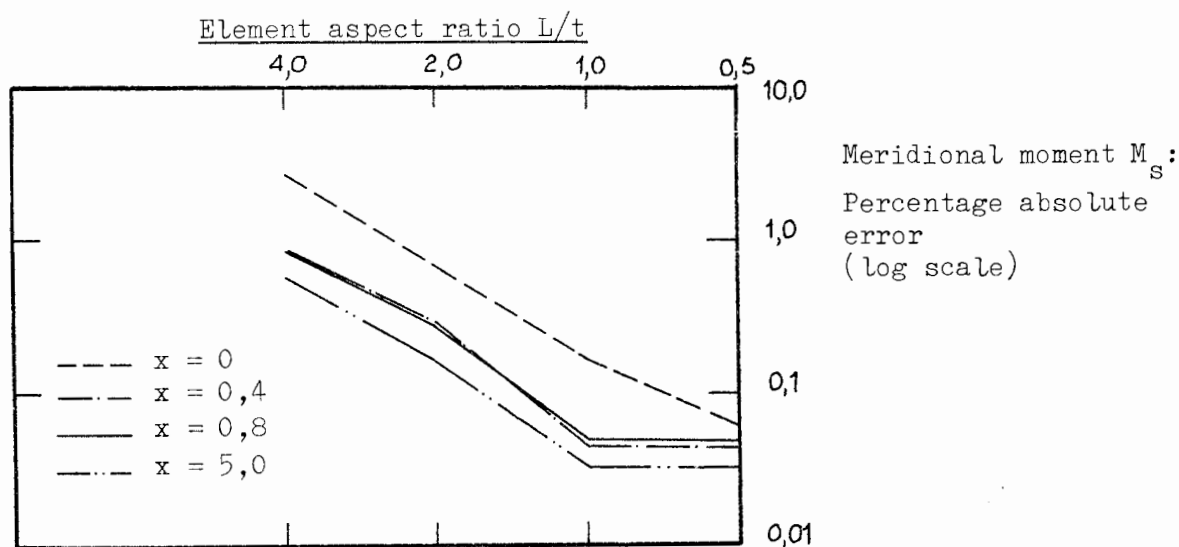


Fig. 4.9

It is also clear from Fig. 4.9 that the limits of the range of L/t ratios which may be expected to yield reasonably accurate moment solutions are far less stringent than those required for an edge loaded cylinder; the range itself may be taken as $\frac{1}{2} \leq L/t \leq 4$ to give less than one percent error for all results.

4.2.3 Conclusions I

In the preceding two examples we have drawn certain conclusions which will be made use of in all the remaining analyses. These conclusions may be summarised as follows:-

- (a) Numerical integration: The Simpson's formulae are the most accurate at our disposal. Of these there is little improvement in accuracy to be gained by using the 7-point formula (or for that matter even greater numbers of points), so that in the interest of programming efficiency the 5-point Simpson's formula will be used.
- (b) Choice of element subdivision: It is clearly not possible to define rigidly the range of L/t ratios for which reasonably accurate results (having errors less than 1%) may be expected, since every shell has different geometry, loading and boundary conditions, all of which affect the accuracy of the solution to a greater or lesser degree.

Every shell should in principle be analysed a number of times, using successively more refined element subdivisions, to ensure that a reasonable degree of convergence has been attained.

However, such a procedure is not always possible, either through lack of time or for economic reasons. We therefore present broad guidelines for the choice of element subdivision based on the analyses of an edge loaded cylinder (representing the class of shell for which more stringent conditions of refinement are required), and the uniformly loaded circular plate (for which the least stringent conditions of refinement are required). These guidelines are:

$$\text{Edge loaded cylinder: } 1/6 \leq L/t \leq 1$$

$$\text{Uniformly loaded plate: } 1/2 \leq L/t \leq 4$$

These guidelines are discussed further in Example 3 (load case 2).

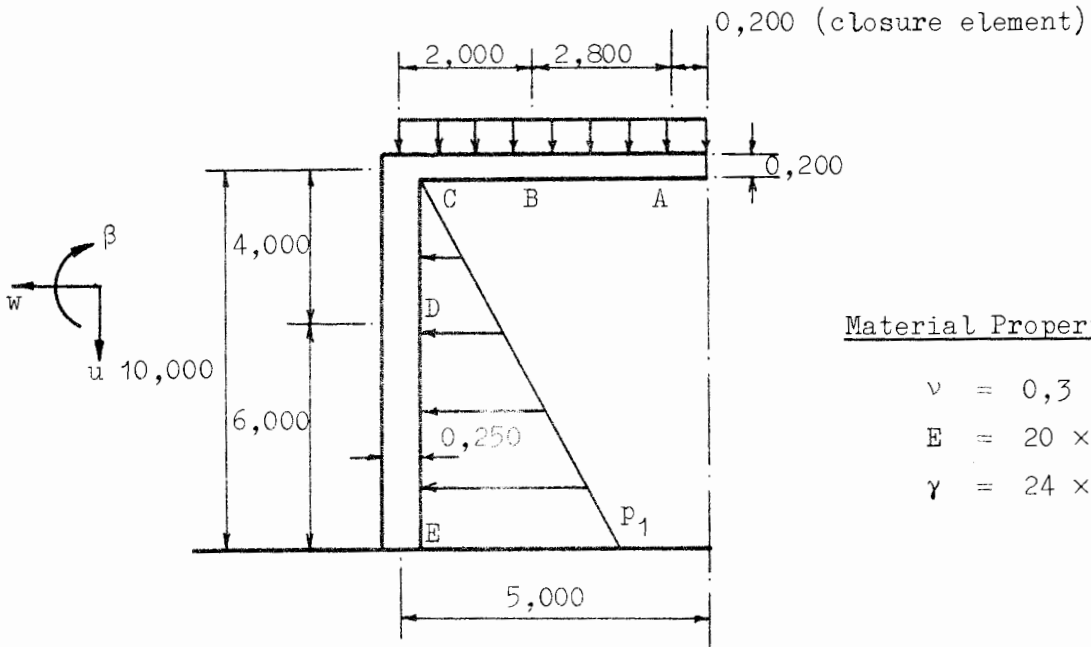
(c) Closure element:

- (i) The logical choice for the size of closure element to use is to make it the same length as the adjacent element to which it is connected. Under these conditions the size of the closure element

itself has no adverse effects on the results in adjacent parts of the shell, the accuracy of the latter results being governed by the element aspect ratios used. In fact, even where the displacements and moments at the axis of symmetry are of importance, closure elements with aspect ratios as high as 2 may be used.

- (ii) Where a circular plate is closed at the axis of symmetry, the errors in the displacement and moment solutions resulting from a small hole at the centre of the plate are very significant, although highly localised, whereas the results obtained using a corresponding closure element are excellent.

TABLE 4.3



Material Properties:

$$\begin{aligned} \nu &= 0,3 \\ E &= 20 \times 10^9 \text{ N/m}^2 \\ \gamma &= 24 \times 10^3 \text{ N/m}^3 \end{aligned}$$

Load Case 1:

Hydrostatic pressure on cylinder wall: $p_1 = 100 \times 10^3 \text{ N/m}^2$

Load Case 2:

Uniformly distributed pressure $p_2 = 4,8 \times 10^3 \text{ N/m}^2$ on the roof (equivalent to the self-weight of the roof).

Analysis I.D. No.	Element Subdivision* (Element lengths in mm)				Remarks**
	AB	BC	CD	DE	
3/1/01	14 @ 200 (1)	10 @ 200 (1)	16 @ 250 (1)	24 @ 250 (1)	Load Case 1
3/1/02	"	20 @ 100 (1/2)	32 @ 125 (1/2)	"	"
3/2/01	-	-	16 @ 250 (1)	24 @ 250 (1)	Open tank, no roof.
3/3/01	14 @ 200 (1)	20 @ 100 (1/2)	32 @ 125 (1/2)	24 @ 250 (1)	Load Case 1, Dead load of entire structure.
3/4/01	"	10 @ 200 (1)	16 @ 250 (1)	"	Load Case 2
3/4/02	"	20 @ 100 (1/2)	32 @ 125 (1/2)	"	"

* L/t ratios given in brackets.

** Unless otherwise stated, all analyses include the circular disc roof.

4.3 Cylinder-Plate and Cylinder-Cone Shells: The Problem of Shell Junctions

The cylinder-plate and cylinder-cone shells are, unlike the previous examples, of considerable practical interest since the former forms the basis of the closed cylindrical water reservoir and the latter is the most common shape used for sludge digester tanks. The examples of this section therefore have practical dimensions and loading so that the accuracy of the results may be evaluated directly, as well as in terms of percentage errors.

Broadly speaking, the objectives of this section are:

- (i) to investigate the general accuracy of results, particularly of the stresses and moments at shell junctions;
- (ii) to examine and enlarge upon various stress and moment solutions, and where some doubt as to the validity or interpretation exists, to give explanations and to compare with solutions in similar structures.

4.3.1 Example 3: A closed cylindrical water tank

Specific objective:

To investigate the performance of the conical frustrum element in analysing the stresses and moments at a shell-plate junction.

Description of the analysis:

The data for this example are given in Table 4.3 together with a description of the element subdivisions used in each of the six analyses. The theoretical solutions used here for comparison have been obtained from another independent program FLUTAN, which is based on the cylindrical water tank equations of Flügge.*

The author's solution for the closed tank is made up of the open tank solution plus the effect of the redundant moment X_1 (Fig. 4.10).

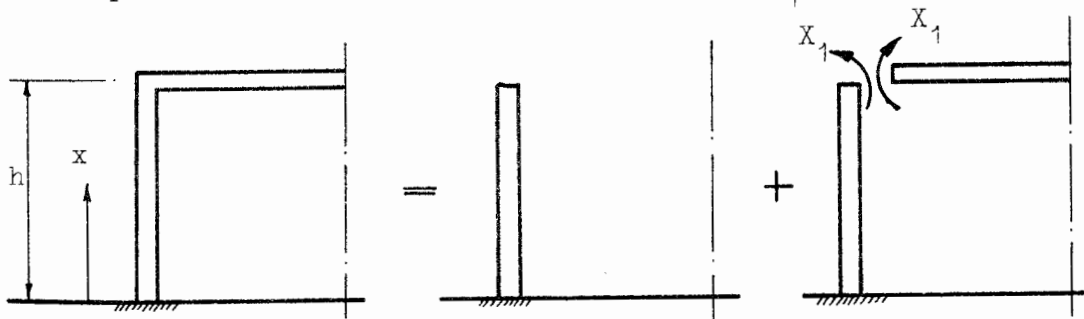
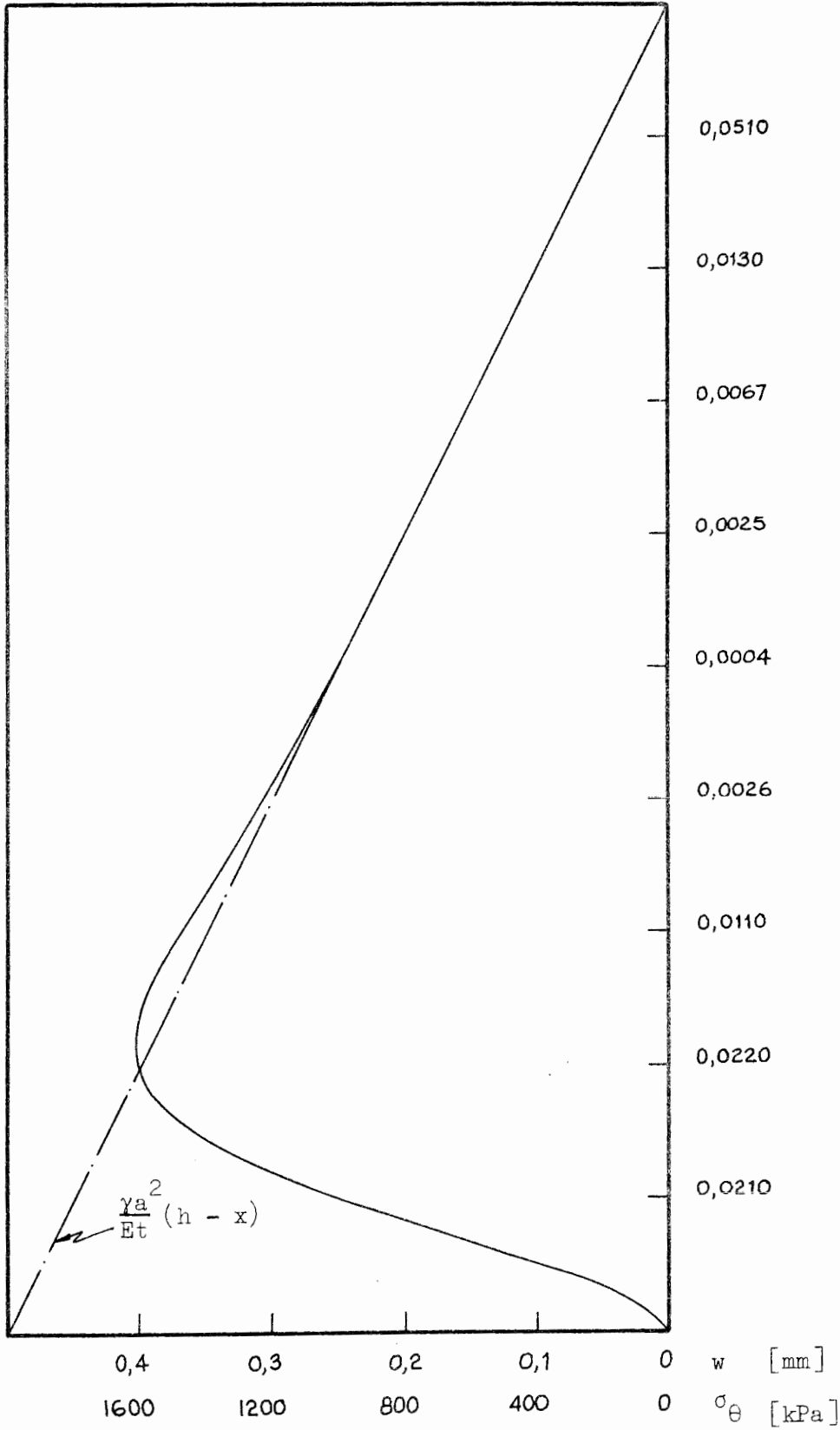


Fig. 4.10

* A slightly modified version of Flügge's theory is given in Appendix G.



Figures to the left refer to percentage error in finite element displacement solution.

Fig. 4.11: Radial displacement w and hoop stress σ_θ

The moment X_1 is found by equating the rotations of the open tank and the circular disc roof at their point of junction. To simplify the procedure it is assumed that the cylinder is infinitely long, thus allowing the two boundary conditions at each end of the cylinder, viz.,

$$\begin{aligned} w(0) &= 0 & w(h) &= 0 \\ \frac{dw}{dx}(0) &= 0 & M_s(h) &= X_1 \end{aligned} \quad (4.2)$$

to be used independently to solve for the four arbitrary constants of integration. The failing of this assumption is that unless h is large the moment at the upper edge of the open tank is not zero; it follows therefore that the moment at the upper edge of the closed tank is not X_1 . Allowance has however been made for this in the theoretical solution used here.

To simplify the programming of the theoretical solution it was considered worthwhile to reformulate Flügge's derivation of the effect of X_1 in terms of x measured from the base of the tank. (Flügge derives this particular case in terms of x measured from the upper edge of the tank.) While results obtained using the writer's formulation agree with those obtained directly from Flügge's equations there is no agreement on the specific results for the author's worked example.* We mention therefore, for future reference, that the author's results appear to be incorrect.

Load cases 1 and 2 in the present example have each been analysed twice to assess the improvement in the results obtained by refining the element breakdown in the region of the shell-plate junction. The refinement resulted in insignificant improvements in the meridional moments, of the order of 0.003%. For these two load cases, therefore, the results quoted here will be for the analyses where the ratio $L/t = 1$ is constant throughout the structure.

Discussion of results:

Load Case 1: We begin by examining the radial displacement w in the cylinder as shown in Fig. 4.11. The theoretical and the finite element solutions coincide for the entire height of the cylinder, as can be appreciated by observing the extremely small percentage errors in the finite element solution, given at metre intervals down the cylinder.

The displacements in the upper half of the cylinder are perfectly linear

* Ref. [1], p 276, Fig. 5.25.

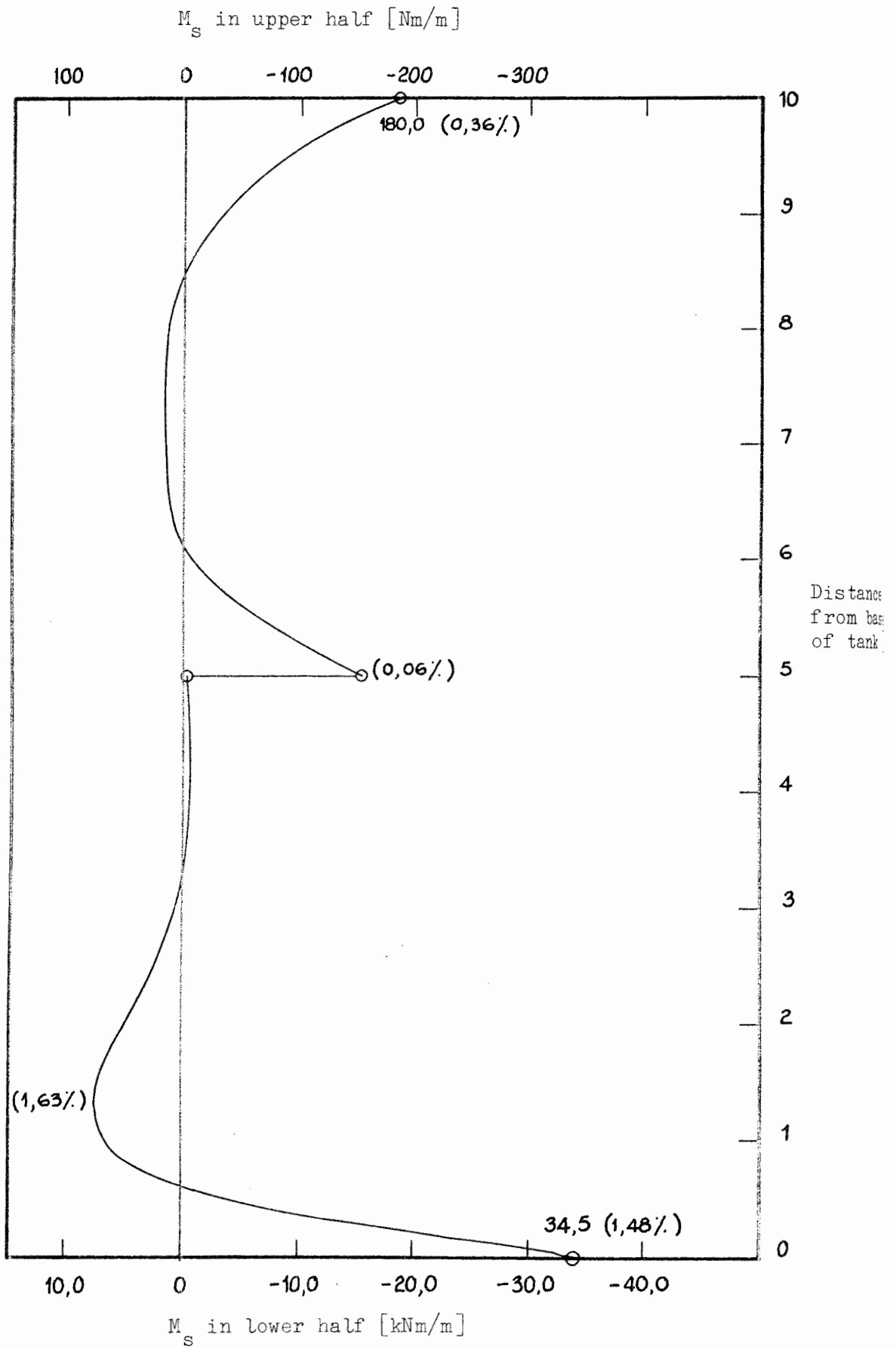


Fig. 4.12: Meridional moment M_s in tank wall

and correspond to the function,

$$\bar{w} = \frac{\gamma a^2}{Et} (h - x) \quad (4.3)$$

These are the displacements which would arise in the absence of kinematic constraints at the base of the tank. The function also satisfies the condition that w be zero at the upper edge of the tank; although no such constraint is imposed on the finite element solution the results show that it is, nevertheless, effectively satisfied.

An interesting observation in this respect is that the circular disc roof is almost totally redundant as a means of restraining the radial deflection of the upper edge of the cylinder. This we conclude by noting that the radial displacement of the open tank at its upper edge is also effectively zero. (In fact, the radial displacement curve for the open tank is identical to that of the closed tank except over a small region near the top of the cylinder where the open tank displacements are of the order 10^{-3} mm larger.)

We turn now to the meridional moment M_s shown in Fig. 4.12.* The theoretical and finite element solutions coincide, notwithstanding that the errors in the finite element solution (given in brackets at points along the curve), are in places greater than 1%. Again it is of interest to note that for the lower half of the tank, the open tank solution corresponds exactly to the closed tank solution.

What is of particular interest here, however, is the moment at the cylinder-disc junction. Although the moments at the junction are very small compared with those at the cylinder base (0,180 and 34,500 kNm/m respectively), the error at the junction is only 0,36%. Furthermore, the moments in the disc roof given by the finite element solution are constant and exactly equal to the value of the moment at the upper edge of the cylinder. The finite element solution therefore maintains perfect continuity of moments at the junction, which in turn indicates a very consistent displacement solution.

The hoop stresses at the cylinder-disc junction are continuous only if Poisson's ratio ν is zero. This can be seen by comparing the expressions for σ_θ in the disc, viz.,

* Different scales have been used to plot the moments because of the vast difference in the magnitudes of moments in the upper and lower halves of the cylinder.

$$\sigma_{\theta} = \frac{E}{1 - \nu^2} \left[\frac{w_2}{a} + \nu \left(\frac{w_2 - w_1}{L} \right) \right] \quad (4.4a)$$

and in the cylinder, viz.,

$$\sigma_{\theta} = \frac{E}{1 - \nu^2} \left[\frac{w_2}{a} + \nu \left(\frac{u_3 - u_2}{L} \right) \right] \quad (4.4b)$$

where the numeric subscripts refer to the nodes shown in Fig. 3.13.

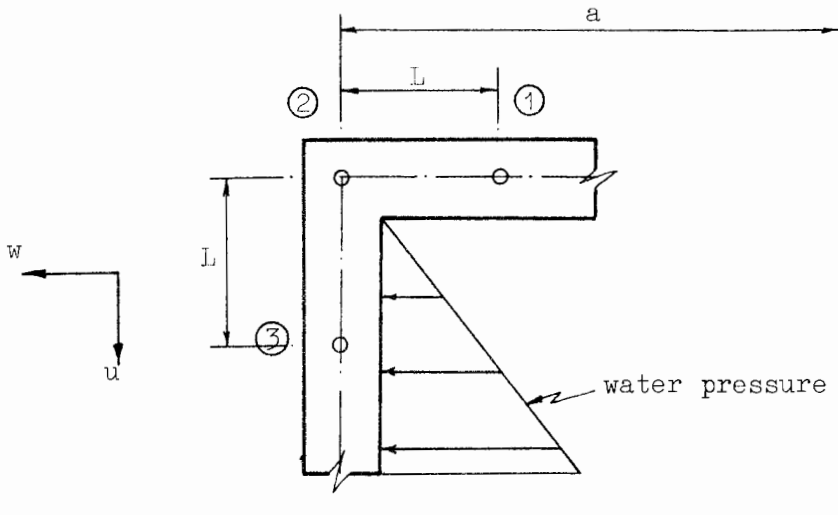


Fig. 4.13

The deformed position of the structure in the region of the cylinder-disc junction is shown digrammatically in Fig. 4.14a, and the corresponding hoop stress distribution in Fig. 4.14(b). Both the circumferential strain w_2/a and the radial strain $(w_2 - w_1)/L$ are positive (tensile) and very small since the radial displacement at node 2 is effectively zero. It follows that the hoop stress at the edge of the disc is tensile and small.

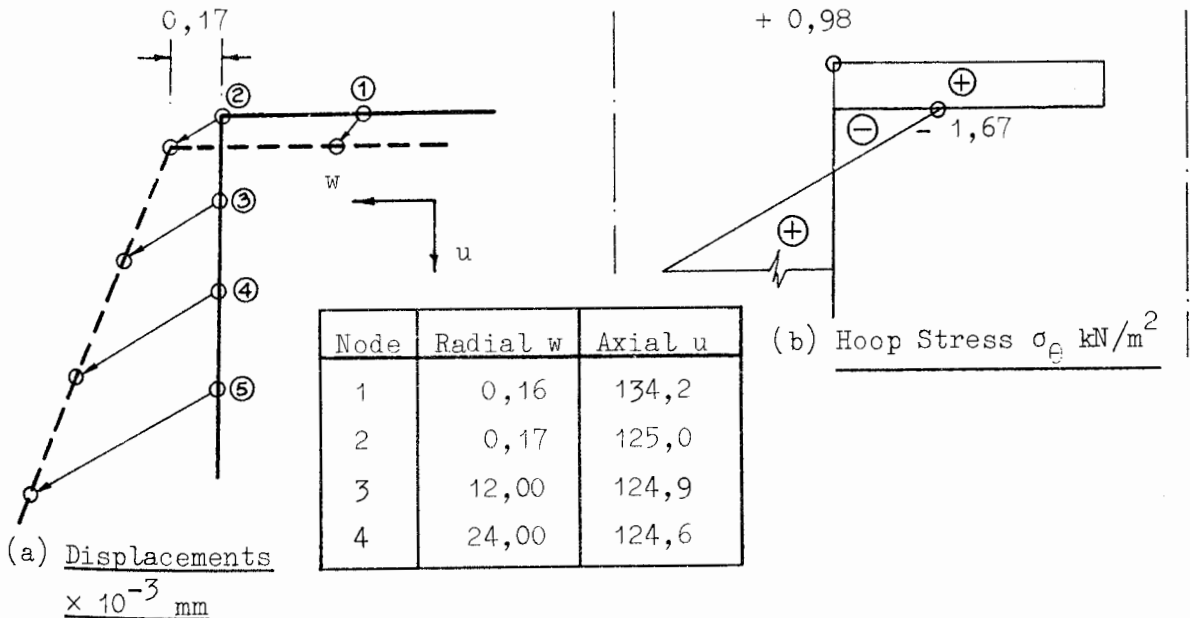


Fig. 4.14

However, the compressive axial strain at the top of the cylinder $(u_3 - u_2)/L$ is greater than the circumferential strain w_2/a . Hence if $\nu > 0$ the hoop stress at the upper edge of the cylinder is compressive. A short distance from the edge the circumferential strain becomes larger than the axial strain and the hoop stress again becomes tensile.

The overall effect is a discontinuity in σ_θ at the cylinder - disc junction.* This discontinuity is a misleading one since it is not caused, as we might expect, by a radial contraction of the cylinder, but by the Poisson contribution of the axial strain.

For practical purposes, however, this compressive stress is negligible. Moreover, since the axial strains decrease towards the base of the cylinder while the radial strains increase, the Poisson effect soon becomes insignificant. The hoop stresses are then given by Eq. (4.1) and may be read off from the radial displacement curve (Fig. 4.11).

Load Case 2: Before entering the main discussion it is of interest to compare two finite element solutions: one (Case A) where the self-weight of the entire structure is included through the use of the body-force load vector (Eqs. 3.24, 3.25a), and the other where the roof is subjected to a uniform pressure equivalent to its own self-weight (Case B).

The only difference between these two analyses is that in Case A the equivalent nodal loads due to the self-weight of the cylinder are included, whereas in Case B they are not; the load vectors for the disc roof are identical. We would therefore expect that the only difference in the solutions will be the larger axial strains in the cylinder of Case A. This is in fact what happens, as indicated diagrammatically in Fig. 4.15.

The relative displacements of the tank roof are in both cases essentially identical, i.e., if axial strain in the cylinder were to be neglected, cases A and B would both yield the same displacements for the roof. However, even when the axial strains in the cylinder are allowed, the difference between the two displacement curves is so small as to have negligible effect on the hoop stresses and moments in the structure, i.e. cases A and B both yield essentially the same hoop stress and moment results for the entire structure.

* Note from Eqs. (4.4) that the hoop stress as such is independent of the thickness of the shell. Hence, the change in thickness at the junction does not in itself give rise to discontinuity in σ_θ .

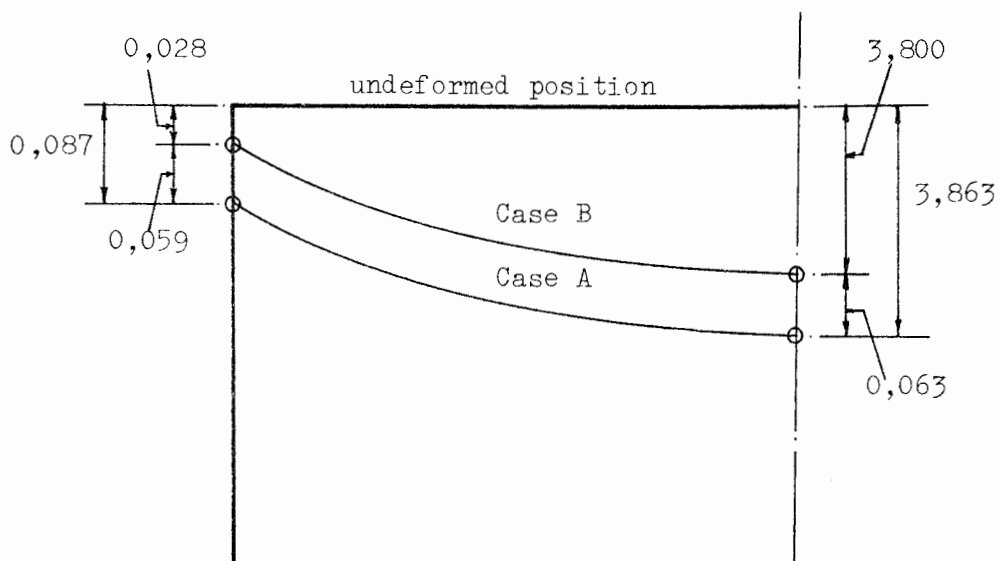


Fig. 4.15: Vertical Displacement of the tank roof (mm)

The preceding comparison serves to clarify two points in connection with equivalent load vectors:

- (i) The body force and surface force load vectors are identical for thin shells.
- (ii) Where the self-weight of the structure is to be included in the analysis it is far easier to use the body force load vector since it requires only one item of data input for the entire structure, viz., the unit weight of the shell material. The surface load vector on the other hand requires the equivalent pressure to be calculated at each node on the structure; although trivial this is a time consuming calculation, particularly in the case of inclined shell walls.

We now turn our attention to the meridional moment M_s for a uniformly distributed pressure on the tank roof. The moments are shown in Fig. 4.16 where, for the plotting scale chosen, the theoretical and finite element solutions coincide. The moments in the lower six metres of the cylinder are effectively zero, so that this part of the diagram has been excluded.

The percentage errors in the finite element solution are given in the accompanying table. From the table it can be seen that there are two regions where the error exceeds 1%. The first, between $x' = 2,0$ and $x' = 4,0$, is

due to the fact that the moments are relatively small, the high errors being thus of little significance.

The second of the high error regions occurs in the cylinder for $x' \geq 5,5$. Here again, part of the error is due to the fact that the moments are small. However, error (if it can be called this) is also likely to arise due to the form of the theoretical expression for M_s (with which the finite element solution is compared) which is given by*

$$M_s = X_1 e^{-\beta(h-x)} \cos \beta(h-x) \quad (4.5)$$

where X_1 is the redundant moment at the junction, β is a constant depending on the geometric and material properties of the cylinder, and x is the distance measured from the base of the cylinder. It is not unreasonable to expect a finite element solution to depart significantly from such an expression.

The finite element solutions for the two critical sections, viz., the centre of the roof and the cylinder-roof junction are, however, reasonably accurate, having errors of only 0,38% and 0,50% respectively. Our only concern here is that a further refinement of the element subdivision in the region of the junction produced no improvement in accuracy. It appears therefore that the 0,50% error at the junction is the best finite element result possible.

Referring back to Table 4.2 it will be noticed that the circular plate of Example 2 is geometrically identical to the roof in the present example. Furthermore, both plates are subject to a certain degree of rotational fixity at their outer edges, as indicated by the moments M_F and X_1 in the free body diagrams of Fig. 4.17(a). The moment M_F is a fixed-end moment due to rigid clamping of the plate, while X_1 is the moment arising from the rotational stiffness of the cylinder-disc junction. By replacing the value of the distributed load in Example 2 with that of Example 3, and multiplying all the stress results of Example 2 by the factor $(48 \times 10^3/100) = 48$, it is possible to compare directly the M_s distributions in each of the examples. The comparison is shown diagrammatically in Fig. 4.17(b)

From these curves we observe the following points:

* Appendix G, Eq. (G-18).

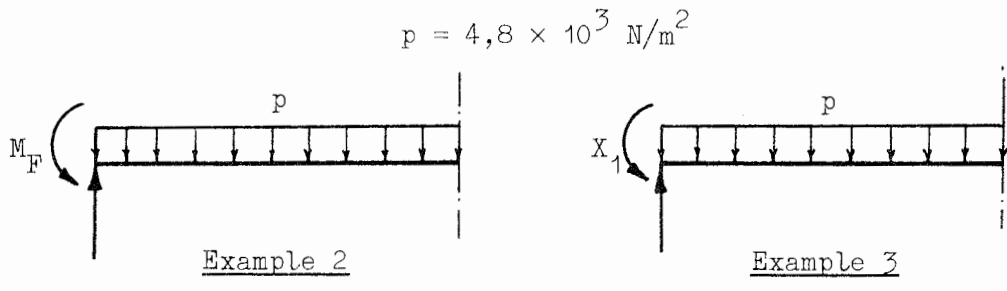


Fig. 4.17(a): Free body diagrams for circular discs

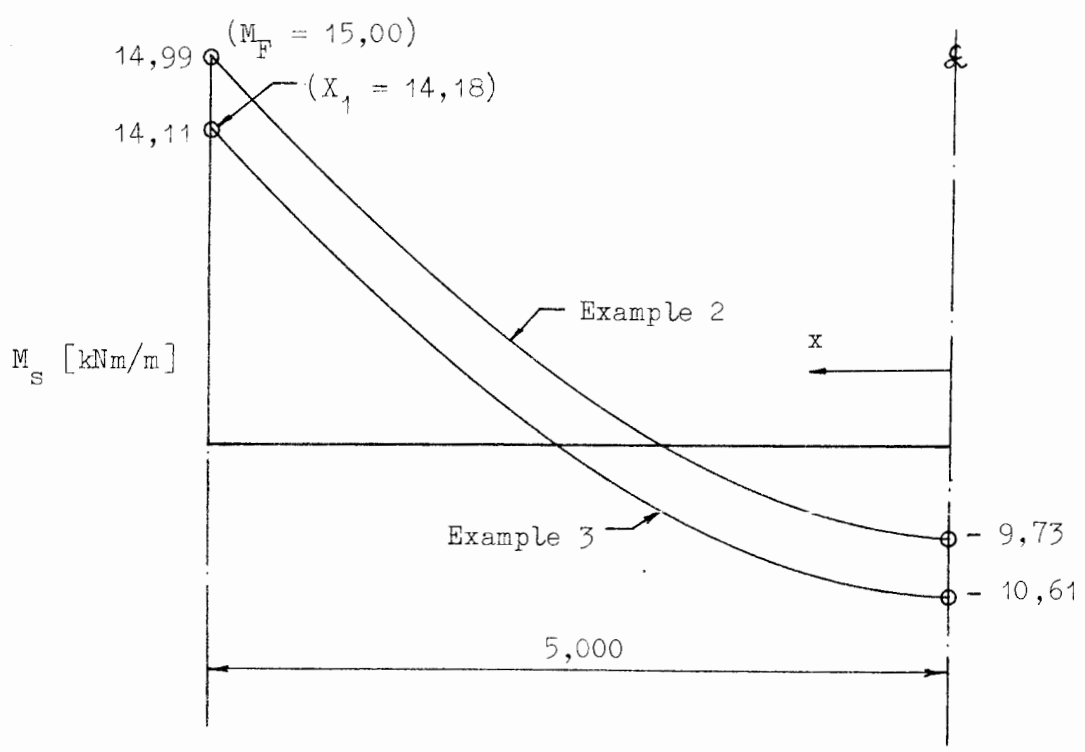


Fig. 4.17(b): Finite element solution for M_S in circular plate

TABLE 4.4

Distance x	M_S		% error in M_S	
	Example 2	Example 3	Example 2	Example 3
0	9,73	10,61	0,17	0,38
5,0	14,99	14,11	0,03	0,50

- (i) The curves are 'parallel', i.e., a constant distance apart, the distance being equal to $M_F - X_1$. The fact that the curves are very close together is trivial since it is clear that by increasing the flexural stiffness of the cylinder, X_1 may be made equal to M_F . The curves would then coincide. We may verify this by taking the limit of X_1 as the flexural stiffness of the cylinder, K_c tends to infinity.* Making use of L'Hôpital's rule,

$$\begin{aligned} K_c^{\lim \rightarrow \infty} \{X_1\} &= K_c^{\lim \rightarrow \infty} \frac{pa^2 K_c \chi}{4[2K_c \chi + K_s(1 + \nu)]} \\ &= \frac{pa^2}{8} = M_F \end{aligned} \quad (4.6)$$

In taking the limit, the flexural stiffness of the disc K_s has been kept constant. In principle then, it is possible to increase the stiffness of the cylinder to such an extent that the cylinder acts as a fixed end to the circular plate roof. Furthermore, the results shown in Fig. 4.17(b) indicate that even in practice fixed end conditions can be very closely simulated. These results will be made use of again in Examples 6 and 7.

- (ii) The finite element solution for the clamped circular plate (Example 2) is far more accurate than the finite element solution for the circular plate forming the roof of a cylindrical tank (Example 3). This can be seen by observing the percentage errors in the two solutions at the centre and edge of the plate, as shown in Table 4.4. Both finite element solutions were obtained using an aspect ratio $L/t = 1$.

The moments at a shell-plate junction are, as we would expect, not as accurately represented as those at a normal fixed end. (In fact, the error in the result for the shell-plate junction is more than 16 times greater than the error in the fixed-end result.) However, the point is that both the results for Example 3 given in Table 4.4 have errors less than 1%, (which may be classified as reasonably accurate), and were obtained using an element aspect ratio $L/t = 1$. Hence our guidelines for the choice of element aspect ratio** appear to be valid for combinations of the basic shell shapes.

* The expression for X_1 is given in Appendix G, Eq. (G-17); the expression for M_F is given in Appendix F, Eq. (F-10).

** See Section 4.2.3, conclusion (b).

The hoop stresses at the cylinder-disc junction are, even allowing for the Poisson effect, consistent with the radial displacements. The hoop stress does however exhibit a very rapid reversal of sign within a short distance from the upper edge of the cylinder. (Fig. 4.18b). The reason for this can be seen by observing the deformed position of the structure in the region of the cylinder-disc junction, as shown diagrammatically in Fig. 4.18(a).

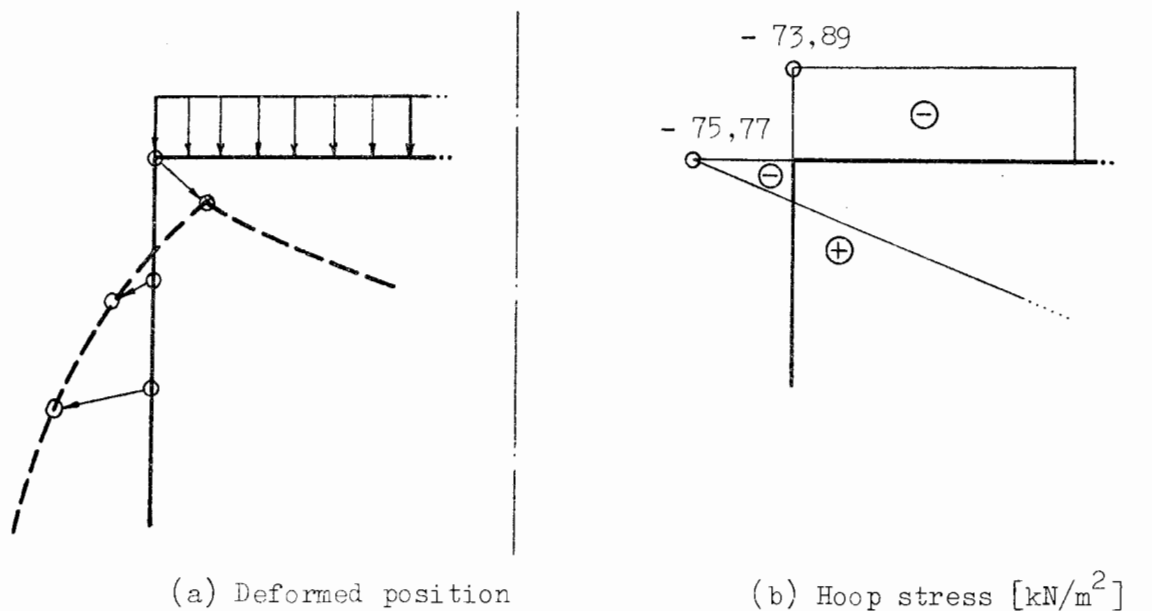


Fig. 4.18

The finite element solution for the hoop stress at a rigidly fixed boundary is often misleading and requires further explanation. For example, at the base node of the cylinder in the present example, the finite element solution for the hoop stress is $\sigma_\theta = -14,43 \text{ kN/m}^2$. Clearly this is the average hoop stress over the base element of the cylinder, (derived from the Poisson contribution of the axial strain), since at the base node the radial displacement is zero and hence the hoop stress must be zero.

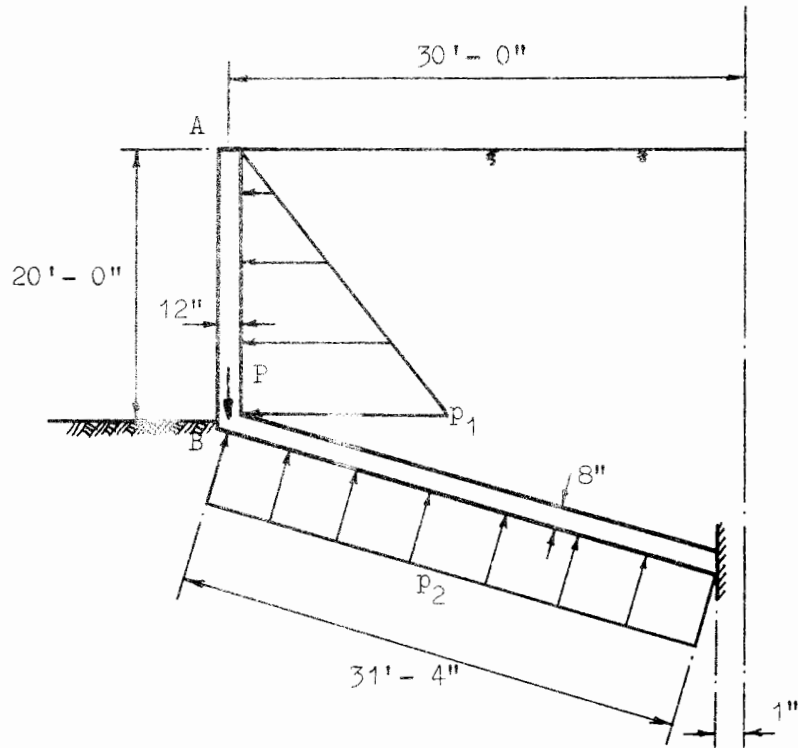
Under certain conditions, for example in axially loaded cylinders, the Poisson contribution of the axial strains to the hoop stresses may be very significant. In such cases the selection of a suitable Poisson ratio bears careful consideration. This point will be examined in more detail in connection with effluent tanks (section 4.6.1).

4.3.2 Example 4: An open sludge digester tank

Description of the analysis:

The data for this example are given in Table 4.5 together with a description of the element breakdown used in each of the four analyses.

TABLE 4.5



Material Properties:

$E = 20 \times 10^9 \text{ lb/ft}^2$

$\nu = 0$

Unit weight of water = 62.4 lb/ft^3

Loading:

$P = 500 \text{ lb/ft}$ (self weight of the cylinder)

$p_1 = 1248 \text{ lb/ft}^2$ (water pressure)

$p_2 = 36,67 \text{ lb/ft}^2$ (soil reaction)

Analysis I.D. No.	Element Subdivision*	
	AB	BC
4/1/01	40 @ 6" ($\frac{1}{2}$)	94 @ 4" ($\frac{1}{2}$)
4/1/02	80 @ 3" ($\frac{1}{4}$)	188 @ 2" ($\frac{1}{4}$)

*L/t ratios given in brackets

The theoretical results used here for comparison have been taken from a worked example of Flügge.* Due, however, to the fact that the general solution for a cone is written in terms of Thomson functions it has not been possible, as in the previous examples, to program the general solution. We are thus obliged to analyse the identical example which Flügge does; this accounts for the Imperial units,** and the fact that only the shape of the meridional moment diagram and its value at the cylinder-cone junction are directly available for comparison.

In determining the loading on the tank Flügge makes the following assumptions:-

- (i) The water pressure acting on the conical bottom is transferred straight through the wall into the ground, and hence does not enter the problem.
- (ii) The weight of the cylinder is assumed to be $P = 550 \text{ lb/ft}$ acting as a point load at the base of the cylinder.
- (iii) The load P causes a vertical soil reaction on the conical bottom given by,

$$\begin{aligned} p_2 &= \frac{550(2\pi)(30)}{\pi(30)^2} \\ &= 36,67 \text{ lb/ft}^2 \end{aligned}$$

which is assumed to act perpendicular to the conical bottom.

The first and third assumptions constitute what appears to be a gross simplification of the actual conditions in the tank bottom. However, as we shall see in the following paragraphs, there is little that can be done within the scope of the present work to improve these assumptions.

If the slope of the tank bottom is small then the tank bottom may be treated in the manner of a circular plate resting on an elastic soil foundation, and subject to a uniformly distributed water pressure p_w and a vertical force V (Fig. 4.19a). Such a procedure would be extremely complex to apply and it

* Ref. [1], p 380

**The program CONFRU is dimensionless and thus independent of the particular units used, provided they are consistent, e.g., N - m or lb - ft.

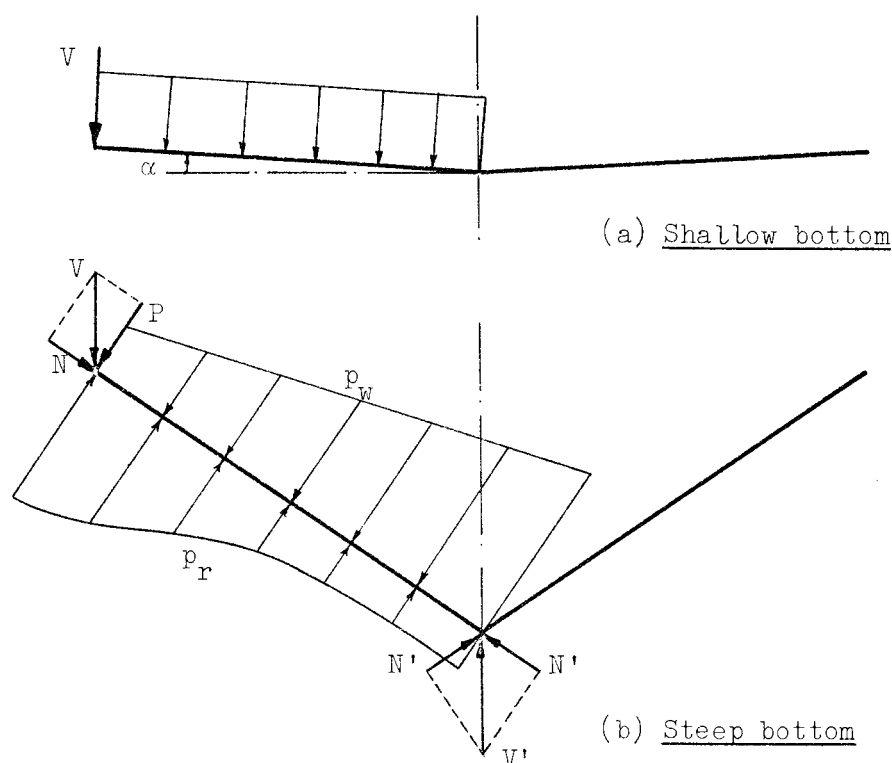


Fig. 4.19

is doubtful whether the end results would justify the effort.

When the slope of the tank bottom is steep* the soil may be considered as supplying a reactive pressure p_r on the tank bottom, not only proportional, as in the case of an elastic foundation, to the deflection of the tank bottom, but also statically connected in some way with the water pressure p_w and the vertical load V (Fig. 4.19b). The axial component N may in this case be fairly substantial, and although part of this force may be transferred to the soil before it reaches the cone apex, it will nevertheless cause a resultant vertical reaction V' at the apex.

The reaction V' suggests the inclusion of a footing at the apex of the conical bottom. With a footing present the conditions of rigid fixity are satisfied (for axisymmetric deformation the conditions of zero rotation and horizontal displacement at the cone apex are already satisfied), and the elastic kinematic boundary conditions may be replaced by a built-in condition at the apex.

With the apex rigidly fixed it is easier to envisage the deflected shape of the tank bottom and to proportion p_r along these lines. Furthermore, the

*In practice the conical bottoms of sludge digesters have slopes of between 30° and 40° .

total reactive pressure need not necessarily equilibrate the water pressure p_w plus the load P , since part of the latter two forces may be transferred directly to the apex footing. Clearly, however, the distribution of p_r remains, in the absence of a detailed investigation, a more or less arbitrary choice.

It is relevant to the discussion of the results to outline briefly the theoretical method of solution employed by Flügge. Basically the solution consists of recognising two redundancies at the cylinder-cone junction, viz., a moment M and a horizontal force H (Fig. 4.20). Expressions for the

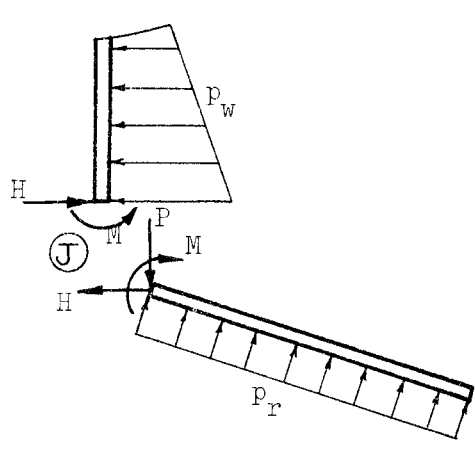


Fig. 4.20

radial deflection w and the rotation χ at J are then derived in terms of the known loading p_w , p_r and P (the self-weight of the cylinder), and the unknowns M and H , for the cylinder and cone separately. By equating the deflections and rotations at J two equations are obtained which may then be solved for M and H .

It is interesting to note again that the solutions for M and H obtained by Flügge are incorrect. This we ascertained by working independently through the example. For all comparisons therefore the writer's own theoretical solutions will be used. Also, for the benefit of the reader who is more familiar with the S.I. units the equivalent stresses in this system are given for all results.

Discussion of results: Two analyses, the one using twice as many elements as the other, have been performed, for which the displacements and rotations at corresponding nodes are effectively identical, the two sets differing only in the sixth significant figure. Convergence of displacements has thus clearly

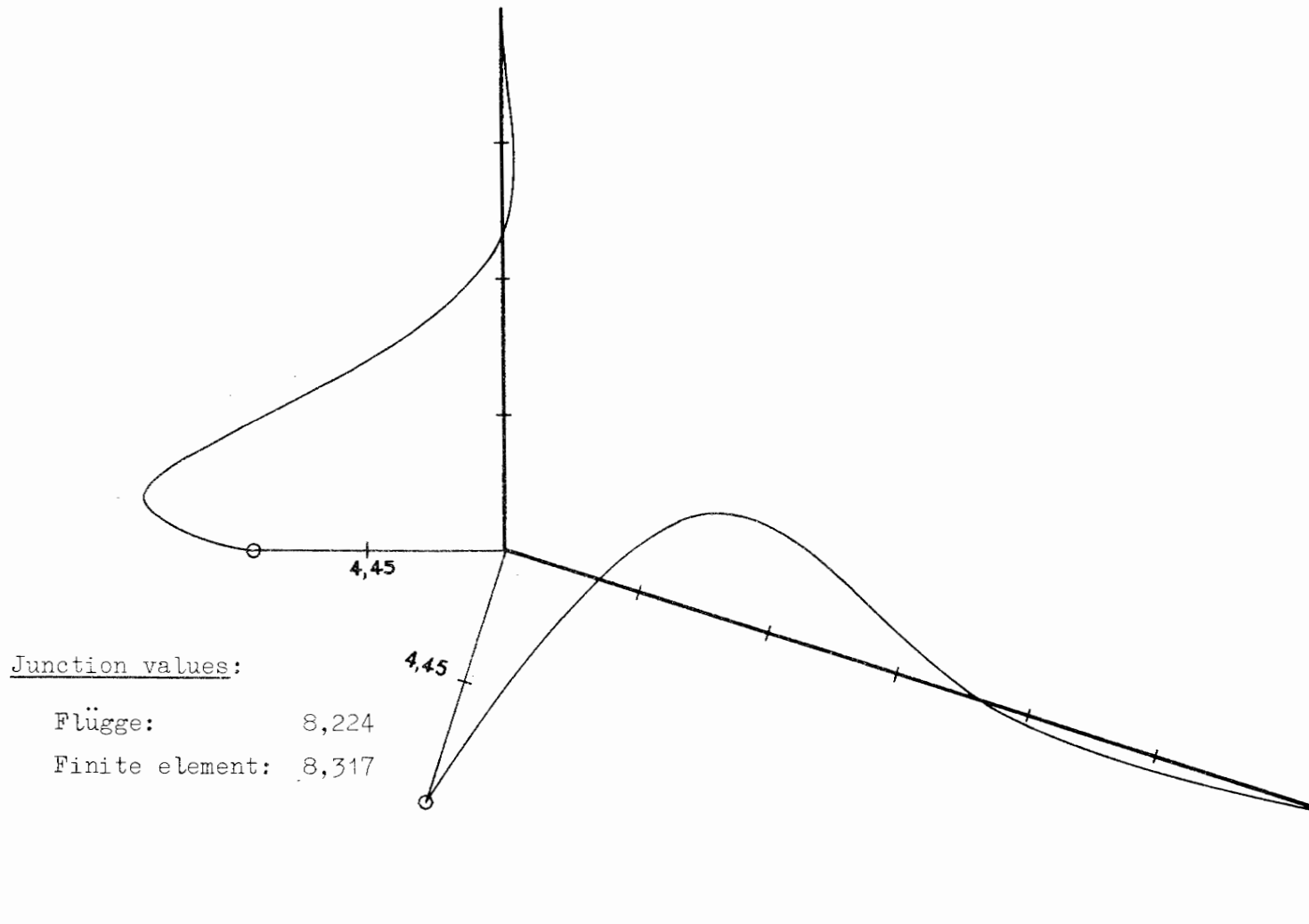


Fig. 4.21: Meridional moment M_s [kNm/m]

been obtained.

The meridional moments M_s given by both finite element solutions are shown in Fig. 4.21 (the solutions coincide for the scale used here). The shape and proportions of this diagram are, in so far as can be judged from Flügge's diagram, identical to the latter. The actual values at the cylinder-cone junction for the theoretical and finite element solutions are given in the following table.

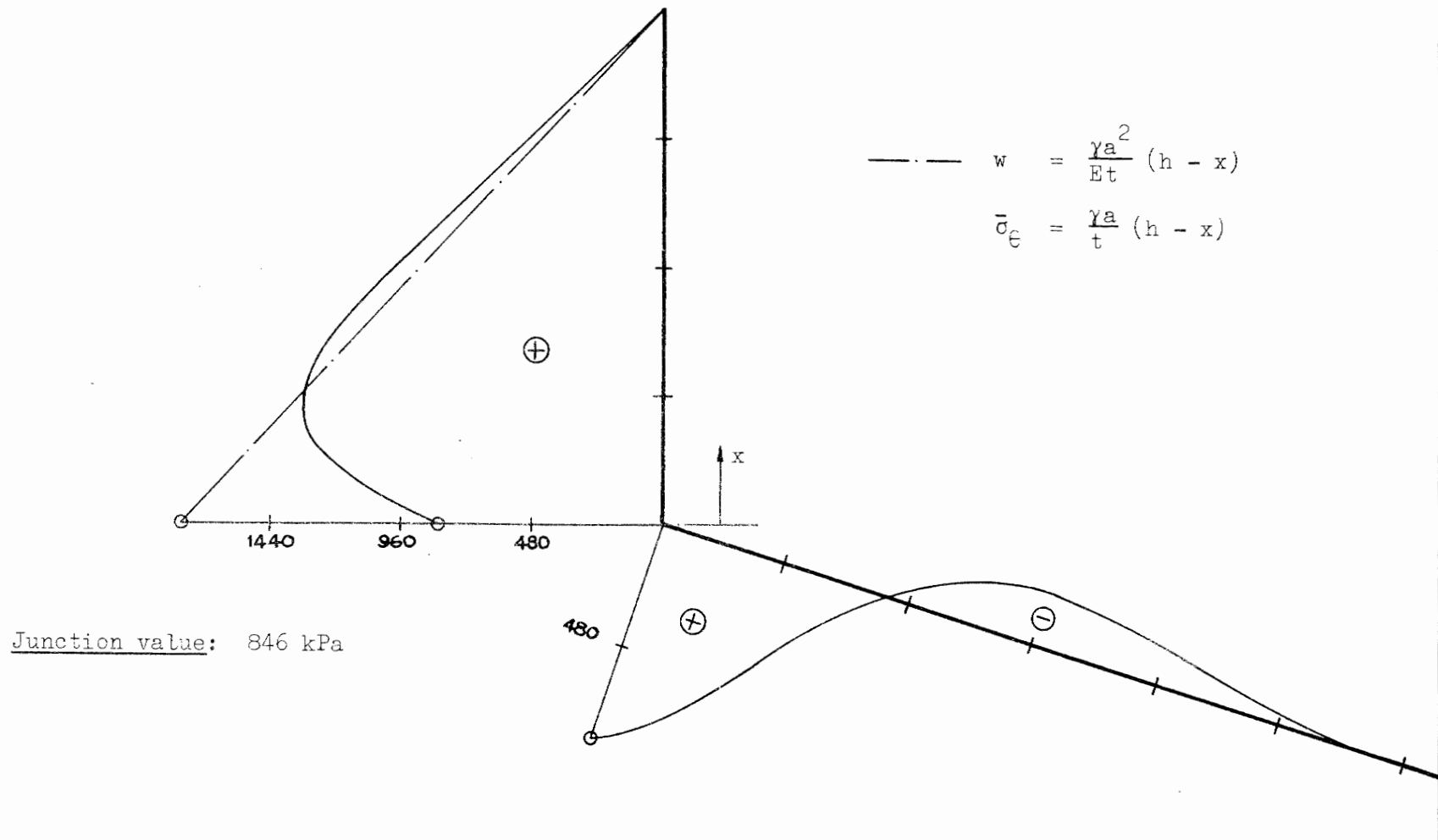
Table 4.7: Meridional Moment M_s at the Shell Junction

Units	Theoretical	Finite Element		Percentage Error	
		L/t = 1/4	L/t = 1/2	L/t = 1/4	L/t = 1/2
ft-lb/ft	1849	1870	1874	1,14	1,35
kNm/m	8,224	8,317	8,335	"	"

The finite element solutions differ only very slightly and the difference between the finite element and theoretical solutions (93 Nm/m) is clearly of no practical significance. The relatively high percentage errors are therefore not a true reflection of the practical value of the results, which are from this point of view very good.

It would be interesting to compare the moments in the cylinder of the present example with those in the water-filled tank of Example 3. However, such a comparison should be avoided since the moments at the base of the cylinder in the present example are very much affected by the point load at the edge of the cone. This edge load is the reason why the moments do not change abruptly at the base of the cylinder, as they do in Example 3. Hence the present results should not be taken as representative of the moments in a cylinder which is partially restrained at its base.

It should also be pointed out that although the moments given for the conical part of the tank are correct, they are not necessarily the true moments that would occur in practice, since very much simplified assumptions have been made for the loading. It seems unlikely, for instance, that there will be such a large moment causing tension on the inside of the cone when



Junction value: 846 kPa

Fig. 4.22: Hoop stress σ_e [kPa]

there is a large water pressure bearing down on this section.

The distribution of the hoop stress σ_{θ} is shown in Fig. 4.22. Since $v = 0$ the hoop stress in the cylinder is directly proportional to the radial displacement w (c.f. Eq. 4.1), so that the σ_{θ} diagram serves also as radial displacement diagram. (The same does not apply to the conical bottom since the hoop stresses there depend on both the radial and vertical displacements).

The hoop stresses in the cylinder are much as we would expect, being linear over the upper part of the cylinder and terminating in a relatively large value at the base, the latter result being due to the large radial displacement at this point. The values over the linear portion, however, are slightly larger than those given by the straight line distribution,*

$$\bar{\sigma}_{\theta} = \frac{\gamma a}{t}(h - x) \quad (4.7)$$

The large hoop stresses at the upper edge of the cone are again caused by the point load acting at this edge. Note that the marked similarity between the M_s and σ_{θ} distributions in the conical bottom is of no particular significance since the meridional bending and hoop stresses act in planes perpendicular to each other.

The axial stress distribution in the conical bottom is shown in Fig. 4.23, the axial stresses in the cylinder being clearly zero. The axial stresses in the conical bottom may easily be explained by referring back to the free-body diagram shown in Fig. 4.20. The outward horizontal reaction H at the edge of the conical bottom is greater than the vertical load P . Hence the resultant of these two forces acts so as to cause tension at the edge of the conical bottom. However, as an edge disturbance, the effect quickly dies out and in the remainder of the conical bottom the horizontal component of the pressure p_r causes axial compression. Both these effects are clearly shown in the finite element solution.

In the present example the theoretical solution for the horizontal reaction is $H = 890 \text{ lb/ft}$ (13 kN/m). Summing the components of H and P in the direction of the conical bottom we find the theoretical solution for

*See Eq. (4.3) and related discussion.

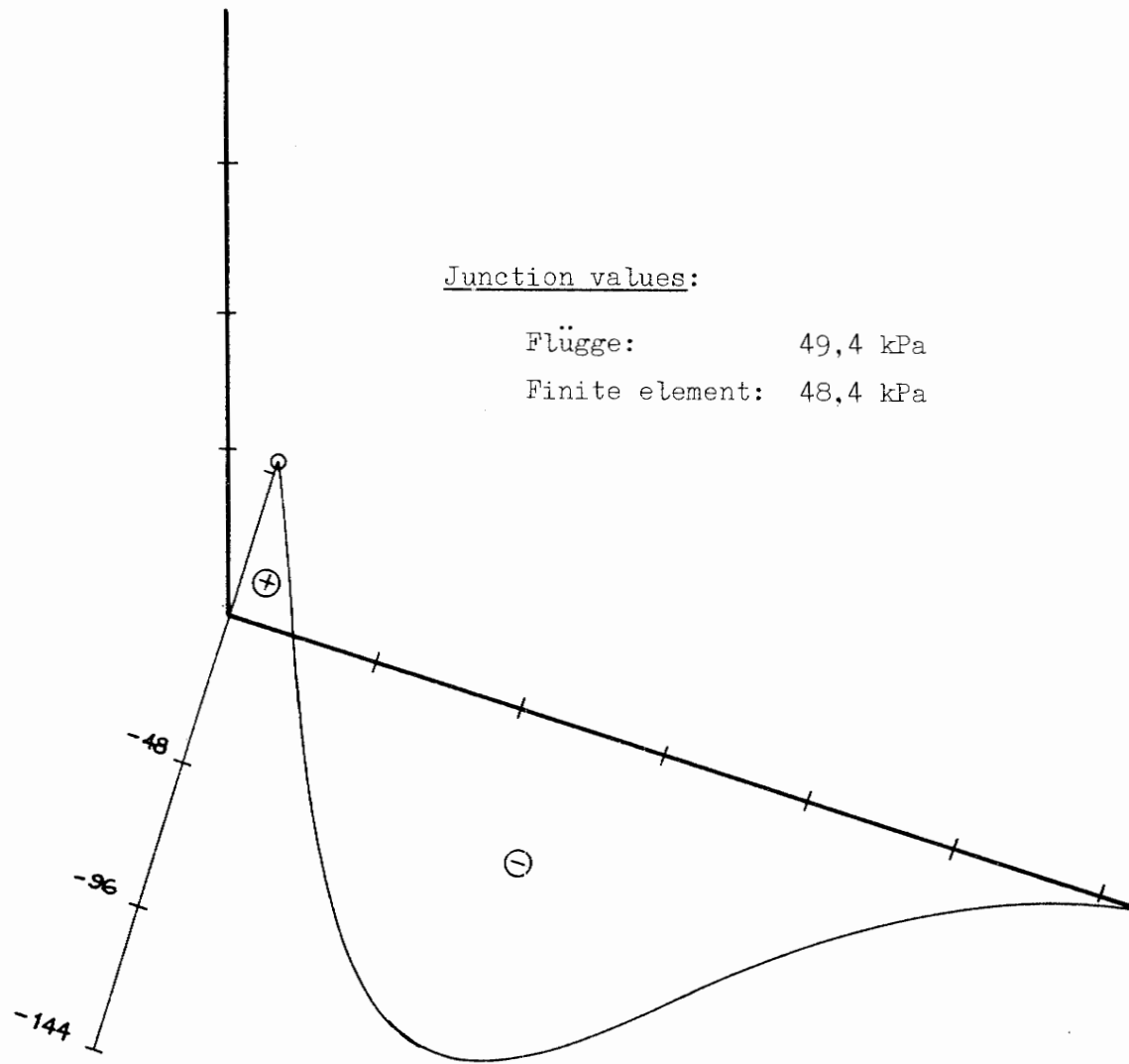


Fig. 4.23: Axial stress σ_e [kPa]

the axial stress at the edge of the conical bottom to be 1029 lb/ft^2 (49,4 kPa). The value obtained from the finite element solution is 1010 lb/ft^2 (48,4 kPa). Considering the complex conditions existing at the cylinder-cone junction, the agreement is extremely good.

4.3.3 Conclusions II

A considerable part of the discussion of the preceding examples has been devoted to enlarging upon various stress and moment solutions. Some of the more common discrepancies which may occur in the results have been pointed out and explained in terms of the mechanical behaviour of the shell, so as to make the general interpretation of the stresses and moments meaningful.

Apart from this the following specific conclusions have been arrived at:

- (a) From the practical point of view the results obtained for both examples are excellent. For instance, in Example 3, where the complete theoretical meridional moment solution is available, the plots of the finite element and theoretical solutions are indistinguishable. In particular, the percentage errors at the shell junctions are:

cylinder-plate ($L/t = 1$): error = 0,50%

cylinder-cone ($L/t = \frac{1}{2}$): error = 1,35%

We conclude therefore that shell junctions present no special problem and that reasonably accurate results can be obtained without excessive refinement of the element subdivision. Furthermore, results have shown that the finite element analyses are capable of maintaining an excellent degree of continuity in meridional moments at the junction, and that there is an accurate transfer of force across the junction.

- (b) Although the surface force and body force load vectors are identical for thin shells, there are distinct advantages to be gained by using the body force formulation where the self-weight of the structure is to be included. These advantages are:
- (i) data input is significantly reduced;
 - (ii) the amount of computation within the program is reduced since the pressure distribution due to the self-weight is not required.

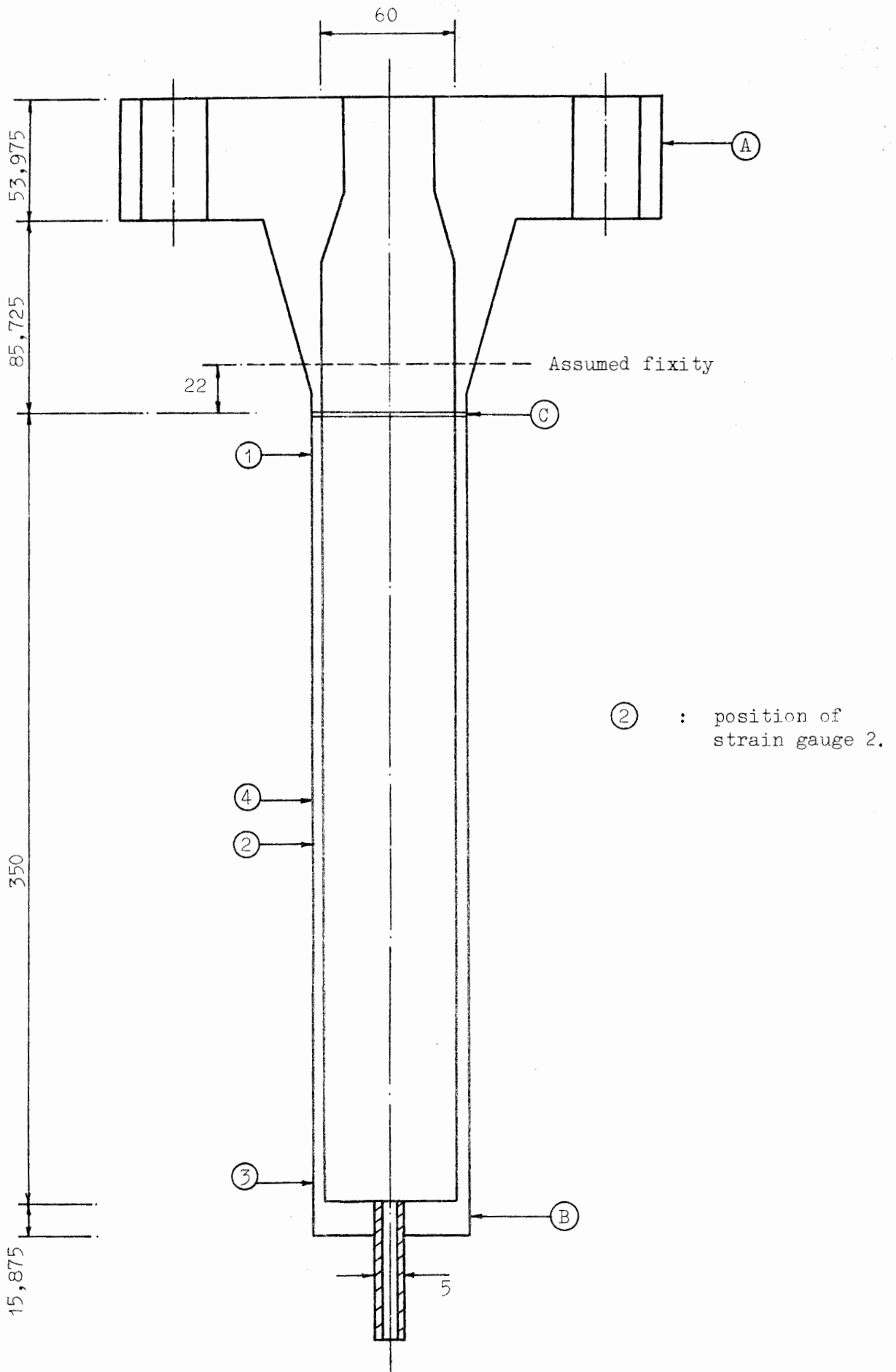


Fig. 4.24: Section through pressure vessel

Scale: 1:2,5 (Dimensions in mm)

4.4 Example 5: The Thin Shell Analysis of a Thick Pressure Vessel: Comparison with Experimental Results

Although the vessel is, as we shall see, a thick shell, this does not prevent us from analysing it as a thin shell in order to compare the results with those obtained from the elementary thin shell equation.

It is also, however, of interest to compare the thin shell finite element results with the experimental results, as well as with the results obtained from elementary thick shell equations, and thereby determine to what extent the thin shell approximation of a thick shell is valid.

The example is of particular relevance since the majority of pressure vessels are axisymmetric shells of revolution, many of which are, by definition, bordering between thick and thin shells.

Description of the analysis

The pressure vessel shown in Fig. 4.24 forms part of a pilot plant for a wine distilling process.* The upper part of the vessel consists of a very thick flange (A) which is bolted to a similar flange (not shown) containing a narrow inlet valve. A similar valve is welded into the end plate at the bottom of the cylinder (B). The vessel is made initially in two separate parts which are welded together at C before final machining takes place.

The relevant technical data for the vessel are given in the following table:

TABLE 4.8

Material:	Austenitic Stainless Steel
Yield Stress:	207 MPa
Young's Modulus:	$E = 188,9 \text{ GPa}$
Poisson's Ratio:	$\nu = 0,3$
Test Pressure:	$p = 26,89 \text{ MPa}$

The vessel is by definition a thick shell since the ratio of internal diameter to shell thickness is,

*This vessel is one of four similar vessels which the Departments of Civil and Mechanical Engineering at the University of Cape Town co-operated in analysing during 1973. See Test Reports, Ref. [21].

$$\frac{D_i}{t} = 10,9 < 20$$

Nevertheless, a comparison of the elementary thick and thin shell equations* for the hoop stress in a cylinder (at a section remote from edge disturbances) shows that the hoop stress obtained from the thin shell equation using the mean diameter of the cylinder wall is very close to the maximum hoop stress at the inside face of the wall obtained from the thick shell equation. The calculations are as follows:

The hoop stress at a section through a thick cylinder wall having a diameter d is given by,

$$\bar{\sigma}_\theta = \frac{(D_o^2 + d^2) D_i^2}{(D_o^2 - D_i^2) d^2} \cdot p \quad (4.8)$$

where the parameters are defined in Fig. 4.25.

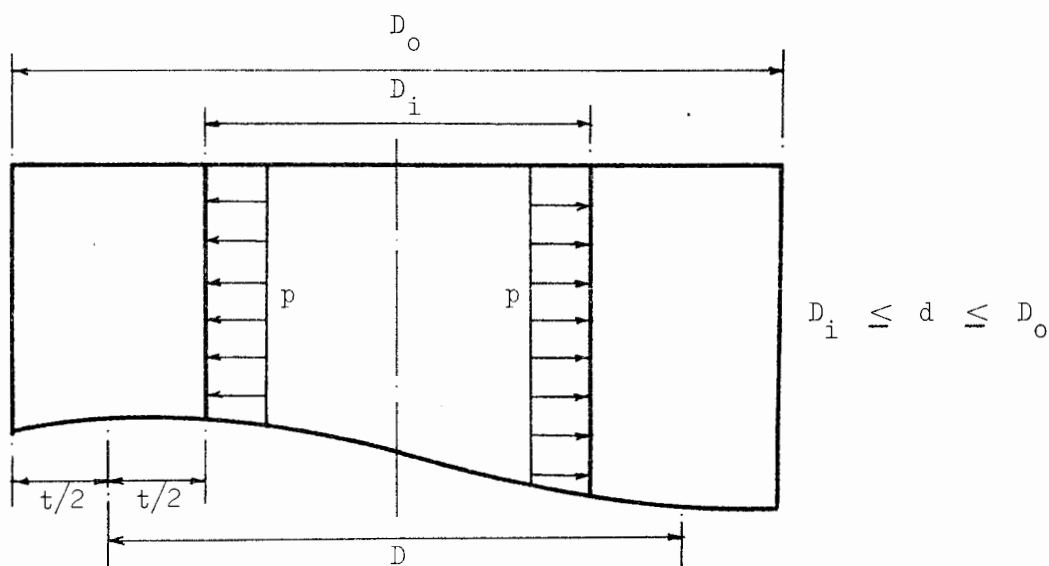


Fig. 4.25

If we write $D_o = D_i + 2t$ and take $D_i/t = 10,9$, then for $d = D_i$ the maximum hoop stress at the inside face of the cylinder is,

$$\bar{\sigma}_\theta = 5,992 p$$

The hoop stress in a thin shell is assumed to be constant over the thickness and is given by,

*The elementary thick shell equations used here are obtained from Ryder [22], p 270.

$$\sigma_{\theta} = \frac{pD}{2t} \quad (4.9)$$

Writing $D = D_i + t$ and taking $D_i/t = 10,9$ we obtain,

$$\sigma_{\theta} = 5,950 p$$

which differs from $\bar{\sigma}_{\theta}$ by a mere 0,7%.

The above result was of particular value since in the experimental work strain gauges could be fixed only to the outside of the cylinder and could thus only estimate the minimum hoop stresses.

For the experimental analysis four 5 mm gauge length electrical strain gauges were cemented to the cylinder in the positions shown in Fig. 4.24. Gauges 1, 2 and 3 measured the hoop strain and gauge 4 the axial strain when the vessel was filled with oil at the required test pressure. The stresses were then calculated from the measured strains using Eqs. (2.15a,b); in the calculations the axial strains were assumed to be constant throughout the length of the cylinder.

For the finite element analysis the upper flange was considered as providing full fixity for the cylinder; the actual point of fixity was chosen more or less arbitrarily at a point 13 mm up from the bottom of flange neck. At the other end of the vessel a small hole was left in the end plate, its diameter being that of the internal diameter of the valve.

Three analyses were carried out using different element L/t ratios and the results presented here are from what appears to be the convergent solution. The element subdivision for this analysis is:

Cylinder: 123 elements @ 0,003 ; $L/t = 0,54$

End plate: 5 elements @ 0,00645; $L/t = 0,41$

Discussion of results

We begin by considering the cylindrical part of the vessel as a thin shell, (this does not in fact seem to be an unreasonable assumption in so far as bending is concerned, since the cylinder wall is very thin), for which the free-body diagram is as shown in Fig. 4.26.

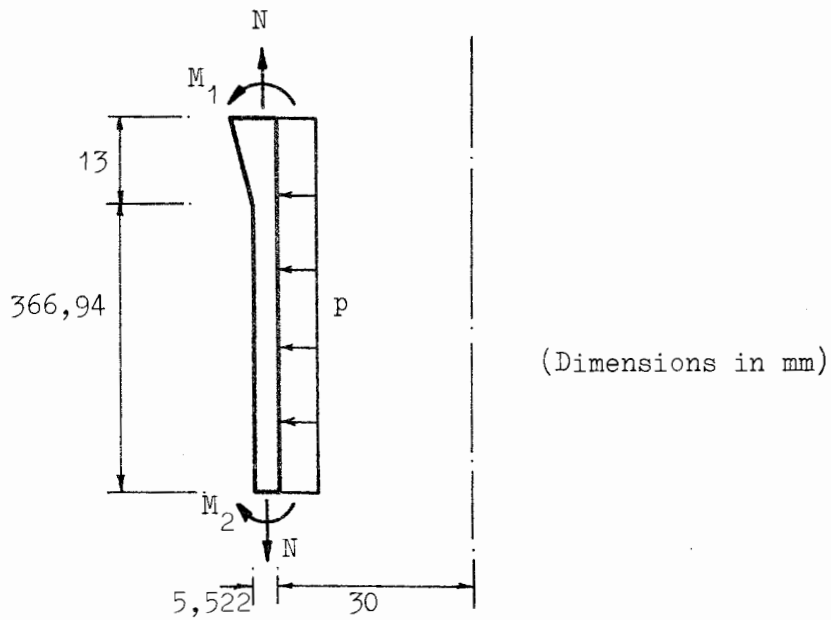
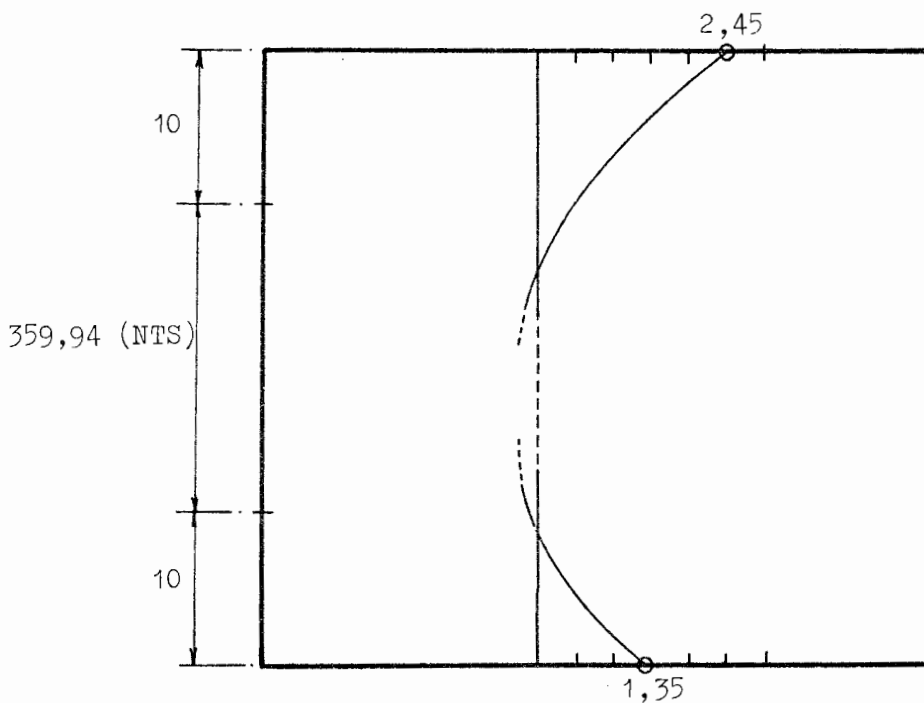


Fig. 4.26

The meridional moments M_1 and M_2 arise from the rotational constraints imposed by the rigid fixity at the upper end of the cylinder and the thick end plate at the lower end. According to thin shell theory these moments give rise to local edge disturbances which quickly die out. This is clearly shown in the finite element results for the meridional moment in the cylinder (Fig. 4.27); notice that the vertical scale is contracted and that over a length constituting 95% of the cylinder, the moments are effectively zero.

Fig. 4.27: M_s in cylinder [kNm/m]

element result is again almost identical to the thin shell theory result. The difference between the thick and thin shell results is due to the fact that for the thin shell calculation, we put $D_i = D$ in Eq. (4.10); this is equivalent to the incorrect assumption that the pressure on the end plate acts over the area contained with the mean diameter D . The experimental result lies conveniently between the thick and thin shell results, and allowing for the fact that the finite element and experimental results do include the Poisson effect, the all round agreement of results is very good.

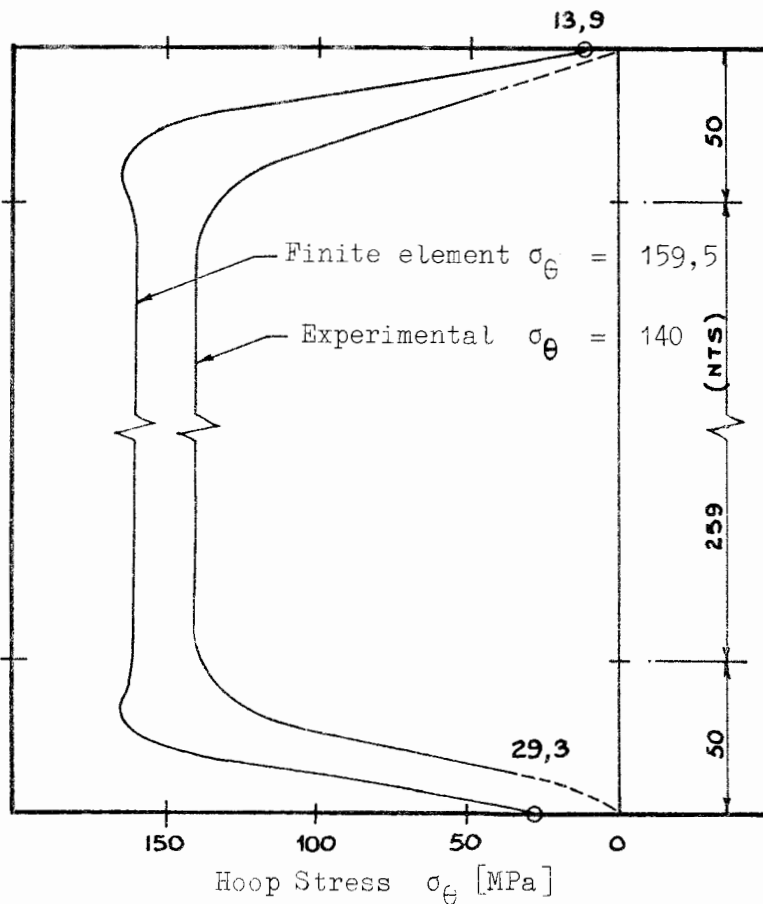


Fig. 4.28

We return now to the regions in which the edge disturbances have a significant effect, and examine the hoop stresses at gauge points 1 and 3. The finite element and experimental results are compared in Fig. 4.28, where the experimental results have been assumed to follow roughly the same distribution as the finite element results. On the basis of this assumption it seems likely that the finite element results continue to give the maximum hoop stress in the cylinder. No adequate explanation can be found for the peaks (or 'humps') in the finite element results at either end of the cylinder, but these peaks probably give rise to a general overestimation of the stresses at the very ends to the cylinder.

We conclude therefore that:

- (i) over regions sufficiently remote from edge disturbances, the finite element solution may be used to predict accurately the maximum hoop stresses and average axial stresses in a thick shell wall, and
- (ii) over regions affected by edge disturbances, the finite element results may be assumed to overestimate slightly the maximum hoop stresses.

4.5 Branched Shells of Revolution

Pian et al^[20] have analysed a complicated branched shell of revolution using the well known SABOR 4 program, and conclude with the statement that, while their results seem plausible, no reliable independent solution is available and so their results are merely provided for possible future comparison. Unfortunately, the program CONFRU cannot be used to provide comparison results since the problem is beyond the reasonable scope of the program in its present state; furthermore, no other solutions for shells of revolution could be found.

The absence of independent solutions for comparison is, however, of little consequence since there are more rigorous and reliable methods of showing that branched shell solutions given by CONFRU are correct.* These methods are outlined in the following section, and are based on the following principle:

If for a given structure a computer program is capable of correctly formulating the system stiffness matrix $[K]$ and the system load vector $\{F\}$ and if the inverse $[K]^{-1}$ is calculated correctly, then it follows that the correct displacements $\{q\}$ must be obtained, since

$$\{q\} = [K]^{-1} \{F\} \quad (4.11)$$

It is assumed in this principle that $\{q\}$ will always be unique.

4.5.1 The Philosophy for testing the branched shell solution

In the preceding five examples it has been shown that the program CONFRU

*For the purposes of this section 'correct' will be taken to mean 'free from, or free of the effects of, logical error'. It is assumed that such solutions are capable of being improved through the process of convergence.

is capable of correctly analysing various single-wall shells of revolution comprising conical frustra, circular plates and circular cylinders, as well as simple combinations of these basic shapes. Closed shells and shell junctions have been found not to create any particular problems.

It has also been shown which numerical factors influence the accuracy of the solution and its convergence, such as the method of numerical integration and the element aspect ratio, and what the general effect of these factors is.

We are therefore satisfied that CONFRU is capable of formulating and solving any single-wall problem correctly.

Now in the branching problem the system stiffness matrix undergoes various major modifications over and above those required in single-wall problems. These modifications have already been investigated and classified into five 'branch types', so that, given an arbitrarily branched shell of revolution, we know exactly what form the system stiffness matrix must assume.

However, we cannot be sure that the computer has set up such a matrix correctly unless we know the actual values of the individual stiffnesses beforehand. Since it is virtually impossible to calculate these stiffnesses by hand (because of the lengthy numerical process involved), there is effectively no direct method of checking that the system stiffness matrix of a branched structure is being set up correctly by the computer.

But suppose that we have analysed the two structures shown in Fig. 4.29(a,b) under some arbitrary loading, and that the solutions are known to be correct. Suppose also that during solution we obtain the actual numerical values of the individual stiffnesses in each of the stiffness matrices $[K_1]$ and $[K_2]$ for these structures. Clearly, if we combine these structures to form the branched structure shown in Fig. 4.29(c), then the system stiffness matrix of the branched structure $[K^*]$ will consist basically of a combination of the stiffness matrices for the two sub-structures. In fact, every single individual stiffness in $[K^*]$ can always be obtained from the corresponding substructure stiffness matrices $[K_1]$ and $[K_2]$.

Hence, knowing the form which $[K^*]$ must assume, and the numerical values of $[K_1]$ and $[K_2]$, the numerical values of $[K^*]$ can be checked exactly.

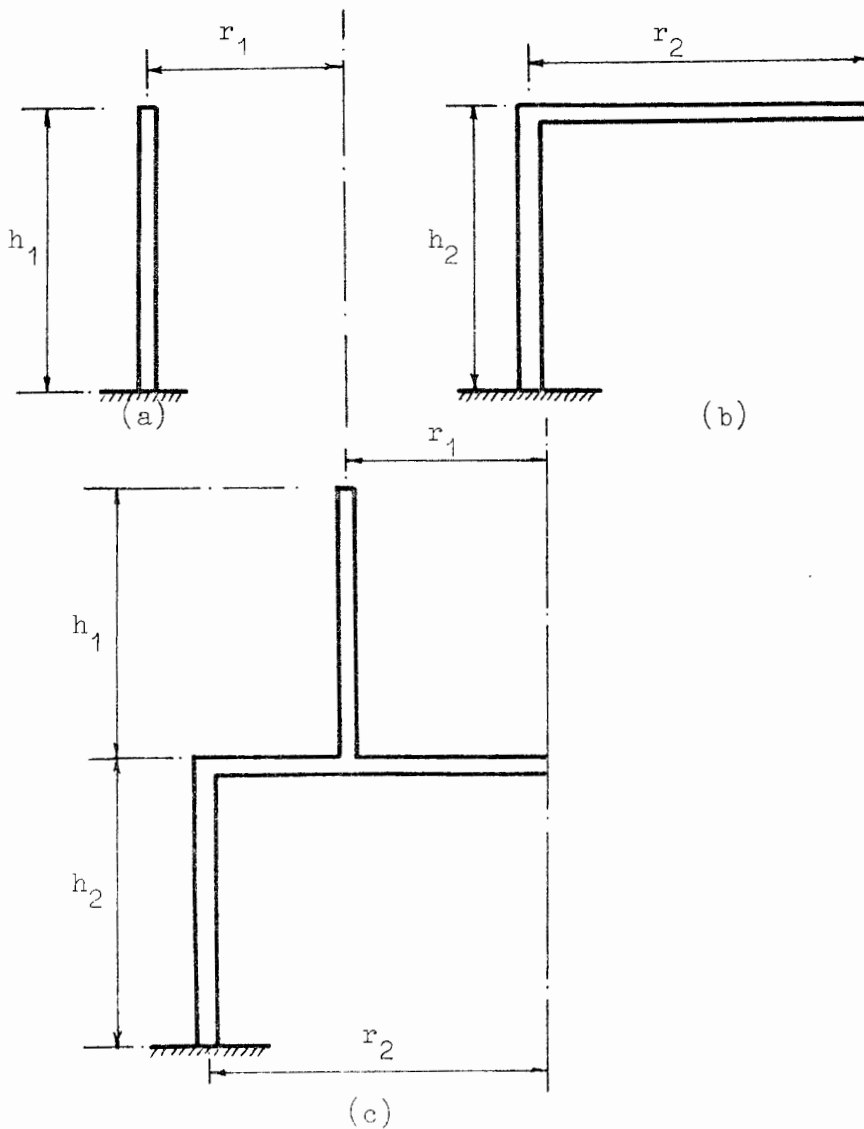


Fig. 4.29: Development of a branched shell from two single-wall shells

Moreover, in so far as $[K_1]$ and $[K_2]$ are correct, $[K^*]$ must also be correct.

Precisely the same procedure may be used to check the load vector $\{F^*\}$ of the branched structure. In this case, however, the process is even simpler since the numerical value of the load vector remains unchanged by any branching in the structure.

There remains then to check that the equation solution subroutine functions correctly and efficiently when $[K^*]$ contains off-diagonal submatrices (as can only occur when the shell is branched). This can be done by substituting the solution back into the $[K^*]$ to obtain the original load vector.*

* This process requires a duplicate copy of $[K^*]$ to be stored. Hence the back-substitution procedure is, for the sake of storage efficiency, not a standard feature of CONFRU.

Each row of $[K^*]$ contains a maximum of 15 non-zero elements so that the recovery of each value of the load vector through back-substitution requires at most 15 multiplications and additions. Hence the rounding error in back-substituting is negligible (the more so because double precision arithmetic is used throughout), and any error which may occur in the back-substituted load vector can be taken to indicate error in the original solution. (Difficulty may be encountered in determining whether such error in the original solution is logical or due to rounding.)

In general, however, logical and rounding errors should be clearly distinguishable, so that back-substitution provides a reliable check on the validity of the equation solution procedure.

A further general check on the validity of the actual solution $\{q\}$ is to analyse the structure several times, each time reordering the node numbering scheme. This has the effect of changing the form of the $[K^*]$ matrix, while obviously not affecting the solution. Hence, if for each such analysis identical solutions are obtained, then this constitutes a necessary (but not sufficient) condition that the solution is correct.

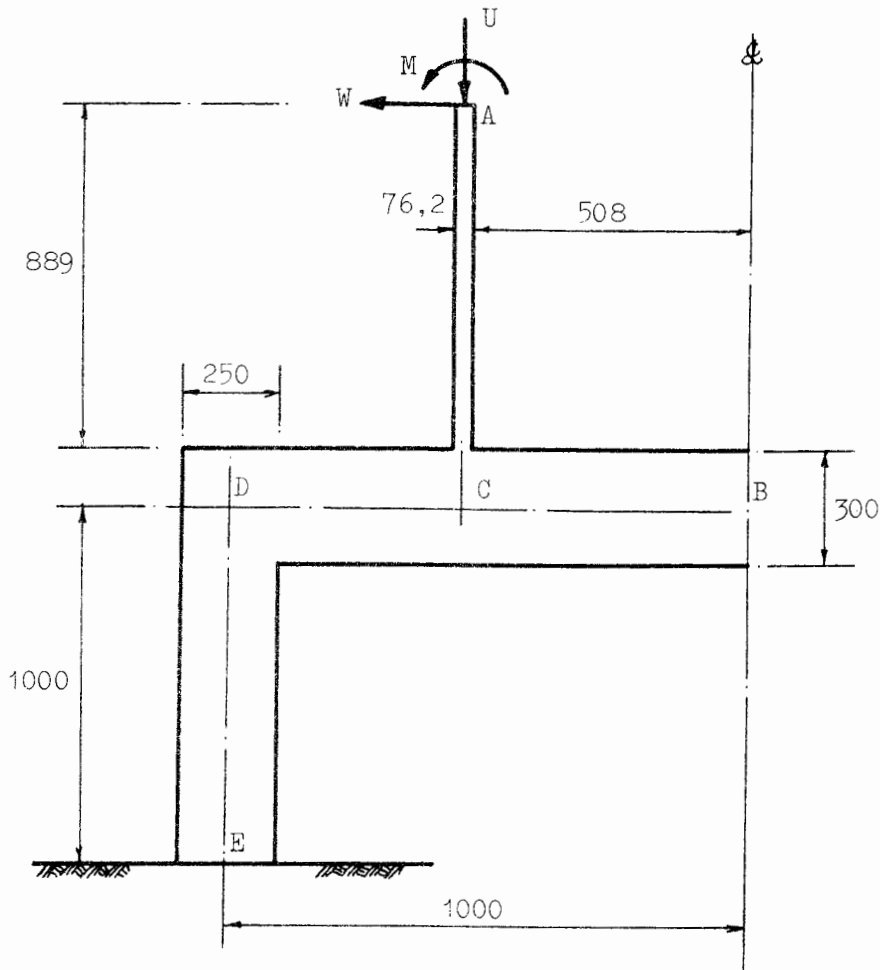
Once the correct displacement solution has been obtained it is a simple matter to check that the stresses and moments are being calculated correctly. This can be done by spot hand calculations since the stress and moment equations are reasonably simple. Checking of the stresses and moments should however be unnecessary since these calculations are completely independent of any branching in the shell.

A final superficial check on the validity of the actual stresses in the branched shell can be made by constructing it in such a way that the stresses in the branched structure are very similar to those in the component sub-structures, when analysed independently. If such correlation is actually obtained it tends to lend plausibility to the results. Plausibility however should never be taken as conclusive.*

Clearly it is both unfeasible and unnecessary to check every branched shell solution in the manner described in this section. However, since any branched shell can be built up of only five branch types (in any combination

* During the initial testing of branched shell solutions, extremely plausible results were often obtained, which later proved to be incorrect.

TABLE 4.10



Loading:

$$M = 4,448 \times 10^3 \text{ Nm/m}$$

$$U = 250 \times 10^3 \text{ N/m}$$

$$W = 264 \times 10^3 \text{ N/m}$$

Material Properties:

$$E = 1,0$$

$$\nu = 0$$

Element Subdivision:

AC: 70 elements @ 0,0127 m; $L/t \div 1/6$

BC: 7 " @ 0,0635 m; $L/t \div 1/5$

CD: 8 " @ 0,0615 m; $L/t \div 1/5$

DE: 20 " @ 0,0500 m; $L/t \div 1/5$

Analysis I.D. No.	Branch Types	Remarks
6/B1/1	2 and 5	For node numbering see Fig. 4.30
6/B2/1	3	" " " see Fig. 4.31
6/B3/1	2 and 5	" " " see Fig. 4.32
6/D/01	-	Lower substructure, see Fig. 4.33
C/C/04	-	Upper substructure, see Example 1

or number) it will suffice to check five arbitrary combinations of these five branch types in order to satisfy ourselves that the program is of general applicability.

In the following section then we will take two hypothetical branched structures which have already been analysed, and apply this method of testing to them.

4.5.2 Example 6: The analysis of a single-branch shell of revolution

Specific objectives:

- (i) To confirm that the system stiffness matrix and load vector of the branched shell are correctly formulated by comparing them with stiffness matrices and load vectors of the component substructure. To confirm also that the equation solution procedure functions correctly and efficiently.
- (ii) To compare the meridional moments in the branched structure with the corresponding moments in the component substructures.

Description of the analyses

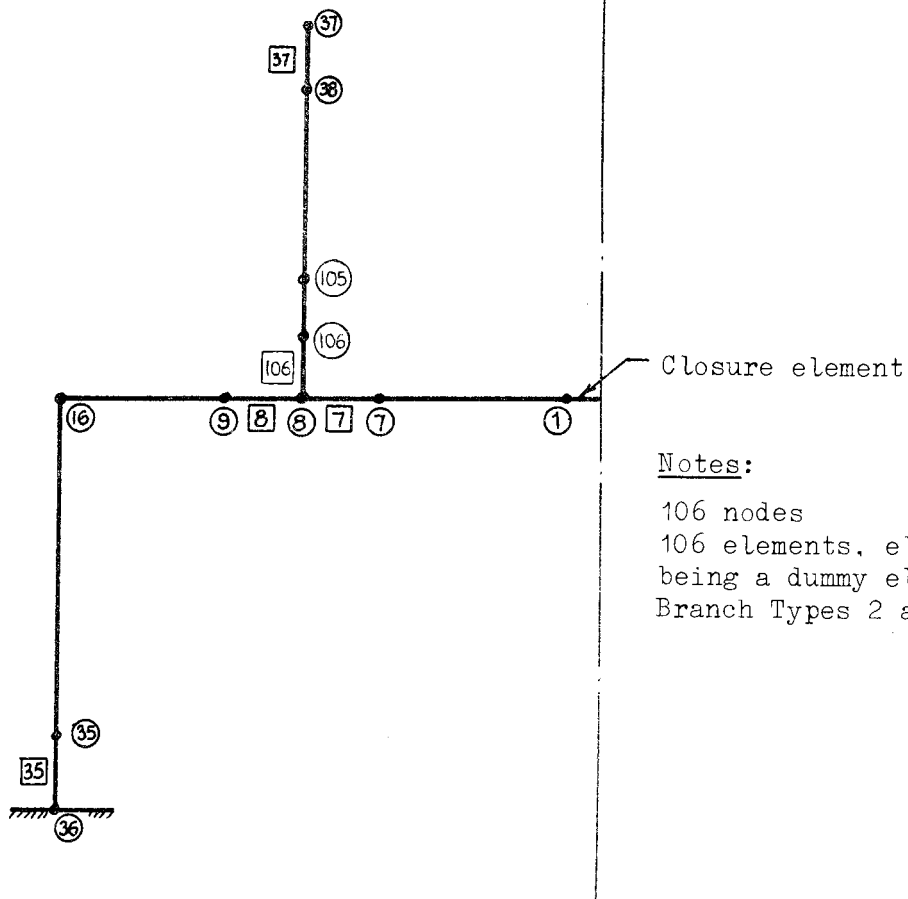
The first branched shell which we will analyse is shown in Tabel 4.10.

The upper cylinder and the edge loads U , W and M are identical to Example 1, and the circular plate and lower cylinder together (referred to as the lower substructure) are of the same form as Example 3. The dimensions of the lower substructure have been chosen so as to make it as stiff as possible relative to the upper cylinder, while maintaining a reasonable balance of proportions for the structure as a whole.

We therefore have two simple substructures for which CONFRU is known to give correct solutions (and hence correct system stiffness matrices and load vectors), and which can therefore be used to test the branched shell solution.

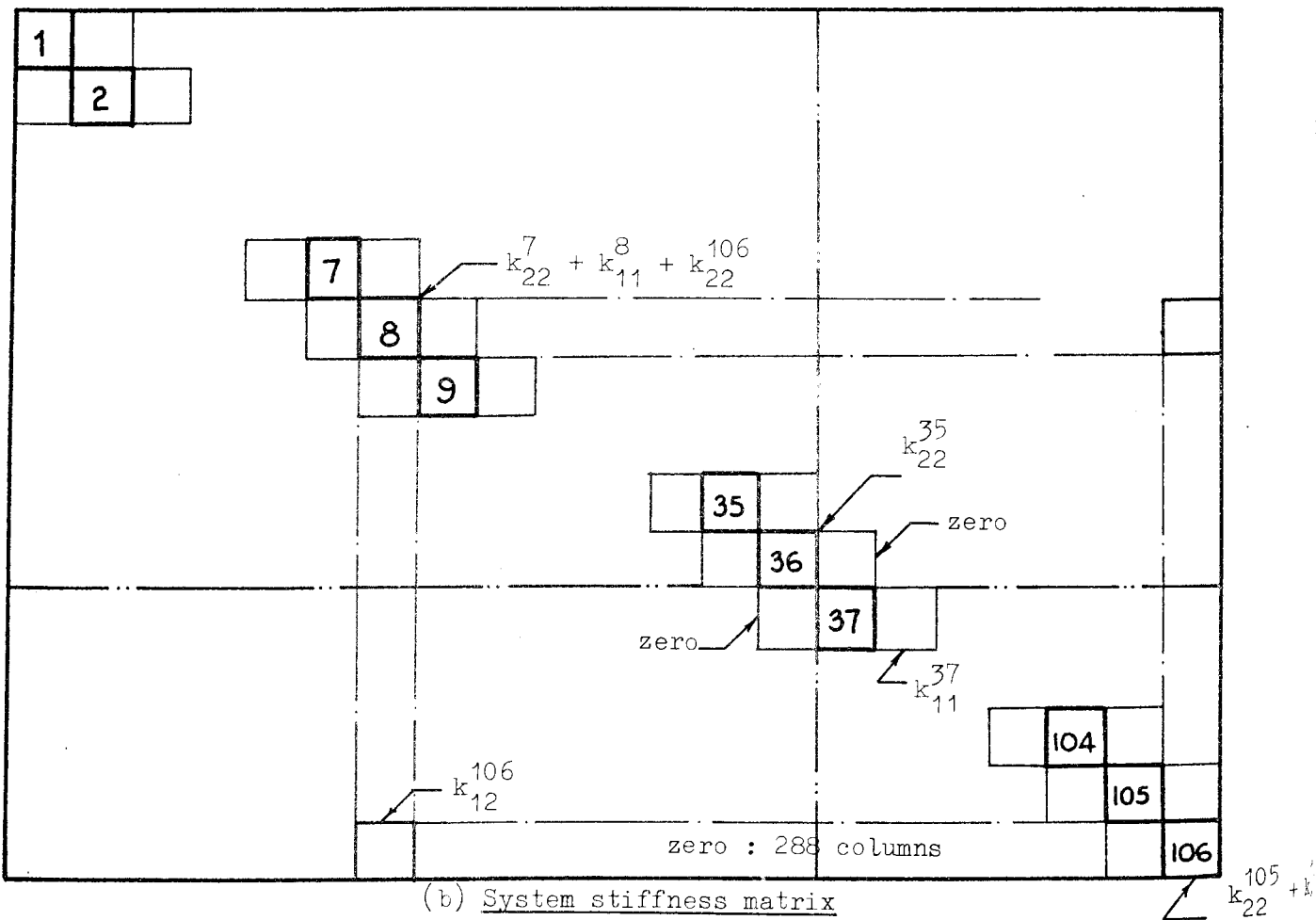
Three analyses of the branched shell have been performed each having the same physical element subdivision, but with different node numbering schemes, resulting in the use of three different branch types (2, 3 and 5).

It will be noticed, however, that analyses 6/B1/1 and 6/B3/1,



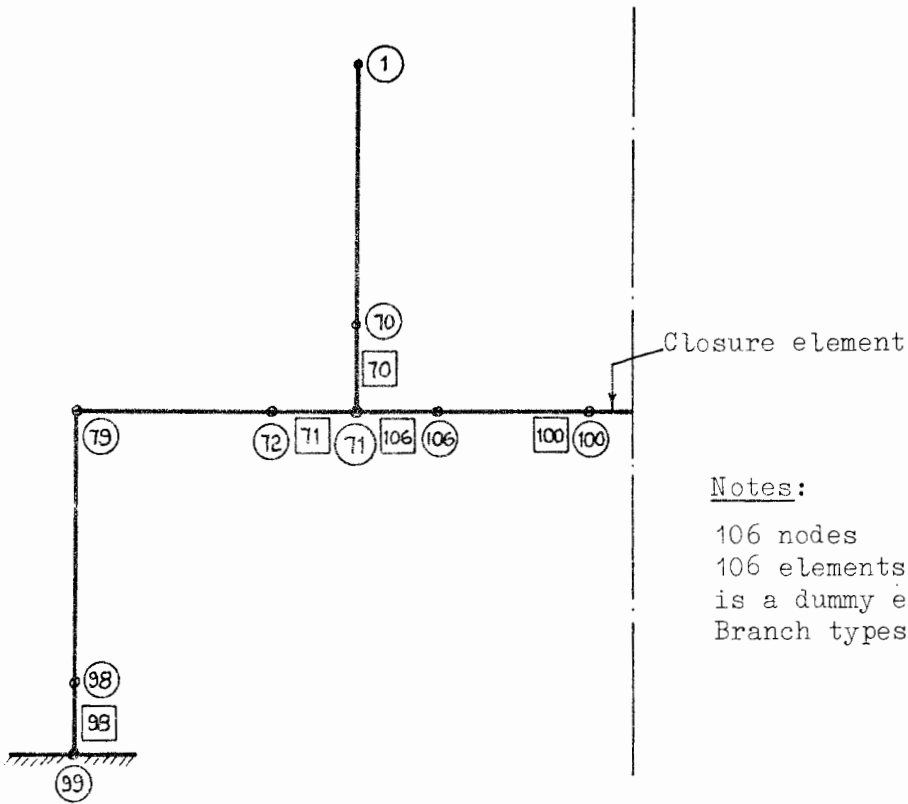
Notes:
 106 nodes
 106 elements, element 36 being a dummy element
 Branch Types 2 and 5.

(a) Node and element numbering schemes



(b) System stiffness matrix

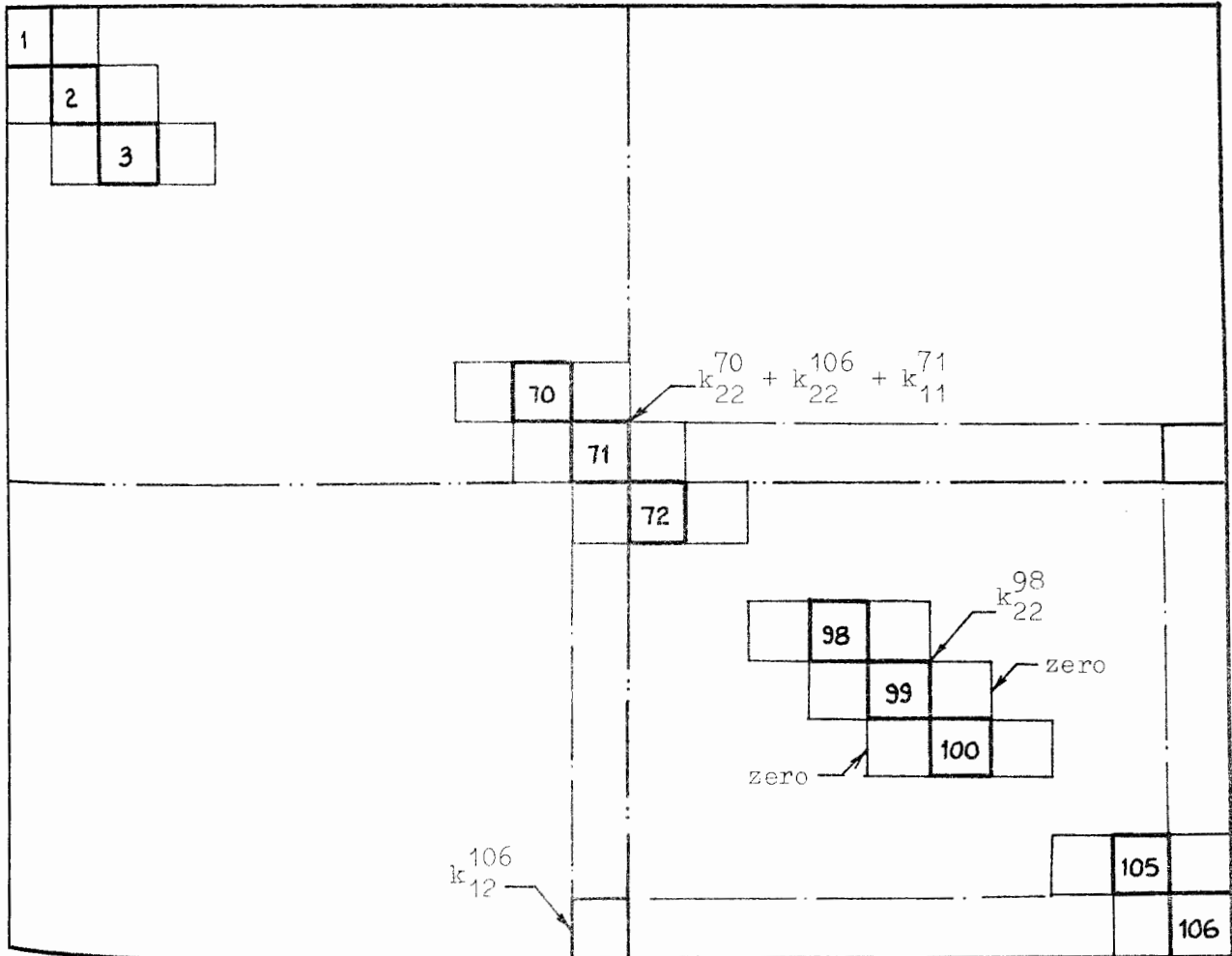
Fig. 4.30: Analysis 6/B1/1



Notes:

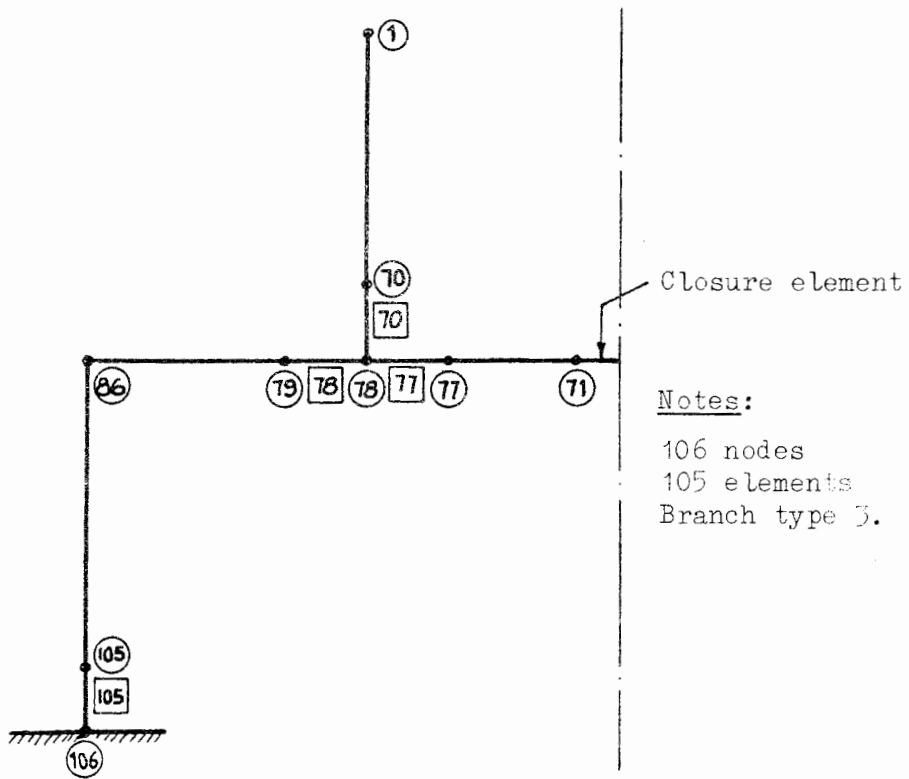
106 nodes
 106 elements; element 99
 is a dummy element.
 Branch types 2 and 5.

(a) Node and element numbering scheme

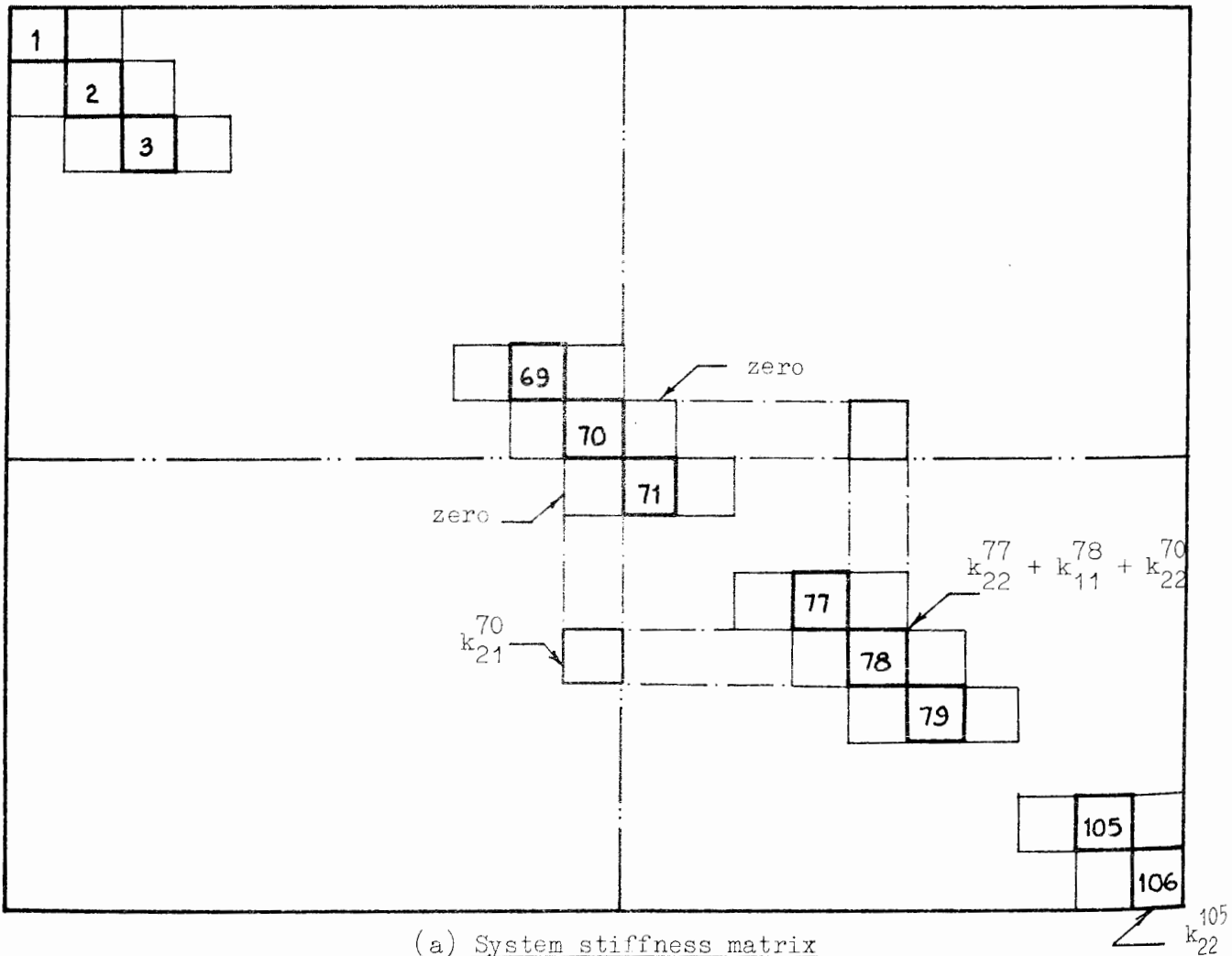


(b) System stiffness matrix

Fig. 4.32: Analysis 6/B3/1



(a) Node and element numbering schemes



(a) System stiffness matrix

although having different node numbering schemes, have the same branch type classification. This apparent ambiguity can be explained by reference to the relevant branch type definitions, but is in all events of no concern to the program user, since use of the program requires no knowledge whatsoever of branch types. The rigid classification of branch types is of use only within the program itself to ensure that specific modifications are made to the system stiffness matrix. As far as the user is concerned, each branch is described essentially by the branch node number and the numbers of the elements meeting at it.*

Discussion of results

The form of the system stiffness matrices for the three branched shell analyses are shown in Figs. 4.30, 4.31 and 4.32, where each differs from the next according to the manner in which the nodes have been numbered.

Each of the matrices is divided into two basic parts, each part essentially identical to the stiffness matrix of the corresponding substructure. This is best illustrated by the stiffness matrix for analysis 6/B2/1 where the upper part, corresponding to nodes 1 to 70, is identical to the stiffness matrix for analysis C/C/04, while the part corresponding to nodes 71 to 106 is identical to the stiffness matrix for analysis 6/D/01, except for the diagonal submatrix at node 78 which is augmented with k_{22}^{70} . (The exact numerical values in the latter submatrix can be obtained from analysis C/C/04.) The connection of the two substructures to form a branch at node 78 is effected by inserting the off-diagonal submatrix,**

$$K_{70,78} = k_{21}^{70} \quad (4.12a)$$

* The tendency during the development CONFRU has been to generate as much data as possible automatically within the program, thus reducing the amount of input data required.

** It will be noticed that in the other two analyses the off-diagonal submatrices are transposed as follows:

$$6/B1/1: \quad K_{106,8} = k_{12}^{106} \quad (4.12b)$$

$$6/B3/1: \quad K_{106,71} = k_{12}^{106} \quad (4.12c)$$

Hence, with only two submatrices in the branched shell stiffness matrix different from the stiffness matrices for the corresponding substructure it is a simple matter to check that the branched shell stiffness matrix has been correctly set up by CONFRU.

The same procedure may be used to check the numerical values of the remaining two branched shell stiffness matrices. In each of the system stiffness matrices shown, modifications to individual submatrices are indicated by noting the new form of the submatrix alongside it.

Needless to say, in all three analyses the system stiffness matrices are set up correctly by the computer.

The load vectors for the branched shells have only three non-zero elements, corresponding to the three edge loads at the top of the upper cylinder. Checking of the load vector is trivial, (the load vector can be simply and accurately calculated on a desk calculator), and in each case it is set up correctly by CONFRU.

When the displacement solutions were substituted back into the stiffness matrices the original load vectors were again obtained. The three non-zero elements were correct to the sixth significant figure, and the worst rounding error in the remaining zero elements was of the order of 10^{-8} . (Spot checks were also carried out to ensure that the back-substitution procedure itself was functioning correctly.)

With the system stiffness matrices and the load vectors set up correctly, and the equation solution procedure working efficiently, all three analyses gave absolutely identical results for both the displacements (to six significant figures) and the stress resultants (to four significant figures).

The excellent agreement was in fact mildly surprising in view of the fact that the stiffness matrices for each of the analyses differ fairly widely in form. In particular, the storage requirements for each matrix, and hence the amount of arithmetic involved in solving the equations, vary significantly for each analysis. These requirements are given in the table below for the diagonal band (9 columns wide), and the off-diagonal submatrix and associated zeros; for each analysis the storage efficiency remains 100%.

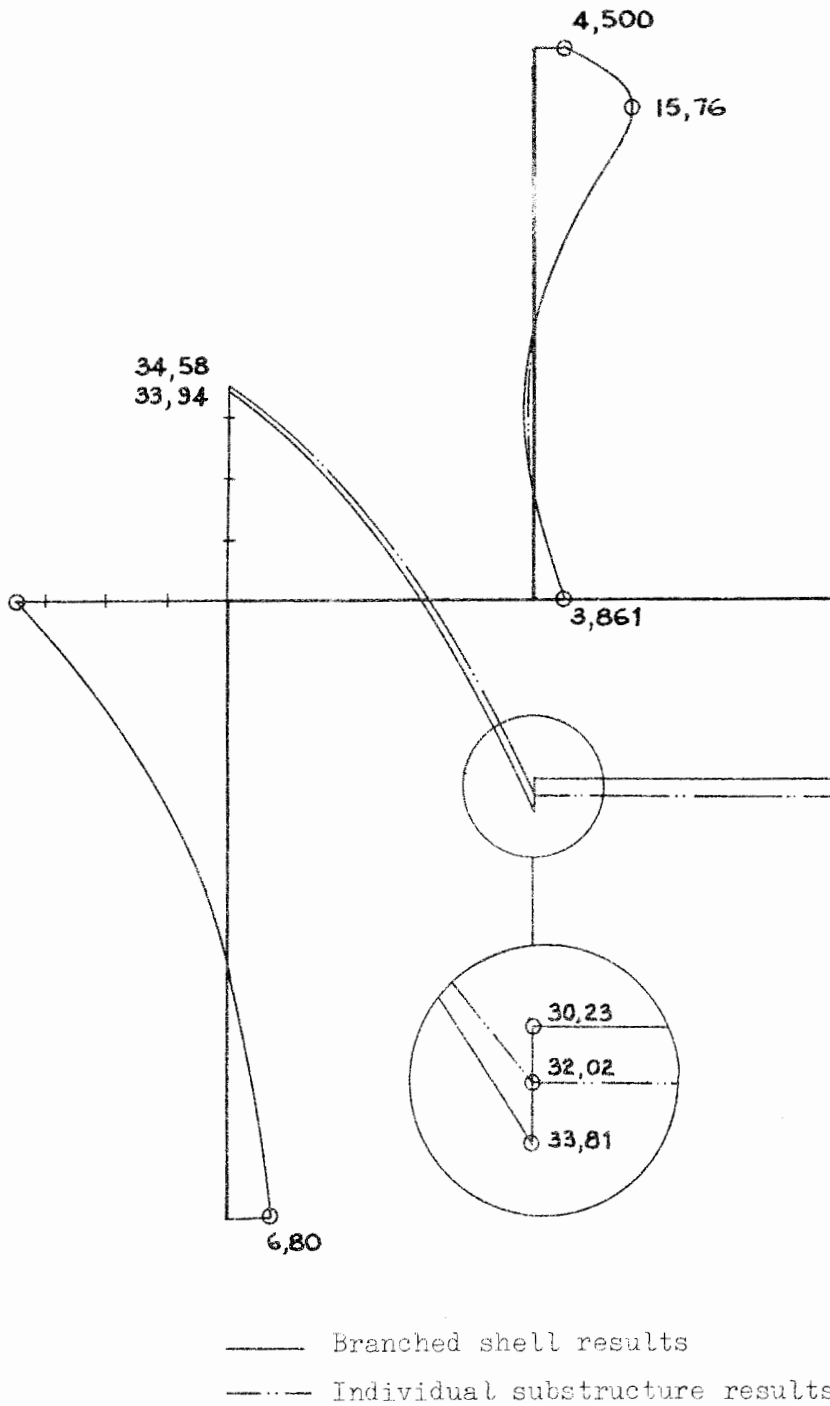


Fig. 4.34: Meridional moment M_s [kNm/m]

TABLE 4.11

Core Storage Requirements, in Double-Precision Words

	6/B1/1	6/B2/1	6/B3/1
Diagonal	1581	1581	1581
Off-diagonal	864	54	307
Total	2445	1635	1888

Discussion of the meridional moments

With the lower substructure relatively stiff we can expect the upper cylinder to behave as if rigidly fixed at its point of connection to the circular plate. Hence, noting from Example 1 that the meridional moment M_s at the base is negligible, we anticipate no tranference of moments from the upper cylinder to the lower substructure. The only force which will be transferred is the axial force U , which can be considered to act as a line load on the circular plate. Thus, for the purpose of comparison of meridional moments, the two substructures will be analysed as shown in Fig. 4.33.

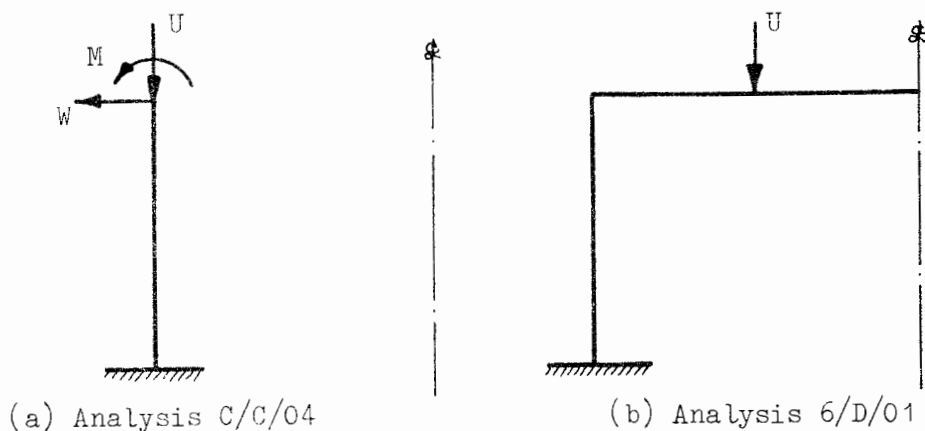
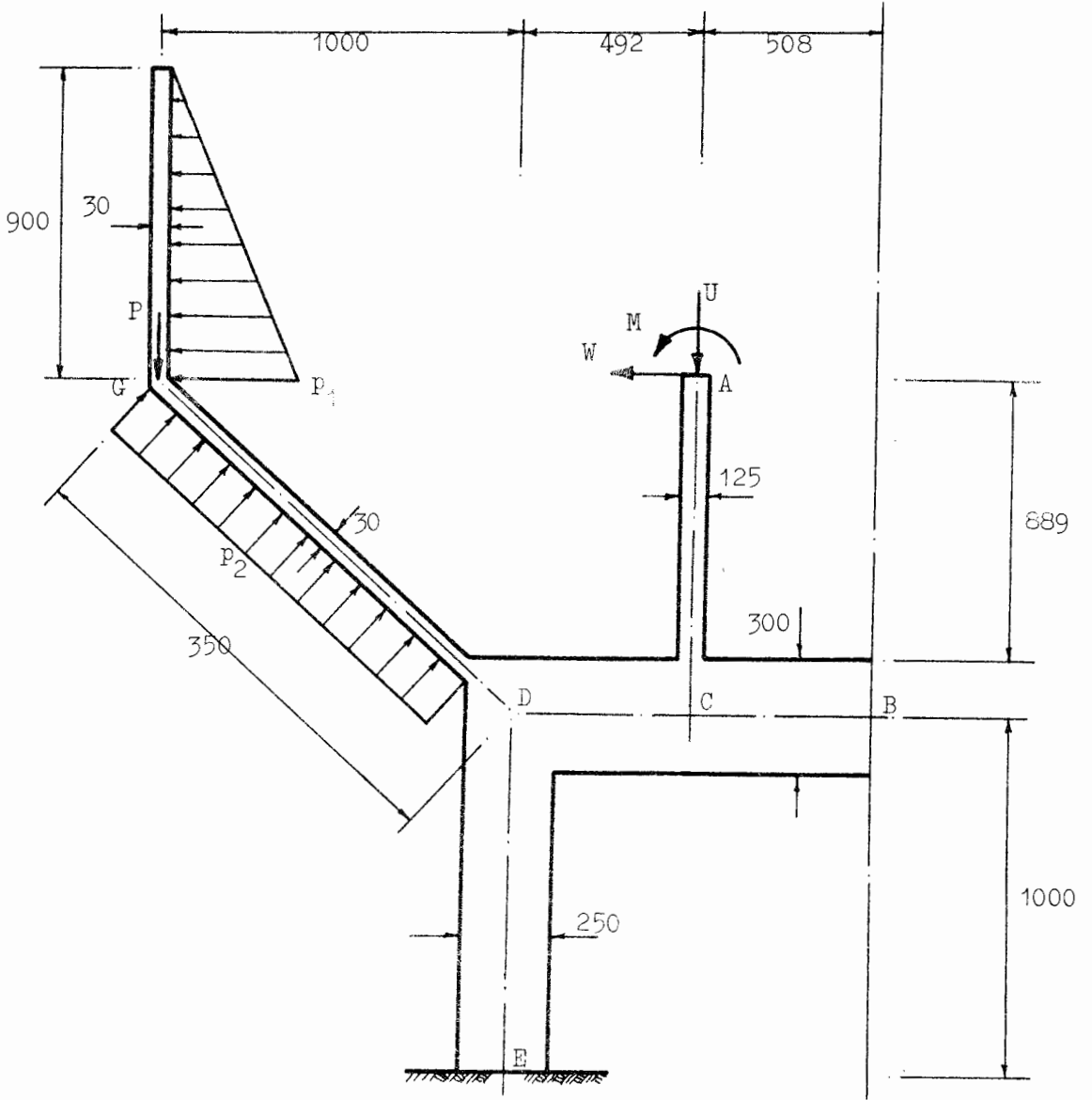


Fig. 4.33

The meridional moments in the branched shell are shown in Fig. 4.34 where they are compared with the corresponding moments in the substructures, analysed independently. The two sets of results are effectively identical, the only region of discrepancy being, as we would expect, at the point where the upper cylinder joins the circular plate. At this point the moments in the cylinder, when analysed independently, are negligible, as compared to

TABLE 4.12



Loading:

$$U = 250 \times 10^3 \text{ N/m}$$

$$P = 10^3 \text{ N/m}$$

$$W = 264 \times 10^3 \text{ N/m}$$

$$P_1 = 8,829 \times 10^3 \text{ N/m}^2$$

$$M = 4,448 \times 10^3 \text{ Nm/m}$$

$$P_2 = 0,250 \times 10^3 \text{ N/m}^2$$

Material Properties:

$$E = 1,0$$

$$\nu = 0$$

Element Subdivision:

AC, BC, CD, DE as for Example 6.

FG: 60 elements @ 0,015 m; $L/t = \frac{1}{2}$

GD: 90 " @ 0,015 m; $L/t = \frac{1}{2}$

Analysis I.D. No.	Branch Types	Remarks
7/B1/1	1, 4, 5	For node numbering, see Fig. 4.36
7/B2/1	1, 4, 5	" " " " , see Fig. 4.37
7/D/01	-	Cone-cylinder substructure: see Fig. 4.35

the value 3,861 kNm/m when it is joined to the circular plate. The moments in the plate itself are discontinuous at the branch point; notice however that the finite element solution maintains very closely equilibrium of the moments at the branch point, as can be seen from the following addition (+ = clockwise moment):

$$30,23 + 3,861 - 33,81 = 0,28 \approx 0.$$

The moments in the circular plate when loaded with a line load are continuous, and at the joint are exactly equal to the mean of the discontinuous moments mentioned above (see inset, Fig. 4.34).

The moments in the branched shell are therefore precisely as we might expect, and so provide us with a final (if superficial) confirmation that the correct solution has been obtained.

4.5.3 Example 7: Analysis of a doubly branched shell of revolution

Specific objectives:

As for Example 6.

Description of the analysis

The second branched shell which we will analyse is shown in Table 4.12. As can be seen from the diagram it consists of the shell analysed in Example 6 with an additional branch in the form of a cone-cylinder (section DGF). The geometry of the cone-cylinder branch and its loading are similar to Example 4.

The complete shell therefore consists of three basic substructures, each of which may be analysed independently to provide the correct numerical values in the system stiffness matrix of the branched shell. For this purpose the cone-cylinder substructure was analysed as shown in Fig. 4.35.

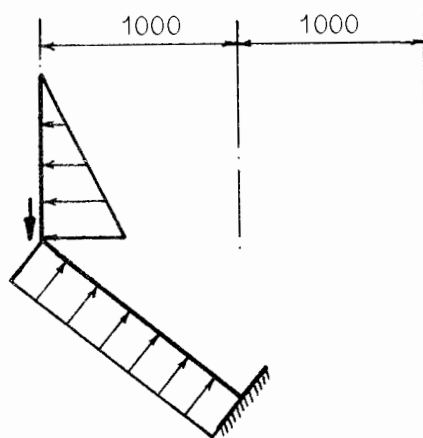


Fig. 4.35

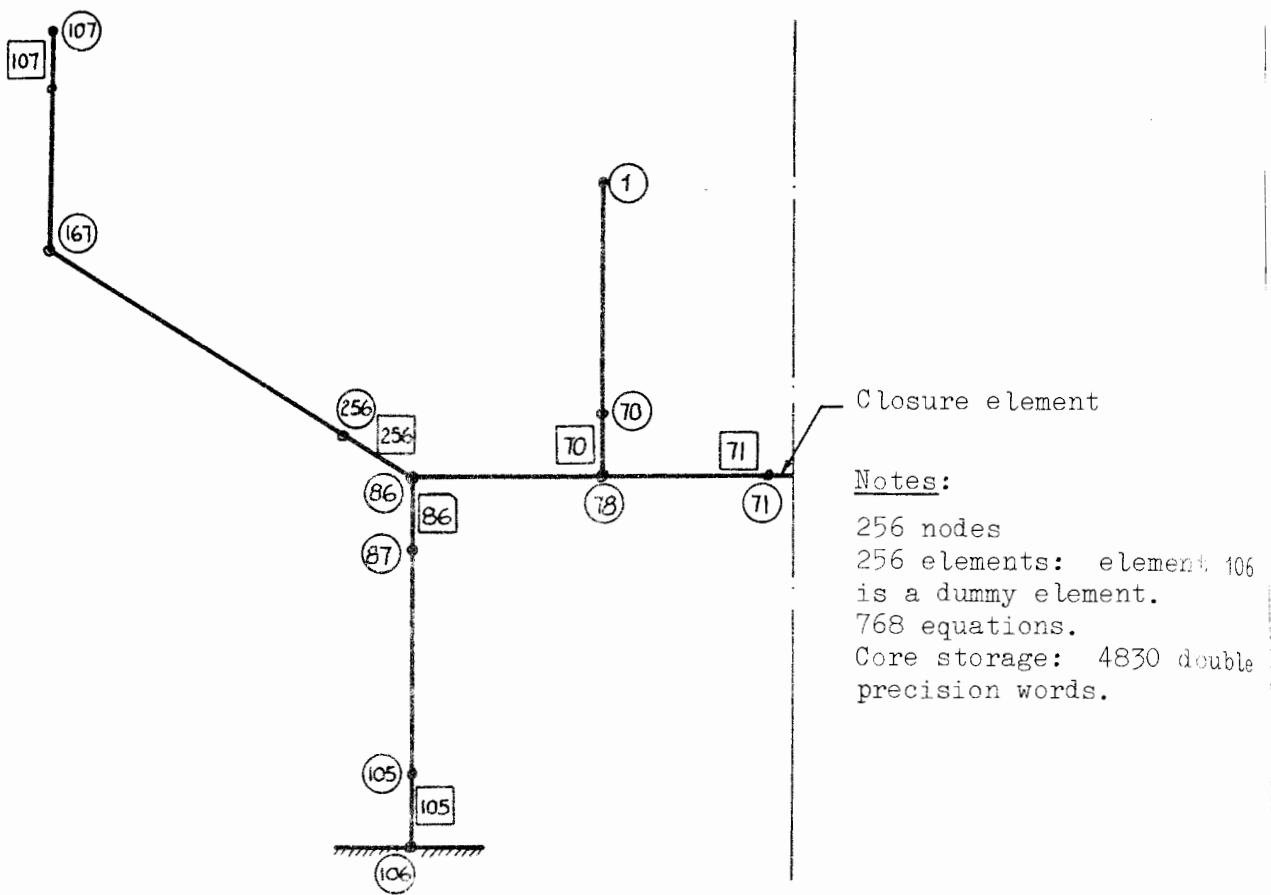


Fig. 4.36: Node and element numbering scheme for analysis 7/B1/1

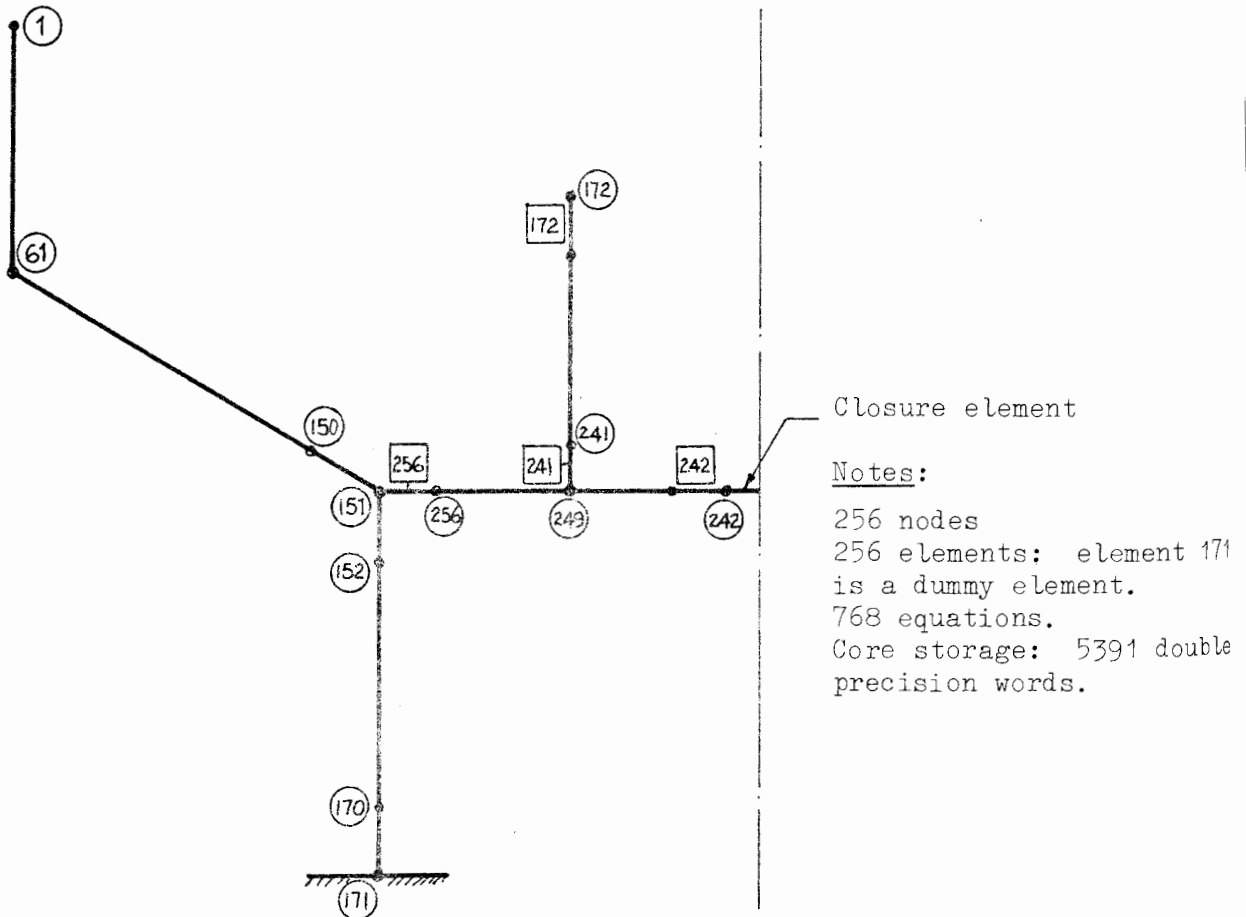


Fig. 4.37: Node and element numbering scheme for analysis 7/B2/1

Two analyses of the branched shell have been performed, each using the same element breakdown, but with different node numbering schemes. The node numbering schemes for the two analyses are shown in Figs. 4.36 and 4.37; the notation used here is the same as that of Example 6.

Discussion of results

Since the methods used in carrying out the objectives of this example are the same as were used in Example 6, it suffices simply to state the following results:

- (i) The system stiffness matrices and load vectors for the two analyses are correctly set up by the program.
- (ii) Both analyses give absolutely identical results for both displacements and stresses. (Note the total core storage requirements for each system stiffness matrix given in the Figures).

As far as the meridional moments M_s are concerned the cone-cylinder branch has, due to its very small relative stiffness, negligible effect on the rest of the shell. Hence the moments in those parts of the structure corresponding to Example 6 remain essentially unchanged.

The moments in the cone-cylinder branch are shown in Fig. 4.38(a) where they are compared with those in the corresponding substructure (Fig. 4.35). When this branch is analysed independently (i.e. fixed at its bottom end) the moments in the lower part of the cone die out (c.f. Example 4, Fig. 4.21). However, when analysed as a branch, the moments have a peak at the branch junction; this is to be expected in view of the fact that the junction D is not infinitely stiff, and as such the equilibrium of moments at the junction must be maintained. Notice that the equilibrium of moments at the junction is very accurately maintained (the unbalanced moment being only 0,030 kN m/m), and that the moments in the conical branch are in fact negligible compared with those in the rest of the shell.

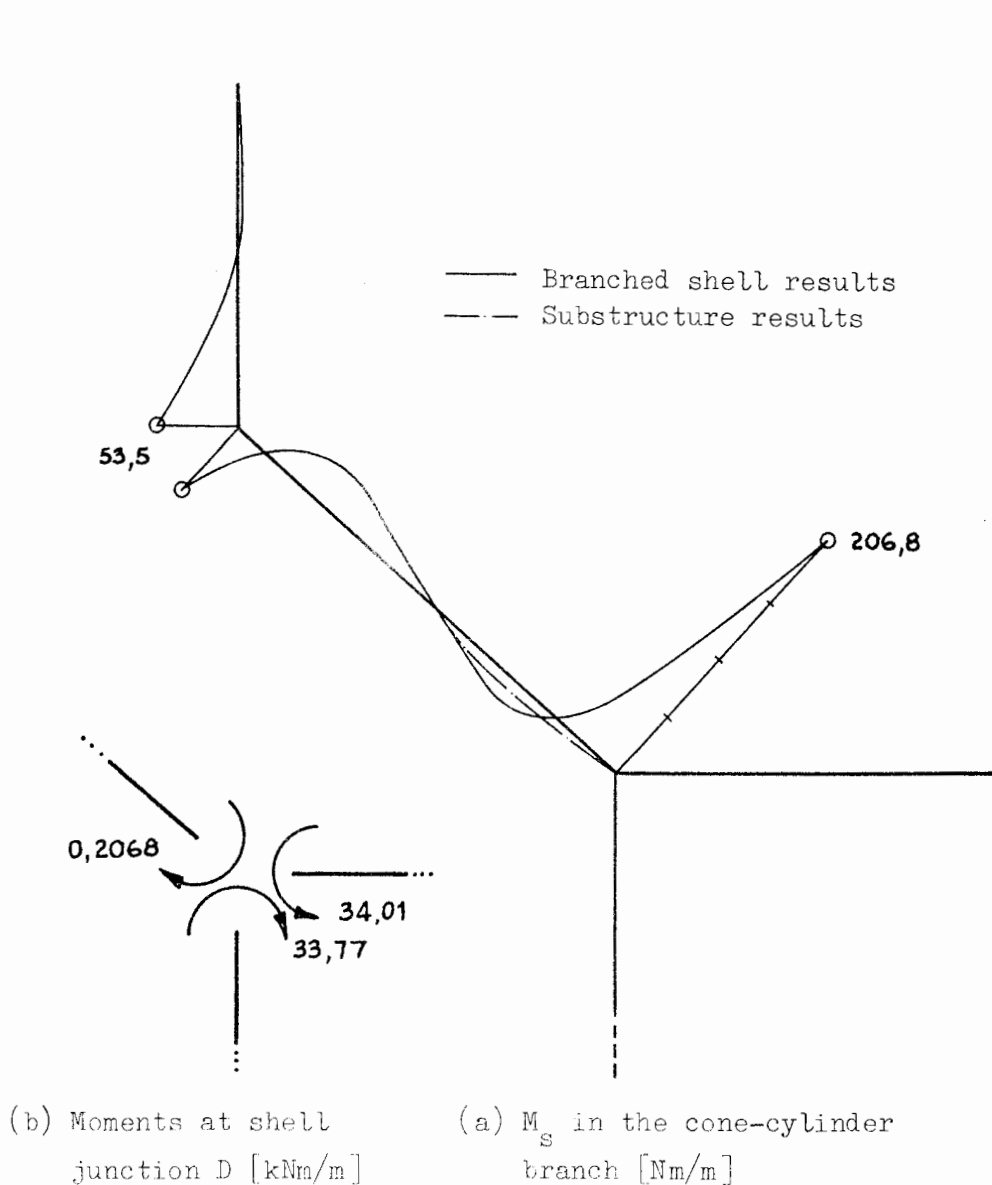


Fig. 4.38

We conclude, therefore, that the solution given by CONFRU for the doubly branched shell is correct.

4.6 An Example from Practice

We have shown in the preceding two examples that the solution given by CONFRU for a single and a double branched shell are correct (i.e., free of logical errors, and hence capable of being improved if necessary by refinement of the element subdivision), and although the full branching logic of the program has been tested only piece by piece, we are nevertheless confident that any arbitrarily branched shell can be equally effectively handled.

Up to now, however, we have avoided the question of the accuracy of the

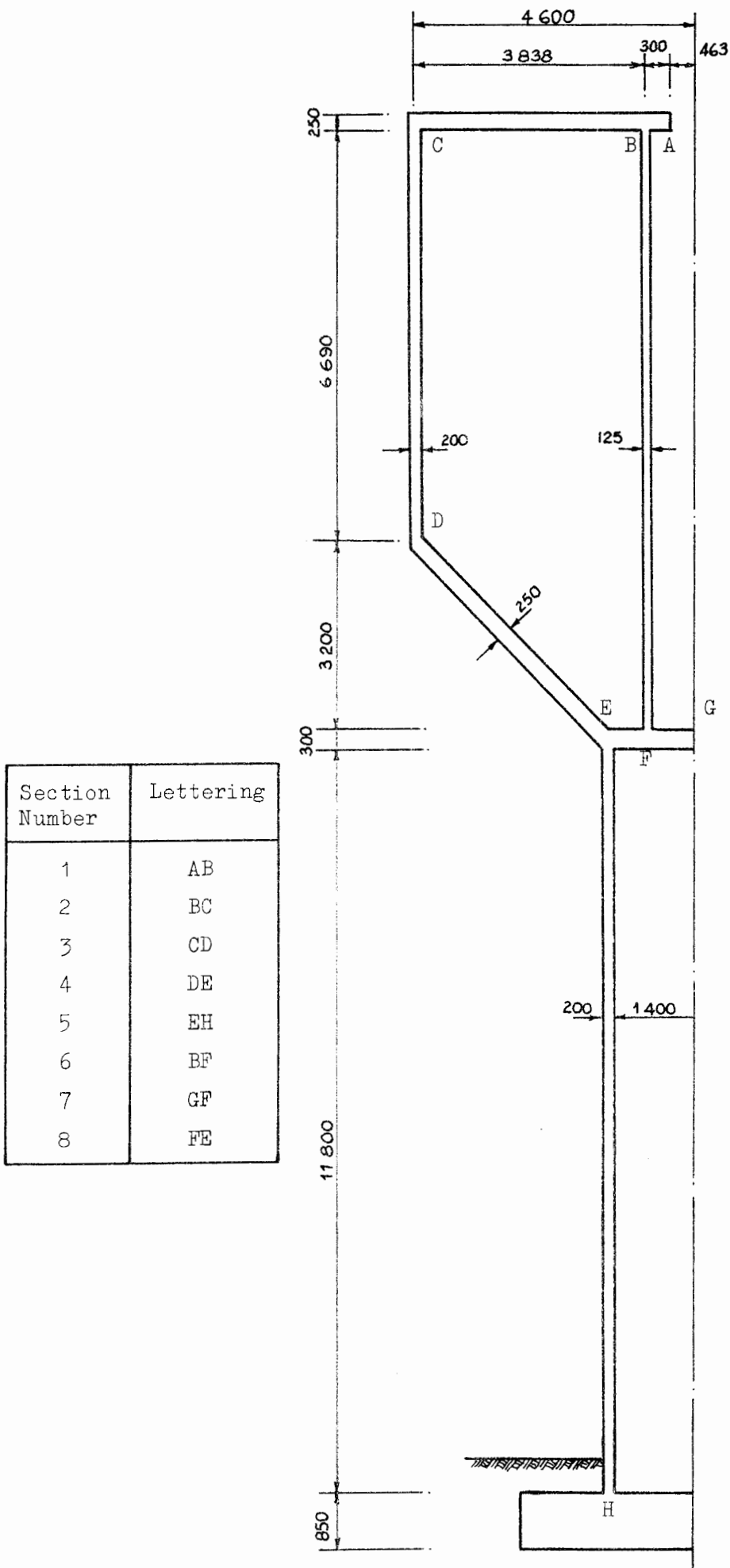


Fig. 4.39: Elevation of elevated effluent tank

Scale 1:1000 Dimensions in mm

branched shell solutions (due to the lack of independent solutions for comparison), and in the following example we will discuss this aspect in relation to practical design requirements.

The example, which is analysed under both live and dead loads, serves also to illustrate the potential of the program.

4.6.1 Example 8: The analysis of an elevated effluent tank

The elevated effluent tank shown in Fig. 4.39 has a capacity of 450 m^3 and forms part of a sewage plant completed recently for the City of Durban. The tank and its supporting tower have an overall height of 21,690 m and the structure as a whole is very slender; in fact the tower and the inner cylinder of the tank are by definition thick shells, having D/t ratios of 14 and 12 respectively.

This structure, being made up entirely of a combination of cylinders, conical frustra and circular plates, is the type of structure for which CONFRU was specifically developed.

Three analyses of the structure have been carried out, for which the data are given in table 4.13. For each analysis the structure is assumed to be rigidly fixed at the base of the tower H, and a closure element is made use of at G where the tank is closed. There are three branch points at B, E and F.

The following objectives are dealt with in this section:

- (i) The automatic plotting facilities attached to CONFRU are illustrated, and the interpretation of plotted output is discussed.
- (ii) The accuracy of the solution is assessed by investigating the improvement in results obtained by refinement of the element subdivision.
- (iii) The live and dead load stress distributions are discussed.

Analysis ST/1/1 is also used as a sample analysis for future reference and the complete data input, as well as the displacement, stress and moment solutions are given in Appendix A.

TABLE 4.13

Material Properties:

Reinforced concrete: $E = 20 \times 10^9 \text{ N/m}^2$
 $\nu = 0,167$
 $\gamma = 24 \times 10^3 \text{ N/m}^3$
 Effluent: $\gamma = 10 \times 10^3 \text{ N/m}^3$

Loading:

Load Case 1: Live load; tank completely filled with effluent.
 Load Case 2: Dead load; self-weight of the structure only.

Analyses:

ST/1/1: Load Case 1, 211 elements
 ST/1/2: Load Case 1, 414 elements
 ST/2/1: Load Case 2, 211 elements.

Section	Element Subdivision*	
	ST/1/1 and ST/2/1	ST/1/2
AB	3 @ 100 (0,4)	3 @ 100 (0,4)
BC	19 @ 202 (0,8)	38 @ 101 (0,4)
CD	9 @ 202 (1,0) + 24 @ 203	18 @ 101 (0,5) + 48 @ 101,5
DE	7 @ 205 (0,8) + 15 @ 206	14 @ 102,5 (0,4) + 30 @ 103
EF	4 @ 159 (0,5)	6 @ 106 (0,4)
FG	4 @ 150 (0,5) + 1 @ 100 + closure element	7 @ 100 (0,3) + closure element
BF	56 @ 150 (1,2) 10 @ 149	112 @ 75 (0,6) 20 @ 74,5
EH	59 @ 200 (1,0)	118 @ 100 (0,5)

*Element lengths in mm; approximate L/t ratio in brackets

Discussion of Results

Computer plotted output: A computer plot of the live and dead load stresses and moments in the shell structure is shown in Fig. 4.40. Plotted output, while always an advantage, is particularly useful where large numbers of elements have been used in an analysis, resulting in many pages of printed output, which are tedious to scan and assess. The plotting facilities available with CONFRU have the following additional advantages:

- (i) The plotting is done automatically following the relevant analysis without any intervention on the part of the user, (other than to specify that the plotting option is to be made use of).
- (ii) The results of up to four analyses may be plotted on one system of axes to facilitate the comparison of different load cases, or the use of different element subdivisions. In such cases the lengths of the axes and the scales used are automatically chosen so as to effect the optimum accommodation of the most diverse ranges of results.

In order to correlate points on the horizontal axis (axial distance) of the computer plots with the corresponding points on the actual structure, it is necessary to refer to the printed stress and moment results, which are set out in the following format:

<u>Node No.</u>	<u>Cumulative Distance</u>	σ_s	σ_e	M_s	M_θ
<u>Section 1</u>					
⋮	⋮	⋮	⋮	⋮	⋮
<u>Section 2</u>					
⋮	⋮	⋮	⋮	⋮	⋮

The cumulative distance in this table is identical to the axial distance in the computer plots. It is the actual distance measured along the middle surface of the structure from the first to the last node. Hence, knowing the nodal numbering scheme used in the analysis (i.e., which node corresponds to which point on the structure), the equivalent cumulative distance may be read off from the table of printed results, and correlation between nodes on

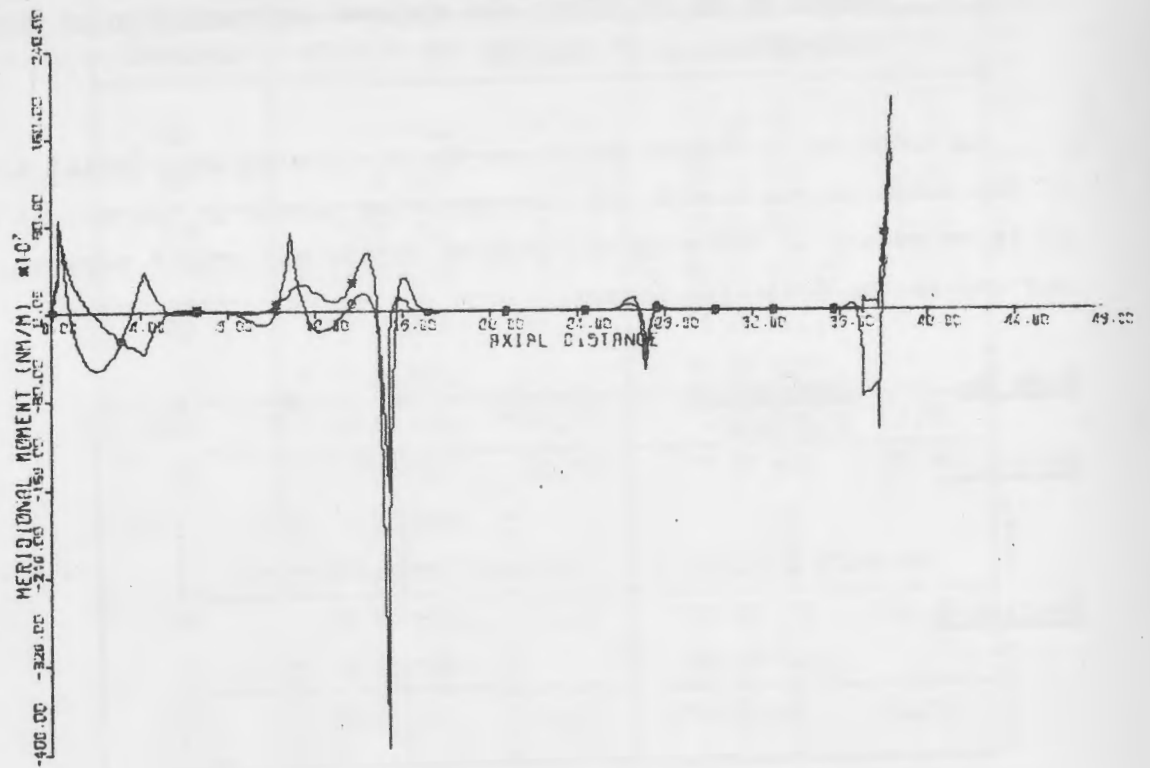
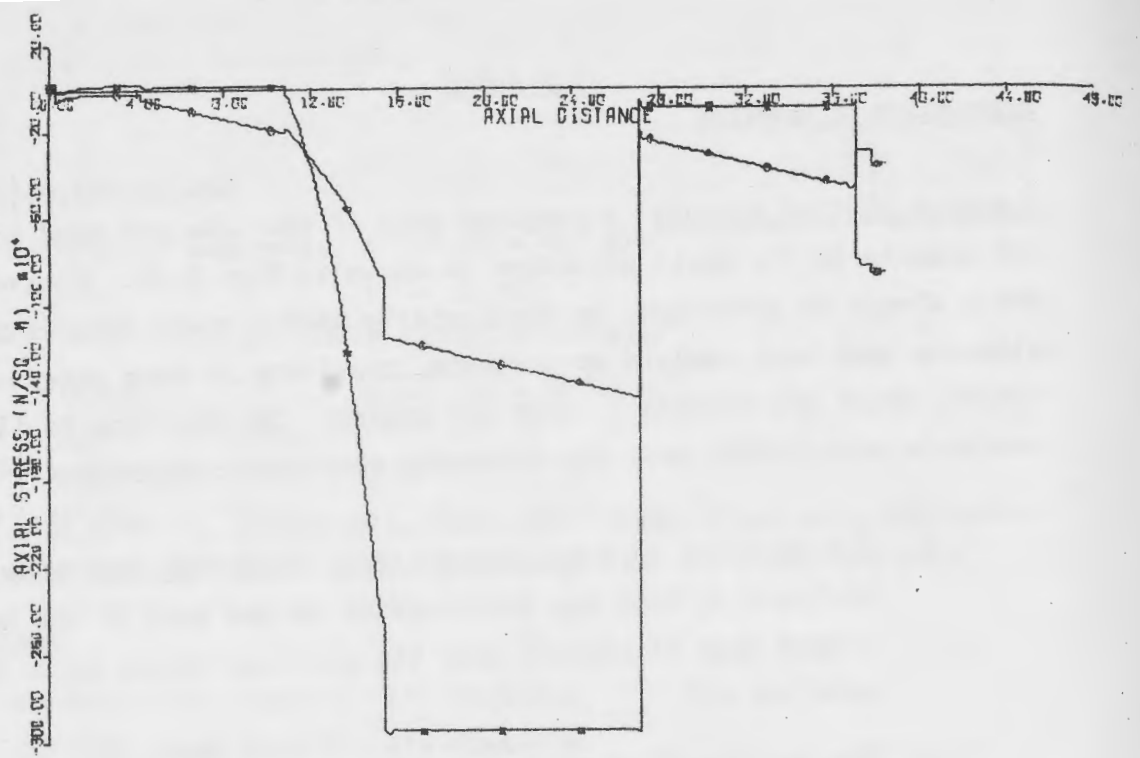
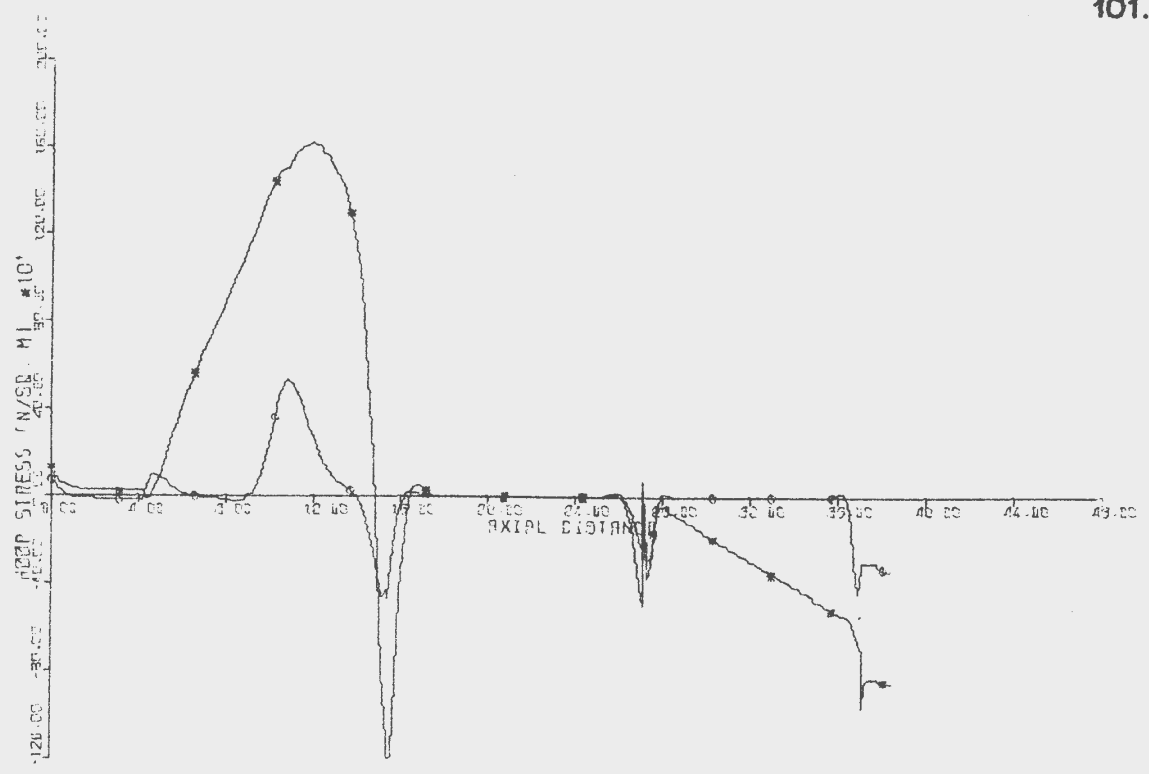
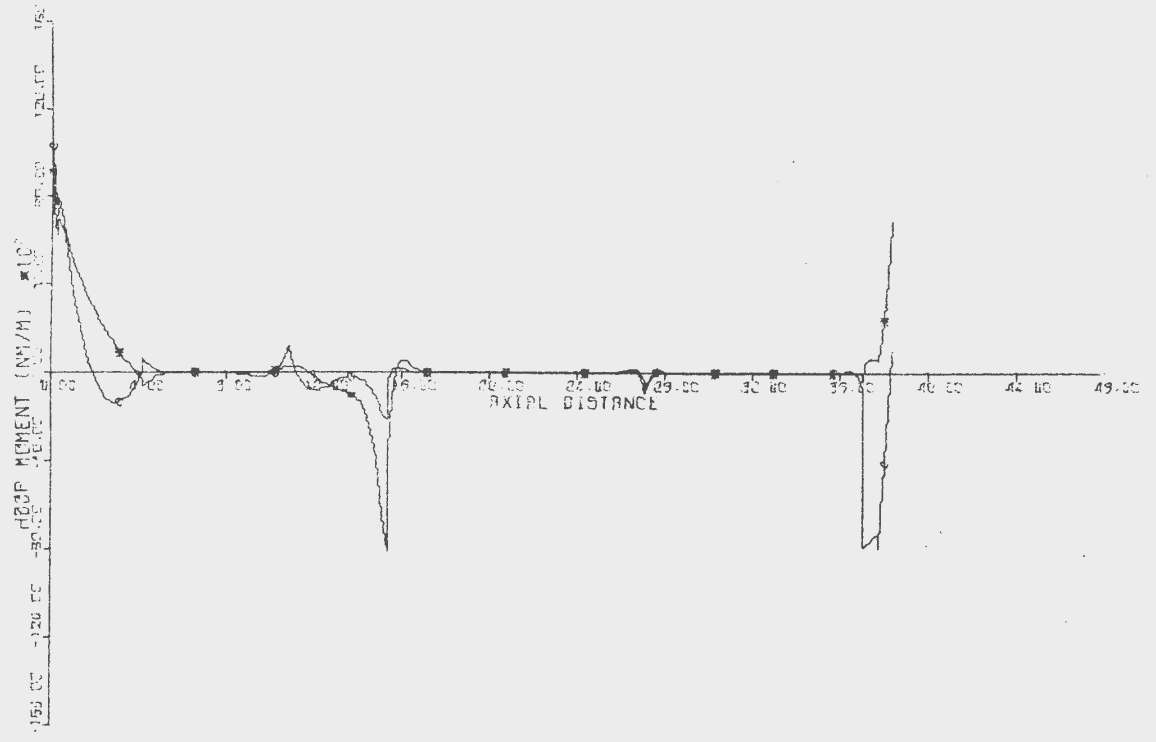


Fig. 4.40



LOAD CASE	
*	ST/1/1
o	ST/2/1
□	
⊗	



UNIVERSITY OF CAPE TOWN	
DEPARTMENT OF CIVIL ENGINEERING	
FINITE ELEMENT ANALYSIS	
OF	
AXISYMMETRIC SHELL	
ANALYSIS:	PLT SERIES: EX. 5
HORIZONTAL AXIS: METERS	DATE:
VERTICAL AXIS: NEWTONS. METERS	
ANALYSIS AND PLOT BY T.B.GRIFFIN	
PROGRAM: STRESSPLOT	

Fig. 4.40 (continued)

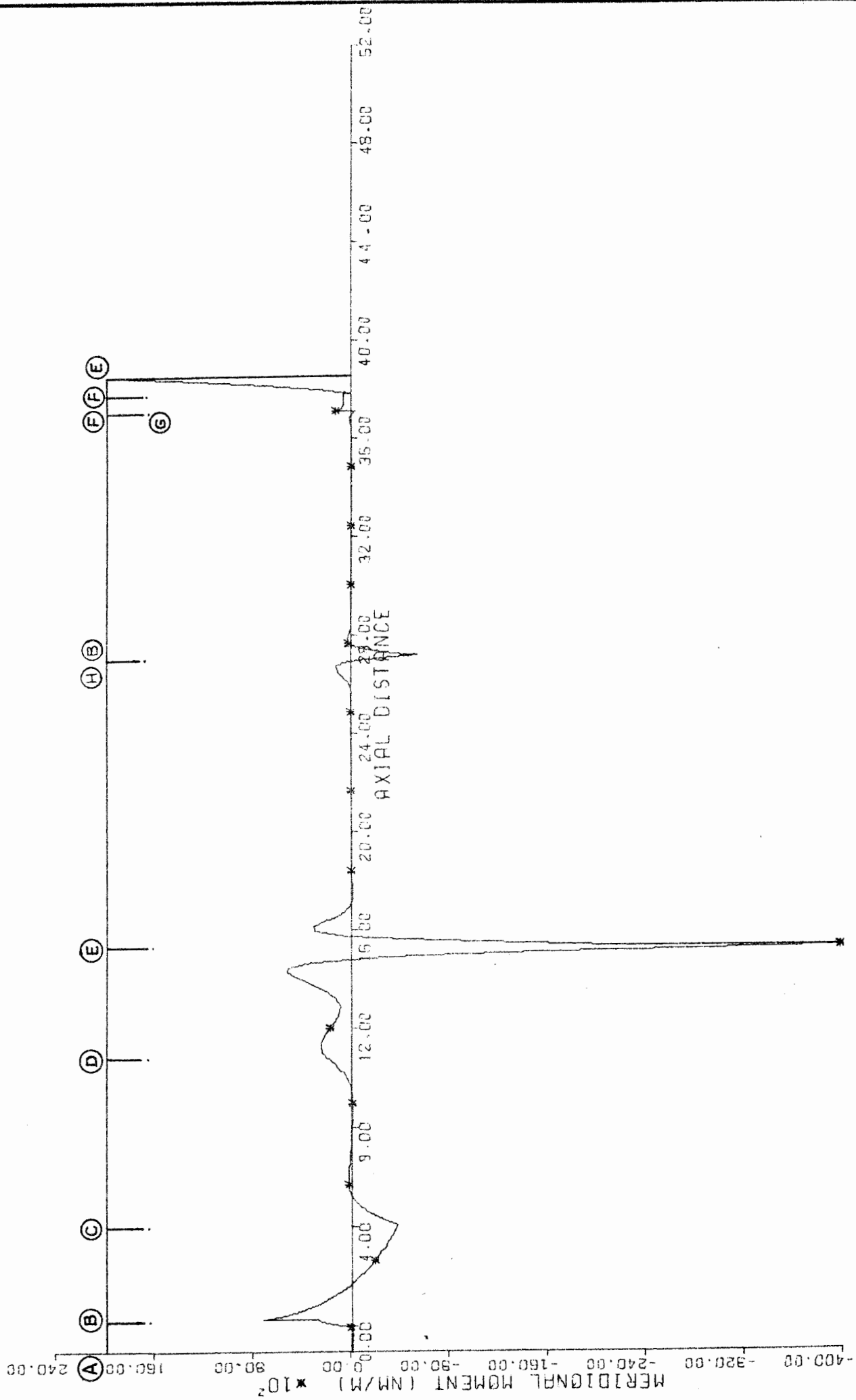


Fig. 4.41

the structure and corresponding points on the horizontal axis of the plots thereby obtained.

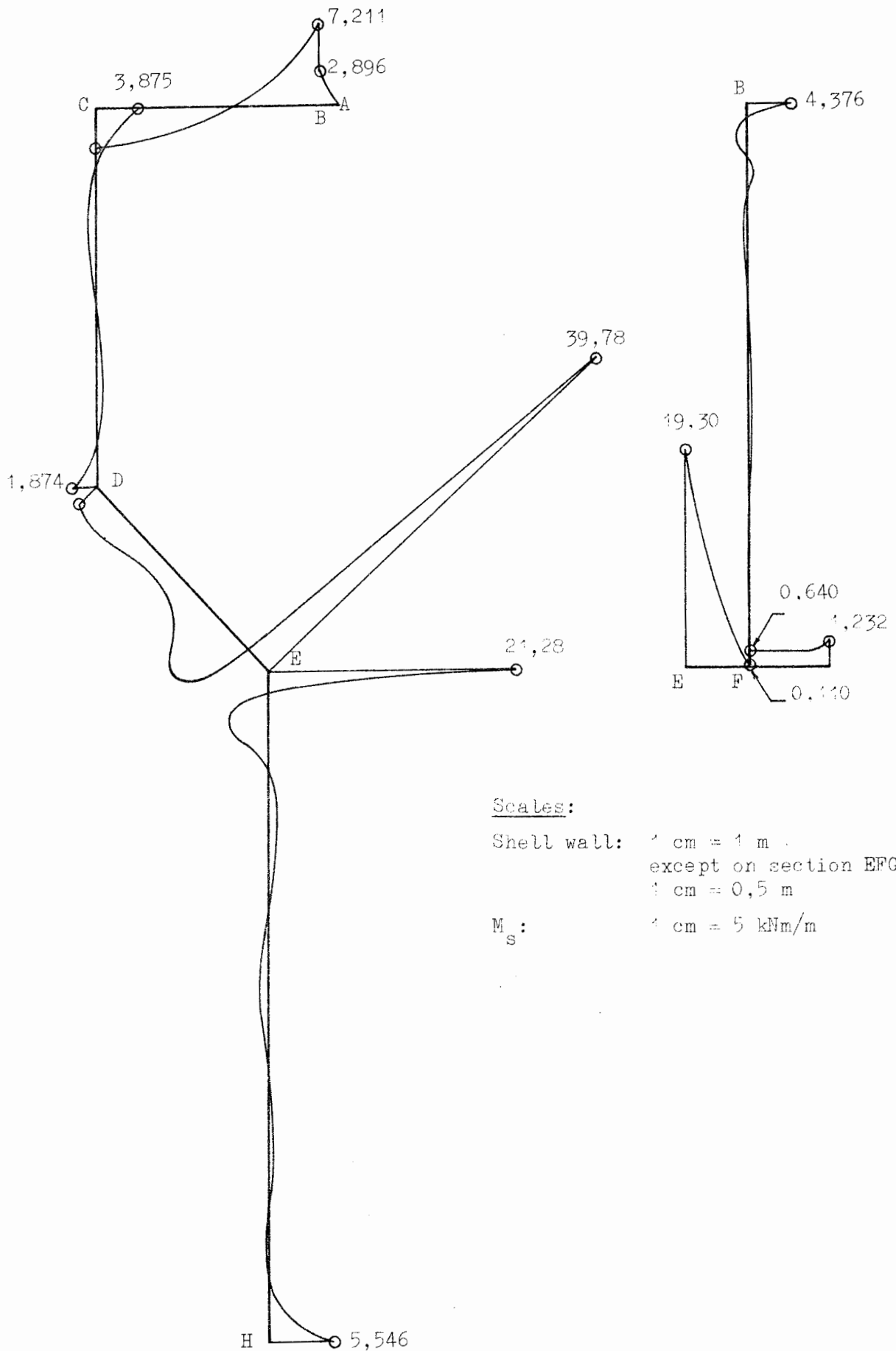
In most cases it is preferable to plot results on a line diagram of the structure. This is easiest done by making use of the computer plot in the following way: (the plot of the meridional moment results for analysis ST/1/1, shown enlarged in Fig. 4.41, will be used to illustrate the procedure).

- (i) From the nodal numbering scheme used in the analysis the cumulative distance to the beginning and end of each section is read off from the table of printed results. (The full set of results for this analysis is given in Appendix A; the section numbers referred to are given in Fig. 4.39).
- (ii) Making use of this information, the horizontal axis of the computer plot is divided into sections (Fig. 4.41).
- (iii) The M_s diagram for each section is transferred to the line diagram of the structure. (Positive stresses denote tension; positive moments denote tension on the side of the positive normal to the shell wall: see 'Sign Convention', Section 3.3.6).

The final result of such a transference is shown in Fig. 4.42 where the meridional moments for analysis ST/1/1 are shown plotted on the tension side of the shell walls. (For clarity the inner cylinder and circular base of the tank separated from the rest of the structure.) The same procedure applies to the plotting of other stresses and moments on a line diagram of the structure.

Accuracy and validity of results: We begin by comparing the results of the two live load analyses ST/1/1 and ST/1/2; the two analyses have average element aspect ratios of approximately 1,0 (211 elements) and 0,5 (414 elements) respectively.

From the M_s diagram already shown (Fig. 4.42) it is clear that the moments are concentrated almost exclusively at the shell junctions. Hence it suffices to compare the moment results obtained from the above analyses at the junction points only, as shown in the following table.



Scales:

Shell wall: 1 cm = 1 m .
 except on section EFG where
 1 cm = 0,5 m

M_s : 1 cm = 5 kNm/m

Fig. 4.42: Live load meridional moment M_s

TABLE 4.14

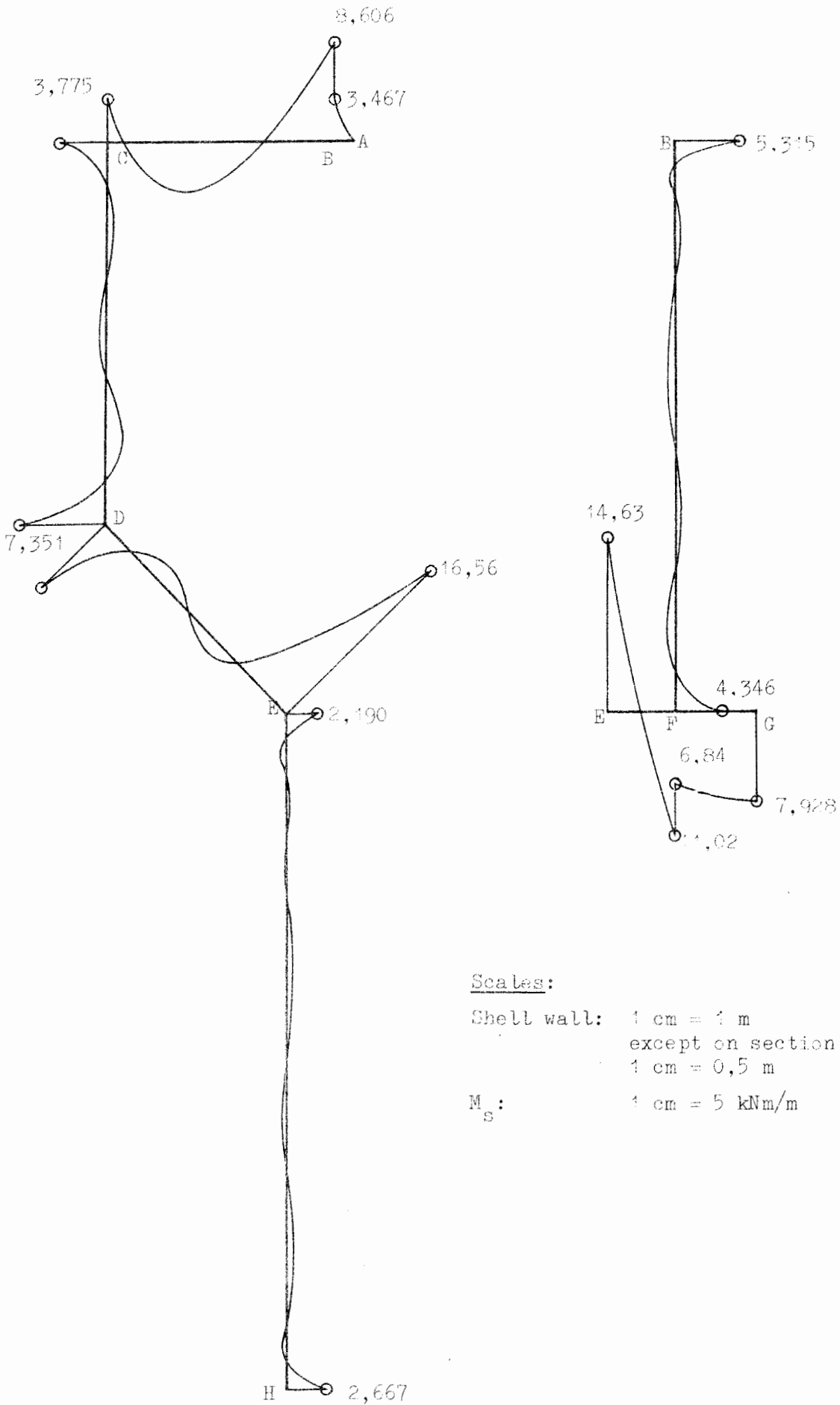
Junction	Section	M_s^* [kN m/m]			Unbalanced Moment at Junction	
		ST/1/1	ST/1/2	Difference	ST/1/1	ST/1/2
B	BA	- 2,896	- 2,896	0		
	BC	7,211	7,266	0,055	0,061	0,040
	BF	- 4,376	- 4,410	0,034		
C	CB	- 3,878	3,876	0,002	0,003	0
	CD	- 3,875	- 3,876	0,001		
D	DC	- 1,862	- 1,859	0,003	0,024	0,006
	DE	1,886	1,865	0,021		
E	ED	39,78	40,82	1,040		
	EF	- 19,30	- 19,34	0,040	0,800	0,240
	EH	- 21,28	- 21,72	0,440		
G	GF	1,232	0,722	0,510	-	-
H	HE	5,546	5,736	0,190	-	-

*Positive moment has clockwise sense.

From this table the following results are apparent:

- (i) The refined element subdivision (analysis ST/1/2) has clearly given rise to an improvement in results, as can be seen by comparing the unbalanced moments at each junction for the two analyses.
- (ii) The improvement in individual results for each section is, however, very small. In fact, for all practical purposes the improvements are negligible, meaning that either set of results would give rise, for instance, to the same steel reinforcement design for the structure.

Hence, for all practical purposes the moments may be said to have converged. Furthermore, there is no doubt that they are correct, and although we cannot state the degree of accuracy of the results, there does not, in view of (ii) above, appear to be any need for this.



Scales:

Shell wall: 1 cm = 1 m
 except on section EFG where
 1 cm = 0,5 m

M_s : 1 cm = 5 kNm/m

Fig. 4.43: Dead load meridional moment M_s

There are some further aspects of the M_s diagram which require comment:

- (i) The surprisingly large moments in the tank roof (which is unloaded) may be explained by reference to the deformed shape of structure, as obtained from the displacement results. The displacements of the points E and F are essentially identical. Hence, and because there is no axial strain in cylinder BF, the displacement of point B remains essentially zero relative to the tank base EG. The point D, on the other hand (and hence the point C, ignoring the axial strain in CD), undergoes a fairly large vertical displacement due to bending in the conical section DE. The net result is that point C undergoes a significantly larger vertical displacement than point B. The moment diagram for the roof corresponds precisely to such a relative displacement, and this in turn accounts for the large edge disturbances at the upper edges of the tank's cylindrical walls.
- (ii) The moments in the circular plate, section FG, are almost exactly constant (as they should be) except for the single value at the axis of symmetry. This error is due to the closure element. Notice, however, that a significant improvement is obtained through the use of a refined element subdivision, as can be seen from the results for section GF in Table 4.14.
- (iii) There are no moments in the cylindrical tower, besides obvious edge disturbances, since there are no lateral loads acting on the tower.

The M_s diagram for the self-weight only of the structure is shown in Fig. 4.43, and the only parts of the diagram requiring comment are the moments at junctions D and E. At junction D the moments due to self-weight of the structure are far higher than those due to water only in the tank, because of the fairly high vertical load at D in the former case, and the zero vertical load at D in the latter. The reason for the difference between the live and dead load moments at junction E is due to the difference in the magnitude and distribution of loads on the conical section DE in each case.

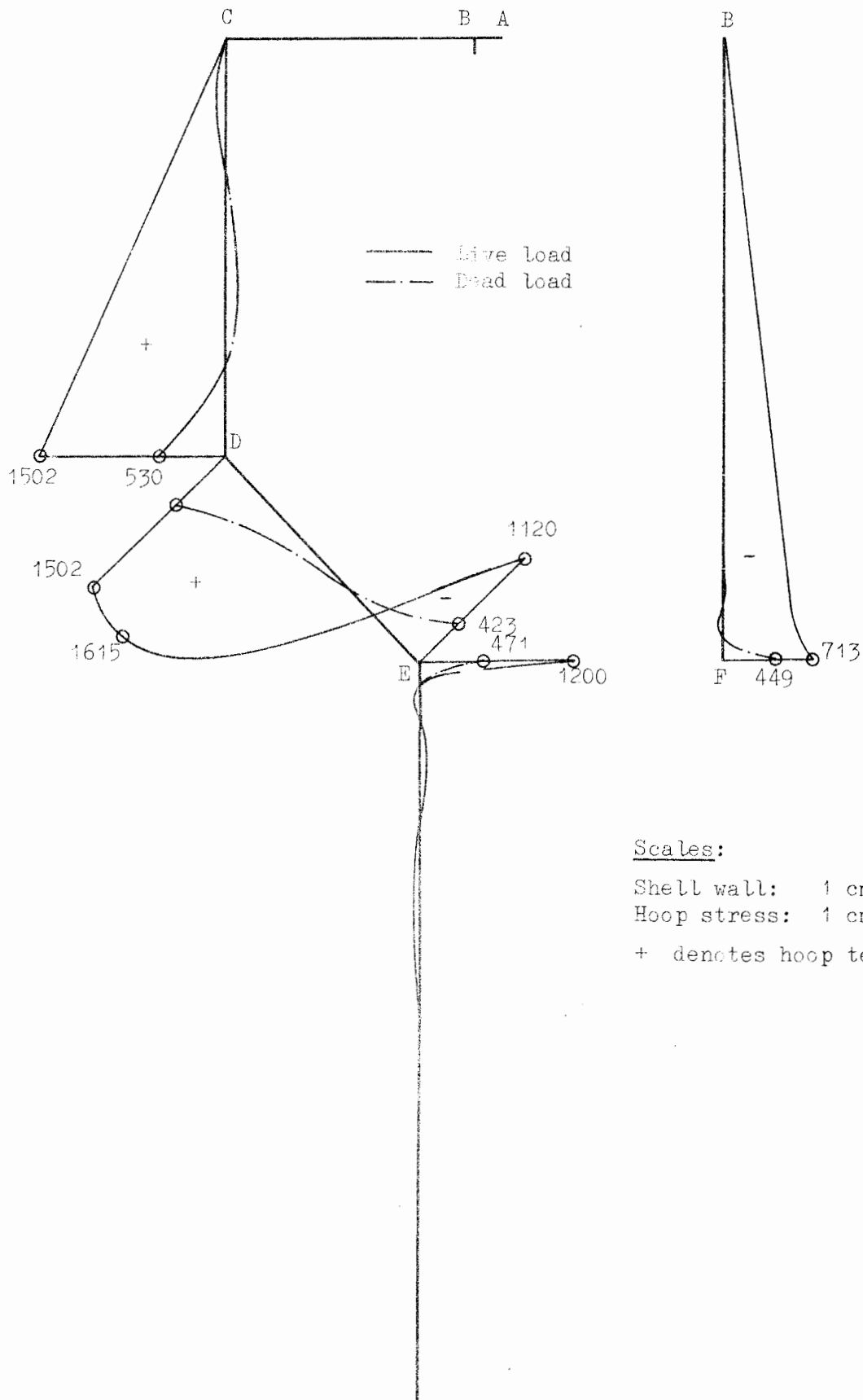


Fig. 4.44: Live and dead load hoop stresses

The hoop stresses in the cylindrical and conical parts of the structure are shown in Fig. 4.44 for both the live and dead load cases. Since the axial strains in the upper cylindrical sections of the structure are negligible, the hoop stress diagrams for these sections may be read also as radial displacement diagrams.

The hoop stresses for the live load case are much as we would expect, i.e.,

- (i) linearly increasing in the cylindrical sections, which are subject to hydrostatic pressure distributions;
- (ii) bulging significantly over most of the conical section, also due to hydrostatic pressure;
- (iii) zero in cylindrical tower, due to zero lateral forces.

The hoop stresses in the inner cylindrical wall of the tank are far smaller than in the outer wall because of the restraining influence of the circular plate at its base which permits only very small radial displacement.

The hoop stresses due to self-weight of the structure are everywhere smaller than the live load hoop stresses. This is clearly due to the fact that all self-weight loading is vertical, and thus not a primary cause of radial displacement.

The axial stresses in the cylindrical and conical sections of the structure are shown in Fig. 4.45 for both the live and dead load cases. Over each section the axial stress diagrams are linear (this may be confirmed by referring to the computer plot in Fig. 4.40), the axial stresses being caused by components in the direction of the shell meridian of the vertical loading. Hence, for the live load case the only axial stresses besides those in the tower are in the conical section, increasing from zero at junction D to a maximum at junction E.

For the self-weight load case the axial stresses begin at junctions B and C, the stresses at these points being due to the weight of the tank roof. The axial stresses increase linearly down the cylindrical and conical sections due to the linear cumulative increase in the weight of the cylinders and cones themselves.

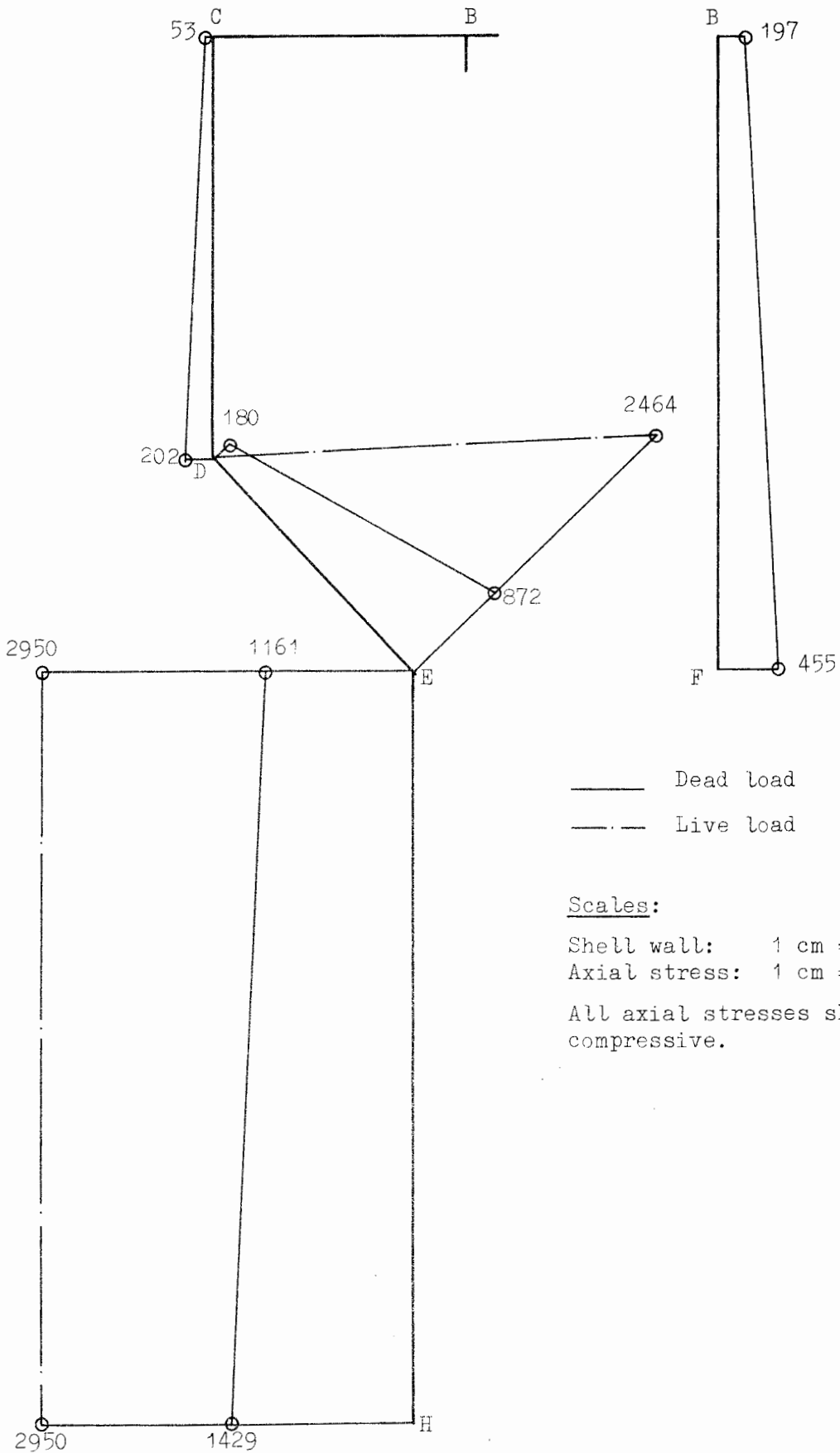


Fig. 4.45: Dead and live load axial stresses

The values given by CONFRU for the axial stresses at the base of the tower may be confirmed by the following simple calculations:

Live Load:

$$\begin{aligned} \text{Volume of effluent in tank}^* &= 550 \text{ m}^3 \\ \text{Weight of effluent in tank} &= 550 \text{ m}^3 \times 10 \text{ kN/m}^3 = 5500 \text{ kN} \\ \therefore \text{Axial stress at tower base} &= \frac{5500}{2\pi r t} = \frac{5500}{2\pi(1,4)(0,2)} = 3125 \text{ kN/m}^2 \end{aligned}$$

The corresponding value given by CONFRU is 2950 kN/m^2 . Although the difference (175 kN/m^2) is fairly large, it is equivalent to a volume of effluent of only 30 m^3 . Furthermore, it should be borne in mind that the effluent loading is input to the program as an equivalent hydrostatic pressure distribution, with the values at junctions C, D, E, F and B only being given. The agreement is, therefore, very reasonable.

Dead Load:

$$\begin{aligned} \text{Volume of material in structure} &= 105 \text{ m}^3 \\ \text{Weight of material in structure} &= 105 \text{ m}^3 \times 24 \text{ kN/m}^3 = 2500 \text{ kN} \\ \therefore \text{Axial stress at base of tower} &= \frac{2500}{2\pi r t} = \frac{2500}{2\pi(1,4)(0,2)} = 1430 \text{ kN/m}^2 \end{aligned}$$

The corresponding value given by CONFRU is 1429 kN/m^2 . The agreement is excellent.

The circumferential moments M_θ , which up until now have not been mentioned, may in general be ignored, and are included in the program CONFRU only for completeness. The reasons for ignoring these moments are:

- (i) The circumferential curvature,

$$\chi_\theta = \frac{-\sin \phi \frac{dw}{ds}}{r} \quad (2.14d)$$

reduces "ad absurdum" in the number and extent of the approximations involved in its derivation (see Section 2.4). The quantity is therefore of doubtful physical significance.

- (ii) For cylinders ($\phi = 0$), $M_\theta = 0$, and for circular plates ($\phi = 90^\circ$), M_θ depends on the slope dw/ds and inversely on the radius r of the plate. Hence we find that where the slope dw/ds is large and the radius small, large values of M_θ result.

*This volume is calculated on the geometry of the middle surface of the tank, assuming the tank to be completely full.

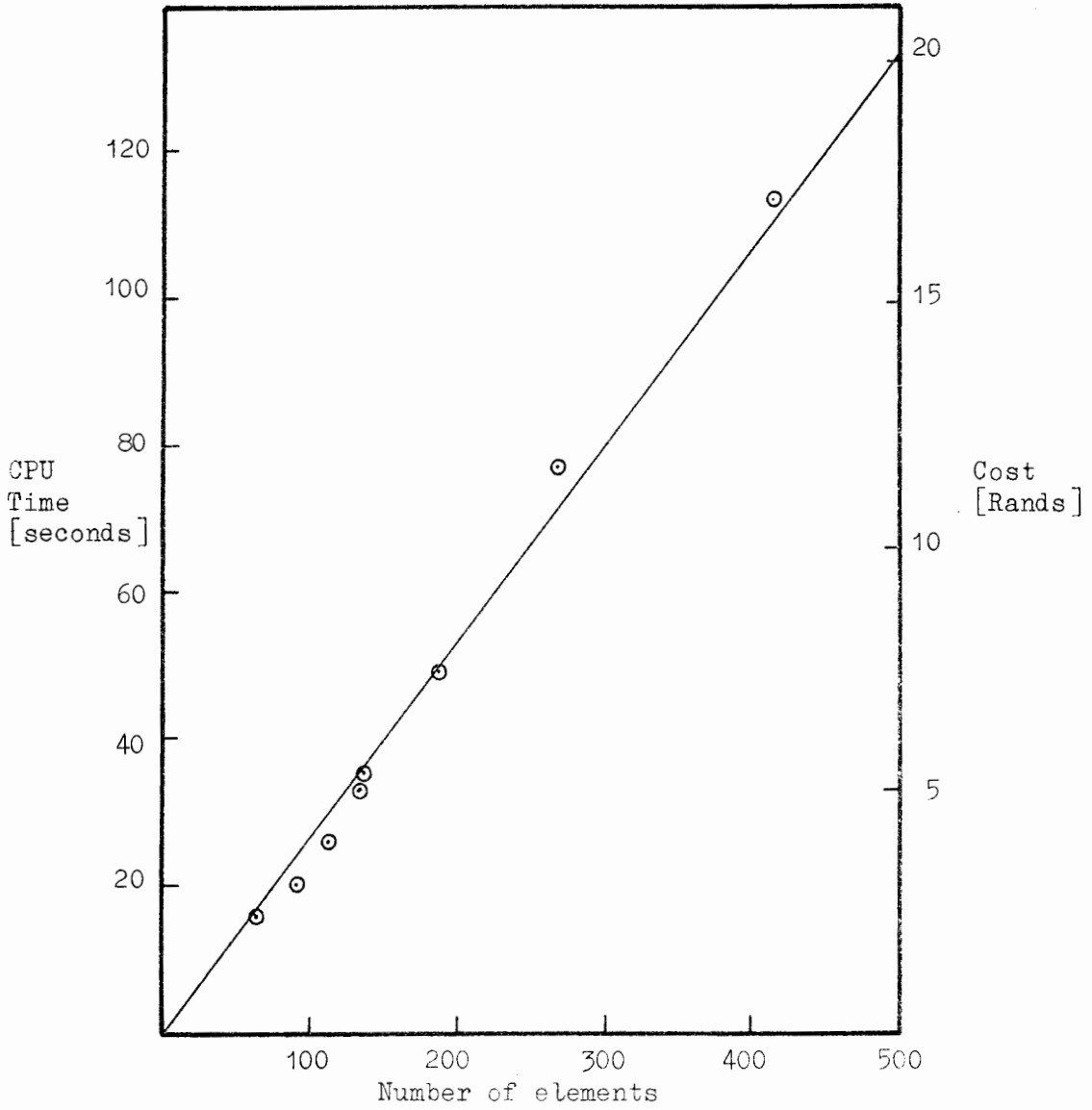


Fig. 4.46

TABLE 4.15: Plotting Times and Costs

Analysis I.D. No.	Total No. of Nodes	Size of Plot	CPU Time [seconds]	Plotting Time [minutes]	Total Cost [rands]
ST/1/1	211	Full	10	10	4-50
"	211	Small	7	6	3-85
ST/1/1 ST/2/1	414	Full	14	11	5-40
"	414	Small	13	7	4-05

This is well illustrated in the present example by the result for M_{θ} at the point A, which is a free end and perhaps the most insignificant part of the structure; at this point M_{θ} has its maximum value for the whole structure.

4.7 Computer Time-Cost Analysis

For the prospective user of a computer program the run-times and costs involved in making use of the program are of paramount importance. The run-times also give a good indication of the overall efficiency of the program.

Computer run-times for finite element analyses depend primarily on the number of elements used in the idealisation of the structure; for CONFRU the type of loading and the actual geometry of the structure have been found to have a negligible effect on run-times.

The actual CPU time for a number of analyses is shown in Fig. 4.46, plotted against the number of elements used in the analyses; the costs of the analyses, based on the CPU time, are also shown. The plotted points are seen to lie very close to a straight line, from which the maximum (extrapolated) cost of a 500 element analysis is approximately R20.

The following points should be noted in connection with Fig. 4.46:

- (i) The costs obtained from the curve should be augmented by a sum of \pm R2-00 to allow for cards read and pages printed.
- (ii) The CPU time depends on the computer system on which the program is run, which is in the present case, a UNIVAC 1106 with 65 K user core. It is envisaged that a new 200 K dual processing system will soon be in operation, which is expected to reduce the CPU times given above by up to 30%.

A representative summary of plotting times and costs is given in Table 4.15 and the following points should be noted:

- (i) The plotting time depends primarily on the number of points plotted, which is $4 \times$ (total number of nodes).

(ii) The user has the choice of three sizes for the overall plot:

- Small: $32 \times 27\frac{1}{2}$ cm: this size intended specifically for Fig. 4.40.
- Medium: 38×38 cm: this size allows two sets of axes to an A4 page.
- Large: 57×46 cm: this size allows one set of axes to an A4 page (see Fig. 4.41).

As can be seen from the table, plotting costs are low and vary over a very narrow range. It will be noticed in particular that plotting the results of two or more analyses on the same system of axes increases the plotting time and cost by almost negligible amounts.

To summarise then, the cost of using CONFRU and its associated plotting facilities is extremely low. For example, for a 250 element analysis with corresponding full size plot of stresses and moments, the user may expect to pay approximately R17.

CHAPTER 5SUMMARY AND CONCLUSIONS

CONFRU is a computer program which uses the finite element method for the linear elastic analysis of variable thickness branched axisymmetric thin shells of revolution, made up of any combination of cylinders, conical frustra or circular plates. The various features contained in the program have been tested, the accuracy of the solutions has been assessed and the potential of the program illustrated. Because the program is intended for commercial use by engineers (with perhaps limited finite element analysis experience), considerable emphasis has been placed on the correct interpretation of results, and on the conditions which should be fulfilled in order to obtain useful solutions from the program. In this respect the chapter of results serves also as a guide to prospective users of the program.

The essential features and capabilities of the program are:

A. Individual element properties

- (a) (i) Conical frustrum element: 2 nodes, 6 degrees of freedom; linear meridional, cubic normal displacement functions; compatible and complete.
- (ii) Closure element: single node, 3 degrees of freedom; linear displacement functions; compatible and complete.
- (b) Strain-displacement and stress-strain relationships:
Approximate thin shell theory of Flügge.
- (c) Stiffness matrix:
Derived by minimisation of total potential energy.
- (d) Equivalent nodal loads:
Axisymmetric; derived through minimisation of total potential energy.
 - (i) Concentrated line loads.
 - (ii) Linearly distributed loads.
 - (iii) Loads due to self-weight of shell.

(e) Material properties:

Linear elastic, isotropic, homogeneous.

(f) Thickness may vary linearly along the length of the element.

B. Properties of the structure

(a) Axisymmetric thin shell of revolution, made up of any combination of cylinders, conical frustra and circular plates.

(b) May be closed at the axis of symmetry, at any number of points.

(c) May contain any system of branching.

(d) Boundary conditions:

(i) Clamped

(ii) Pinned-clamped

(iii) Pinned-sliding

(iv) Clamped-sliding

(v) Free.

(e) Young's modulus E and Poisson's ratio ν must be constant for the structure.

C. Solution procedure(a) Numerical integration:

5 or 7 point Simpson's quadrature.

(b) Solution of equations:

Gauss-Jordan; K matrix stored in single dimension array ensuring 100% storage efficiency. Technique developed for symmetric, sparsely populated matrices.

(c) Back-substitutions: (optional)D. Output(a) Printed output: (all optional)

(i) Geometry of structure,

(ii) Loading on structure,

(iii) System stiffness matrix,

(iv) Load vector.

(v) Boundary conditions,

(vi) Displacements and rotation at each node,

(vii) Stresses and moments at each node, printed section by section.

(b) Plotted output: (optional)

Up to four sets of stress and moment results automatically plotted on a single system of axes; overall size of the plot is optional.

Of the features mentioned above, the following constitute original work by the writer:

- (i) The development and implementation of a circular plate closure element.
- (ii) The development of a general algorithm for setting up the system stiffness matrix for an arbitrarily branched shell of revolution. It is interesting to note that since the conical frustrum element is one dimensional, this algorithm may also be used for symmetric plane frame analyses.
- (iii) The development of an algorithm for the solution of sparsely populated symmetric systems of equations; the algorithm ensures 100% storage efficiency.

The correctness of the solutions given by CONFRU for single wall shells has been demonstrated by comparison with exact theoretical solutions. In the case of branched shells the solutions have been checked by making use of the method of substructures, the philosophy of which is outlined in Section 4.5.1. All solutions obtained were found to exhibit convergence as the element subdivision was refined; in particular, shell junctions, including the cylinder - circular plate junction, have no significantly adverse effects on either the convergence or the general accuracy of the solutions.

In connection with the accuracy of the solutions we have found that:

- (i) For numerical integration of the element stiffness matrix the 5 point Simpson's quadrature formula is both accurate and efficient, and there is very little to be gained in the way of accuracy by using 7 or more points.
- (ii) In Examples 1 to 4, where quantitative accuracy assessment could be performed, convergent displacement solutions were obtained by using element aspect ratios within the general range

$$1/6 \leq L/t \leq 1.$$

The maximum meridional moment error recorded was 1,65 % occurring in the wall of the hydrostatically loaded closed cylindrical tank. The errors in the moments at the shell junctions did not exceed this value.

- (iii) From Examples 6 and 7 it would appear that the branched shell solutions are of the same order of accuracy as the single wall shell solutions. Rounding errors were found to be negligible, and the choice of nodal numbering scheme had no effect on the solution.
- (iv) In Example 8, confirmation of solution convergence was obtained using two element subdivisions having aspect ratios within the range suggested above. It was pointed out that the solution obtained using an element aspect ratio of 1 was quite suitable for design purposes, although no quantitative measure of the accuracy could be given.
- (v) The program appears to operate equally efficiently when very large numbers of elements are used; significant improvements in accuracy (as gauged by the diminishing out of balance moments at shell junctions) have been obtained using over 400 elements.

It has been shown in Example 5 that CONFRU may be used to estimate the maximum hoop and axial stresses in thick wall shells, in those parts of the shell sufficiently remote from edge disturbances. This is particularly useful in the analyses of pressure vessels (which must often be classified as thick shells by definition), where analytical thick shell solutions are not available, or where the high cost of experimental analysis is prohibitive.

Throughout the development of CONFRU one of the primary aims has been to make the program simple to use. This aim we feel has been realised. Data input is kept to a minimum by relying as far as possible on automatic data generation at execution time. The user need have only a rudimentary knowledge of finite element methods, and no technical knowledge of the program is required: for example, branch points are denoted by simply naming the branch node and the numbers of the elements meeting at it. In this way the possibility of technical errors in the data input is greatly reduced.

Finally, computer run-times and associated costs are, even for large analyses, very low.

CONFURU has certain limitations which provide scope for further improvement.* Among the items requiring further attention are:

- (i) At present Young's modulus E , Poisson's ratio ν and the unit weight of the structural material γ are constant for the entire structure. Modifications which would allow these properties to vary from section to section appear to be desirable (c.f. Pian et al. [21], p 119)
- (ii) The loading conditions applicable to a shell of revolution resting on a soil foundation require investigation. Until such time, the user should bear in mind that the solutions obtained from CONFURU, while correct, are valid only in so far as the assumptions made for the loading are valid.
- (iii) It has been shown that where sharp edges occur between two sections of a shell high stress and moment concentrations arise.** In fact, the majority of shells of revolution are stiffened at these edges with ring beams designed to absorb these stress concentrations. In axisymmetric shells the ring beams are subject primarily to torsion (due to the meridional moment in the shell wall), and hoop stresses (due to radial displacement). In order to perform their function the beams are designed to be very much stiffer than the adjacent shell, the stiffness being derived from the heavy steel reinforcement in them. It is this very large relative stiffness which precludes their idealisation as shell elements, even as an approximation, since the relative stiffness of the ring beam is not simply proportional to its linear dimensions, as is the case in a normal shell element idealisation. Clearly what is required is a special ring stiffener element having prescribed torsional and hoop stiffnesses which take into account the reinforcement in the beam. The chief problem in developing such an element is to make it compatible with the adjacent shell elements; (this problem is discussed by Jones and Strome [27], p 216). Hence, until such an element has been developed for CONFURU there is no alternative but to ignore the effects of ring beams.

* We mention here only these improvements which fall within the stated scope of the program.

** See for example junctions D and E in Figs. 4.42 and 4.43. A discussion of this phenomenon is also given by Flugge [1], p 350.

There remains a final detail which while not a limitation of the program (since it does not fall within the stated scope) nevertheless deserves attention. This is the question of the elastic boundary condition and the initial temperature strain facilities, for which the fundamental theory has been given. Although both these facilities were at one stage available in CONFRU in a specialised form, they have since been deleted from the system due to lack of commercial interest.* The theory, however, remains useful for future possible reference.

*In liquid containing structures the temperature gradient occurs mainly across the thickness of the shell wall. Since the initial strain vector (Eq. 3.20) takes no account of changes in curvature, the effects of temperature gradients across the shell wall cannot be analysed. The formulation given here is suitable only for uniform heating or cooling of the shell wall as a whole.

BIBLIOGRAPHY

- [1] FLÜGGE, W., Stresses in Shells, Second edition, Springer, 1973.
- [2] TIMOSHENKO, S., and GOODIER, J., Theory of Elasticity, Third edition, McGraw-Hill, 1970.
- [3] TIMOSHENKO, S., and WOINOWSKY-KRIEGER, S., Theory of Plates and Shells, Second edition, McGraw-Hill, 1959.
- [4] ZIENKIEWICZ, O.C., The Finite Element Method in Engineering Science, London, McGraw-Hill, 1971.
- [5] WASHIZU, K., Variational Methods in Elasticity and Plasticity, Pergamon Press, Oxford, 1968.
- [6] TOTTENHAM, H., and BREBBIA, C., Finite Element Techniques in Structural Mechanics, Stress Analysis Publishers, Southampton, 1970.
- [7] ARGYRIS, J.H., and KELSEY, S., Energy Theorems and Structural Analysis, Butterworths, London, 1968.
- [8] COURANT, R., and HILBERT, D., Methods of Mathematical Physics, Vol. II, 1962.
- [9] RALSTON, A., A First Course in Numerical Analysis, McGraw-Hill, 1965.
- [10] McCracken, D.D., and DORN, W.S., Numerical Methods and FORTRAN Programming, John Wiley and Sons, 1966.
- [11] GREENBAUM, G.A., Comments on "Numerical Analysis of Unsymmetrical Bending of Shells of Revolution", AIAA, v 2, n 3, March 1964.
- [12] NOVOZHILOV, V.V., Thin Shell Theory, Second Edition, Walters-Noordhoff, 1970.
- [13] PERCY, J.H., PIAN, T.H.H., KLEIN, S., and NAVARATNA, D.R., Application of Matrix Displacement Method to Linear Elastic Analysis of Shells of Revolution, AIAA, v 3, n 11, 1965.
- [14] PARDOEN, G.C., and HAGEN, R.L., Symmetrical Bending of Circular Plates using Finite Elements, Computers and Structures, v 2, 1972, p 547.
- [15] HADLEY, E., Linear Algebra, Addison-Wesley, 1965.
- [16] KLEIN, S., A Study of the Matrix Displacement Method as Applied to Shells of Revolution, Proc. Conf. Matrix Meth. Struct. Mech., WPAFB, Oct. 1965.
- [17] GRAFTON, P.E., and STROME, D.R., Analysis of Axisymmetric Shells by Direct Stiffness Method, AIAA, v 1, n 10, 1963.
- [18] SABIR, A.B., and ASHWELL, D.G., A Stiffness Matrix for Shallow Shell Finite Elements, Int. J. Mech. Sci., v 11, 1969, p 269.

- [19] AHMAD, S., IRONS, B.M. and ZIENKIEWICZ, O.C., Analysis of Thick and Thin Shell Curved Structures by Finite Elements, Int. J. Num. Meths. in Eng., v 2, 1970, p 419.
- [20] PIAN, T.H.H., WITMER, E.A., MACK, E.W. and BERG, B.A., An Improved Discrete Element Analysis and Program for the Linear-Elastic Static Analysis of Meridionally-Curved, Variable Thickness, Branched Thin Shells of Revolution Subject to General External Mechanical and Thermal Loads, Parts I and II, ASRL TR 146-4, M.I.T., Cambridge, Massachusetts, March 1968.
- [21] (a) GRIFFIN, T.B., Consani Pressure Vessels: Results of Computer Analyses, Dept. of Civil Engineering, U.C.T., Dec. 1973.
 (b) MILES, A.W., Consani Pressure Vessels: Results of Hydrostatic Pressure Tests, Dept. of Mechanical Engineering, U.C.T., Nov. 1973.
- [22] RYDER, G.H., Strength of Materials, Third Edition, MacKilloan, 1961.
- [23] DESAI, C.S. and ABEL, J.F., Introduction to the Finite Element Method, Van Nostrand Reinhold, 1972.
- [24] Correspondence; Computer Science Division, C.S.I.R., Pretoria, May 1973.
- [25] BREBBIA, C.A. and DEBNATH, J.M., Comparison of Recent Shallow Shell Finite Element Analyses, Int. J. Mech. Sci., v 12, n 10, Oct. 1970.
- [26] KRAUS, H., Computers and the Analysis of Pressure Vessels, Computers and Structures, v 2, n 5/6, Dec. 1972.
- [27] JONES, R.E. and STROME, D.R., A Survey of Analyses of Shells by the Displacement Method. Proc. Conf. Matrix Meth. Struct. Mech., WPAFB, Oct. 1965, p 205.
- [28] GALLETLY, G.D., Influence Coefficients for Open Crown Hemispheres. Trans. ASME, v 82A, 1960.
- [29] GREEN, B.E., STROME, D.R. and WEIKEL, R.C., Applications of the Stiffness Method to the Analysis of Shell Structures, ASME Paper No. 61 - AV - 58, March 1961.
- [30] CLOUGH, R.W. and JOHNSON, C.P., Finite Element Approximation for the Analysis of Thin Shells, Int. J. Solids and Structures, v 4, n 1, Jan. 1969.
- [31] POPOV, E.P., PENZIEN, J. and LU, Z.A., Finite Element Solution for Axisymmetric Shells, ASCE, v 90, EM5, Oct. 1964.
- [32] PERCY, J.H., PIAN, T.H.H., KLEIN, S. and NAVARATNA, D.R., Application of Matrix Displacement Method to Linear Elastic Analysis of Shells of Revolution, AIAA, v 3, n 11, Nov. 1965.
- [33] JONES, R.E. and STROME, D.R., Direct Stiffness Method of Analysis of Shells of Revolution utilising Curved Elements, AIAA, v 4, n 9, Sept. 1966.
- [34] STRICKLIN, J.A., NAVARATNA, D.R. and PIAN, T.H.H., Improvement on the Analysis of Shells of Revolution by Matrix Displacement Methods, AIAA, v 4, n 11, Nov. 1965.

- [35] UTKU, S., Stiffness Matrices for Thin Triangular Elements of Non-Zero Gaussian Curvature, AIAA, v 5, Sept. 1967.
- [36] CONNOR, A. and BREBBIA, C.A., Stiffness Matrix for a Shallow Rectangular Shell Element, ASCE, v 93, EM5, 1967.
- [37] BONNES, G., DHATT, G., GIROUX, Y.M. and ROBICHAUD, L.P.A., Curved Triangular Elements for the Analysis of Shells, Proc. Conf. Matrix Meth. Struct. Mech., WPAFB, Oct. 1968.
- [38] POPOV, E.P. and SHARIFI, P., A Refined Curved Element for Thin Shells of Revolution, Int. J. Num. Meth. Eng., v 3, 1971, p 495.
- [39] MUNROE, J.A. and CHEN, Y., A Finite Element Analysis of an Axisymmetrically Loaded Orthotropic Shell of Revolution, Computers and Structures, v 2, 1972, p 723.
- [40] ICES STRUDL II, Engineering User's Manual, Volume 2, Additional Design and Analysis Facilities, Second Edition, June 1971, M.I.T., Cambridge.
- [41] Correspondence; The Genesys Center, University of Technology, Loughborough, Leicestershire, Feb. 1974.
- [42] HARTUNG, R.F., An Assessment of Current Capabilities for Computer Analysis of Shell Structures, Computers and Structures, v 1, n 1/2, Aug. 1971.

APPENDIX ACONFRU User's ManualList of Contents

	Page
A.1 <u>Introduction</u>	119
A.2 <u>The Internal Logic of CONFRU and STRESSPLOT</u>	
A.2.1 General description: CONFRU main program	120
A.2.2 Description of CONFRU subroutines	122
A.2.3 Plotter program STRESSPLOT	137
A.3 <u>CONFRU Input Data</u>	
A.3.1 Preparation of input data	140
A.3.2 Coding of input data	145
A.3.3 Maximum size of analysis	155
A.3.4 Sample runstreams for the execution of CONFRU and STRESSPLOT, including STRESSPLOT input data.	156
A.4 <u>A Complete Sample Analysis and Plot</u>	
A.4.1 Input data	159
A.4.2 Partial listing of results	160
A.5 <u>Listings of Programs</u>	172

A.1 Introduction

CONFURU is a finite element computer program capable of the linear elastic, static analysis of variable thickness branched axisymmetric thin shells of revolution subject to any system of axisymmetric mechanical loads. The shell and finite element theory upon which the program is based has been given in Chapters 2 and 3, and numerous results obtained from the program are discussed in Chapter 4.

A description of the internal logic of CONFURU is given in section A.2, including descriptions of the individual subroutines. This information serves primarily to supplement the input data, a detailed description of which is given in section A.3. Included in this section are typical run-streams showing the relationship between the analysis program CONFURU and the plotter program STRESSPLOT.

Sample data input and results for the analysis of Example 8 of Chapter 4 are shown in section A.4, and complete listings of all programs are given in section A.5.

CONFURU is written in FORTRAN V as implemented on the UNIVAC 1106 series computer. A complete deck of cards for the program is available and the program is maintained permanently on both disc and magnetic tape at the University of Cape Town Computer Centre. CONFURU is therefore immediately available to any interested user.

In the descriptions that follow (except for the input of data), it is assumed that the user has a basic knowledge of FORTRAN V.

A.2 The Internal Logic of CONFRU and STRESSPLOT

A.2.1 General Description: CONFRU main program

CONFRU is structured in modular form, i.e., it consists of a main program and a series of independent subroutines. The functions of the main program are to coordinate the steps in the analysis by making decisions and calling the relevant subroutines, and to perform all input/output. The actual analysis is performed by the various subroutines acting either alone or in conjunction, each of which has a specific function.

A macro flow chart for the main program (MAIN) showing the steps in the analysis and the fourteen subroutines called, is given in Fig. A.1; a description of each subroutine is given in section A.2.2. Among the general features of the program are the following:

- (a) All arithmetic is performed in double precision.
- (b) All real variable arrays are dynamically dimensioned.* The advantages of this form of dimensioning are:
 - (i) Compatibility of dimensions of variables in the main program and the corresponding variables in the subroutines is ensured.
 - (ii) The dimensions of all similarly dimensioned variables in both the main program and the subroutines may be changed by changing a single number which appears on the first card of the main program.
- (c) All printed output is optional. The user may select exactly which output is required. This is particularly useful in those cases where the program is executed from a remote terminal.
- (d) The modular form of the program allows subsidiary steps in the analysis to be ignored if not required. For example, if there are no concentrated line loads acting on the structure, the subroutine PTLOAD is ignored.
- (e) Stress and moment results are automatically written into a computer disc file for future plotting. The actual plotting is performed by a separate program STRESSPLOT, described in section A.2.3

*See also "Maximum size of analysis possible", section A.3.3.

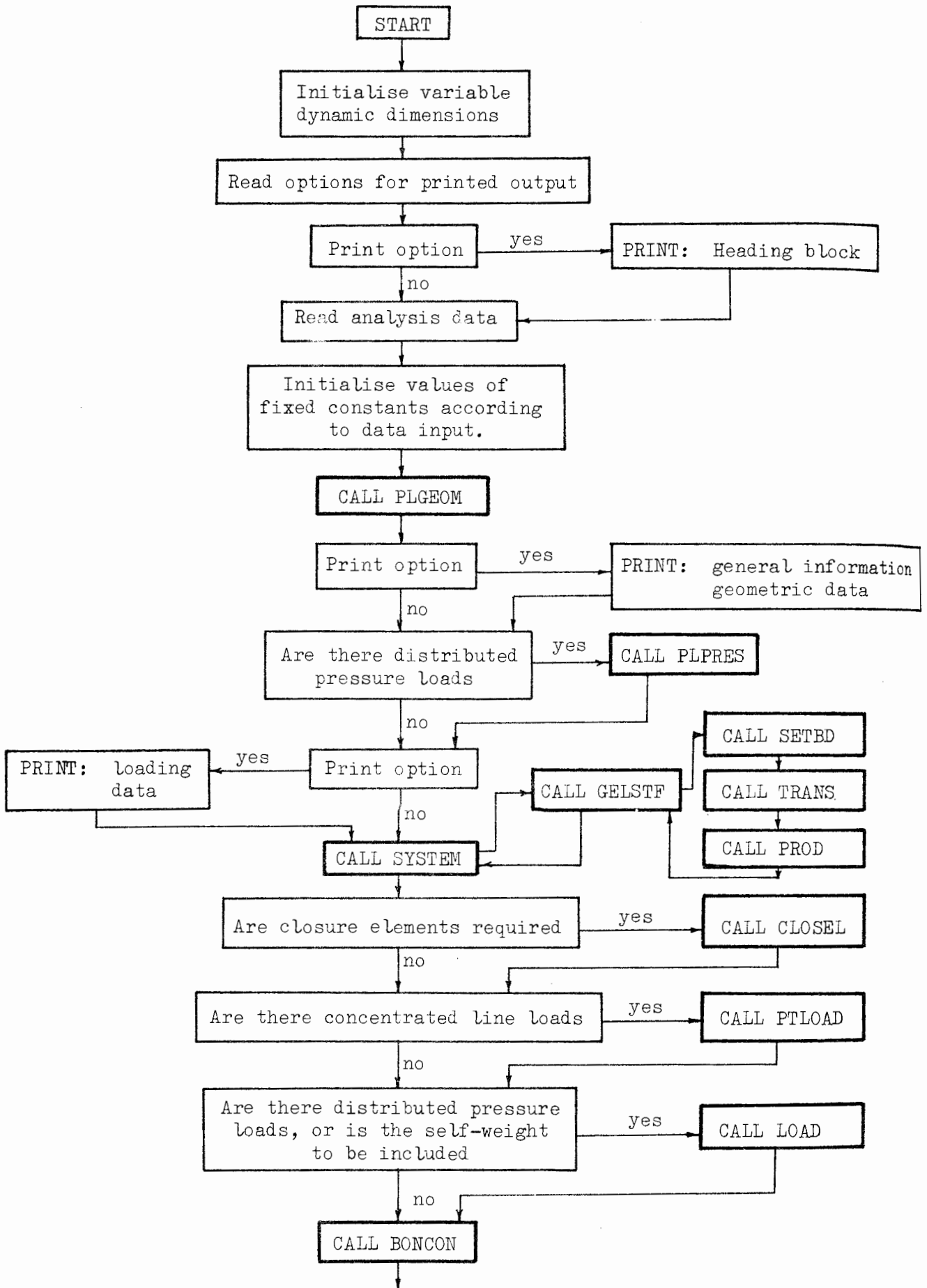


Figure A.1: Macro flow chart for CONFRU main program

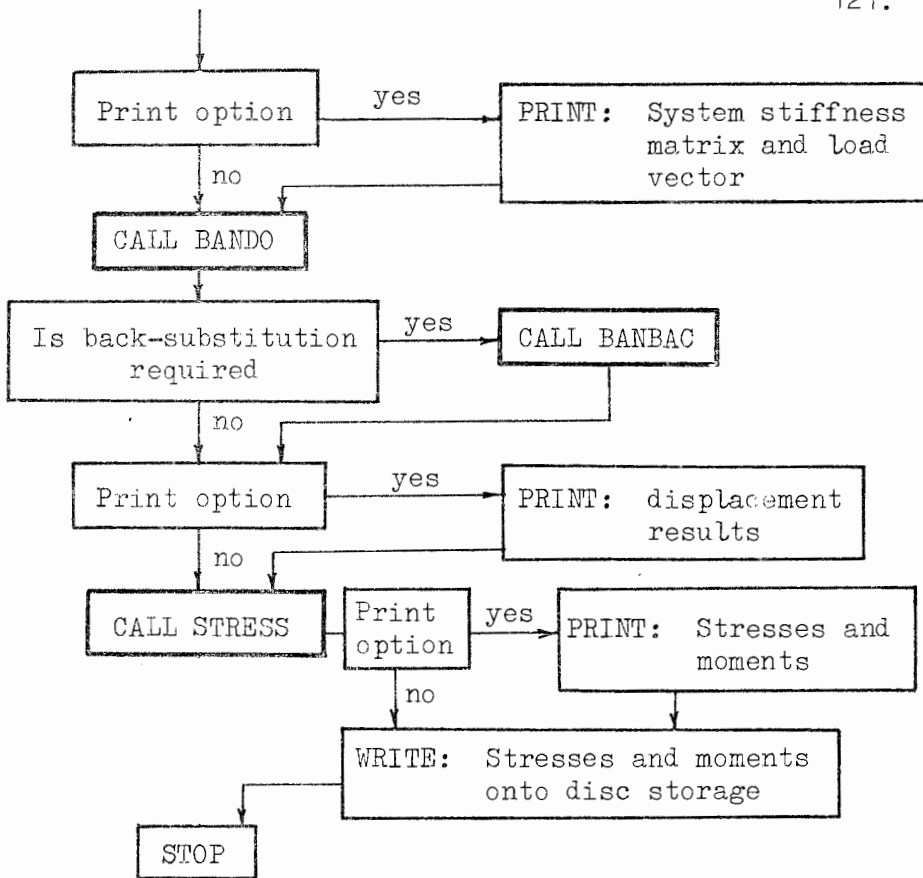


Figure A.1: (Continued)

A.2.2 Description of CONFRU subroutines

There follows a description of each of the subroutines used in CONFRU. In each subroutine, its function, input and output variables, and a brief description of its salient features are given. The subroutines are described in the order in which they appear in the macro flow chart of Fig. A.1.

The information given here serves only as the first step towards a programmer's reference and is not intended to be complete. The descriptions should be viewed rather as augmenting the preparation and coding of input data, and to this end particular attention has been paid to the input and output variables associated with each subroutine

In many cases the information given here is sufficient for compiling flow charts from the listings of the subroutines. Particular attention has been paid to describing the use of SYSTEM and BANDO since these subroutines are useful outside the context of CONFRU:

Notation used for input and output variables:

- (i) Variables beginning with the letters I, J, K, L, M and N are integers, with the exception of the length of element i $L(I)$ which is real.
- (ii) Subscripted variables are arrays having the number of dimensions indicated. All the other variables are constants.
- (iii) Variables preceded by a star (*) are transferred to or from the subroutine through a COMMON statement. All other variables are transferred via the subroutine argument list.
- (iv) When a variable which has already been defined is encountered in an input or output list the name of the subroutine in which it was defined is given in square brackets.

Subroutine PLGEOM (NSEC, NELB, NELE, RB, RE, TB, TE, L, T, R1, R2)

Function: To calculate the geometry of every element.

Input variables:

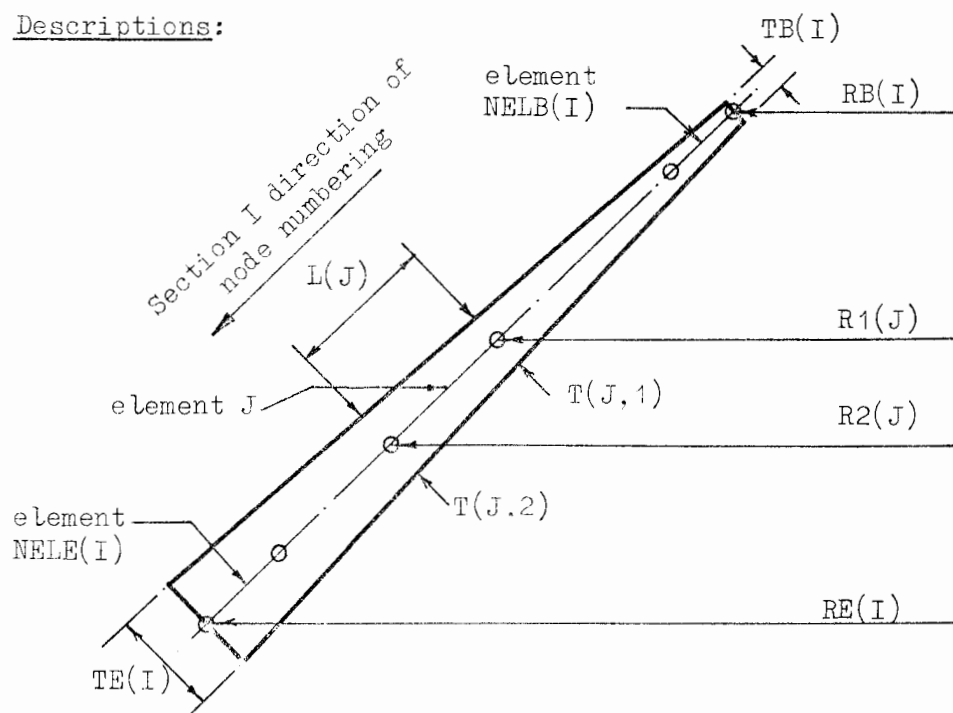
NSEC : number of sections (see definition, section A.3.1)
 NELB(I): number of the first element in section I

NELE(I) : number of the last element in section I
 RB(I) : radius of the first node in section I
 RE(I) : radius of the last node in section I
 TB(I) : thickness of shell at start of section I
 TE(I) : thickness of shell at end of section I
 L(J) : length of element J.

Output variables:

T(J,1) : thickness of element J at its start
 T(J,2) : thickness of element J at its end
 R1(J) : radius of element J at its start
 R2(J) : radius of element J at its end.

Descriptions:



Given the radius and thickness of the shell at the ends of each section, and the length of each element, PIGEOM calculates the radius and thickness at the ends (nodes) of each element.

Subroutine PLPRES (NPS, NELP1, NELP2, PR1, PR2, L, P1, PDA)

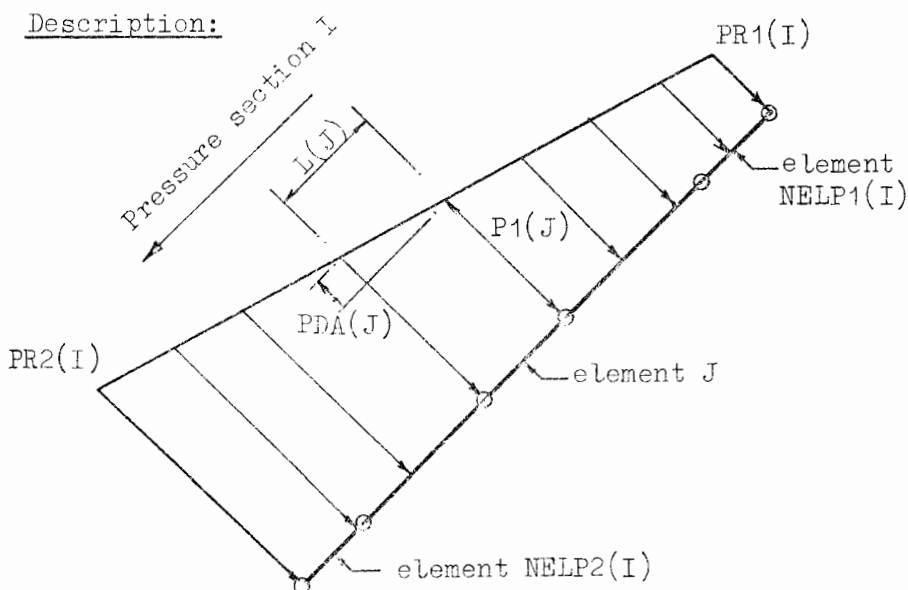
Function: To calculate the value of the pressure loading at the beginning of each element.

Input variables:

NPS : number of pressure sections (see definition, section A.3.1).
 NELP1(I): the number of the first element in pressure section I.
 NELP2(I): the number of the last element in pressure section I.
 PR1(I) : the value of the pressure at the beginning of pressure section I [N/m^2].
 PR2(I) : the value at the end of pressure section I.
 L(J) : [PLGEOM]

Output variables:

P1(J) : the value of the pressure at the beginning (first node) of element J.
 PDA(J) : the pressure difference across element J.

Description:

Given the pressures and element numbers at the beginning and end of each pressure section, PLPRES calculates the pressure at the beginning of each element, as well as the pressure difference across each element within the pressure section.

Subroutine SYSTEM (ND, L, R1, R2, T, NC, NM, NF, A)

Function: To set up the system stiffness matrix in a form suitable for solution by subroutine BANDO.

Input variables:

ND(K,M): branching information (see corresponding data input description section A.3.2, point 10).

L(J) :
 R1(J) :
 R2(J) : } [PLGEOM]
 T(J,1) :
 T(J,2) :

*NBP : number of branch points.

*NELT : total number of elements.

*N : total number of stiffness equations.

Output variables:

NC, NM, NF: counters which describe the form of A. [BANDO]

A(I) : an array which contains the coefficients of the system stiffness matrix. [BANDO]

Description:*

SYSTEM builds up the system stiffness matrix, beginning at node 1 and working sequentially through the nodes. Each node has associated with it 3 rows of the K matrix and between 1 and 3 elements. Hence, on finding itself at node I, SYSTEM determines which elements are joined to node I, CALLS for their individual element stiffness matrices (which are set up by subroutine GELSTF), and inserts these k matrices into their correct position in K. At the same time SYSTEM generates the counters NC, NM and NF which describe the form which the K matrix is taking.

The program is divided into five main parts:

- (i) a part which inserts the k matrix for element 1 into K;
- (ii) a decision-making part which interprets the branching information and selects which of the remaining parts of the program to go to;
- (iii) a part which deals with all standard parts of K, i.e. those nodes which are not associated with branching;

*K refers to the system stiffness matrix, and k to an element stiffness matrix.

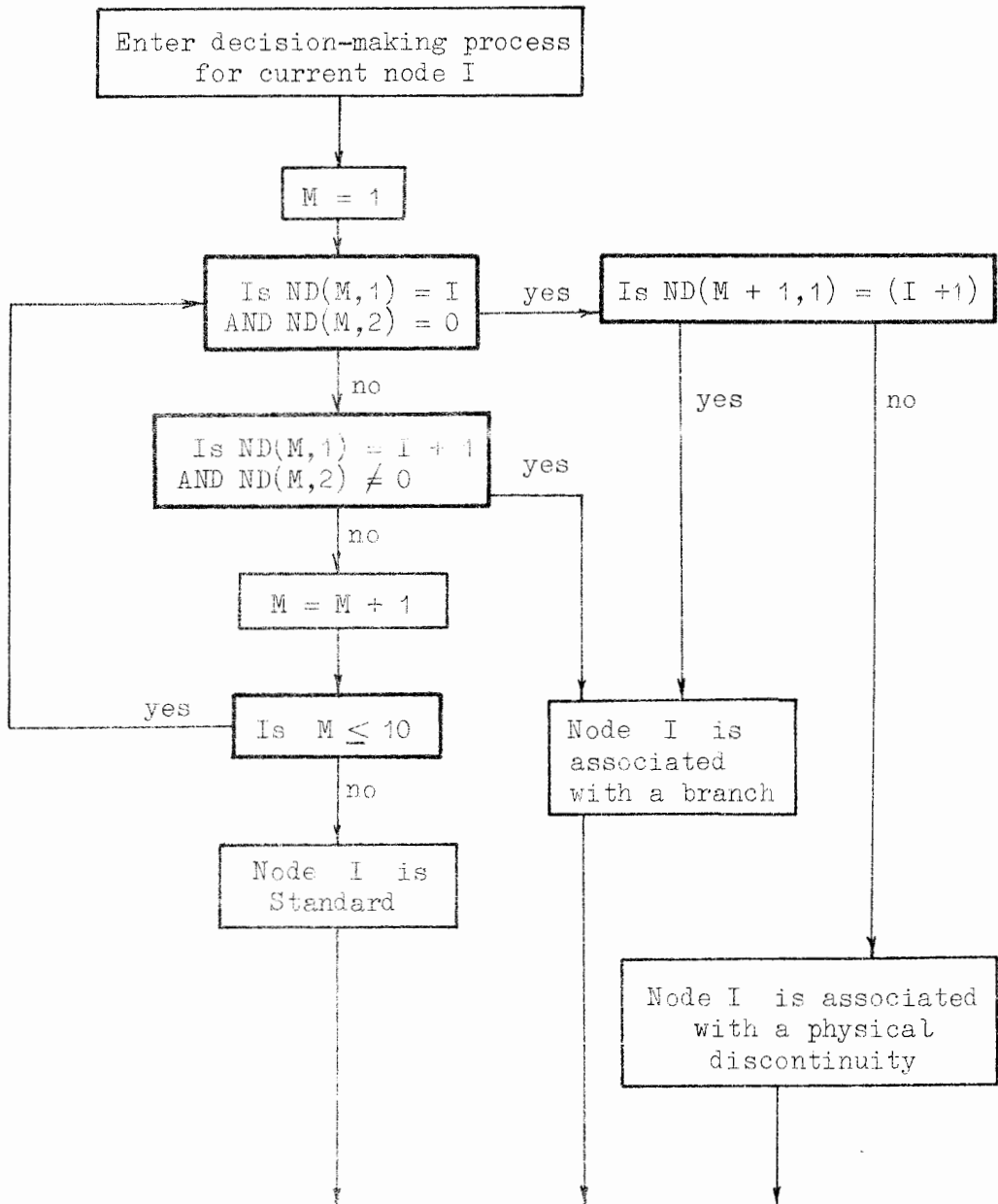


Fig. A.2

- (iv) a part which deals with all branching;
- (v) a part which deals with physical discontinuities associated with boundary conditions.

Part (i), although it deals with a standard part of the K matrix, is necessary because the required subscript notation for $A(I)$ ($I = 1,6$) is not compatible with the logic of part (iii).

Part (ii) uses the branching information in $ND(K,M)$ to decide which of the remaining three parts of the program to go to. A flow chart of the decision-making process is shown in Fig. A.2. Notice that the process is entered once for every node and that the entire set of branching information is scanned for every node, whether or not the information for a particular branch point has already been used. (The latter fact is clearly necessary since the information for one branch may affect more than one node).

If the decision is to go to part (iv) then once this part is entered further decisions are made as to what type of branch is being dealt with. However, since all the branch types have certain features in common there is no necessity for having a special section for each branch type.

SYSTEM may also be used to set up the system stiffness matrix for a symmetrical plane frame when only half the frame need be analysed. This is clear from the fact that the axisymmetric shell is idealised as a plane structure and is analysed using a one-dimensional element having three degrees of freedom at each node (two translations and one rotation). The only changes to SYSTEM that would be required are as follows:

- (i) the statement CALL GELSTF which sets up the element stiffness matrix should be replaced by a CALL to another subroutine which sets up a corresponding plane frame element stiffness matrix;
- (ii) the geometric arguments L, R1, R2 and T which are used to calculate the element stiffness matrix should be replaced by the corresponding plane frame parameters (length, depth and breadth of element). Note that SYSTEM itself is independent of the geometrical parameters used, such parameters being required only by subroutine GELSTF.

The above changes necessitate the replacement of only 10 out of the 227 cards of SYSTEM.

For plane frames there is no problem with closing the structure at the axis of symmetry since the symmetric plane frame must have a node on the axis of symmetry.

Once SYSTEM has been used to set up a plane frame K, matrix BANDO may be used to solve the resulting set of stiffness equations. Hence the major programming effort required for a symmetrical plane frame analysis is already available in CONFRU.

Subroutine GELSTF (L, R1, R2, T1, T2, KE)

Function: To derive, using numerical integration, a conical frustrum element stiffness matrix for the *i*th element.

Input variables:

L : length of element *i*,
 R1 : radius at start of element *i*,
 R2 : radius at end of element *i*,
 T1 : thickness of element *i* at its start,
 T2 : thickness of element *i* at its end,
 *NGP : number of integration points to be used.

Output variable:

KE(I,J) : the (6 × 6) element stiffness matrix.

Internal variable (numbers in brackets after each, refer to dimensions):

B(4,6) : the matrix [B],
 D(4,4) : the matrix [D*],
 BT(6,4) : matrix [B]^t
 Z(6,4) : matrix product [B]^t [D*],
 ZK(6,6) : matrix product [B]^t [D*] [B],
 SD : the distance from the start of the element to the *j*th integration point
 T(J) : the thickness of the element at the *j*th integration point.

Description:

GELSTF derives a (6×6) element stiffness matrix given by,*

$$k = \frac{2\pi EL}{1 - \nu^2} \int_0^1 [B]^t [D^*] [B] r ds'$$

The program algorithm follows the procedure described in section 3.1.2, with the following additional features:

- (i) numerical integration may be either 5 or 7 point Simpson's quadrature, as selected by NGP;
- (ii) the matrices $[B]$ and $[D^*]$ are set up by subroutine SETBD;
- (iii) matrix transposition is performed by subroutine TRANS;
- (iv) matrix products are calculated by subroutine PROD.

It is important to note that GELSTF ignores the factor $2\pi E/(1 - \nu^2)$ since it is constant for the entire structure. This factor is applied only after the system stiffness equations have been solved by BANDO, whence the solution obtained from BANDO is multiplied by the inverse factor $(1 - \nu^2)/2\pi E$ to yield the actual displacements. This multiplication is performed in the MAIN program directly after the CALL BANBAC statement.

The form of the element stiffness matrix required by SYSTEM is the complete (6×6) matrix using standard subscript notation, e.g., KE(3,4) is the stiffness in the fourth column of the third row.

Subroutine SETBD (RNU, L, R1, R2, SD, T, B, D)

Function: To set up from their explicit formulae the matrices $[B]$ and $[D^*]$ (see subroutine GELSTF) for a given point along the length of a given element.

Input variables:

RNU : Poisson's ratio ν .

(All other variables in the argument list have the same meaning as given in subroutine GELSTF.)

*Chapter 3, section 3.1.2, Eq. (3.17).

Description:

The logic of the program is trivial except for one feature: if the angle of inclination of the element, as defined by

$$\text{SINQ} = \sin \phi = \frac{r_2 - r_1}{L}$$

$$\text{and } \text{COSQ} = \cos \phi = \left[1 - \left(\frac{r_2 - r_1}{L} \right)^2 \right]^{\frac{1}{2}}$$

is close to 0° (a cylinder) or 90° (a circular plate), then the limiting values are assumed and $\sin \phi$ and $\cos \phi$ are given the values 0 or 1 as the case may be. This is to ensure that cylinders and circular plates have their exact sine and cosine values.

Subroutine TRANS (NR, NC, B, BT)

Function: To transpose the matrix B having NR rows and NC columns. The transpose is contained in the matrix BT.

Subroutine PROD (NR1, NC1, A, NR2, NC2, B, C)

Function: To multiply two matrices A and B, and to insert the product into a matrix C. Matrix A has NR1 rows and NC1 columns: matrix B has NR2 rows and NC2 columns. Clearly, for a valid operation $\text{NC1} = \text{NR2}$ whence matrix C has NR1 rows and NC2 columns.

Subroutine CLOSEL (ICLOSE, NF, GC, P1, R1, T, A, VEC)

Function: To augment the system stiffness matrix and system load vector with the required closure element stiffness matrices and load vectors.

Input variables:

ICLOSE(I) : the node number of the ith closure element

NR, A, VEC: [BANDO]

P1, R1, T : [PLPRES]

GC : [LOAD]

Output variables:

A, VEC: (augmented)

Description:

From the closure element node number the corresponding rows in system stiffness matrix are selected and the required stiffness coefficients (diagonal elements only) are augmented. The same applies to the augmentation of the system load vector.

Explicit expressions for the closure element stiffnesses are given in section 3.2.1, together with the equivalent nodal loads for a uniformly distributed load acting on the closure element, and its self-weight.

Subroutine LOAD (NELT, GC, L, R1, R2, T, P1, PDA, VEC)

Function: To set up the system load vector for the self-weight of the structure and all distributed loads acting on the structure.

Input variables:

NELT : total number of elements used in the structural idealisation,
 GC : the unit weight of the structural material,
 L, R1, R2, T, P1, PDA: [PLPRES]

Output variable:

VEC(I): the ith component of the system load vector.

Internal variables:

SQ, SINQ : $\sin \phi$ } where ϕ is the angle of inclination of the element.
 CQ, COSQ : $\cos \phi$ }

Functions U1, W1, M1, U2, W2, M2: the explicit expressions for the equivalent nodal loads at nodes 1 and 2 of an element loaded with a linearly distributed load and/or its own self-weight. These expressions are given in Appendix E.

Description:

The program works through the entire structure, element by element, performing the following functions for each element I:

- (i) if $P1(I) > 0$ element I has a linearly distributed load on it, whose shape is defined by $PDA(I)$. The equivalent nodal loads are calculated and inserted into VEC .
- (ii) if $GC > 0$ the self-weight of the structure is to be included and the same procedure as above is followed.

The procedure is described in more detail in section 3.3.2.

Subroutine PTLOAD (NNPL, NPTL, R1, R2, L, UU, WW, MM, VEC)

Function: To insert all concentrated line loads into the system load vector.

Input variables:

NNPL : the number of nodes at which line loads are applied,
 NPTL(I) : the node number of the i th node at which line loads are applied,
 R1, R2, L: [PLGEOM],
 UU(I) : the axial component of the line load at node NPTL(I)
 WW(I) : the radial component of the line load at node NPTL(I) } [N/m]
 MM(I) : the applied moment at node NPTL(I) [Nm/m]

Output variable:

VEC: [LOAD]

Description:

The input line loads per unit of circumference are converted to total loads acting at the node and superimposed into the appropriate position in the system load vector.

Subroutine BONCON (NNBC, NBC, NC, NM, NF, UBC, WBC, MBC, A, VEC)

Function: To apply the structural boundary condition.

Input variables:

NNBC : number of nodes at which boundary conditions are to be applied,
 NBC(I) : the node number of the i th node at which a boundary condition is to be applied
 UBC(I) = $\begin{cases} 'U' & \text{if the axial displacement at node NBC(I) is zero} \\ 0 & \text{otherwise} \end{cases}$

$$WBC(I) = \begin{cases} 'W' & \text{if the radial displacement at node } NBC(I) \text{ is zero} \\ 0 & \text{otherwise} \end{cases}$$

$$MBC(I) = \begin{cases} 'M' & \text{if the rotation at node } NBC(I) \text{ is zero} \\ 0 & \text{otherwise} \end{cases}$$

NC, NM, NF, A: [BRANDO]
 VEC : [LOAD]

Output variable:

A, VEC : (augmented).

Description:

For every displacement component which is known to be zero the corresponding row and column of the system stiffness matrix and load vector are set to zero, including the diagonal element. The row and column are not removed from the system since this would require a partial redefinition of NC, NM and NF which would be both a time consuming and lengthy process. The size and form of A remains unchanged.

Subroutine BANDO (N, NC, A, VEC, NM, NF, NR, NWR)

BANDO is a subroutine for the solution of a system of linear simultaneous equations, whose matrix of coefficients is symmetric.

The subroutine is designed specifically for sparsely populated, irregularly formed matrices; for example, a matrix with a diagonal band and scattered elements away from the band. The normal methods of storing such systems in two-dimensional arrays results in excessive waste of storage space since the storage of the scattered off-diagonal elements necessitates also the storage of large numbers of zeros which are not required for the solution. BANDO overcomes this problem by storing only half the matrix of coefficients in a single dimension array (i.e. a vector), in such a way that 100% storage efficiency is always obtained.

The basis of the solution procedure itself is the Gauss-Jordan method. However, although the solution procedure is straightforward, because the matrix of coefficients is stored in vector form a somewhat complex system of logic is required to put the method into practice. In particular, three counter variables NC, NF and NM must be generated with the matrix of coefficients to describe its exact form.

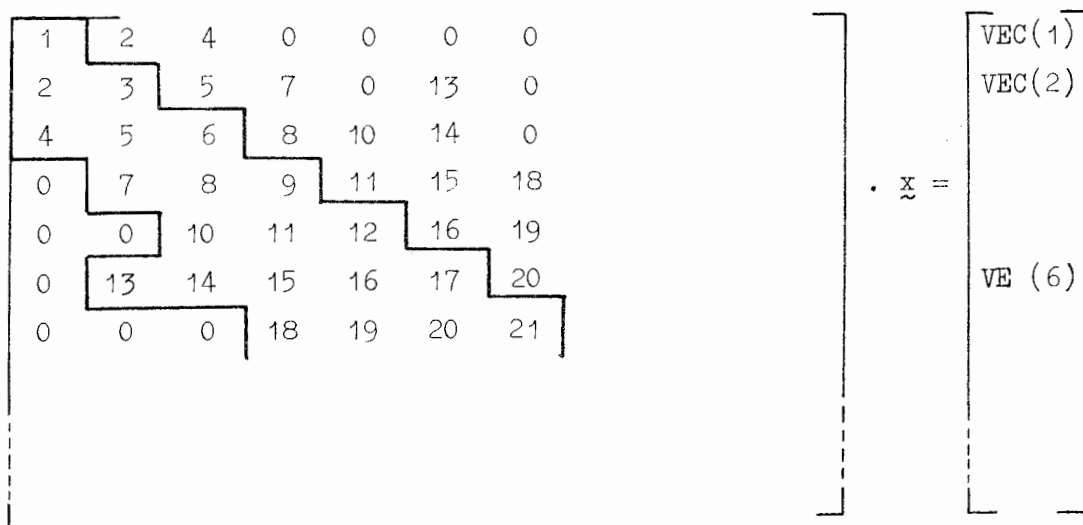
Input variables:

- A(J) : the coefficients of the lower diagonal half of the system stiffness matrix, stored row by row in a single dimension vector. Each row begins with the first non-zero element and ends with the diagonal element.
- NC(I) : the number of the column in which row I has its first non-zero element.
- NF(I) : the value of the subscript of the element of A which contains the first non-zero element of row I.
- NM(I) = I - NC(I) + 1; the total number of elements in row I between the first non-zero element and the diagonal, both inclusive.
- VEC(I) : the element of the load vector corresponding to row I.
- N : the total number of equations.
- NR, NWR : (these are internal variable arrays and are included in the list of arguments only so that they may be dynamically dimensioned to the same dimensions as NC, NM and NF.)

Output variable:

- VEC(I) : the solution of the system of equations is contained in the vector VEC(I).

The above variables are illustrated in the figure below. The shaded area represents the part of the system stiffness matrix stored in A; the numerals refer to the subscript of A. Note that all the elements between the first non-zero element and the diagonal (both inclusive) must be stored.



Row I	NC(I)	NF(I)	NM(I)
1	1	1	1
2	1	2	2
3	1	4	3
4	2	7	3
5	3	10	3
6	2	13	5

Boundary conditions:

In finite element applications where the boundary conditions result in complete rows and columns of the coefficient matrix being set to zero, these rows and columns must not be deleted from the system. If BANDO encounters a zero diagonal element (corresponding to a zero displacement boundary condition), it simply skips that row, and the corresponding displacement component remains zero.

Description of logic:

The logic used in BANDO depends primarily on the following fact: the process of reducing the elements of a column below the diagonal to zero (which is the basis of the Gauss-Jordan method) leaves the matrix symmetrical, except of course for those columns (and rows) which have already been reduced. The process may be illustrated as follows.

Assume that column 1 of the matrix shown in the previous figure must be reduced to zero:^{*}

Row 2 - Row 1:

$$A'_{21} = A_{21} - \frac{A_{21}}{A_{11}} \cdot A_{11} \quad (= 0)$$

$$A'_{22} = A_{22} - \frac{A_{21}}{A_{11}} \cdot A_{12}$$

$$A'_{23} = A_{23} - \frac{A_{21}}{A_{11}} \cdot A_{13}$$

$$A'_{24} = A_{24} - 0$$

*Standard double subscript notation is used here to avoid confusion between upper and lower diagonal halves of the matrix.

$$A'_{26} = A_{26} - 0$$

$$(\text{VEC})'_2 = (\text{VEC})_2 - \frac{A_{21}}{A_{11}} \cdot (\text{VEC})_1$$

Row 3 - Row 1:

$$A'_{31} = A_{31} - \frac{A_{31}}{A_{11}} \cdot A_{11} (= 0)$$

$$A'_{32} = A_{32} - \frac{A_{31}}{A_{11}} \cdot A_{12}$$

$$A'_{33} = A_{33} - \frac{A_{31}}{A_{11}} \cdot A_{13}$$

$$A'_{34} = A_{34} - 0$$

$$A'_{35} = A_{35} - 0$$

$$A'_{36} = A_{36} - 0$$

$$(\text{VEC})'_3 = (\text{VEC})_3 - \frac{A_{31}}{A_{11}} \cdot (\text{VEC})_1$$

From the above illustration it is possible to make the following generalisation:

- (i) If A'_{21} and A'_{31} are not set to zero in practice, (i.e. if there zero values are taken as implied rather than real), the matrix remains symmetrical.
- (ii) Where the matrix is symmetrical the subtraction of row n from row i is equivalent to the subtraction of column n from column i , but including only those elements of column n below (and including) its diagonal element. The elements to the left of the diagonal (in the row n) or above the diagonal (in the column n) are not included in the subtraction since their values have already been obtained in the preceding row subtractions. For example, in the above illustration, for row 3 - row 1 it is not necessary to evaluate A'_{32} since its value has already been set in the preceding row subtraction, i.e. $A'_{32} = A'_{23}$ by symmetry.

These generalisations allow a significant reduction in the amount of

arithmetic required; in fact a large proportion of the arithmetic is merely implied rather than actually performed. For example, in the above illustration A'_{21} and A'_{31} are not set to zero; the calculation is merely implied. In this way the reduction of the lower diagonal matrix to zero is entirely implied and what in fact the lower diagonal matrix (the only part of which is actually stored and operated on) finally contains, is the transpose of the upper diagonal matrix as it appears at the end of the reduction process.

Hence, the upper diagonal matrix is reduced to a diagonal matrix, beginning this time from the last element and working backwards.

The final solution is then obtained by dividing each element of the reduced load vector by its corresponding diagonal so that the original load vector now contains the solution.

Subroutine STRESS (NSEC, NODS, NOD1, NOD2, NEL1, NEL2, L, R1, R2, T, VEC)

Function: To calculate from the displacements the stresses and bending moment at every node in the structure.

Input variables:

NSEC : the number of sections into which the structure is divided
(see section A.3.1),

NOD1(I) } : the node numbers of the first and last nodes in section i,
NOD2(I) }

NEL1(I) } : the element numbers of the first and last elements in section i,
NEL2(I) }

L, R1, R2, T : [PLGEOM]

VEC(J) : the jth component of the system load vector,

NODS : (an internal variable included in the argument list so that it may be dynamically dimensioned).

Output variable:

There are no output variables as such. Stresses and moments are written into a disc file for future plotting and printed on the line printed.

Description:

For the purposes of calculating stresses and moments, each section is

considered to be independent of any other. Hence the calculation of stresses and moments is completely independent of any branching in the structure and Eq. (3.51) (section 3.3.5) may be applied at each node in turn to yield the stress resultants at that node. The hoop and circumferential stresses are then calculated from the corresponding stress resultants by dividing by the element thickness at the node.

The advantage of calculating the stresses by section is that stresses and moments at abrupt changes in the geometry of the shell are not given as the mean of the stresses on either side of the abrupt change; instead the stresses and moments on either side of the abrupt change are given separately. For example, at a shell junction (which must, by definition, constitute a division of the shell into separate sections), two moments are given for the junction node. These moments should be (but seldom are) equal, and a comparison of these moments gives some idea of the accuracy of the solution.

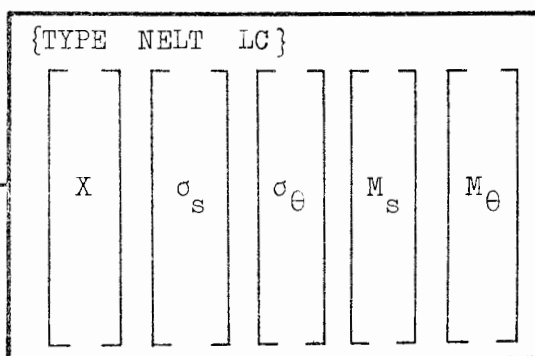
A.2.3 Plotter program STRESSPLOT

STRESSPLOT is an independent plotter program developed specifically for the plotting of stress and moment results obtained from CONFRU. A description of the input data required when STRESSPLOT is used in conjunction with CONFRU is given in section A.3.3, and a description of the output, including sample plots, is given in section 4.6.1. The internal logic of the program will be briefly described here.

Assume that we have the following general data input:

```
{PLTS  NLC  SIZE}
```

```
@ ADD PLOT1.
@ ADD PLOT2.
```



The above input will plot the results of two separate analyses on the same system of axes. The plot files PLOT1. and PLOT2. (the general contents of which are shown alongside), are set up automatically by CONFRU and contain vectors of the cumulative distance X and the stress results for the two

analyses.

The basic part of the program consists of a sequence of steps which is repeated four times, once for each of the stresses which is to be plotted. Hence in the first sequence, all M_s curves are plotted, in the second all σ_s curves, etc. The procedure for one complete sequence, say for σ_s , is as follows:

- (i) Read X and σ_s from PLOT1. Pick out the maximum and minimum values of σ_s in the set. Hence calculate the absolute range of σ_s values in the set.
Repeat for PLOT2.
- (ii) Determine which set of σ_s has the maximum range. Hence re-define the variable arrays containing the sets of σ_s values so that the set having the maximum range will be plotted first.
- (iii) Determine the length l of the X axis:^{*}

SIZE = F,	$l = 13$ inches
SIZE = H,	$l = 10$ inches
SIZE = S,	$l = 12$ inches.

[Note: this step is performed only once in the very first sequence so that all four X axes have the same length and scale].
- (iv) Determine the starting value and scale of X axis. Starting value is clearly zero, and the scale is given by (total meridional length of structure)/ l .
- (v) Determine the starting value and scale of the σ_s axis. The starting value is the lowest of the minima found in (i) and the scale is calculated from (the highest of the maxima) - (lowest of minima) $\div 8$, where 8 inches is the standard length of the stress axis.
- (vi) Draw the X and σ_s axes.
- (vii) Plot the curve for first analysis.
Plot the curve for second analysis, etc.

^{*}Note that SIZE also affects the overall size of the plot. Hence the figures for l given here are again modified depending on the scale factors applied to the overall plot. The user should bear in mind that the objective of SIZE is to fit the axes onto A4 pages (see section 4.6.1).

The procedure above is repeated for the remaining three stresses. Finally, the heading box is drawn in the lower right hand corner, the load case information is drawn in the centre of the four sets of axes, and a box is drawn around the whole plot.

A complete listing of STRESSPLOT follows the CONFRU listings in section A.5.

A.3 CONFRU Input Data

The analysis of an axisymmetric shell of revolution using CONFRU involves two essential steps:

- (i) preparation of input data, and
- (ii) coding of the input data in the accepted CONFRU format.

Each of these steps is described in detail in what follows. Note in particular that throughout the description the left hand side of the structure is taken to be the side being analysed.

Units:

CONFRU is dimensionless with respect to units and any consistent set of units may be used. For the purposes of printed headings and in describing the dimensions of input data, Newtons and metres are used here.

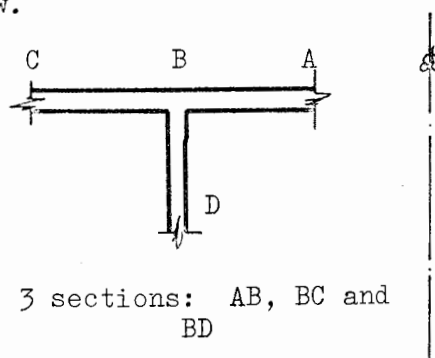
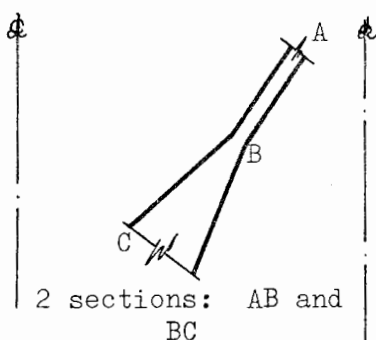
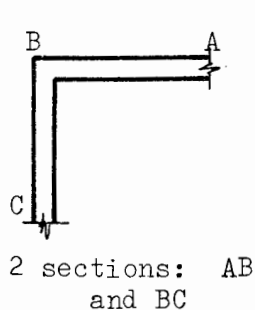
Sign convention:

Part of the data is input in global coordinates and part in local coordinates. Hence the relevant sign conventions are described where required.

A.3.1 Preparation of input data

The following procedure is suggested for the preparation of the input data:

- (a) From a study of a working drawing of the structure, divide the structure into sections; the concept of a section is of fundamental importance to the preparation of input data and is defined as a part of the structure whose middle surface is a straight line, and whose thickness is either constant or varies linearly from one end of the section to the other; furthermore, a section may not be joined to another section except at its end points. Examples of the subdivision of parts of a structure into sections are given below.

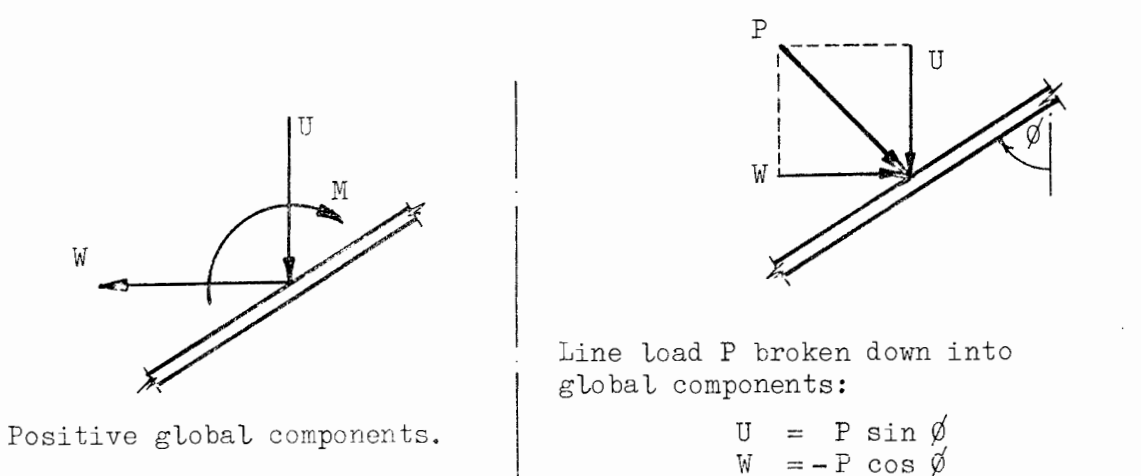


(b) Determine the radius r and thickness t of the shell wall at the beginning and end of each section; determine the length of each section.

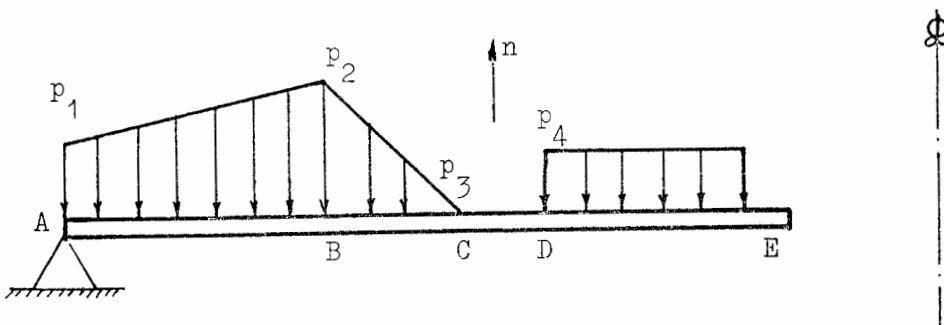
(c) Define the loading acting on the structure:

(i) If self-weight of the structure is to be included, the only preparation required is a choice of the unit weight of the material

(ii) The positions at which concentrated line loads act must be defined, and where applicable they must be broken down into their global components, as shown in the following example:



(iii) The region over which a constant or linearly varying distributed load acts is called a pressure section. Pressure sections have the same characteristics as sections, with the additional constraint that the distributed load over a pressure section must be continuous. Thus, in the example below, AB constitutes one pressure section, BC a second, and DE a third.



Distributed loading may only act perpendicular to the middle surface of the shell (or plate) and is positive if it acts in the direction of the positive normal n to the middle surface

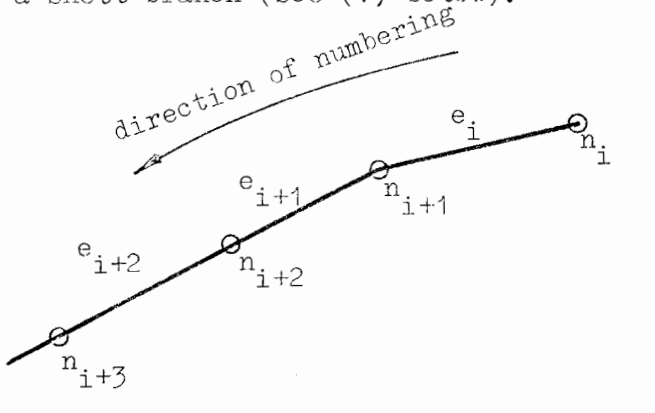
(see 'Sign Convention', section 3.3.5).

- (d) Subdivide each section into a suitable number of elements, (without attempting to number them). The choice of subdivision should be performed primarily on the basis of element aspect ratio, taking into account the geometry of the section (whether it is cylindrical, a conical frustrum or a circular plate), and the type of loading acting on the section. The choice is also governed by the positions of concentrated line loads and the beginnings and ends of pressure sections, since each of these must occur at a node.

In general the element aspect ratios should lie within the range $1/6 \leq L/t \leq 1$, the lower values being used in the regions of shell junctions and concentrated loads. Large discontinuities in L/t ratios should be avoided and the user should aim at using fairly constant aspect ratios throughout a given section, and similar aspect ratios throughout the structure, even at the expense of using large numbers of elements. Such a procedure greatly simplifies the preparation of input data. (The user should in any case study a similar example from Chapter 4, as well as the relevant comments in the Summary and Conclusions).

- (e) Select the element and nodal numbering scheme to be used in the analysis. It is best to begin by choosing Node 1 at the top of the structure, as close to the axis of symmetry as the structural geometry allows. Thereafter, the numbering is subject to the following constraints:

- (i) Element i must always follow node i , except at the start of a shell branch (see (v) below).

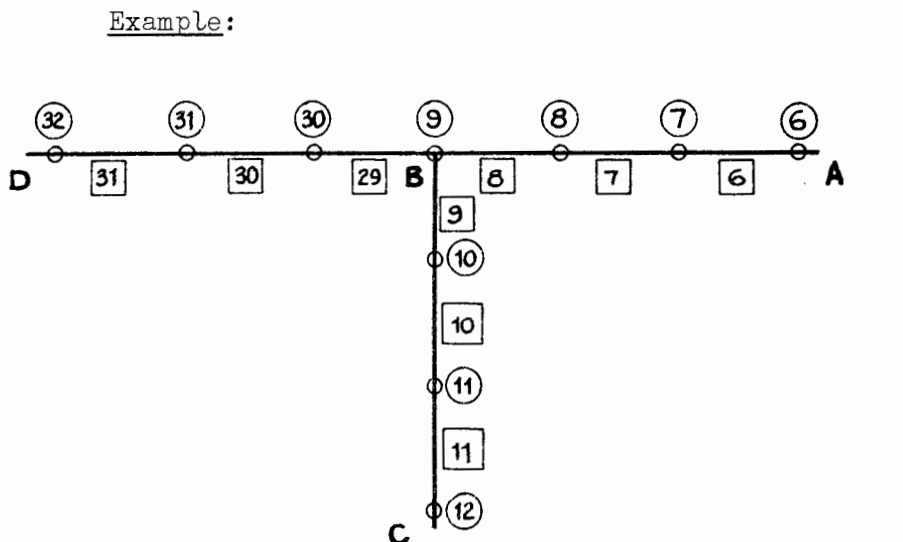


- (ii) Nodes and elements in circular plates must be numbered radially

outward from the axis of symmetry. If the shell is branched it is advisable to number the nodes and elements in cylinders and conical frustra from top to bottom; this allows a greater degree of consistency in specifying the branching information.

- (iii) The numbering of nodes and elements within any section must be continuous.
- (iv) At a branch point (i.e. a node at which 3 sections meet), the numbering of the nodes and elements in any two of the sections must be continuous; these two sections constitute the main shell at the branch point. The nodes and elements of the third section may be numbered independently of the main shell; this section then constitutes the shell branch at that branch point.

Example:



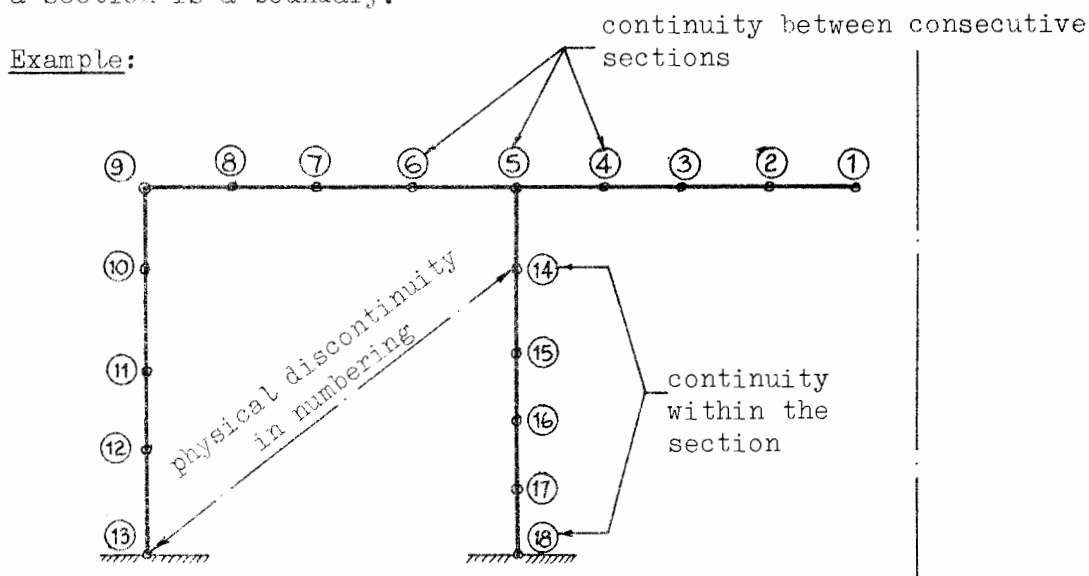
Main shell : Sections AB and BC; numbering of nodes and elements is continuous over these two sections.

Shell branch: Section BD; numbering of nodes and elements is independent of main shell numbering.

- (v) The only exception to rule (i) occurs at the start of a shell branch. The number of the first element in a shell branch is $(n - 1)$ where n is the number of the first node within the shell branch. Hence in the example above $n = 30$ and the number of the first element in the shell branch BD is 29.
- (vi) When the nodes and elements have been numbered, the sections are numbered accordingly, i.e. in the order of increasing node (element) numbers so that the lowest numbered section contains element 1 and the highest numbered section contains the highest numbered element.

The above are the general rules for the numbering of elements and nodes. However, in practice the numbering process may be simplified by summarising it as follows:

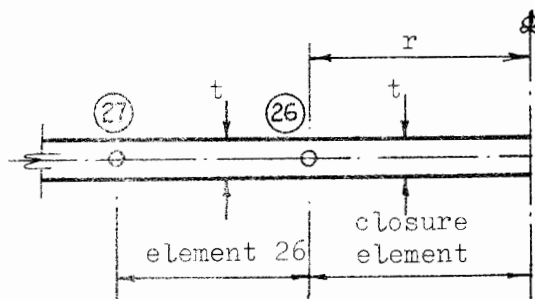
- (i) Number all nodes first, maintaining continuity of numbering within each section, and as far as possible continuity of numbering between consecutive sections. In branched shells physical discontinuities* in the numbering scheme may be necessary at physical discontinuities in the shell, e.g. where the end of a section is a boundary.



- (ii) Fill in the relevant element numbers according to the rules given, but subject to the following special cases:

Closure elements: Closure elements are not numbered. They are defined in terms of their single node and the adjacent element.

Example:



The length of the closure element is equal to the radius of node 26; its thickness is assumed to be the same as adjacent element 26.

*Defined alternatively as a jump in the nodal numbering scheme from the end of one section to the beginning of another totally unconnected section.

TABLE A-1

Sequence of input data for CONFRU

ISYM IGEN IG IL IS IBON IV IB ID ISP

LCASE HEAD(I)

RNU E GC

NSEC NPS NNBC NNPL NBP

{ NOD1(I) NEL1(I) NOD2(I) NEL2(I) RS1(I) RS2(I) T1(I) T2(I) }
I = 1, NSEC

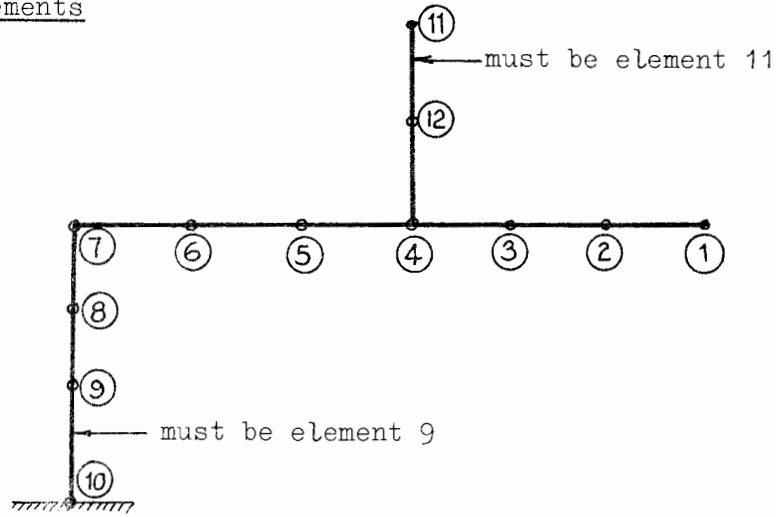
* { NELP1(I) NELP2(I) PR1(I) PR2(I) }
I = 1, NPS

{ NBC(I) UBC(I) WBC(I) MBC(I) }
I = 1, NNBC

* { NP TL(I) UU(I) WW(I) MM(I) }
I = 1, NNPL

* { ND(I,1) ND(I,2) ND(I,3) ND(I,4) }
I = 1, NBP

{ L(I) NREP }

Dummy elementsExample:

When the above nodal numbering scheme is used there can be no element 10 since according to rule (i) (subsection (e) above), element i must follow node i . In such cases element 10 is referred to as a dummy element and is specified by assigning zero length to it.

A.3.2 Coding of input data

The sequence of input data, given in terms of the corresponding variables used within CONFRU, is shown in Table A-1. The following general points augment the information in the table:

- (i) Each line corresponds to a single data card; where a set of variables is enclosed in chain brackets and is followed by $I = 1, 'x'$, it means that a total number of 'x' cards containing the same type of information is required.
- (ii) A star in front of the chain brackets means that the entire set of data is optional and may be ignored. (Note that blank cards are not required for optional data).
- (iii) Except in the first line (SYM, etc.) two blank columns are left between every data number. This greatly facilitates the checking of the data once it has been punched into cards.
- (iv) Three types of input format are used, viz., I format for integers, E and F format for reals, and A format for alphanumeric data, e.g. headings). The format used for each particular variable is given where the variable is described.

General description of input data

In the description of data that follows chain brackets around a set of

variables have the same meaning as given above in (i) and (ii), except that where the brackets are not followed by I = 1, 'x', only one data card containing the variables within the brackets is required.

1. Options for printed output:

```
{ ISYM  IGEN  IG  IL  IS  IBON  IV  IB  ISP }
  FORMAT (10I1)
```

If the value of any of the printed output options is set to zero the corresponding print-out is given. If set to any other positive value, the corresponding print-out is not given. The printed output corresponding to the above variables is:

ISYM: program and analysis title blocks

IGEN: general analysis information such as Young's modulus and Poisson's ratio; shell branching information, which acts as a check on the validity of the corresponding data input (see 10. below).

IG : shell geometry, i.e. length, thickness and radii of each element.

IL : loading on the structure, i.e. concentrated line loads, pressure at every node.

IS : contents of A as set up by subroutine SYSTEM.

IBON: boundary conditions.

IV : system load vector.

IB : back substituted load vector.

ID : displacements and rotations at each node.

ISP : stresses and moments at each node. (Note: ISP > 0 does not prevent the writing of results to data files for future plotting; see 3. below.)

Example:

```
0 1 1 1 1 1 1 1 0 1
```

Only the title blocks and the displacement results are printed.

2. Heading information:

```
{ LCASE  HEAD(I) }
  FORMAT (A6, 2X, 10A5)
```

LCASE : the analysis identification number, chosen by the user. It may be up to 6 alphanumeric characters in length.

HEAD(I): a general heading chosen by the user for the analysis. It may be up to 50 alphanumeric characters in length and is optional.

Example:

```
ST/1/1     ANALYSIS OF AN ELEVATED EFFLUENT TANK
```

3. Miscellaneous data:

```
{ NPLOT  NGP  ICLOSE(1)  ICLOSE(2)  .....  ICLOSE(5) }
  FORMAT (2 (I2, 2X), 5(I3, 2X))
```

NPLOT : is an integer chosen by the user and used to identify the data file into which the stresses and moments will be written for future plotting. If no plotting is required the number 15 should be used. (See also Runstreams, section A.3.4).

NGP : the number of points to be used in the numerical integration. Must be either 5 or 7.

ICLOSE(I): the numbers of the closure element nodes. Up to five closure elements may be included.

Example:

```
15  5  20  100
```

NPLOT = 15, NGP = 5, and there are two closure elements at nodes 20 and 100.

4. Material properties:

```
{ RNU  E  GC }
  FORMAT (3 (E8.3, 2X))
```

RNU : Poisson's ratio ν

E : Young's modulus E [N/m²]

GC : Unit of structural material [N/m³].

If GC > 0, the self-weight of the entire structure is included in the analysis (together with any other loading present).

If $GC = 0$, the self-weight of the structure is ignored.

Example:

$0.167E00$ $20.00E09$ $24.00E03$

$\nu = 0.167$, $E = 20 \times 10^9$, and $GC = 24 \times 10^3$

5. General constants:

{ NSEC NPS NNBC NNPL NBP }
 FORMAT (5 (I3,2X))

NSEC : the number of sections into which the shell is divided (see section A.3.1(a)).

NPS : the number of pressure sections (see section A.3.1(c)(iii))

NNBC : the number of nodes at which zero displacement boundary conditions are to be applied.

NNPL : the number of nodes at which concentrated line loads are to be applied.

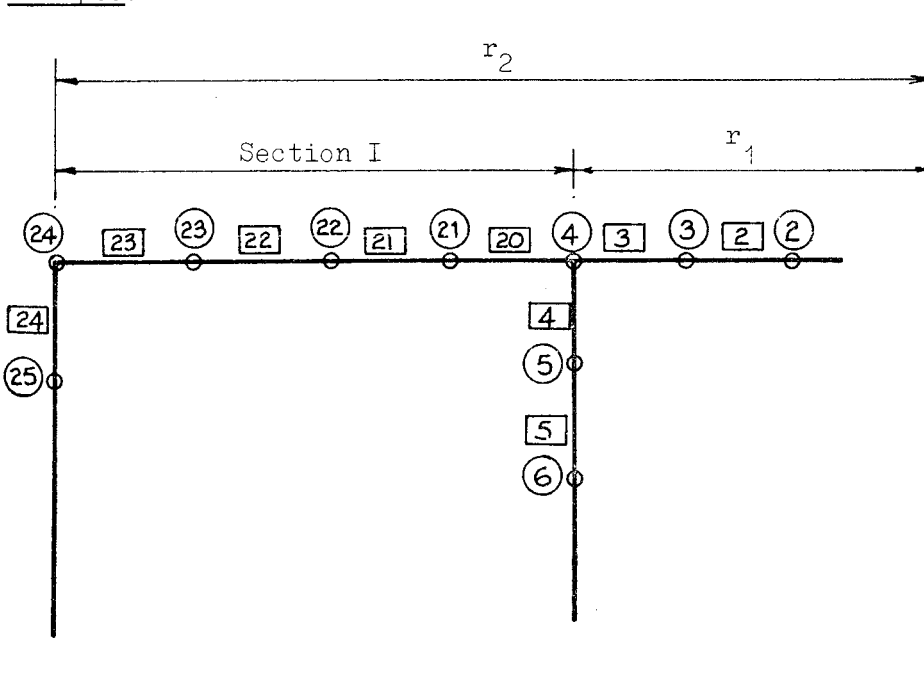
NBP : the number of data cards required to describe the branching information for the structure (see point 10. below).

6. Sectional geometry:

{ NOD(I) NEL1(I) NOD2(I) NEL2(I) RS1(I) RS2(I) T1(I) T2(I) }
 I = 1, NSEC
 FORMAT (4(I3, 2X), 4(E8.3, 2X))

Number of data cards required = NSEC; cards must be input in the order of increasing section number, i.e. the i th card refers to section i .

Example:



Data card for section I (see also subroutine PLGEOM, section A.2.2):

```

NOD1(I)   = 4
NEL1(I)   = NELB(I) = 20
NOD2(I)   = 24
NEL2(I)   = NELE(I) = 23
RS1(I)    = RB(I)   = r1
RS2(I)    = RE(I)   = r2
T1(I)     = TB(I)
T2(I)     = TE(I)

```

Note that the total number of elements used in the analysis is automatically given by NEL2(NSEC).

If RS2(I) = RS1(I), RS2(I) may be left blank, in which case the value given for RS1(I) is assumed.

If T2(I) = T1(I), T2(I) may be left blank, in which case the value given for T1(I) is assumed.

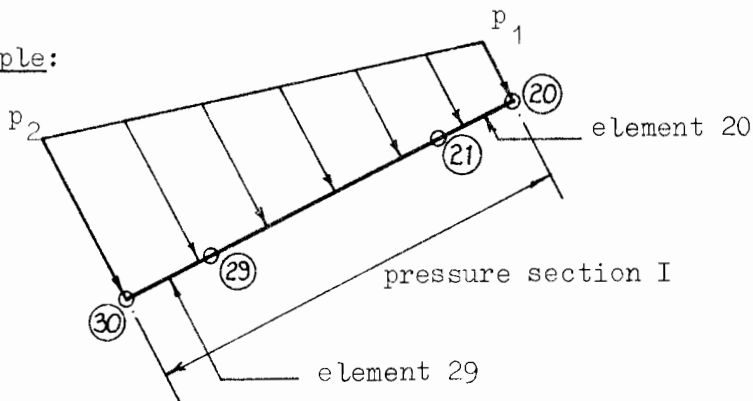
7. Distributed loading

$$\{ \text{NELP1(I)} \quad \text{NELP2(I)} \quad \text{PR1(I)} \quad \text{PR2(I)} \} \quad I = 1, \text{NPS}$$

FORMAT (2 (I3, 2X), 2 (E8.3, 2X))

Number of data cards required = NPS; cards must be input in order of increasing pressure section number, i.e. the *i*th card refers to pressure section *i*.

Example:



Data card for pressure section *i* (see also subroutine PLPRES, section A.2.2):

```

NELP1(I) = 20
NELP2(I) = 29
PR1(I)   = p1
PR2(I)   = p2

```

8. Boundary conditions:

$$\left\{ \text{NBC}(I) \quad \text{UBC}(I) \quad \text{WBC}(I) \quad \text{MBC}(I) \right\} I = 1, \text{NNBC}$$

FORMAT (I3, 2X, 3 (A1, 1X))

Number of data cards required = NNBC; cards input in order of increasing boundary node number.

NBC(I) : the number of the node at which the *i*th boundary condition occurs

UBC(I) : if UBC(I) = 'U' there is zero axial displacement at the specified node.

WBC(I) : if WBC(I) = 'W' there is zero radial displacement at the specified node.

MBC(I) : if MBC(I) = 'M' there is zero rotation at the specified node.

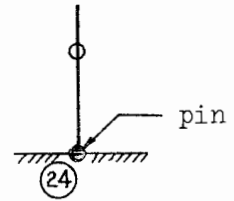
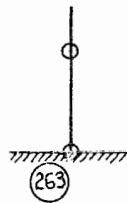
If UBC(I), WBC(I) or MBC(I) is left blank, the corresponding displacement or rotation remains unaffected, i.e. an unknown quantity to be solved for.

Example:

```

┌ 263)XUXWXM
└
┌ 24 U W
└

```



Node 263 is rigidly fixed, and node 24 is a clamped-pin.

9. Concentrated line loads:

$$\left\{ \text{NPTL}(I) \quad \text{UU}(I) \quad \text{WW}(I) \quad \text{MM}(I) \right\} I = 1, \text{NNPL}$$

FORMAT (I3, 3 (E8.3, 2X))

Number of data cards required = NNPL; cards input in order of increasing node numbers.

NPTL(I) : the number of the node at which the *i*th concentrated line load or moment is applied.

UU(I) : the axial component of the load [N/m].

WW(I) : the radial component of the load [N/m].

MM(I) : the value of the line moment applied at the node [Nm/m].

Example:

$$\sqrt{106 \times 20.00 \times 10^6 \times 40.00 \times 10^6 \times 60.00 \times 10^3}$$

At node 106 there is an axial load $U = 20 \times 10^6$ [N/m], a radial load $W = 40 \times 10^6$ [N/m] and a moment $M = 60 \times 10^3$ [Nm/m].

10. Shell branching information:

$$\left\{ \begin{array}{cccc} \text{ND(I,1)} & \text{ND(I,2)} & \text{ND(I,3)} & \text{ND(I,4)} \end{array} \right\} \text{ I} = 1, \text{NBP}$$

FORMAT (4 (I3, 2X))

The branching information required consists of a specification of:

- (i) physical discontinuities in the node numbering scheme (see section A.3.1, summary of process, point (i)).
- (ii) shell branches (see section A.3.1, (e), (iv)).

It is suggested that these specifications be given in the order of the sections in which they occur. Hence, the user should begin at section 1, node 1, and work through the structure in the order of increasing section numbers (which corresponds to the order of increasing node and element numbers), noting as he goes the physical discontinuities and shell branches.

The specifications take the following form:

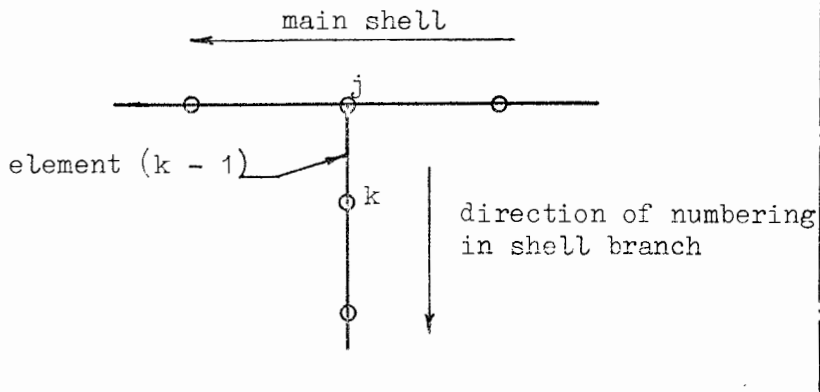
A. Physical discontinuity at node k: (where node k occurs at the end of a section).
$$\begin{aligned} \text{ND(I,1)} &= k \\ \text{ND(I,2)} &= \text{ND(I,3)} = \text{ND(I,4)} = 0 \end{aligned}$$

The physical interpretation of this information is: node k is not joined to node (k + 1), but node k is not a branch point. Note that node (k + 1), the other side of the discontinuity so to speak, is ignored (except, of course, if it constitutes the beginning of a shell branch).

B. Shell branches:

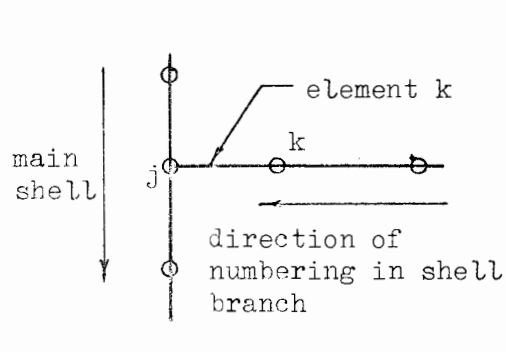
Shell branches take two distinct forms:

- (i) where the nodes of the shell branch are numbered away from the branch point node;



$ND(I,1) = k$, first node of shell branch,
 $ND(I,2) = j$, branch point node,
 $ND(I,3) = k - 1$, first element of shell branch,
 $ND(I,4) = j$ ($j < k$ always);

- (ii) where the nodes of the shell branch are numbered towards the branch point node;



In this case two specifications are required:

- (a) the shell branch generally constitutes a "physical discontinuity at node k " as previously described, and is always treated as such, except when k is the very last node in the idealisation.

Hence the first specification is

$ND(I,1) = k$
 $ND(I,2) = ND(I,3) = ND(I,4) = 0$

- (b) the branch is specified as

$ND(I + 1,1) = \begin{cases} k, & \text{if } k > j \\ j, & \text{if } k < j \end{cases}$ the higher of j and k
 $ND(I + 1,2) = \begin{cases} j, & \text{if } k > j \\ k, & \text{if } k < j \end{cases}$ the lower of j and k

$$ND(I + 1,3) = k, \text{ the first element of the shell branch}$$

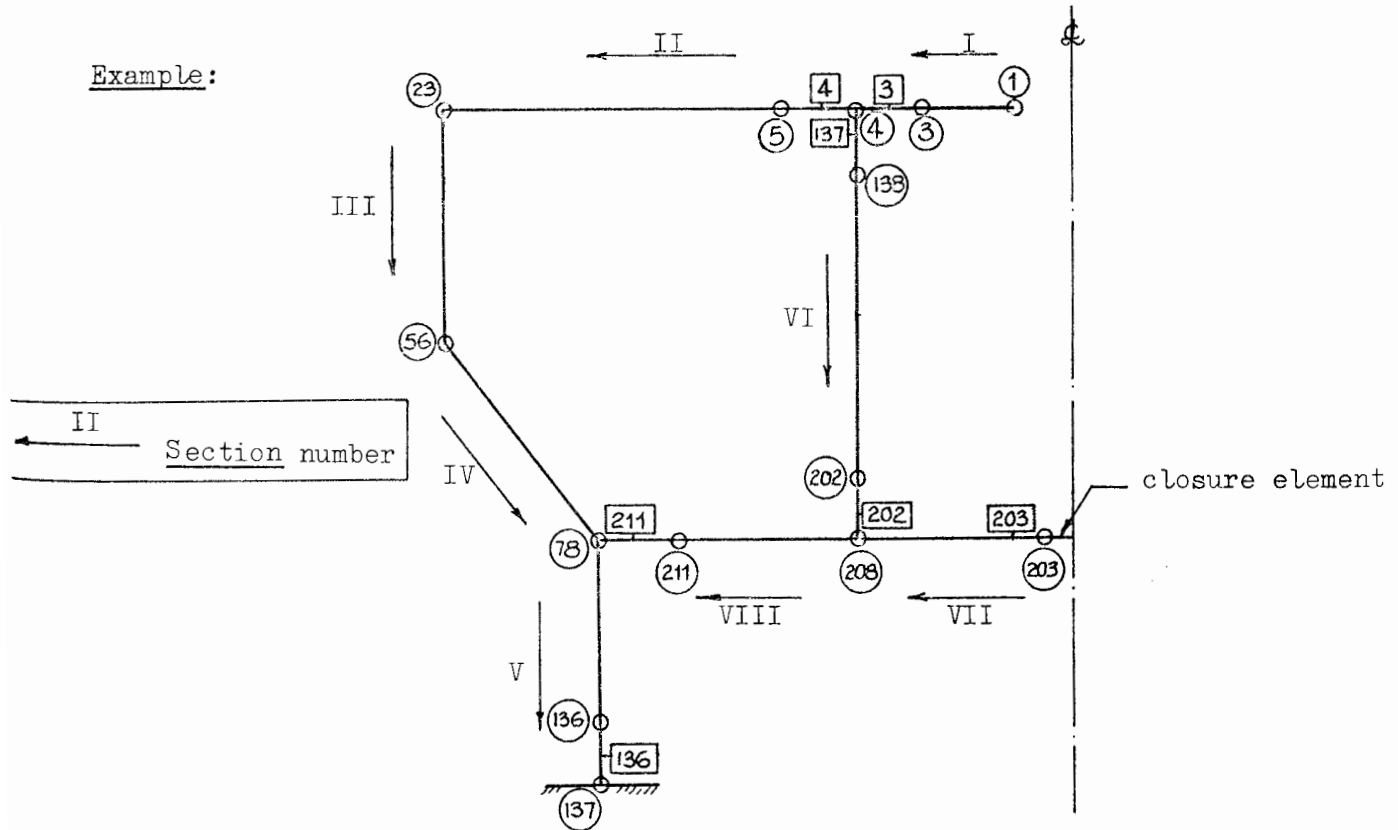
$$ND(I + 1,4) = \begin{cases} 0, & \text{if } j > k \\ j, & \text{if } j < k \end{cases}$$

There are two exceptions to the above rules, both of which deal with the last node (i.e. the highest numbered node) in the element idealisation. These exceptions are:

- (i) If the last node is a boundary it is not included in the branching information.
- (ii) If the last node occurs at a branch the "physical discontinuity of node k" specification is not required.

Note, finally, that closure element nodes are never specified as a "physical discontinuity" because circular plate nodes must always be numbered away from the axis of symmetry, and hence closure element nodes always occur at the beginning of a section.

Example:



Begin at node 1; proceed along the shell in the direction of increasing section numbering.

Section I : no discontinuity or shell branch

Section II : no discontinuity or shell branch

Section III: no discontinuity or shell branch

Section IV : no discontinuity or shell branch

Section V : end of section, discontinuity, node 137 not joined to node
138; data card required is:

137

Section VI : beginning of section is a shell branch; data card
required is:

138 4 137 4

end of section is a shell branch; data cards required are:

202

208 202 202

Section VII : no discontinuity or shell branch

Section VIII: end of section is a shell branch; data card required is:

211 78 211 78

In this example five data cards are required to describe the branching;
thus $NBP = 5$.

Note on the debugging of branching information input data

When the branching information has been read in, CONFRU compiles and prints out a description of each discontinuity and branch exactly according to the information given. For example, for the fourth data card in the preceding example, the following description would be printed:

NODE 208 IS CONNECTED TO NODE 202 THROUGH ELEMENT 202

Hence, if this information is incorrect (or nonsensical) the user may infer that the corresponding input data is invalid, and the card must be corrected.

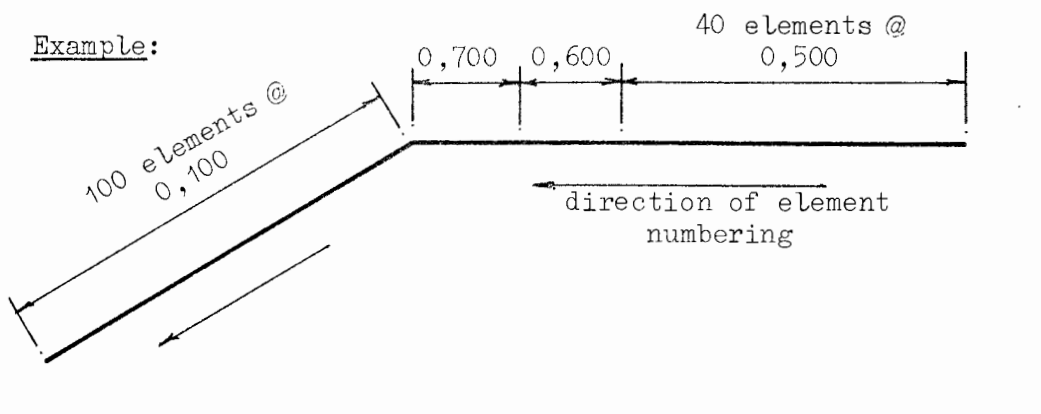
11. Element lengths:

$$\{ L(I) \quad NREP \}$$

$$\text{FORMAT} \quad (\text{F7.0}, 2\text{X}, \text{I3})$$

$L(I)$: the length of element i [m].

$NREP$: the total number of times the corresponding element length is repeated in sequence.

Example:

The element length for the above idealisation would be specified as:

0.500	40
0.600	
0.700	
0.100	100

If $NREP = 0$, $NREP$ is ignored.

i.e. $L(I)$ through $L(I + 39) = 0.500$
 $L(I + 40) = 0.600$
 $L(I + 41) = 0.700$
 $L(I + 42)$ through $L(I + 142) = 0.100$

Note that if element i is a dummy element, $L(I)$ must be specified as zero.

A.3.3 Maximum size of analysis

The maximum size of analysis is governed by the dimension limits of the variables used in the program. These dimensions are dynamically set by 4 variables whose values are in turn set by the user at the beginning of the main program. These variables, their current values, and the analysis variables which they govern are:

IX = IXX = 500; the maximum number of elements which may be used.

IY = IYY = 15000; the maximum number of coefficients in half the system stiffness matrix.

IW = IWW = 1503; the maximum number of equations, which is equal to $3 \times (\text{number of nodes} + 1)$.

IZ = IZZ = 30; twice the maximum number of sections; the maximum number of pressure sections; the maximum number of concentrated line loads.

Certain other variables whose dimensions are always likely to be small are not dynamically dimensioned. These variables and their maximum limits are:

maximum number of boundary conditions	=	10
maximum number of closure elements	=	5
maximum number of branch points	=	10

The above dimensions result in a total computer storage requirement of 63526 words, which is just below the maximum core storage of 65 K at present available on the UNIVAC 1106 system at U.C.T.

A.3.4 Sample runstreams for the execution of CONFRU and STRESSPLOT, including STRESSPLOT input data

The execution of both CONFRU and STRESSPLOT requires the use of the UNIVAC EXEC 8 Control System and it is assumed for the purposes of the following description that the user has some knowledge of this system.

Preparation of necessary computer disc files

- (i) CONFRU main program and subroutines, as well as the plotter program STRESSPLOT, are stored as elements of a disc program file CONFRU.
- (ii) Executable versions of CONFRU and STRESSPLOT are MAPped into absolute elements CONFRU . CONFRUABS and CONFRU . CONPLOTABS respectively.
- (iii) A sufficient number of disc data files are made available for storing stress results for plotting. These will be denoted by PLOT1, PLOT2, etc.

A complete and up-to-date deck of cards is available for both CONFRU and STRESSPLOT. These decks contain all the control cards necessary for performing the above three steps. Hence, after inputting these decks the user should be in a position to use directly the sample runstreams given below.

STRESSPLOT input data:

Besides the actual stress values that are to be plotted (which are automatically generated and stored by CONFRU), there is only one card of input data required for STRESSPLOT. This card is,

```
{ PLTS  NLC  SIZE }
  FORMAT (A6, 2X, I1, 2X, A1)
```

PLTS : a 6-character alphanumeric word chosen by the user to identify the plot.

NLC : the number of sets of results which are to be plotted on this set of axes.

SIZE : the overall of the plot (see footnote p 138)

```
F : Full   : 57 × 46 cm
=  H : Half  : 38 × 38 cm
S : Small  : 32 × 27½ cm
```

The remaining data is given in the form of the ADDition of computer data files containing the points to be plotted. For each set of results (i.e. analysis), which is to be plotted, the corresponding data file is ADDED four times, once for each of the four stresses and moments.

Sample runstreams:

(a) A single analysis, no plotting required:

```
@ RUN
@ ASG, AX CONFRU
@ XQT CONFRU.CONFRUAABS
```

CONFRU data

```
@ FIN
```

(b) A single analysis, with plot:

```
@ RUN
@ ASG, AX  CONFRU
@ ASG, AX  PLOT1
@ USE  16, PLOT1
@ XQT  CONFRU.CONFRUABS
```

```
CONFRU data:
```

```
NPLOT = 16
```

```
@ XQT  CONFRU.CONPLOTABS
```

```
STRESSPLOT data
```

```
@ ADD  PLOT1.
@ ADD  PLOT1.
@ ADD  PLOT1.
@ ADD  PLOT1.
@ FIN
```

(c) Two analyses, with the results of both analyses plotted on the same set of axes:

```
@ RUN
@ ASG, AX  CONFRU
@ ASG, AX  PLOT1
@ ASG, AX  PLOT2
@ USE  16, PLOT1
@ USE  17, PLOT2
@ XQT  CONFRU.CONFRUABS
```

```
CONFRU data for first analysis
```

```
NPLOT = 16
```

```
@ XQT  CONFRU.CONFRUABS
```

```
CONFRU data for second analysis
```

```
NPLOT = 17
```

```
@ XQT  CONFRU.CONPLOTABS
```

```
STRESSPLOT data
```

```
@ ADD  PLOT1.
@ ADD  PLOT2.
@ ADD  PLOT1.
@ ADD  PLOT2.
```

TABLE A-2

Data input for analysis ST/1/1

000001	0000000000						
000002	ST/1/1 EX. 8: ELEVATED EFFLUENT TANK FILLED WITH LIQUID						
000003	16 5 203						
000004	0.167E00 20.00E09						
000005	8	4	1		5		
000006	1	1	4	3	0.4625E0	.7625E00	0.250E00
000007	4	4	23	22	.7625E00	4.600E00	0.250E00
000008	23	23	56	55	4.600E00		0.200E00
000009	56	56	78	77	4.600E00	1.400E00	0.250E00
000010	78	78	137	136	1.400E00		0.200E00
000011	4	137	208	202	.7625E00		0.125E00
000012	203	203	208	207	.0625E00	.7625E00	0.300E00
000013	208	208	78	211	.7625E00	1.400E00	0.300E00
000014	23	55			0.669E05		
000015	56	77	0.669E05		.989E05		
000016	137	202			-.989E05		
000017	208	211	-.989E05		-.989E05		
000018	137	U W M					
000019	137						
000020	138	4	137	4			
000021	202						
000022	208	202	202				
000023	211	78	211	78			
000024	0.100		3				
000025	0.202		28				
000026	0.203		24				
000027	0.205		7				
000028	0.206		15				
000029	0.200		59				
000030	0.150		56				
000031	0.149		10				
000032	0.100						
000033	0.150		4				
000034	0.1594		4				

```

@ ADD PLOT1.
@ ADD PLOT2.
@ ADD PLOT1.
@ ADD PLOT2.
@ FIN

```

A.4 A Complete Sample Analysis

The input data and partial results for a complete analysis and plot are given in the following pages. The information given takes the following form:

- (a) Input data for analysis ST/1/1 (Example 8, Chapter 4);
 Input data for analysis ST/2/1 (Example 8, Chapter 4);
 Input data for the plotting on the same set of axes of the above two analyses.
- (b) The complete runstream for the above analyses and the corresponding plot is identical to runstream (c) of section A.3.4.
- (c) The plotted output for the two analyses is shown in Fig. 4.40 of Chapter 4.
- (d) A partial listing of the printed output for analysis ST/1/1 showing,
 - (i) heading page,
 - (ii) general information, branching information,
 - (iii) displacement results,
 - (iv) stress results.

A.4.1 Input data

A complete listing of the data input required for analysis ST/1/1 is shown in Table A-2.

The input data for analysis ST/2/1 is identical to that for analysis ST/1/1 except for the following changes; (line numbers refer to the data listing given in Table A-2).

Line 2: replace entire line with:

```
ST/2/1 EX.8: ELEVATED EFFLUENT TANK, SELF-WEIGHT ONLY
```

Line 3: change N PLOT = 16 to N PLOT = 17

Line 4: insert GC = 24.00E03.

The input data required for STRESSPLOT consists of the following single line:

```
EX. 88882888
```

i.e. plot identification is 'EX. 8',
number of sets of results to be plotted = 2,
size of plot is 'small'.

A.4.2 Partial listing of results

A partial listing of the results for analysis ST/1/1 follows on the next page.

```
*****  
*                CONFRU                *  
*  FINITE ELEMENT AXISYMMETRIC  *  
*    THIN SHELL PROGRAM    *  
*                               *  
*          T.B.GRIFFIN          *  
*  DEPT. OF CIVIL ENGINEERING  *  
*    UNIVERSITY OF CAPE TOWN    *  
*                               *  
*          AUGUST 1974          *  
*                               *  
*    UNIVAC 1106 EXEC 8        *  
*****
```

```
*****  
*  LOAD CASE: ST/1/1          *  
*                               *  
*  DATE... 11 August 1974    *  
*                               *  
*****
```

 EX. 8: ELEVATED EFFLUENT TANK FILLED WITH LIQUID

POISSON RATIO: .167
 MODULUS OF ELASTICITY: .200+11
 UNIT WEIGHTS: STRUCTURE MATERIAL: .000

NUMERICAL INTEGRATION: 5 POINT SIMPSON QUADRATURE.

 CHECK NODE AND ELEMENT NUMBERS
 FOR SECTIONS AND BRANCHES

SECTIONS	NODE	(ELEMENT)*****	(ELEMENT)	NODE
1	1	(1)	(3)	4
2	4	(4)	(22)	23
3	23	(23)	(55)	56
4	56	(56)	(77)	78
5	78	(78)	(136)	137
6	4	(137)	(202)	208
7	203	(203)	(207)	208
8	208	(208)	(211)	78

CLOSURE ELEMENTS

THERE ARE CLOSURE ELEMENTS AT THE FOLLOWING NODES: 203

BRANCH POINTS

NODE 137 IS NOT CONNECTED TO NODE 138

NODE 138 IS CONNECTED TO NODE 4 THROUGH ELEMENT 137

NODE 202 IS NOT CONNECTED TO NODE 203

NODE 208 IS CONNECTED TO NODE 202 THROUGH ELEMENT 202

NODE 211 IS CONNECTED TO NODE 78 THROUGH ELEMENT 211

 DISPLACEMENTS AT EACH NODE, IN GLOBAL COORDINATES:

NODE	U	W	M
1	.167909-02	.285525-05	-.161572-03
2	.169508-02	.281828-05	-.159362-03
3	.171113-02	.287001-05	-.162212-03
4	.172763-02	.297566-05	-.168131-03
5	.176584-02	.267397-05	-.207848-03
6	.181030-02	.253785-05	-.235613-03
7	.186046-02	.249432-05	-.254846-03
8	.191331-02	.250778-05	-.267469-03
9	.196815-02	.255880-05	-.274699-03
10	.202398-02	.263587-05	-.277367-03
11	.207994-02	.273175-05	-.276078-03
12	.213528-02	.284165-05	-.271289-03
13	.218933-02	.296230-05	-.263362-03
14	.224149-02	.309134-05	-.252587-03
15	.229120-02	.322708-05	-.239203-03
16	.233797-02	.336824-05	-.223411-03
17	.238131-02	.351386-05	-.205383-03
18	.242080-02	.366318-05	-.185267-03
19	.245603-02	.381561-05	-.163191-03
20	.248660-02	.397068-05	-.139269-03
21	.251217-02	.412801-05	-.113602-03
22	.253239-02	.428729-05	-.862798-04
23	.254692-02	.444826-05	-.573834-04
24	.254701-02	-.187206-05	-.763729-05
25	.254712-02	.410748-06	.280163-04
26	.254718-02	.862184-05	.514413-04
27	.254717-02	.205366-04	.651187-04
28	.254706-02	.344459-04	.715997-04
29	.254685-02	.491340-04	.731822-04
30	.254653-02	.638093-04	.717533-04
31	.254610-02	.780171-04	.697463-04
32	.254558-02	.915456-04	.651673-04
33	.254495-02	.104412-03	.616447-04
34	.254423-02	.116604-03	.585633-04
35	.254342-02	.128230-03	.560845-04
36	.254253-02	.139417-03	.542350-04
37	.254155-02	.150288-03	.529641-04
38	.254050-02	.160954-03	.521880-04
39	.253937-02	.171504-03	.518193-04
40	.253816-02	.182015-03	.517855-04
41	.253688-02	.192549-03	.520383-04
42	.253551-02	.203160-03	.525542-04
43	.253407-02	.213903-03	.533289-04
44	.253255-02	.224830-03	.543651-04
45	.253094-02	.235993-03	.556546-04
46	.252926-02	.247440-03	.571537-04
47	.252749-02	.259204-03	.587533-04
48	.252563-02	.271287-03	.602446-04
49	.252368-02	.283633-03	.612619-04
50	.252163-02	.296102-03	.613495-04
51	.251950-02	.308428-03	.597391-04
52	.251728-02	.320182-03	.555510-04

53	.251497-02	.330736-03	.477354-04
54	.251260-02	.339242-03	.351943-04
55	.251017-02	.344633-03	.169688-04
56	.250772-02	.345710-03	-.746399-05
57	.250348-02	.345515-03	-.237052-04
58	.249626-02	.343184-03	-.423959-04
59	.249583-02	.338524-03	-.616727-04
60	.247219-02	.331580-03	-.801662-04
61	.245543-02	.322560-03	-.969710-04
62	.243598-02	.311776-03	-.111604-03
63	.241397-02	.299583-03	-.123960-03
64	.238962-02	.286263-03	-.134319-03
65	.236327-02	.272176-03	-.143163-03
66	.233502-02	.257526-03	-.151333-03
67	.230485-02	.242380-03	-.159948-03
68	.227254-02	.226630-03	-.170392-03
69	.223767-02	.209949-03	-.184280-03
70	.219954-02	.191765-03	-.203352-03
71	.215722-02	.171254-03	-.229227-03
72	.210960-02	.147381-03	-.262889-03
73	.205555-02	.119046-03	-.303680-03
74	.199430-02	.854318-04	-.347479-03
75	.192616-02	.466968-04	-.383582-03
76	.185383-02	.527404-05	-.389631-03
77	.178460-02	-.318755-04	-.323946-03
78	.173371-02	-.495791-04	-.115193-03
79	.170629-02	-.484923-04	.915714-04
80	.167849-02	-.233768-04	.141267-03
81	.165004-02	.320376-05	.117697-03
82	.162104-02	.224141-04	.738733-04
83	.159168-02	.331601-04	.355612-04
84	.156215-02	.375553-04	.107100-04
85	.153256-02	.382776-04	-.172992-05
86	.150298-02	.374176-04	-.584537-05
87	.147342-02	.362247-04	-.563656-05
88	.144389-02	.352632-04	-.388028-05
89	.141438-02	.346741-04	-.207099-05
90	.138488-02	.343990-04	-.780771-06
91	.135538-02	.343228-04	-.679912-07
92	.132588-02	.343433-04	.217579-06
93	.129638-02	.343937-04	.259085-06
94	.126688-02	.344402-04	.197380-06
95	.123738-02	.344714-04	.115632-06
96	.120788-02	.344876-04	.507671-07
97	.117838-02	.344935-04	.115036-07
98	.114888-02	.344937-04	-.653746-08
99	.111938-02	.344917-04	-.113059-07
100	.108988-02	.344896-04	-.971317-08
101	.106038-02	.344880-04	-.622604-08
102	.103088-02	.344871-04	-.307127-08
103	.100137-02	.344867-04	-.979325-09
104	.971873-03	.344866-04	.926362-10
105	.942372-03	.344867-04	.460667-09
106	.912870-03	.344868-04	.446292-09
107	.883369-03	.344868-04	.276247-09
108	.853868-03	.344869-04	.770280-10
109	.824367-03	.344869-04	-.895393-10

110	.794866-03	.344868-04	-.181259-09
111	.765364-03	.344868-04	-.137531-09
112	.735363-03	.344868-04	.140130-09
113	.706362-03	.344869-04	.773822-09
114	.676861-03	.344871-04	.183833-08
115	.647360-03	.344876-04	.320723-08
116	.617858-03	.344884-04	.430422-08
117	.588357-03	.344892-04	.379952-08
118	.558856-03	.344897-04	-.599436-09
119	.529355-03	.344885-04	-.119381-07
120	.499853-03	.344842-04	-.328475-07
121	.470352-03	.344748-04	-.627403-07
122	.440852-03	.344591-04	-.928513-07
123	.411351-03	.344392-04	-.994614-07
124	.381852-03	.344238-04	-.376464-07
125	.352352-03	.344330-04	.158535-06
126	.322851-03	.345009-04	.558737-06
127	.293348-03	.346720-04	.118686-05
128	.263839-03	.349836-04	.192478-05
129	.234321-03	.354233-04	.236731-05
130	.204792-03	.358553-04	.166224-05
131	.175266-03	.359211-04	-.156172-05
132	.145729-03	.349505-04	-.897335-05
133	.116247-03	.319721-04	-.217055-04
134	.868709-04	.259827-04	-.385451-04
135	.576777-04	.166960-04	-.529472-04
136	.287302-04	.598071-05	-.492789-04
137	.000000	.000000	.000000
138	.172713-02	-.102999-04	-.272680-04
139	.172681-02	-.977043-05	.229240-04
140	.172639-02	-.574260-05	.262135-04
141	.172585-02	-.260426-05	.149351-04
142	.172524-02	-.120642-05	.439071-05
143	.172460-02	-.104376-05	-.143962-05
144	.172396-02	-.144638-05	-.345442-05
145	.172335-02	-.198464-05	-.353714-05
146	.172275-02	-.247997-05	-.304232-05
147	.172216-02	-.290062-05	-.259699-05
148	.172159-02	-.326961-05	-.235594-05
149	.172103-02	-.361549-05	-.227528-05
150	.172048-02	-.395614-05	-.227410-05
151	.171995-02	-.429883-05	-.229574-05
152	.171942-02	-.464471-05	-.231452-05
153	.171891-02	-.499276-05	-.232448-05
154	.171840-02	-.534174-05	-.232770-05
155	.171791-02	-.569093-05	-.232765-05
156	.171743-02	-.604002-05	-.232671-05
157	.171696-02	-.638897-05	-.232592-05
158	.171650-02	-.673784-05	-.232551-05
159	.171606-02	-.708667-05	-.232538-05
160	.171562-02	-.743548-05	-.232539-05
161	.171520-02	-.778431-05	-.232543-05
162	.171479-02	-.813313-05	-.232546-05
163	.171439-02	-.848197-05	-.232548-05
164	.171400-02	-.883080-05	-.232548-05
165	.171362-02	-.917963-05	-.232548-05
166	.171326-02	-.952847-05	-.232548-05

167	.171290-02	-.987730-05	-.232548-05
168	.171256-02	-.102261-04	-.232548-05
169	.171223-02	-.105750-04	-.232548-05
170	.171191-02	-.109238-04	-.232548-05
171	.171160-02	-.112726-04	-.232548-05
172	.171130-02	-.116215-04	-.232548-05
173	.171102-02	-.119703-04	-.232548-05
174	.171075-02	-.123191-04	-.232548-05
175	.171048-02	-.126680-04	-.232548-05
176	.171023-02	-.130168-04	-.232548-05
177	.170999-02	-.133656-04	-.232548-05
178	.170976-02	-.137145-04	-.232548-05
179	.170955-02	-.140633-04	-.232548-05
180	.170934-02	-.144121-04	-.232549-05
181	.170915-02	-.147610-04	-.232550-05
182	.170897-02	-.151098-04	-.232552-05
183	.170879-02	-.154587-04	-.232551-05
184	.170864-02	-.158075-04	-.232542-05
185	.170849-02	-.161563-04	-.232521-05
186	.170835-02	-.165051-04	-.232485-05
187	.170823-02	-.168538-04	-.232455-05
188	.170811-02	-.172025-04	-.232487-05
189	.170801-02	-.175513-04	-.232694-05
190	.170792-02	-.179007-04	-.233210-05
191	.170784-02	-.182512-04	-.234040-05
192	.170777-02	-.186028-04	-.234724-05
193	.170772-02	-.189546-04	-.233845-05
194	.170767-02	-.193000-04	-.228789-05
195	.170764-02	-.196328-04	-.216551-05
196	.170762-02	-.199417-04	-.197253-05
197	.170760-02	-.202222-04	-.181902-05
198	.170760-02	-.205016-04	-.203471-05
199	.170761-02	-.208771-04	-.323213-05
200	.170763-02	-.215491-04	-.610601-05
201	.170763-02	-.227814-04	-.106017-04
202	.170779-02	-.246675-04	-.140983-04
203	.170480-02	-.259803-05	.750876-06
204	.170484-02	-.582178-05	-.133302-05
205	.170520-02	-.109596-04	-.336990-05
206	.170584-02	-.161483-04	-.522832-05
207	.170676-02	-.213509-04	-.703920-05
208	.170796-02	-.265594-04	-.883058-05
209	.170959-02	-.323510-04	-.132728-04
210	.171282-02	-.381109-04	-.295436-04
211	.171988-02	-.438514-04	-.621486-04

 NODAL STRESSES (N/SQ.M) AND MOMENTS (NM/M)

NODE	CUMULATIVE LENGTH	SIGMA-S	SIGMA-THETA	MS	MTHETA
SECTION 1					
1	.000	.1361+05	.1257+06	.9675+02	.9114+04
2	.100	.1873+05	.1033+06	.1535+04	.7634+04
3	.200	.3107+05	.9183+05	.2363+04	.6771+04
4	.300	.3515+05	.8392+05	.2896+04	.6226+04
SECTION 2					
4	.300	-.1732+05	.7516+05	.7211+04	.6946+04
5	.502	-.1277+05	.5332+05	.5286+04	.6495+04
6	.704	-.1673+04	.4323+05	.3939+04	.5918+04
7	.906	.4732+04	.3725+05	.2896+04	.5334+04
8	1.108	.8770+04	.3340+05	.2046+04	.4777+04
9	1.310	.1148+05	.3079+05	.1327+04	.4258+04
10	1.512	.1339+05	.2894+05	.7027+03	.3776+04
11	1.714	.1479+05	.2757+05	.1512+03	.3329+04
12	1.916	.1585+05	.2654+05	-.3435+03	.2913+04
13	2.118	.1666+05	.2574+05	-.7922+03	.2526+04
14	2.320	.1730+05	.2511+05	-.1203+04	.2163+04
15	2.522	.1782+05	.2460+05	-.1582+04	.1823+04
16	2.724	.1824+05	.2419+05	-.1934+04	.1503+04
17	2.926	.1859+05	.2385+05	-.2263+04	.1201+04
18	3.128	.1887+05	.2356+05	-.2571+04	.9145+03
19	3.330	.1912+05	.2332+05	-.2861+04	.6429+03
20	3.532	.1932+05	.2311+05	-.3135+04	.3944+03
21	3.734	.1950+05	.2293+05	-.3395+04	.1380+03
22	3.936	.1966+05	.2278+05	-.3643+04	-.9743+02
23	4.138	.1972+05	.2263+05	-.3878+04	-.3228+03
SECTION 3					
23	4.138	.1255+05	.2144+05	-.3875+04	-.6472+03
24	4.340	.8493+04	-.6721+04	-.2877+04	-.4804+03
25	4.542	.8827+04	.3260+04	-.1967+04	-.3284+03
26	4.744	.9105+04	.3901+05	-.1216+04	-.2030+03
27	4.946	.9317+04	.9085+05	-.6425+03	-.1073+03
28	5.148	.9468+04	.1513+06	-.2390+03	-.3974+02
29	5.350	.9566+04	.2152+06	.2296+02	.3635+01
30	5.552	.9623+04	.2790+06	.1711+03	.2959+02
31	5.754	.9648+04	.3408+06	.2374+03	.3964+02
32	5.956	.9642+04	.3996+06	.2439+03	.4156+02
33	6.159	.9647+04	.4556+06	.2273+03	.3796+02
34	6.362	.9633+04	.5086+06	.1892+03	.3160+02
35	6.565	.9618+04	.5591+06	.1459+03	.2436+02
36	6.768	.9602+04	.6078+06	.1042+03	.1740+02
37	6.971	.9589+04	.6550+06	.6763+02	.1129+02
38	7.174	.9577+04	.7014+06	.3729+02	.6227+01
39	7.377	.9568+04	.7473+06	.1257+02	.2098+01

40	7.580	.9560+04	.7930+06	-.7996+01	-.1335+01
41	7.783	.9553+04	.8388+06	-.2617+02	-.4371+01
42	7.986	.9547+04	.8849+06	-.4357+02	-.7276+01
43	8.189	.9540+04	.9316+06	-.6116+02	-.1021+02
44	8.392	.9534+04	.9791+06	-.7893+02	-.1318+02
45	8.595	.9528+04	.1028+07	-.9539+02	-.1593+02
46	8.798	.9523+04	.1077+07	-.1073+03	-.1791+02
47	9.001	.9523+04	.1129+07	-.1090+03	-.1820+02
48	9.204	.9530+04	.1181+07	-.9261+02	-.1547+02
49	9.407	.9547+04	.1235+07	-.4762+02	-.7953+01
50	9.610	.9580+04	.1289+07	.3849+02	.6427+01
51	9.813	.9633+04	.1343+07	.1792+03	.2993+02
52	10.016	.9711+04	.1394+07	.3869+03	.6462+02
53	10.219	.9817+04	.1440+07	.6696+03	.1118+03
54	10.422	.9949+04	.1477+07	.1026+04	.1713+03
55	10.625	.1010+05	.1500+07	.1438+04	.2402+03
56	10.828	.9654+04	.1505+07	.1862+04	.3109+03

SECTION 4

56	10.828	-.2870+05	.1498+07	.1886+04	.2850+03
57	11.033	-.5022+05	.1543+07	.2335+04	.2919+03
58	11.238	-.1043+06	.1575+07	.2502+04	.2367+03
59	11.443	-.1632+06	.1598+07	.2458+04	.1378+03
60	11.648	-.2270+06	.1612+07	.2266+04	.1113+02
61	11.853	-.2959+06	.1615+07	.1984+04	-.1295+03
62	12.058	-.3702+06	.1610+07	.1666+04	-.2727+03
63	12.263	-.4502+06	.1596+07	.1359+04	-.4098+03
64	12.469	-.5364+06	.1575+07	.1102+04	-.5351+03
65	12.675	-.6293+06	.1548+07	.9369+03	-.6440+03
66	12.881	-.7293+06	.1514+07	.8985+03	-.7352+03
67	13.087	-.8373+06	.1475+07	.1022+04	-.8104+03
68	13.293	-.9540+06	.1427+07	.1338+04	-.8750+03
69	13.499	-.1080+07	.1368+07	.1871+04	-.9393+03
70	13.705	-.1217+07	.1292+07	.2625+04	-.1021+04
71	13.911	-.1365+07	.1188+07	.3558+04	-.1150+04
72	14.117	-.1523+07	.1042+07	.4539+04	-.1371+04
73	14.323	-.1691+07	.8363+06	.5266+04	-.1748+04
74	14.529	-.1865+07	.5502+06	.5140+04	-.2369+04
75	14.735	-.2042+07	.1675+06	.3065+04	-.3334+04
76	14.941	-.2213+07	-.3072+06	-.2841+04	-.4717+04
77	15.147	-.2375+07	-.8090+06	-.1559+05	-.6464+04
78	15.353	-.2464+07	-.1120+07	-.3978+05	-.8159+04

SECTION 5

78	15.353	-.2943+07	-.1200+07	-.2128+05	-.3553+04
79	15.553	-.2960+07	-.1187+07	-.7130+04	-.1191+04
80	15.753	-.2950+07	-.8267+06	.2846+03	.4752+02
81	15.953	-.2947+07	-.4464+06	.2960+04	.4943+03
82	16.153	-.2947+07	-.1719+06	.3074+04	.5134+03
83	16.353	-.2943+07	-.1852+05	.2201+04	.3676+03
84	16.553	-.2949+07	.4408+05	.1221+04	.2039+03
85	16.753	-.2949+07	.5426+05	.4923+03	.8222+02
86	16.953	-.2950+07	.4189+05	.7452+02	.1244+02
87	17.153	-.2950+07	.2481+05	-.1032+03	-.1723+02
88	17.353	-.2950+07	.1106+05	-.1386+03	-.2315+02

89	17.553	-.2950+07	.2652+04	-.1105+03	-.1846+02
90	17.753	-.2950+07	-.1269+04	-.6715+02	-.1121+02
91	17.953	-.2950+07	-.2350+04	-.3101+02	-.5178+01
92	18.153	-.2950+07	-.2053+04	-.8321+01	-.1390+01
93	18.353	-.2950+07	-.1331+04	.2602+01	.4345+00
94	18.553	-.2950+07	-.6659+03	.5893+01	.9842+00
95	18.753	-.2950+07	-.2200+03	.5363+01	.8957+00
96	18.953	-.2950+07	.1150+02	.3569+01	.5960+00
97	19.153	-.2950+07	.9424+02	.1838+01	.3070+00
98	19.353	-.2950+07	.9697+02	.6465+00	.1080+00
99	19.553	-.2950+07	.6911+02	.1035-01	.1729-02
100	19.753	-.2950+07	.3816+02	-.2296+00	-.3834-01
101	19.953	-.2950+07	.1528+02	-.2506+00	-.4185-01
102	20.153	-.2950+07	.2222+01	-.1838+00	-.3070-01
103	20.353	-.2950+07	-.3281+01	-.1042+00	-.1741-01
104	20.553	-.2950+07	-.4326+01	-.4339-01	-.7245-02
105	20.753	-.2950+07	-.3402+01	-.7304-02	-.1220-02
106	20.953	-.2950+07	-.2044+01	.9277-02	.1549-02
107	21.153	-.2950+07	-.9923+00	.1414-01	.2361-02
108	21.353	-.2950+07	-.4899+00	.1330-01	.2221-02
109	21.553	-.2950+07	-.5213+00	.9640-02	.1610-02
110	21.753	-.2950+07	-.9331+00	.2989-02	.4992-03
111	21.953	-.2950+07	-.1433+01	-.9013-02	-.1505-02
112	22.153	-.2950+07	-.1504+01	-.2923-01	-.4881-02
113	22.353	-.2950+07	-.3018+00	-.5804-01	-.9693-02
114	22.553	-.2950+07	.3323+01	-.8855-01	-.1479-01
115	22.753	-.2950+07	.1050+02	-.9995-01	-.1669-01
116	22.953	-.2950+07	.2143+02	-.5108-01	-.8531-02
117	23.153	-.2950+07	.3365+02	.1206+00	.2015-01
118	23.353	-.2950+07	.3957+02	.4852+00	.8103-01
119	23.553	-.2950+07	.2380+02	.1076+01	.1797+00
120	23.753	-.2950+07	-.3761+02	.1803+01	.3011+00
121	23.953	-.2950+07	-.1725+03	.2313+01	.3863+00
122	24.153	-.2950+07	-.3969+03	.1833+01	.3061+00
123	24.353	-.2950+07	-.6821+03	-.9238+00	-.1543+00
124	24.553	-.2950+07	-.9027+03	-.7590+01	-.1268+01
125	24.753	-.2950+07	-.7732+03	-.1943+02	-.3244+01
126	24.953	-.2950+07	.1934+03	-.3568+02	-.5959+01
127	25.153	-.2950+07	.2635+04	-.5081+02	-.8485+01
128	25.353	-.2950+07	.7087+04	-.5080+02	-.8483+01
129	25.553	-.2950+07	.1338+05	-.1012+02	-.1690+01
130	25.753	-.2950+07	.1957+05	.1073+03	.1791+02
131	25.953	-.2950+07	.2056+05	.3368+03	.5624+02
132	26.153	-.2949+07	.6759+04	.6839+03	.1142+03
133	26.353	-.2949+07	-.3572+05	.1069+04	.1786+03
134	26.553	-.2949+07	-.1213+06	.1249+04	.2086+03
135	26.753	-.2949+07	-.2540+06	.7335+03	.1225+03
136	26.953	-.2952+07	-.4075+06	-.1239+04	-.2070+03
137	27.153	-.2955+07	-.4936+06	-.5546+04	-.9261+03

SECTION 6

4	27.153	-.5446+05	.6895+05	-.4376+04	-.7309+03
138	27.303	-.1025+06	-.2873+06	-.1899+04	-.3171+03
139	27.453	-.9474+05	-.2721+06	-.3680+03	-.6146+02
140	27.603	-.9153+05	-.1659+06	.2188+03	.3654+02
141	27.753	-.9096+05	-.8350+05	.2899+03	.4842+02

142	27.903	-.9138+05	-.4690+05	.1859+03	.3105+02
143	28.053	-.9189+05	-.4272+05	.7726+02	.1290+02
144	28.203	-.9221+05	-.5334+05	.1373+02	.2293+01
145	28.353	-.9234+05	-.6748+05	-.9966+01	-.1664+01
146	28.503	-.9236+05	-.8047+05	-.1235+02	-.2063+01
147	28.653	-.9234+05	-.9150+05	-.7743+01	-.1293+01
148	28.803	-.9232+05	-.1012+06	-.3138+01	-.5241+00
149	28.953	-.9231+05	-.1102+06	-.5046+00	-.8426-01
150	29.103	-.9230+05	-.1192+06	.4503+00	.7519-01
151	29.253	-.9230+05	-.1282+06	.5257+00	.8779-01
152	29.403	-.9230+05	-.1372+06	.3221+00	.5379-01
153	29.553	-.9231+05	-.1464+06	.1273+00	.2125-01
154	29.703	-.9231+05	-.1555+06	.1818-01	.3036-02
155	29.853	-.9231+05	-.1647+06	-.2020-01	-.3374-02
156	30.003	-.9231+05	-.1738+06	-.2234-01	-.3730-02
157	30.153	-.9231+05	-.1830+06	-.1339-01	-.2235-02
158	30.303	-.9231+05	-.1921+06	-.5151-02	-.8602-03
159	30.453	-.9231+05	-.2013+06	-.6379-03	-.1065-03
160	30.603	-.9231+05	-.2104+06	.9012-03	.1505-03
161	30.753	-.9231+05	-.2196+06	.9478-03	.1583-03
162	30.903	-.9231+05	-.2287+06	.5557-03	.9280-04
163	31.053	-.9231+05	-.2379+06	.2081-03	.3475-04
164	31.203	-.9231+05	-.2470+06	.2155-04	.3599-05
165	31.353	-.9231+05	-.2562+06	-.4001-04	-.6682-05
166	31.503	-.9231+05	-.2653+06	-.4020-04	-.6713-05
167	31.653	-.9231+05	-.2745+06	-.2307-04	-.3852-05
168	31.803	-.9231+05	-.2836+06	-.8344-05	-.1394-05
169	31.953	-.9231+05	-.2928+06	-.4798-06	-.8013-07
170	32.103	-.9231+05	-.3019+06	.2251-05	.3759-06
171	32.253	-.9231+05	-.3111+06	.2431-05	.4060-06
172	32.403	-.9231+05	-.3202+06	.1451-05	.2423-06
173	32.553	-.9231+05	-.3294+06	-.7585-06	-.1267-06
174	32.703	-.9231+05	-.3385+06	-.5080-06	-.8484-06
175	32.853	-.9231+05	-.3477+06	-.1168-04	-.1950-05
176	33.003	-.9231+05	-.3568+06	-.1716-04	-.2866-05
177	33.153	-.9231+05	-.3660+06	-.1065-04	-.1779-05
178	33.303	-.9231+05	-.3751+06	.2862-04	.4779-05
179	33.453	-.9231+05	-.3843+06	.1249-03	.2085-04
180	33.603	-.9231+05	-.3934+06	.2776-03	.4635-04
181	33.753	-.9231+05	-.4026+06	.3988-03	.6660-04
182	33.903	-.9231+05	-.4117+06	.2233-03	.3729-04
183	34.053	-.9231+05	-.4209+06	-.7423-03	-.1240-03
184	34.203	-.9231+05	-.4300+06	-.3053-02	-.5098-03
185	34.353	-.9231+05	-.4392+06	-.6635-02	-.1108-02
186	34.503	-.9231+05	-.4483+06	-.9291-02	-.1552-02
187	34.653	-.9231+05	-.4575+06	-.4602-02	-.7685-03
188	34.803	-.9231+05	-.4666+06	.1912-01	.3193-02
189	34.953	-.9231+05	-.4758+06	.7452-01	.1245-01
190	35.103	-.9231+05	-.4849+06	.1584+00	.2646-01
191	35.253	-.9231+05	-.4941+06	.2160+00	.3608-01
192	35.403	-.9231+05	-.5034+06	.9219-01	.1540-01
193	35.553	-.9231+05	-.5126+06	-.4901+00	-.8185-01
194	35.702	-.9232+05	-.5216+06	-.1807+01	-.3017+00
195	35.851	-.9232+05	-.5304+06	-.3753+01	-.6267+00
196	36.000	-.9233+05	-.5385+06	-.5011+01	-.8368+00
197	36.149	-.9231+05	-.5458+06	-.1955+01	-.3266+00
198	36.298	-.9224+05	-.5531+06	.1177+02	.1965+01

199	36.447	-.9209+05	-.5630+06	.4264+02	.7121+01
200	36.596	-.9188+05	-.5806+06	.8791+02	.1468+02
201	36.745	-.9179+05	-.6129+06	.1163+03	.1942+02
202	36.894	-.9225+05	-.6624+06	.4241+02	.7082+01
208	37.043	-.9627+05	-.7127+06	-.2846+03	-.4753+02

SECTION 7

203	37.043	-.8061+06	-.9660+06	.1232+04	-.3349+03
204	37.143	-.8071+06	-.8513+06	.7063+03	.4871+03
205	37.293	-.8287+06	-.8398+06	.6639+03	.5961+03
206	37.443	-.8326+06	-.8373+06	.6499+03	.6172+03
207	37.593	-.8338+06	-.8364+06	.6436+03	.6246+03
208	37.743	-.8341+06	-.8359+06	.6403+03	.6281+03

SECTION 8

208	37.743	-.8672+06	-.8415+06	.1224+02	.5232+03
209	37.902	-.8660+06	-.8465+06	.2772+04	.1111+04
210	38.062	-.8633+06	-.8491+06	.6999+04	.2398+04
211	38.221	-.8615+06	-.8508+06	.1254+05	.4348+04
78	38.381	-.8609+06	-.8521+06	.1930+05	.6925+04

A.5 Listing of Programs

There follow complete listings of all the CONFRU programs, including the plotter program STRESSPLOT. The programs are listed in the following order:

1. CONFRU MAIN program
2. Subroutine PLGEOM
3. Subroutine PLPRES
4. Subroutine SYSTEM
5. Subroutine GELSTF
6. Subroutine SETBD
7. Subroutine TRANS
8. Subroutine PROD
9. Subroutine PTLOAD
10. Subroutine LOAD
11. Subroutine CLOSEL
12. Subroutine BONCON
13. Subroutine BANDO
14. Subroutine BANBAC
15. Subroutine STRESS
16. Plotter program STRESSPLOT

C ** CONFRU MAIN PROGRAM **

PARAMETER IXX=500,IYY=15000,IZZ=30,IWW=1503

LOGICAL PCS

DIMENSION HEAD(10),NEL1(IZZ),NEL2(IZZ),NOD1(IZZ),NOD2(IZZ)

DIMENSION NPTL(IZZ),NELP1(IZZ),NELP2(IZZ),NODS(IXX),NL(IZZ)

DIMENSION NBC(10),UBC(10),WBC(10),MBC(10),ICLOSE(5)

DIMENSION NC(IWW),ND(10,4),NF(IWW),NM(IWW),NR(IWW),NWR(IWW)

DOUBLE PRECISION L(IXX),R1(IXX),R2(IXX),T(IXX,2),TL(IXX)

DOUBLE PRECISION A(IYY),VEC(IWW)

DOUBLE PRECISION RS1(IZZ),RS2(IZZ),T1(IZZ),T2(IZZ)

DOUBLE PRECISION P1(IXX),PR1(IZZ),PR2(IZZ),PDA(IXX)

DOUBLE PRECISION QU(IZZ),WW(IZZ),MM(IZZ)

DOUBLE PRECISION RNU,E,GC,FAC

C DOUBLE PRECISION BA(IYY),BVEC(IWW)

COMMON /BLK1/IX,IY,IZ,IW

COMMON /BLK2/NPLOT/BLK3/IBON/BLK4/NCP/BLK5/RNU,E/BLK6/NELT,N

COMMON /BLK7/NBP/BLK8/ISP

C NOTE: IF BACK SUBSTITUTION IS REQUIRED

C CHANGE: IXX=250,IYY=7500,IWW=750

C AND REMOVE RELEVANT COMMENT CARDS

C -----

IX = 500

IY = 15000

IZ = 30

IW = 1503

C -----

C *****

C *****

C ** MAIN HEADER TITLE

C *****

500 READ(8,500) ISYM,IGEN,IG,IL,IS,IBON,IV,IB,IO,ISP

500 FORMAT(10I1)

500 IF(1SYM),501

PRINT 301

301 FORMAT(1H1,6(/),1H0,39X,31('*')),/,

140X,'* CONFRU *'/,

140X,'* FINITE ELEMENT AXISYMMETRIC *'/,

240X,'* THIN SHELL PROGRAM *'/,

340X,'*',29X,'*',/,

640X,'* T.B.GRIFFIN *'/,

740X,'* DEPT. OF CIVIL ENGINEERING *'/,

240X,'* UNIVERSITY OF CAPE TOWN *'/,

540X,'*',29X,'*',/,

340X,'* AUGUST 1974 *'/,

340X,'*',29X,'*',/,

640X,'* UNIVAC 1106 EXEC 8 *'/,

840X,31('*'))

C *****

C READ IN ANALYSIS DATA

C *****

501 CONTINUE

```

READ(8,200) LCASE,(HEAD(I),I = 1,10)
READ(8,201) NPLOT,NBP,(LCLOSE(I),I = 1,5)
READ(8,202) RNC,E,GC
READ(8,203) NSEC,NPS,NNBC,NNPL,NBP

```

```

DO 254 I = 1,NSEC
254 READ(8,204)NCD1(I),NEL1(I),NCD2(I),NEL2(I),RS1(I),RS2(I),T1(I),
1T2(I)

```

```

IF(NPS),256,
DO 255 I = 1,NPS
255 READ(8,208) NELP1(I),NELP2(I),PR1(I),PR2(I)

```

```

256 DO 253 I = 1,NNBC
253 READ(8,205) NBC(I),UBC(I),WBC(I),MBC(I)

```

```

IF(NNPL),257,
DO 251 I = 1,NNPL
251 READ(8,207) NPTL(I),UU(I),WW(I),MM(I)

```

```

257 IF(NBP),252,
DO 258 I = 1,NBP
258 READ(8,203) ND(I,1),ND(I,2),ND(I,3),ND(I,4)

```

252 NELT = NEL2(NSEC)

```

I = 1
263 READ(8,206) L(I),NREP
IF(NREP - 1) 261,261,
NREPI = NREP - 1
DO 262 J = 1,NREPI
I = I + 1
262 READ(8,206) L(I)
261 I = I + 1
IF(I-NELT) 263,263

```

```

200 FORMAT(A6,2X,10A5)
201 FORMAT(2(I2,2X),5(I3,2X))
202 FORMAT(8(E8.3,2X))
203 FORMAT(5(I3,2X))
204 FORMAT(4(I3,2X),4(E8.3,2X))
205 FORMAT(13,2X,3(A1,1X))
206 FORMAT(F7.0,2X,I3)
207 FORMAT(13,2X,3(E8.3,2X))
208 FORMAT(2(I3,2X),2(E8.3,2X))

```

```

221 TL(1) = 0.
DO 13 I = 1,NELT
13 TL(I+1) = TL(I) + L(I)

```

```

C *****
C HEADING: ANALYSIS INFORMATION
C *****
IF(ISYM),,502

```

PRINT 302,LCASE

```

302 FORMAT(1H0,5(/),1H0,39X,31('*'),/,
340X,'* LOAD CASE: ',A6,11X,'*',/,
440X,'*',29X,'*',/,
540X,'* DATE.....',10X,'*',/,
640X,31('*'))
C *****
C FIXED CONSTANTS
C *****
502 NELTP1 = NELT + 1
IF(NBP)503,,505
DO 504 I = 1,10
DO 504 J = 1,4
504 ND(I,J) = 0.
503 CONTINUE
N = (NELT + 1)*3
IF(ND(NBP,1).EQ.NELT) N = NELT*3

NS2 = NSEC*2
M = 0
DO 5 J = 1,NSEC
NL(2*J - 1) = MOD1(J)
5 NL(2*J) = MOD2(J)
DO 6 K = 1,NS2
NT = NL(K)
DO 7 I = K,NS2
IF(NL(I+1).NE.NT) GO TO 7
M = M + 1
GO TO 6
7 CONTINUE
6 CONTINUE

NPP = (N/3) + N

DO 150 I = 1,NELT
P1(I) = 0.
150 PDA(I) = 0.
C *****
C GEOMETRIC DATA GENERATION
C *****

CALL PLGEOM(NSEC,NEL1,NEL2,RS1,RS2,T1,T2,L,T,R1,R2)

C *****
C PRINT OUT GENERAL INFORMATION, BRANCHING ETC.
C *****
IF(IGEN),,400

PRINT 309 , (HEAD(I),I = 1,10)
309 FORMAT(1H1,50('*'),/,1H ,10A5,/,1H ,50('*'))
PRINT 305,RNU,E,GC
303 FORMAT(1H0,'POISSON RATIO: ',8X,F5.3,/,
1' MODULUS OF ELASTICITY: ',E8.3,/,
2'DUNIT WEIGHTS: STRUCTURE MATERIAL: ',E8.3,/,)
IF(NGP.NE.5.AND.NGP.NE.7) PRINT 318,NGP
318 FORMAT(1H0,'NUMERICAL INTEGRATION: ',I2, ' POINT GAUSS QUADRATURE
1.')
IF(NGP.EQ.5.OR.NGP.EQ.7) PRINT 319,NGP

```

```

319 FORMAT('UNNUMERICAL INTEGRATION: ',I2,' POINT SIMPSON QUADRATURE.')

PRINT 331
331 FORMAT(1H0,3(/),1H ,30('-'),/, ' CHECK NODE AND ELEMENT NUMBERS',/,
1' FOR SECTIONS AND BRANCHES',/,1H ,30('-'),/,1H0,'SECTIONS',3X,'NO
2DE',2X,'(ELEMENT)',5('*'),'(ELEMENT)',2X,'NODE',/,1H ,8('-'))
DO 332 J = 1,NSEC
PRINT 333,J,NOD1(J),NEL1(J),NEL2(J),NOD2(J)
333 FORMAT(1H ,3X,12,6X,I3,5X,'(',I3,')',9X,'(',I3,')' ,I3)
332 CONTINUE

PRINT 430
430 FORMAT(1H0,'CLOSURE ELEMENTS',/,1H ,16('-'))
IF(ICLOSE(1).EQ.0) PRINT 431
431 FORMAT(1H , 'THE STRUCTURE HAS NO CLOSURE ELEMENTS')
IF(ICLOSE(1).GT.0) PRINT 321,ICLOSE(1)
321 FORMAT('THERE ARE CLOSURE ELEMENTS AT THE FOLLOWING NODES: ',I3)
DO 322 J = 2,5
IF(ICLOSE(J).GT.0) PRINT 323,ICLOSE(J)
323 FORMAT(1H ,51X,I3)
322 CONTINUE

PRINT 338
338 FORMAT(1H0,'BRANCH POINTS',/,1H ,13('-'))
IF(NBP.EQ.0) PRINT 435
435 FORMAT(' THE STRUCTURE HAS NO BRANCH POINTS')
IF(NBP),400,
DO 335 M = 1,NBP
ND2 = ND(M,1) + 1
IF(ND(M,2).GT.0) PRINT 336,ND(M,1),ND(M,2),ND(M,3)
IF(ND(M,2).EQ.0) PRINT 337,ND(M,1),ND2
336 FORMAT('UNODE ',I3,' IS CONNECTED TO NODE ',I3,' THROUGH ELEMENT '
1,I3)
337 FORMAT('UNODE ',I3,' IS NOT CONNECTED TO NODE ',I3)
335 CONTINUE
C *****
C PRINT OUT GEOMETRIC DATA
C *****
400 IF(I3),,402

330 PRINT 304
304 FORMAT(1H1,15('-'),/, ' GEOMETRIC DATA:',/,1H ,15('-'),/,
1'NELEMENT',4X,'LENGTH',4X,'RADIUS(1)',4X,'RADIUS(2)',5X,
2'T(1)',7X,'T(2)')
DO 350 I = 1,NELT
350 PRINT 305,I,L(I),R1(I),R2(I),T(I,1),T(I,2)
305 FORMAT(1H ,2X,I3,4X,F8.6,4X,F8.3,7X,F6.3,5X,5(F8.6,3X))
PRINT 306,TL(NELT,1)
306 FORMAT(1H ,18('-'),/,1H , 'TOTAL',2X,F9.6)
C *****
C PRESSURE DATA GENERATION
C *****

402 CONTINUE

IF(NFS.GT.0) CALL PLPRES(NPS,NELP1,NELP2,PR1,PR2,L,P1,POA)

```

```

C *****
C PRINT OUT LOADING DATA
C *****

      IF(IL),,401

      PRINT 307
307 FORMAT(1H1,13(' '),/, ' LOADING DATA:',/,1H ,13(' '))
311 IF(GC.GT.0.) PRINT 314
314 FORMAT('0** THE SELF WEIGHT OF THE STRUCTURE IS INCLUDED SEPARATEL
      1Y IN THIS ANALYSIS **')
      PRINT 315
315 FORMAT(1HD,2X,'NODE',6X,'PRESSURE',7X,'UU',12X,'WW',12X,'MM')

      J = 1
      ZERO = 0.
      DO 351 I = 1,NELTP1
      IF(NPTL(J).EQ.I) PRINT 308,I,P1(I),UU(J),WW(J),MM(J)
      IF(NPTL(J).NE.1) PRINT 308,I,P1(I),ZERO,ZERO,ZERO
      IF(NPTL(J).EQ.I) J = J + 1
308 FORMAT(1H ,2X,I3,6X,E9.4,5X,4(E9.4,5X))
351 CONTINUE
C *****
C SET UP SYSTEM STIFFNESS MATRIX
C *****

401 CONTINUE

      CALL SYSTEM(ND,L,R1,R2,T,NC,NM,NF,A)

C *****
C CLOSURE ELEMENT STIFFNESS & LOAD VECTOR
C *****

      IF(ICLOSE(1).GT.0)CALL CLOSEL(ICLOSE,NF,GC,P1,R1,T,A,VEC)

C *****
C SET UP SYSTEM LOAD VECTOR
C *****

      POS = .FALSE.
      DO 410 I = 1,NELT
      IF(DABS(P1(I)).GT.0.) POS = .TRUE.
410 CONTINUE

      IF(NNPL.GT.0) CALL PTLOAD(NNPL,NPTL,R1,R2,L,UU,WW,MM,VEC)
      IF(GC.GT.0.OR.POS) CALL LOAD(NELT,GC,L,R1,R2,T,P1,PCA,VEC)

C *****
C BOUNDARY CONDITIONS
C *****

      CALL BCNCCN(NNBC,NBC,NC,NM,NF,UBC,WBC,MBU,A,VEC)

C *****
C PRINT OUT SYSTEM STIFFNESS & LOAD VECTOR
C *****

```

```

      IF(IS),,605
      PRINT 603
603  FORMAT(1H1,'SYSTEM STIFFNESS',/,1H ,16(' '),/)
      NNN = NELT*15
      PRINT 604,(A(I),I = 1,NNN)
604  FORMAT(1H0,10E11.6)
605  IF(IV),,606

      PRINT 601
601  FORMAT(1H1,18(' '),/,,' SYSTEM LOAD VECTOR',/,1H ,18(' '),/,1H0,'NO
      1DE',9X,'U',13X,'W',13X,'M',/)
      J = 0
      DO 420 I = 1,N,3
      J = J + 1
      PRINT 421,J,VEC(I),VEC(I+1),VEC(I+2)
421  FORMAT(1H ,I4,3(5X,E9.4))
420  CONTINUE

606  CONTINUE

C      DO 645 I = 1,IYY
C 645  BA(I) = A(I)

C      *****
C      SOLVE SYSTEM STIFFNESS EQUATIONS
C      *****

      CALL BANDC(N,NC,A,VEC,NM,NF,NR,NWR)

C      *****
C      BACK SUBSTITUTION
C      *****

C      IF(IB.EG.0) CALL BANBAC(NC,NM,NF,ND,VEC,BA,BVEC)

C -----

      FAC = (1. - RND*RND)/(6.283185307*E)
      DO 8 I = 1,N
      8  VEC(I) = VEC(I)*FAC

C -----

C      *****
C      PRINT OUT DISPLACEMENT RESULTS
C      *****

      IF(ID),,404

      PRINT 9
      9  FORMAT(1H1,50(' '),/,,' DISPLACEMENTS AT EACH NODE, IN GLOBAL COORD
      1INATES:',/,1H ,50(' '),/,1H0,'NODE',9X,'U',13X,'W',13X,'M')
      J = 0
      DO 11 I = 1,N,3
      J = J + 1
      PRINT 10 ,J,VEC(I),VEC(I+1),VEC(I+2)

```

```
10 FORMAT(1H ,I3,5X,E11.6,2(4X,E11.6))
11 CONTINUE
```

```
C *****
C PRINT OUT STRESS HEADINGS
C *****
```

```
404 IF(ISP),407,
PRINT 406,NPLOT
406 FORMAT('RESULTS TO PLOT FILE ',I2,' ONLY')
GO TO 405
```

```
407 PRINT 50
50 FORMAT(1H1,42(' '),/, ' NODAL STRESSES (N/SQ.M) AND MOMENTS (NM/M) '
1,/,1H ,42(' ')
1,/, 'NODE ',2X, 'CUMULATIVE ',4X, 'SIGMA-S ',4X, 'SIGMA-THETA ',7X, 'MS '
2,9X, 'NTHETA ',/,1H ,8X, 'LENGTH ',/)
```

```
C *****
C STRESS RESULTANTS
C *****
```

```
405 WRITE(NPLOT,51) NFP,LCASE
51 FORMAT(7X,I3,2X,A6)
```

```
CALL STRESS(NSEC,NODS,NOD1,NOD2,NEL1,NEL2,L,R1,R2,T,VEC)
```

```
STOP
END
```

```

1      SUBROUTINE PLGEOM(NSEC,NELB,NELE,RE,RE,TB,TE,L,T,R1,R2)
2      COMMON /BLK1/IX,IY,IZ,IW
3      INTEGER EL1,EL2
4      DOUBLE PRECISION RB(IZ),RE(IZ),TB(IZ),TE(IZ)
5      DOUBLE PRECISION L(IX),R1(IX),R2(IX),T(IX,2)
6      DOUBLE PRECISION TL,SINA,DELT,SL
7      DIMENSION NELB(IZ),NELE(IZ)
8      DO 1 M = 1,NSEC
9      TL = 0.
10     EL1 = NELB(M)
11     EL2 = NELE(M)
12     DO 2 J = EL1,EL2
13     2 TL = TL + L(J)
14     IF(RE(M).EQ.0.)RE(M) = RB(M)
15     SINA = (RE(M) - RB(M))/TL
16     R1(EL1) = RB(M)
17     DO 3 I = EL1,EL2
18     R2(I) = R1(I) + L(I)*SINA
19     3 R1(I+1) = R2(I)
20
21     IF(TE(M).EQ.0.)TE(M) = TB(M)
22     K = EL2 - EL1 + 1
23     DELT = TE(M) - TB(M)
24     SL = 0.
25     T(EL1,1) = TB(M)
26     DO 4 I = 1,K
27     SL = SL + L(EL1-1+I)
28     T(EL1+I,1) = (SL/TL)*DELT + T(EL1,1)
29     4 T(EL1+I-1,2) = T(EL1+I,1)
30
31     1 CONTINUE
32
33     RETURN
34     END

```

```
1      SUBROUTINE PLPRES(NPS,NELP1,NELP2,PR1,PR2,L,P1,PDA)
2      COMMON /BLK1/IX,IY,IZ,IW
3      INTEGER EL1,EL2
4      DIMENSION NELP1(IZ),NELP2(IZ)
5      DOUBLE PRECISION PR1(IZ),PR2(IZ),L(IX),P1(IX),PDA(IX)
6      DOUBLE PRECISION TL,DELP
7
8      DO 200 I = 1,NPS
9      EL1 = NELP1(I)
10     EL2 = NELP2(I)
11     DELP = PR2(I) - PR1(I)
12     TL = 0.
13     DO 210 J = EL1,EL2
14 210 TL = TL + L(J)
15     P1(EL1) = PR1(I)
16     DO 220 K = EL1,EL2
17     PDA(K) = (L(K)/TL)*DELP
18     IF(K - EL2),220,
19     P1(K+1) = P1(K) + PDA(K)
20 220 CONTINUE
21
22 200 CONTINUE
23     99 RETURN
24     END
```

```

SUBROUTINE SYSTEM(ND,L,R1,R2,T,NC,NM,NF,A)
COMMON /BLK1/IX,IY,IZ,IW
COMMON /BLK4/N6P/BLK6/NELT,N
COMMON /BLK7/NBP
DIMENSION NC(1W),ND(10,4),NM(1W),NF(1W)
DOUBLE PRECISION A(IY),KE(6,6),KA(6,6),KB(6,6)
DOUBLE PRECISION L(IX),R1(IX),R2(IX),T(IX,2)

```

C *****

```

DO 90 I = 1,IY
90 A(I) = 0.

```

C *****

C ELEMENT 1 STIFFNESS MATRIX

C *****

```

I = 1
J = 1
K1 = J
K2 = J + 20
CALL GELSTF(L(I),R1(I),R2(I),T(I,1),T(I,2),KE)
K3 = 1
K4 = 1
DO 40 K = K1,K2
A(K) = A(K) + KE(K3,K4)
IF(K3 - K4) 41,,41
K3 = K3 + 1
K4 = 1
GO TO 40
41 K4 = K4 + 1
40 CONTINUE
DO 42 K5 = 1,6
42 NC(K5) = 1
J = 10
I = I + 1

```

C *****

```

80 DO 50 M = 1,10
IF(ND(M,1).EQ.I.AND.ND(M,2).EQ.0) GO TO 51
GO TO 52
51 IF(ND(M+1,1).EQ.(I+1)) GO TO 20
GO TO 50
52 IF(ND(M,1).EQ.(I+1).AND.ND(M,2).NE.0) GO TO 20
50 CONTINUE

```

C *****

C ALL STANDARD ELEMENT STIFFNESS MATRICES

C *****

```

DO 82 MM = 1,10
IF(ND(MM,4) - I),83,
82 CONTINUE
DO 85 KK = 1,6
DO 85 JJ = 1,6

```

```

85 KB(KK,JJ) = U.
GO TO 84
83 NEL = ND(MM,3)
K3 = 4
IF(ND(MM,1).GT.ND(MM,3)) K3 = 1
K4 = K3
CALL GELSTF(L(NEL),R1(NEL),R2(NEL),T(NEL,1),T(NEL,2),KB)
84 CALL GELSTF(L(I),R1(I),R2(I),T(I,1),T(I,2),KE)
A(J) = A(J) + KE(1,1) + KB(K3,K4)
A(J+4) = A(J+4) + KE(2,1) + KB(K3+1,K4)
A(J+5) = A(J+5) + KE(2,2) + KB(K3+1,K4+1)
A(J+9) = A(J+9) + KE(3,1) + KB(K3+2,K4)
A(J+10) = A(J+10) + KE(3,2) + KB(K3+2,K4+1)
A(J+11) = A(J+11) + KE(3,3) + KB(K3+2,K4+2)
J1 = J + 12
J2 = J1 + 14
K3 = 4
K4 = 1
DO 45 K = J1,J2
A(K) = A(K) + KE(K3,K4)
IF(K4 - K3) 44,,44
K3 = K3 + 1
K4 = 1
GO TO 45
44 K4 = K4 + 1
45 CONTINUE

NROW = (I*3) + 1
NCOL = (I-1)*3 + 1
KB = NROW + 2
DO 46 K = NROW,KB
46 NC(K) = NCOL

I = I + 1
J = J1 + 3
IF(I - 1 - NELT) 80,70,80

```

```

C *****
C BRANCH POINT STIFFNESS MATRICES
C *****

```

```

20 NROW = (I*3) + 1
MM = M
IF(ND(M+1,1).EQ.(I+1)) MM = M + 1
DO 38 K = 1,3
38 NC(NROW+K-1) = (ND(MM,2)-1)*3 + 1

N1 = J
N2 = J + 4
N3 = J + 9
NB = (NROW-1) - (NC(NROW)+2) - 3
N4 = N3 + 3
N7 = N4 + NB + 3
N5 = N7 + 4
N8 = N5 + NB + 3
N6 = N8 + 5
N9 = N6 + NB + 3

```

```

NN1 = N9 + 6
NN2 = NN1 + 4
NN3 = NN2 + 5

NFLAG = 0
IF(ND(M+1,1).EQ.(1+1)) NFLAG = 1
K1 = ND(M+1,3)
K2 = ND(M,3)

K3 = 1
IF(ND(M,3).EQ.ND(M,2)) K3 = 4
K4 = K3

IF(NFLAG.EQ.0) CALL GELSTF(L(I),R1(I),R2(I),T(I,1),T(I,2),KA)

IF(NFLAG.EQ.1) CALL GELSTF(L(K1),R1(K1),R2(K1),T(K1,1),T(K1,2),KB)

IF(NFLAG.EQ.0) CALL GELSTF(L(K2),R1(K2),R2(K2),T(K2,1),T(K2,2),KB)
IF(NFLAG - 1) 21,,21
DO 22 KK = 1,6
DO 22 JJ = 1,6
22 KA(KK,JJ) = 0.
21 IF(I - (NELT-1)),,6,
IF(ND(M-1,1) - (I+1)) 35,,35
36 DO 34 K1 = 1,6
DO 34 K2 = 1,6
34 KE(K1,K2) = 0.
GO TO 33

35 CALL GELSTF(L(I+1),R1(I+1),R2(I+1),T(I+1,1),T(I+1,2),KE)

33 A(N1) = A(N1) + KA(1,1)
A(N2) = A(N2) + KA(2,1)
A(N2+1) = A(N2+1) + KA(2,2)

DO 23 K1 = 1,3
23 A(N3 + K1 - 1) = A(N3+K1-1) + KA(3,K1)

K5 = 4
K6 = 1
IF(ND(M,4).GT.0.AND.ND(M,1).EQ.ND(M,3)) K5 = 1
IF(K5.EQ.1) K6 = 4
DO 24 K1 = 1,3
A(N4 + K1 - 1) = KB(K5,K6+K1-1)
A(N5 + K1 - 1) = KB(K5+1,K6+K1-1)
24 A(N6 + K1 - 1) = KB(K5+2,K6+K1-1)

DO 29 K1 = 1,3
29 A(N7+K1-1) = KA(4,K1)

A(N7+3) = KA(4,4) + KE(1,1) + KB(K3,K4)

DO 30 K1 = 1,3
30 A(N8+K1-1) = KA(5,K1)

A(N8+3) = KA(5,4) + KE(2,1) + KB(K3+1,K4)
A(N8+4) = KA(5,5) + KE(2,2) + KB(K3+1,K4+1)

```

```

DO 31 K1 = 1,3
31 A(N9+K1-1) = KA(6,K1)

A(N9+3) = KA(6,4) + KE(3,1) + KB(K3+2,K4)
A(N9+4) = KA(6,5) + KE(3,2) + KB(K3+2,K4+1)
A(N9+5) = KA(6,6) + KE(3,3) + KB(K3+2,K4+2)

IF(I-(NELT-1)),70,

NROW = (I+1)*3 + 1
NCOL = (I*3) + 1
DO 28 K1 = 1,3
28 NC(NROW + K1 - 1) = NCOL

DO 25 K1 = 1,4
25 A(NN1+K1-1) = KE(4,K1)
DO 26 K1 = 1,5
26 A(NN2+K1-1) = KE(5,K1)
DO 27 K1 = 1,6
27 A(NN3+K1-1) = KE(6,K1)

69 J = NN1 + 3
I = I + 2
GO TO 80

60 CALL GELSTF(L(I),R1(I),R2(I),T(I,1),T(I,2),KE)

A(J) = A(J) + KE(1,1)
A(J+4) = A(J+4) + KE(2,1)
A(J+5) = A(J+5) + KE(2,2)
A(J+9) = A(J+9) + KE(3,1)
A(J+10) = A(J+10) + KE(3,2)
A(J+11) = A(J+11) + KE(3,3)

LROW = (I*3) + 1
NCOL = (I-1)*3 + 1
DO 61 K = 1,3
61 NC(LROW + K - 1) = NCOL
I = I + 1
J = J + 15
GO TO 80

70 CONTINUE

NF(1) = 1
DO 10 I = 1,N
NM(I) = I - NC(I) + 1
10 NF(I+1) = NF(I) + NM(I)

```

C *****

```

RETURN
END

```

```

SUBROUTINE GELSTF(L,R1,R2,T1,T2,KE)
DOUBLE PRECISION B(4,6),BT(6,4),D(4,4),Z(6,4),KE(6,6)
DOUBLE PRECISION T(10),ABS(10),H(10),ZK(6,6)
DOUBLE PRECISION RNU,L,R1,R2,T1,T2,SD,E
COMMON /BLK1/IX,IY,IZ,IW
COMMON /BLK4/NGP/BLK5/RNU,E

```

```

DEFINE R(R1,R2,SD) = R1 + (SD*(R2 - R1))

```

```

C *****
C GAUSSIAN HALF-FORMULA COEFFICIENTS FOR N=4,6,8 AND 10
C *****

```

```

IF(NGP - 4) 1,,1
ABS(1) = 0.339981043584856
ABS(2) = 0.861136311594053
H(1) = 0.652145154862546
H(2) = 0.347854845137454
GO TO 10

```

```

1 IF(NGP - 6) 2,,2
ABS(1) = 0.238619186083197
ABS(2) = 0.661209386466265
ABS(3) = 0.932469514203152
H(1) = 0.467913934572691
H(2) = 0.360761575048139
H(3) = 0.171324492379170
GO TO 10

```

```

2 IF(NGP - 8) 3,,3
ABS(1) = 0.183434642495650
ABS(2) = 0.525532409916329
ABS(3) = 0.796666477413627
ABS(4) = 0.960289856497536
H(1) = 0.362683783378362
H(2) = 0.313706645877887
H(3) = 0.222381004453374
H(4) = 0.101228536290376
GO TO 10

```

```

3 IF(NGP - 10) 4,,4
ABS(1) = 0.148874338981631
ABS(2) = 0.433395394129247
ABS(3) = 0.679409568299024
ABS(4) = 0.805063366688985
ABS(5) = 0.973906528517172
H(1) = 0.295524224714753
H(2) = 0.269266719309996
H(3) = 0.219086362515982
H(4) = 0.149451349150581
H(5) = 0.066671344308668

```

```

GO TO 10

```

```

C *****
C SIMPSON'S COEFFICIENTS FOR N=5 AND 7
C *****

```

```

4 IF(NGP - 5) 5,,5

```

```

ABS(1) = 0.
ABS(2) = 0.25
ABS(3) = 0.50
ABS(4) = 0.75
ABS(5) = 1.0
H(1) = 1./12.
H(2) = 1./3.
H(3) = 1./6.
H(4) = 1./3.
H(5) = 1./12.

```

```

GO TO 10

```

```

5 IF (NGP - 7)10,,10

```

```

ABS(1) = 0.
ABS(2) = 1./6.
ABS(3) = 1./3.
ABS(4) = 1./2.
ABS(5) = 2./3.
ABS(6) = 5./6.
ABS(7) = 1.0
H(1) = 1./18.
H(2) = 2./9.
H(3) = 1./9.
H(4) = 2./9.
H(5) = 1./9.
H(6) = 2./9.
H(7) = 1./18.

```

```

10 DO 12 I = 1,6

```

```

DO 12 J = 1,6

```

```

12 KE(I,J) = 0.

```

```

IF (NGP.EQ.4.OR.NGP.EQ.6.OR.NGP.EQ.8.OR.NGP.EQ.10)NGP = NGP/2

```

```

DO 20 NPT = 1,NGP

```

```

SD = ABS(NPT)

```

```

T(NPT) = T1 + (SD*(T2-T1))

```

```

CALL SETBD(RNU,L,R1,R2,SD,T(NPT),B,D)

```

```

NR = 4

```

```

NC = 6

```

```

CALL TRANS(NR,NC,B,BT)

```

```

CALL PROD(NC,NR,BT,NR,NR,D,Z)

```

```

CALL PROD(NC,NR,Z,NR,NC,B,ZK)

```

```

DO 25 I = 1,6

```

```

DO 25 J = 1,6

```

```

25 ZK(I,J) = ZK(I,J) *R(R1,R2,SD)*H(NPT)

```

```

DO 26 I = 1,6

```

```

DO 26 J = 1,6

```

```

26 KE(I,J) = KE(I,J) + (ZK(I,J)*L)

```

```

20 CONTINUE

```

```

RETURN

```

```

END

```

```

SUBROUTINE SETBD(RNU,L,R1,R2,SD,T,B,D)
DOUBLE PRECISION B(4,6),D(4,4),L,R1,R2,SD,R,T,RNU,COSQ,SINQ
COSQ = DSQRT(DABS(1.-(((R2-R1)**2)/(L*L))))
SINQ = (R2-R1)/L
IF(U.996.LE.COSQ.AND.COSQ.LE.1.1) COSQ = 1.
IF(DABS(SINQ).LE.D.1) SINQ = 0.
IF(DABS(COSQ).LE.D.1) COSQ = 0.
IF(U.996.LE.SINQ.AND.SINQ.LE.1.1) SINQ = 1.
R = R1 + (SD*(R2-R1))

DO 2 I = 1,4
DO 2 J = 1,6
2 B(I,J) = 0.

B(1,1) = -(COSQ/L)
B(1,2) = -(SINQ/L)
B(1,3) = 0.
B(1,4) = COSQ/L
B(1,5) = SINQ/L
B(1,6) = 0.
B(2,1) = ((1.-SD)*SINQ*COSQ/R) - ((1.-((3.*SD*SD) + (2.*(SD**3))))*SINQ*COSQ/R)
B(2,2) = ((1.-SD)*SINQ*SINQ/R) + ((1.-((3.*SD*SD) + (2.*(SD**3))))*COSQ*COSQ/R)
B(2,3) = L*COSQ*(SD-(2.*SD*SD) + (SD**3))/R
B(2,4) = (SD*SINQ*COSQ/R)-((3.*SD*SD)-(2.*(SD**3)))*SINQ*COSQ/R
B(2,5) = (SD*SINQ*SINQ/R) + ((3.*SD*SD)-(2.*(SD**3)))*COSQ*COSQ/R
B(2,6) = L*COSQ*(-SD*SD + SD**3)/R
B(3,1) = SINQ*(6.-12.*SD)/(L*L)
B(3,2) = COSQ*(-6. + 12.*SD)/(L*L)
B(3,3) = (-4. + 6.*SD)/L
B(3,4) = -SINQ*(6. - 12.*SD)/(L*L)
B(3,5) = COSQ*(6. - 12.*SD)/(L*L)
B(3,6) = (-2. + 6.*SD)/L
B(4,1)=-SINQ*SINQ*(-6.*SD+6.*SD*SD)/(L*R)
B(4,2)=SINQ*COSQ*(-6.*SD+6.*SD*SD)/(L*R)
B(4,3)=SINQ*(1.-4.*SD+3.*SD*SD)/R
B(4,4)=-SINQ*SINQ*(6.*SD-6.*SD*SD)/(L*R)
B(4,5)=SINQ*COSQ*(6.*SD-6.*SD*SD)/(L*R)
B(4,6)=SINQ*(-2.*SD+3.*SD*SD)/R

DO 1 I = 1,4
DO 1 J = 1,4
1 D(I,J) = 0.
D(1,1) = T
D(1,2) = RNU*T
D(2,1) = RNU*T
D(2,2) = T
D(3,3) = (T**3)/12.
D(3,4) = RNU*(T**3)/12.
D(4,3) = RNU*(T**3)/12.
D(4,4) = (T**3)/12.
RETURN
END

```

```

SUBROUTINE LOAD(NELT,GC,L,R1,R2,T,P1,PDA,VEC)
COMMON /BLK1/IX,IY,IZ,IW
DOUBLE PRECISION L(IX),R1(IX),R2(IX),P1(IX),T(IX,2),VEC(IW)
DOUBLE PRECISION SQ,CQ,GC,PDE,PDA(IX)

```

```

*****

```

```

DEFINE COSQ(SQ) = DSQRT(DABS(1.-SQ*SQ))
DEFINE SING(L,R1,R2) = (R2-R1)/L

```

```

DEFINE U1(L,R1,P1,CQ,SQ,PD,GC,T) = 6.283*L*((-R1*P1*SQ/2.) - 0.15*
1((R1*PD*SQ) + (P1*L*SQ*SQ)) - (PD*L*SQ*SQ/15.)) + 6.283*GC*T*L*((R
21/2.) + L*SQ*((CQ*CQ/6.) + (3.*SQ*SQ/20.)))

```

```

DEFINE W1(L,R1,P1,CQ,SQ,PD,GC,T) = 6.283*L*((R1*P1*CQ/2.) + 0.15*(
1(R1*PD*CQ) + (P1*L*SQ*CQ)) + (PD*L*SQ*CQ/15.)) + (6.283*GC*T*L*L*S
2Q*CQ*SQ/60.)

```

```

DEFINE M1(L,R1,P1,SQ,PD,GC,T) = 6.283*L*((R1*P1*L/12.) + 0.0333
1*((R1*PD*L) + (P1*L*L*SQ)) + (PD*L*L*SQ/60.)) + 6.283*GC*T*L*L*(-(R
21*SQ/12.) - (L*SQ*SQ/60.))

```

```

DEFINE U2(L,R1,P1,CQ,SQ,PD,GC,T) = 6.283*L*(-(R1*P1*SQ/2.) - 0.35*
1((R1*PD*SQ) + (P1*L*SQ*SQ)) - (4.*PD*L*SQ*SQ/15.)) + 6.283*GC*T*L*
2((R1/2.) + L*SQ*((CQ*CQ/3.) + (0.35*SQ*SQ)))

```

```

DEFINE W2(L,R1,P1,CQ,SQ,PD,GC,T) = 6.283*L*((R1*P1*CQ/2.) + 0.35*(
2(R1*PD*CQ) + (P1*L*SQ*CQ)) + (4.*PD*L*SQ*CQ/15.)) - (6.283*GC*T*L*
3L*SQ*SQ*CQ/6L.)

```

```

DEFINE M2(L,R1,P1,SQ,PD,GC,T) = 6.283*L*(-(R1*P1*L/12.) - 0.05*
1((R1*PD*L) + (P1*L*L*SQ)) - (PD*L*L*SQ/30.)) + 6.283*GC*T*L*L*((R1
3*SQ/12.) + (L*SQ*SQ/20.))

```

```

*****

```

```

NC = (NELT*3) + 1
NN = (NELT + 1)*3
J = 0

```

```

*****

```

```

DO 2 I = 1,NC,3
IF(J),3,
SQ = SING(L(J),R1(J),R2(J))
CQ = COSQ(SQ)
IF(DABS(CQ).LE.0.1) CQ = 0.
IF(DABS(SQ).LE.0.1) SQ = 0.
IF(0.99.LE.SQ.AND.SQ.LE.1.1) SQ = 1.
IF(0.99.LE.CQ.AND.CQ.LE.1.1) CQ = 1.
PDE = PDA(J)
VEC(I) = VEC(I) + U2(L(J),R1(J),P1(J),CQ,SQ,PDE,GC,T(J,1))
VEC(I+1) = VEC(I+1) + W2(L(J),R1(J),P1(J),CQ,SQ,PDE,GC,T(J,1))
VEC(I+2) = VEC(I+2) + M2(L(J),R1(J),P1(J),SQ,PDE,GC,T(J,1))

IF(J-NELT),2,

```

```
3 SQ = SINQ(L(J+1),R1(J+1),R2(J+1))
  CQ = COSQ(SQ)
  IF(DABS(CQ).LE.0.1) CQ = 0.
  IF(DABS(SQ).LE.0.1) SQ = 0.
  IF(0.99.LE.SQ.AND.SQ.LE.1.1) SQ = 1.
  IF(0.99.LE.CQ.AND.CQ.LE.1.1) CQ = 1.
  PDE = PDA(J+1)
  VEC(I) = VEC(I) +U1(L(J+1),R1(J+1),P1(J+1),CQ,SQ,PDE,GC,T(J+1,1))
  VEC(I+1) = VEC(I+1)
  1+W1(L(J+1),R1(J+1),P1(J+1),CQ,SQ,PDE,GC,T(J+1,1))
  VEC(I+2) = VEC(I+2)
  1+M1(L(J+1),R1(J+1),P1(J+1),SQ,PDE,GC,T(J+1,1))
  J = J + 1
2 CONTINUE

RETURN
END
```

```

SUBROUTINE CLOSEL(ICLOSE,NF,GC,P1,R1,T,A,VEC)
COMMON /BLK1/IX,IY,IZ,IW
COMMON /BLK5/RNU,E
DIMENSION ICLOSE(5),NF(IW)
DOUBLE PRECISION P1(IX),R1(IX),T(IX,2),A(IY),VEC(IW)
DOUBLE PRECISION RNU,E,GC

```

C *****

```

DO 1 I = 1,5
  IF(ICLOSE(I)).EQ.1,
  IC = ICLOSE(I)
  NROW = ICLOSE(I)*3
  NCOEF1 = NF(NROW) - 1
  NCOEF2 = NF(NROW+1) - 1
  A(NCOEF1) = A(NCOEF1) + T(IC,1)*(1.+RNU)
  A(NCOEF2) = A(NCOEF2) + (T(IC,1)**3)*(1.+RNU)/12.

```

C *****

C ****PRESSURE LOAD

C *****

```

  IF(P1(IC).EQ.0.OR.IC.EQ.0) GO TO 2
  VEC(NROW) = VEC(NROW) - (P1(IC)*R1(IC)*R1(IC)/8.)*6.283185*R1(IC)
  VEC(NROW-2) = VEC(NROW-2) - (P1(IC)*R1(IC)/2.)*6.283185*R1(IC)

```

C *****

C ****DEAD LOAD

C *****

```

2 IF(GC.EQ.0..OR.IC.EQ.0) GO TO 1
  P1(IC) = -(GC*T(IC,1))
  VEC(NROW-2) = VEC(NROW-2) - (P1(IC)*R1(IC)/2.)*6.283185*R1(IC)
  VEC(NROW) = VEC(NROW) - (P1(IC)*R1(IC)*R1(IC)/8.)*6.283185*R1(IC)
  P1(IC) = 0.

```

1 CONTINUE

```

RETURN
END

```

```

SUBROUTINE BONCON(NNBC,NBC,NC,NM,NF,UBC,WBC,MBC,A,VEC)
COMMON /BLK1/IX,IY,IZ,IW
COMMON /BLK3/IBON
COMMON /BLK6/NELT,N
DIMENSION NC(IW),NM(IW),NF(IW),NBC(10),UBC(10),WBC(10),MBC(10)
DOUBLE PRECISION A(IY),VEC(IW)

IF(IBON),,7

PRINT 100
100 FORMAT(1H1,37('-'),/,,' ZERO DISPLACEMENT BOUNDARY CONDITIONS',/,
11H ,37('-'),/,,'ONCODE')
DO 10 I = 1,NNBC
10 PRINT 101,NBC(I),UBC(I),WBC(I),MBC(I)
101 FORMAT(1HU,1X,I3,2X,3(A1,3X))

7 DO 1 M = 1,NNBC
K = (NBC(M) - 1)*3 + 1
J = 1
5 I = 0
IF(UBC(M).EQ.'U'.AND.J.EQ.1) I = K
IF(WBC(M).EQ.'W'.AND.J.EQ.2) I = K+1
IF(MBC(M).EQ.'M'.AND.J.EQ.3) I = K+2

IF(I),6,

VEC(I) = 0.
K1 = NF(I)
K2 = NM(I) + NF(I) - 1
DO 4 JJ = K1,K2
4 A(JJ) = 0.
K3 = I + 1
DO 2 JJ = K3,N
IF(NC(JJ).LE.I) GO TO 3
GO TO 2
3 NCC = I - NC(JJ) + NF(JJ)
A(NCC) = 0.
2 CONTINUE

6 J = J + 1
IF(J-3)5,5,

1 CONTINUE
RETURN
END

```

```

1      SUBROUTINE BANDO(N,NC,A,VEC,NM,NF,NR,NWR)
2      COMMON /BLK1/IX,IY,IZ,IW
3      DIMENSION NC(IW),NM(IW),NF(IW),NR(IW),NWR(IW)
4      DOUBLE PRECISION A(IY),VEC(IW),MULT,DIAG
5
6      N1 = N - 1
7
8      C      *****
9      C      FORWARD REDUCTION
10     C      *****
11
12     DO 20 I = 1,N1
13     K = NF(I+1) - 1
14     DIAG = A(K)
15     IF(DIAG),20,
16     NRC = 0
17     L = I + 1
18     DO 22 J = L,N
19     IF(NC(J).LE.I) NRC = NRC + 1
20     IF(NC(J).LE.I) NR(NRC) = NF(J) + I - NC(J)
21     IF(NC(J).LE.I) NWR(NRC) = J
22     CONTINUE
23     DO 30 JJ = 1,NRC
24     KK = NR(JJ)
25     MULT = A(KK)/DIAG
26     K1 = NWR(JJ)
27     VEC(K1) = VEC(K1) - MULT*VEC(I)
28     KB = NRC-JJ + 1
29     DO 40 LL = 1,KB
30     K2 = NR(JJ+LL-1)
31     MM = K2 + NWR(JJ) - I
32     40 A(MM) = A(MM) - MULT*A(K2)
33     30 CONTINUE
34     20 CONTINUE
35
36     C      *****
37     C      REVERSE REDUCTION
38     C      *****
39
40     I = N
41     50 K = NF(I) + NM(I) - 1
42     DIAG = A(K)
43     IF(DIAG),70,
44     NRC = NM(I) - 1
45     DO 60 J = 1,NRC
46     MULT = A(K-J)/A(K)
47     60 VEC(I-J) = VEC(I-J) - MULT*VEC(I)
48     VEC(I) = VEC(I) /DIAG
49     70 I = I - 1
50     IF(I-2),90,50
51
52     VEC(1) = VEC(1)/A(1)
53
54     RETURN
55     END

```

```

SUBROUTINE BANBAC(NC,NM,NF,ND,VEC,BA,BVEC)
COMMON /BLK1/IX,IY,IZ,IW/BLK6/NELT,N/BLK7/NBP
DOUBLE PRECISION BA(IY),BVEC(IW),VEC(IW)
DIMENSION NC(IW),NM(IW),NF(IW),ND(10,4),NS(10),NB(10),NROWS(10)
1 ,NROWB(10)

C *****
C **** STANDARD NODES, LAST NODE, BIGGER NODE OF BRANCH.
C *****

      K = 0
      DO 100 I = 1,N
      BVEC(I) = 0.
      IF(I.EQ.(N-1)) NEX = 1
      IF(I.EQ.(N-2)) NEX = 2
      IF(I.EQ.(N-1).OR.I.EQ.(N-2)) GO TO 77
      IF(NM(I).GT.6) GO TO 70
      GO TO 75
70 NEX = 5
      IF(K.EQ.1) NEX = 4
      IF(K.EQ.2) NEX = 3
      IF(K.EQ.2) K = 0
      K = K + 1
      GO TO 77

75 IF(NM(I).EQ.6.OR.I.EQ.3) NEX = 3
      IF(NM(I).EQ.5.OR.I.EQ.2) NEX = 4
      IF(NM(I).EQ.4.OR.I.EQ.1) NEX = 5

77 NFI = NF(I)
      NCI = NC(I)
      NMI = NM(I)

      DO 10 J = 1,NMI
10 BVEC(I) = BVEC(I) + BA(NFI+J-1)*VEC(NCI+J-1)

      DO 15 J = 1,NEX
      NFIJ = NF(I+J)
      NMIJ = NM(I+J)
15 BVEC(I) = BVEC(I) + BA(NFIJ + NMIJ -1-J)*VEC(NCI + NMI -1 + J)

100 CONTINUE

      IF(NBP),60,

      J = 1
      DO 40 M = 1,10
      IF(ND(M,2))40,40,
      IF(ND(M,2) - ND(M,1)),,45
      NS(J) = ND(M,2)
      NB(J) = ND(M,1)
      GO TO 50
45 NS(J) = ND(M,1)
      NB(J) = ND(M,2)
50 NROWS(J) = (NS(J) - 1)*3 + 1
      NROWB(J) = (NB(J) - 1)*3 + 1

```

```

      J = J + 1
40 CONTINUE

```

```

C *****
C *** AUGMENT SMALLER NODE AT BRANCH
C *****

```

```

      K = 1
      DO 80 I = 1,N
      IF (1 - NROWS(K))80,,80
      NK = NROWB(K)
      DO 90 M = 1,3
      DO 90 MM = 1,3
      NFK = NF(NK + MM - 1)
      NCK = NC(NK + MM - 1)
      NMK = NM(NK + MM - 1)
      BVEC(I+M-1) = BVEC(I+M-1) + BA(NFK+M-1)*VEC(NCK+NMK-1)

```

```

90 CONTINUE
      K = K + 1

```

```

80 CONTINUE
60 RETURN
END

```

```

SUBROUTINE STRESS(NSEC,NODS,NOD1,NOD2,NEL1,NEL2,L,R1,R2,T,VEC)
COMMON /BLK1/IX,IY,IZ,IW
COMMON /BLK2/NPLOT/BLK5/RNU,E /BLK8/ISP
DOUBLE PRECISION SM(4,9),DVEC(9,1),B(4,6),D(4,4),DB(4,6)
DOUBLE PRECISION L(IX),R1(IX),R2(IX),T(IX,2),VEC(IW),STR(4)
DOUBLE PRECISION TL,RNU,E,SD,SIGN,AV,TLN
DIMENSION NODS(IX),NOD1(IZ),NOD2(IZ),NEL1(IZ),NEL2(IZ)

```

```

N1 = 4
N2 = 6
N3 = 9
N4 = 1
TL = 0.

```

C*****

```

DO 100 I = 1,NSEC

NN = NEL2(I) - NEL1(I) + 2
JN = NN - 1
NODS(I) = NOD1(I)
DO 10 JK = 2,JN
10 NODS(JK) = NEL1(I) + JK - 1
NODS(NN) = NOD2(I)
J = NEL1(I)
JL = NEL1(I)

IF(ISP),,13
PRINT 15,I
15 FORMAT(1H0,'SECTION ',I2,'/',I1H ,10('-',))
13 CONTINUE

```

C*****

```

DO 50 K = 1,NN

DO 20 M = 1,4
DO 20 MM = 1,3
20 SM(M,MM) = 0.
DO 21 M = 1,9
21 DVEC(M,1) = 0.
IF(K-1),60,

SD = 1.
CALL SETBD(RNU,L(J-1),R1(J-1),R2(J-1),SD,T(J-1,1),B,D)
CALL PROD(N1,N1,D,N1,N2,B,DB)
DO 55 MM = 1,4
DO 55 JJ = 1,6
55 SM(MM,JJ) = DB(MM,JJ)

IF(K-NN),56,

60 SD = 0.
CALL SETBD(RNU,L(J),R1(J),R2(J),SD,T(J,1),B,D)
CALL PROD(N1,N1,D,N1,N2,B,DB)

```

```

IF(K-1),,65

DO 66 MM = 1,4
DO 66 JJ = 1,6
66 SM(MM,JJ) = DB(MM,JJ)
GO TO 56

65 DO 67 MM = 1,4
DO 67 JJ = 4,9
67 SM(MM,JJ) = SM(MM,JJ) + DB(MM,JJ-3)

56 IF(K-1)40,,40
NROW1 = (NODS(K) - 1)*3 + 1
NROW2 = (NODS(K+1) - 1)*3 + 1
GO TO 49

40 CONTINUE
NROW1 = (NODS(K-1) - 1)*3 + 1
NROW2 = (NODS(K) - 1)*3 + 1
IF(K.NE.NN) NROW3 = (NODS(K+1) - 1)*3 + 1

49 DO 42 M = 1,3
DVEC(M,1) = VEC(NROW1 + M - 1)
DVEC(M+3,1) = VEC(NROW2 + M - 1)
IF(K.EQ.1.OR.K.EQ.NN) GO TO 42
DVEC(M+6,1) = VEC(NROW3 + M - 1)
42 CONTINUE

CALL PROD(N1,N3,SM,N3,N4,DVEC,STR)

AV = 2.
IF(K.EQ.1.OR.K.EQ.NN) AV = 1.
SIGN = 1.
DO 30 M = 1,4
IF(M.EQ.3.OR.M.EQ.4) SIGN = -1.
30 STR(M) = (STR(M)*E*SIGN)/((1. - RNU*RNU)*AV)

```

```

C *****
C SIGMA STRESSES FROM STRESS RESULTANTS
C *****

```

```

IF(K-1) 31,,31
DO 32 M = 1,2
32 STR(M) = STR(M)/T(J,1)
GO TO 33
31 IF(K-NN)34,,34
DO 35 M = 1,2
35 STR(M) = STR(M)/T(J-1,2)
GO TO 33
34 DO 36 M = 1,2
36 STR(M) = STR(M)/((T(J,1) + T(J-1,2))/2.)
33 CONTINUE

IF(ISP),,70

```

```
      PRINT 80,NCDS(K),TL,(STR(M),M = 1,4)
80  FORMAT(1H ,I3,5X,F6.3,5X,4(E10.4,3X))

70  WRITE(NPLOT,81) TL,(STR(M),M = 1,4)
81  FORMAT(F6.3,2X,4(E10.4,2X))
      TLN = TL
      TL = TL + L(JL+K-1)
      J = J + 1

50  CONTINUE

      TL = TLN

100 CONTINUE

      RETURN
      END
```

```

C      $$$$$$$$$$$$$$$$$$$$$$$$$$$$$$$$$$$$$$$$$$$$$
C      **STRESSPLOT PLOTTER PROGRAM**
C      $$$$$$$$$$$$$$$$$$$$$$$$$$$$$$$$$$$$$$$$$$$$$

      DATA LCDUM/'      '/
      DIMENSION XT(3,500),YT(3,500),X(500),Y(500),XX(3,500),YY(3,500),
1RANGE(3),UPP(3),LCT(3),LC(3),FOR(20),NN(3)
      DIMENSION LOW(5),SCAL(10)
      DIMENSION BUFF(2000)

C  -----
C  **** PLOT IDENTIFICATION
C  -----

      CALL PLGTS(BUFF,2000,17)
      CALL SYMBCL(0.,0.,0.26,4HGRAF,0.0,4)
      CALL PLOT(1.2,0.,3)
      CALL PLOT(1.2,0.3,2)
      CALL PLOT(-0.1,0.3,2)
      CALL PLOT(-0.1,0.,2)
      CALL PLOT(1.2,0.0,2)

C  -----
C  **** READ IN MAIN DATA
C  -----

      READ(8,1) PLTS,NLC,SIZE
1  FORMAT(A6,2X,11,2X,A1)

C  -----
C  PLOT SCALE DOWN
C  -----

      CALL PLOT(0.,4.0,-3)
      IF(SIZE.EQ.'S') CALL FACTOR(0.45)
      IF(SIZE.EQ.'H') CALL FACTOR(0.625)
      IF(SIZE.EQ.'F') CALL FACTOR(0.750)

C  -----
C  -----

      DO 20 NST = 1,4

      NSP = 38
      IF(NST.EQ.1) NSP = 26
      IF(NST.EQ.2) NSP = 2
      IF(NST.EQ.3) NSP = 14
      XR = 3.0
      YR = 4.0
      IF(NST.EQ.2) XR = 0.
      IF(NST.EQ.2) YR = 11.
      IF(NST.EQ.3) YR = 0.
      IF(NST.EQ.4) XR = 0.
      IF(NST.EQ.4) YR = -11.

```

```

C -----
C **** READ IN ALL DATA RELEVANT TO ONE STRESS
C -----

```

```

4 FORMAT(' (F6.3, ', I2, 'X, E10.4) ')
ENCODE(4, FOR) NSP
DO 50 J = 1, NLC
  READ(8, 2) TYPE, NELT, LC(J)
2 FORMAT(A5, 2X, I3, 2X, A5)
  NN(J) = NELT
  NJ = NN(J)
  READ(8, FOR) (XT(J, I), YT(J, I), I = 1, NJ)

```

```

C -----
C **** FIND WHICH DATA HAS THE MAXIMUM RANGE
C -----

```

```

DO 51 K = 1, NJ
51 Y(K) = YT(J, K)
  CALL SCALE(Y, 8.0, NJ, +1)
  LOW(J) = Y(NJ + 1)
  UPP(J) = Y(NJ+1) + 8.0*Y(NJ+2)
50 RANGE(J) = ABS(Y(NJ+1) - UPP(J))

```

```

L = 0
DO 57 M = 1, NLC
  SCAL(L + M) = LOW(M)
  SCAL(L + M + 1) = UPP(M)
57 L = L + 1

```

```

UB = RANGE(1)
NLCM1 = NLC - 1
DO 52 J = 1, NLCM1
  IF(RANGE(J+1).GT.UB) JMAX = J + 1
  IF(RANGE(J+1).GT.UB) UB = RANGE(J+1)
52 CONTINUE

```

```

C -----
C **** REARRANGE DATA SO THAT MAX RANGE DATA IS PLOTTED FIRST
C -----

```

```

DO 53 J = 1, NLC
  IF(JMAX-J)54,,54
  NNJMAX = NN(JMAX)
  DO 55 L = 1, NNJMAX
  YY(1, L) = YT(JMAX, L)
55 XX(1, L) = XT(JMAX, L)
  LCT(1) = LC(JMAX)
  NN(1) = NN(JMAX)
  GO TO 53
54 K = J
  IF(J.LT.JMAX) K = J+1
  NJ = NN(J)
  DO 56 L = 1, NJ
  YY(K, L) = YT(J, L)
56 XX(K, L) = XT(J, L)
  LCT(K) = LC(J)

```

```

NN(K) = NN(J)
53 CONTINUE

```

```

C -----
C **** PLOT ALL CURVES FOR ONE STRESS
C -----

```

```

DO 30 NLOAD = 1,NLC
IF(LCT(NLOAD).EQ.LC(1)) MARK = 11
IF(LCT(NLOAD).EQ.LC(2)) MARK = 5
IF(LCT(NLOAD).EQ.LC(3)) MARK = 0
N = NN(NLOAD)
DO 35 I = 1,N
X(I) = XX(NLOAD,I)
35 Y(I) = YY(NLOAD,I)
IF(NST-1) 10,10
IF(SIZE.EQ.'S') XL = 12.
IF(SIZE.EQ.'H') XL = 10.
IF(SIZE.EQ.'F') XL = 13.

LTYPE = N/IFIX(XL)
10 IF(NST.EQ.3) XR = XL + 1.5
IF(NLOAD-1),21,
X(N+1) = SX1
X(N+2) = SX2
Y(N+1) = SY1
Y(N+2) = SY2
GO TO 22
21 CALL PLOT(XR,YR,-3)
CALL SCALE(X,XL,N,+1)
NLC2 = 2*NLC
CALL SCALE(SCAL,8.0,NLC2,+1)
Y(N+1) = SCAL(NLC2+1)
Y(N+2) = SCAL(NLC2+2)
YOR = 0.
XOR = 0.
IF(Y(N+1).LT.0.) YOR = -Y(N+1)/Y(N+2)
IF(X(N+1).LT.0.) XOR = -X(N+1)/X(N+2)
IF(NST.EQ.1) CALL AXIS(XOR,0.,24HMERIDIONAL MOMENT (NM/M),+24,8.0,
190.,Y(N+1),Y(N+2))
IF(NST.EQ.2) CALL AXIS(XOR,0.,22HAXIAL STRESS (N/SQ. M),+22,8.0,
190.,Y(N+1),Y(N+2))
IF(NST.EQ.3) CALL AXIS(XOR,0.,21HHOOP STRESS (N/SQ. M),+21,8.0,
190.,Y(N+1),Y(N+2))
IF(NST.EQ.4) CALL AXIS(XOR,0.,18HHOOP MOMENT (NM/M),+18,8.0,
190.,Y(N+1),Y(N+2))
CALL AXIS(0.,YOR,14HAXIAL DISTANCE,-14,XL,0.,X(N+1),X(N+2))
22 CALL LINE(X,Y,N,1,LTYPE,MARK)
SX1 = X(N+1)
SX2 = X(N+2)
SY1 = Y(N+1)
SY2 = Y(N+2)
30 CONTINUE
20 CONTINUE

```

```

C -----
C **** PLOT HEADING BOX

```

```

C -----
XP = XL - 6.
YP = -0.5
CALL PLOT(XP,YP,-3)
CALL PLOT(7.0,0.,2)
CALL SYMBOL(1.0,-0.31,0.21,23HUNIVERSITY OF CAPE TOWN,0.,23)
CALL SYMBOL(0.25,-0.62,0.21,31HDEPARTMENT OF CIVIL ENGINEERING,0.,
131)
CALL PLOT(0.,-0.72,3)
CALL PLOT(7.0,-.72,2)
CALL SYMBOL(0.25,-1.10,0.28,23HFINITE ELEMENT ANALYSIS,0.,23)
CALL SYMBOL(3.4,-1.43,0.28,2HCF,0.,2)
CALL SYMBOL(1.0,-1.86,0.28,18HAXISYMMETRIC SHELL,0.,18)
CALL PLOT(0.,-1.96,3)
CALL PLOT(7.0,-1.96,2)
CALL SYMBOL(0.2,-2.20,0.14,10HANALYSIS: ,0.,10)
CALL SYMBOL(999.,999.,0.14,TYPE,0.,6)
CALL PLOT(3.0,-1.96,3)
CALL PLOT(3.0,-2.3,2)
CALL SYMBOL(3.25,-2.20,0.14,13HPLOT SERIES: ,0.,13)
CALL SYMBOL(999.,999.,0.14,PLTS ,0.,0)
CALL PLOT(0.,-2.30,3)
CALL PLOT(7.0,-2.30,2)
CALL SYMBOL(0.2,-2.54,0.14,23HHORIZONTAL AXIS: METERS, 0.,23)
CALL SYMBOL(5.0,-2.54,0.14,5HDATE:,0.,5)
CALL SYMBOL(0.2,-2.73,0.14,30HVERTICAL AXIS: NEWTONS, METERS,0.,
130)
CALL PLOT(4.90,-2.30,3)
CALL PLOT(4.90,-2.68,2)
CALL PLOT(0.,-2.68,3)
CALL PLOT(7.0,-2.68,2)
CALL SYMBOL(0.2,-3.12,0.14,32HANALYSIS AND PLOT BY T.B.GRIFFIN,0.,
132)
CALL SYMBOL(0.2,-3.40,0.14,19HPROGRAM: STRESSPLOT,0.,20)

CALL PLOT(0.,0.,3)
CALL PLOT(0.,-3.5,2)
CALL PLOT(7.0,-3.5,-3)
XP = (2.*XL) + 4.
YP = 24.
CALL PLOT(-XP,0.,2)
CALL PLOT(-XP,YP,2)
CALL PLOT(0.,YP,2)
CALL PLOT(0.,0.,2)

```

```

C -----
C **** WRITE OUT THE LOAD CASE DATA
C -----

```

```

LC1 = LC(1)
LC2 = LC(2)
LC3 = LC(3)
LC4 = LCDUM
IF(LC(2).EQ.0) LC2 = LCDUM
IF(LC(3).EQ.0) LC3 = LCDUM
XLC = -XL + 6.

```

```
CALL PLOT(XLC,12.5,-3)

CALL SYMBOL(-8.3,0.3,0.2,12,0.,-1)
CALL SYMBOL(-7.85,0.2,0.14,LC4,0.,6)
CALL PLOT(-7.0,0.44,3)
CALL PLOT(-8.5,0.44,2)
CALL SYMBOL(-8.3,0.64,0.2,0,0.,-1)
CALL SYMBOL(-7.85,0.54,0.14,LC3,0.,6)
CALL PLOT(-7.0,0.78,3)
CALL PLOT(-8.5,0.78,2)
CALL SYMBOL(-8.3,0.98,0.2,5,0.,-1)
CALL SYMBOL(-7.85,0.88,0.14,LC2,0.,6)
CALL PLOT(-7.0,1.12,3)
CALL PLOT(-8.5,1.12,2)
CALL SYMBOL(-8.3,1.32,0.20,11,0.,-1)
CALL SYMBOL(-7.85,1.22,0.14,LC1,0.,6)
CALL PLOT(-7.0,1.46,3)
CALL PLOT(-8.5,1.46,2)
CALL SYMBOL(-8.3,1.56,0.14,9HLOAD CASE,0.,9)
CALL PLOT(-7.0,1.87,3)
CALL PLOT(-8.5,1.87,2)
CALL PLOT(-8.5,0.,2)
CALL PLOT(-8.0,1.46,3)
CALL PLOT(-8.0,0.,2)
CALL PLOT(-7.0,0.,3)
CALL PLOT(-8.0,0.,3)
CALL PLOT(-7.0,0.,2)
CALL PLOT(-7.0,1.87,2)

CALL PLOT(8.,0.,999)
STOP
END
```

APPENDIX B

Integration of Eq. (2.10b) for the Stress Resultant N_{θ}^*

$$N_{\theta}^* = \int_{-t/2}^{t/2} \sigma_{\theta}^* dz$$

Substituting for σ_{θ}^* from Eqs. (2.6) and (2.7),

$$\begin{aligned} N_{\theta}^* &= D \int_{-t/2}^{t/2} \left\{ \frac{u \sin \phi + w \cos \phi - zw' \sin \phi}{r + z \cos \phi} + \nu \frac{du}{ds} - \nu z \frac{d^2 w}{ds^2} \right\} dz \\ &= D \int_{-t/2}^{t/2} \left\{ \frac{u \tan \phi}{\frac{r}{\cos \phi} + z} + \frac{w}{\frac{r}{\cos \phi} + z} - w' \tan \phi + \frac{rw' \frac{\tan \phi}{\cos \phi}}{\frac{r}{\cos \phi} + z} \right. \\ &\quad \left. + \nu \frac{du}{ds} - \nu z \frac{d^2 w}{ds^2} \right\} dz \\ &= D \left[u \tan \phi \log \left(\frac{r}{\cos \phi} + z \right) + w \log \left(\frac{r}{\cos \phi} + z \right) - w' z \tan \phi \right. \\ &\quad \left. + rw' \frac{\sin \phi}{\cos^2 \phi} \log \left(\frac{r}{\cos \phi} + z \right) + \nu z \frac{du}{ds} - \nu \frac{z^2}{2} \frac{d^2 w}{ds^2} \right]_{-t/2}^{t/2} \quad (B-1) \end{aligned}$$

To begin with we will consider the log function alone:

$$\begin{aligned} \left[\log \left(\frac{r}{\cos \phi} + z \right) \right]_{-t/2}^{t/2} &= \log \left(\frac{r}{\cos \phi} + \frac{t}{2} \right) - \log \left(\frac{r}{\cos \phi} - \frac{t}{2} \right) \\ &= \log \frac{\left(1 + \frac{t \cos \phi}{2r} \right)}{\left(1 - \frac{t \cos \phi}{2r} \right)} \end{aligned}$$

Expanding the log functions in Taylor's series we have,

$$\begin{aligned} \log \left(1 + \frac{t \cos \phi}{2r} \right) &= \frac{t \cos \phi}{2r} - \frac{t^2 \cos^2 \phi}{8r^2} + \frac{t^3 \cos^3 \phi}{24r^3} - \dots \\ \log \left(1 - \frac{t \cos \phi}{2r} \right) &= -\frac{t \cos \phi}{2r} - \frac{t^2 \cos^2 \phi}{8r^2} - \frac{t^3 \cos^3 \phi}{24r^3} - \dots \end{aligned}$$

Subtracting the second series from the first, and neglecting terms of order higher than cubic gives,

$$\log \frac{\left(1 + \frac{t \cos \phi}{2r}\right)}{\left(1 - \frac{t \cos \phi}{2r}\right)} = \left(\frac{t \cos \phi}{r} + \frac{t^3 \cos^3 \phi}{12r^3}\right)$$

Making use of this result in equation (B-1) and simplifying, we have,

$$N_{\theta}^* = D\left[\frac{u \sin \phi + w \cos \phi}{r} + v \frac{du}{ds}\right] + K\left[\frac{\cos^2 \phi}{r^3}(u \sin \phi + w \cos \phi + rw' \sin \phi)\right]$$

APPENDIX C

Notes on the Principle of Minimum Total Potential Energy

Statement of the Principle: Proof of the Principle is adequately covered in the texts^[5,6], and it is sufficient for the present purpose to state it as follows:

Of all the admissible displacement functions, the actual displacements make the total potential energy a minimum.

The elastic strain energy density: In physical terms the elastic strain energy density \bar{U} is the area under the stress-strain curve for a particular material (Fig. C-1).

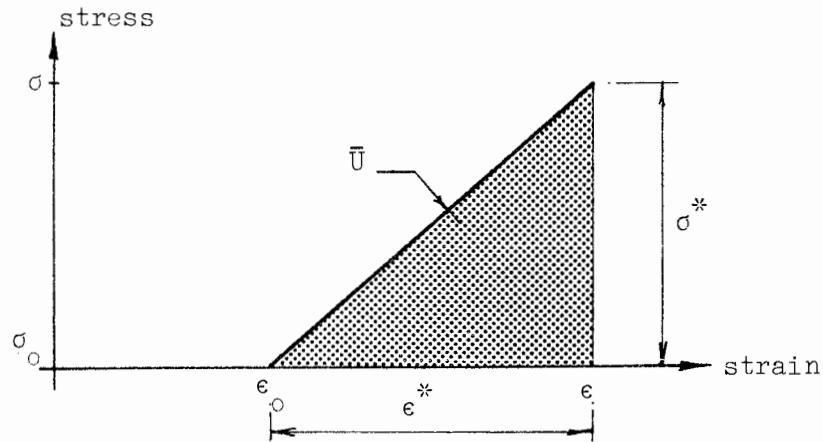


Fig. C-1

Let ϵ = actual (total) strain,
and ϵ_0 = initial strain
so that $(\epsilon - \epsilon_0)$ = strain due to applied loads.

Then for a linear elastic material having an elastic constant D ,

$$\begin{aligned}\sigma^* &= D(\epsilon - \epsilon_0) \\ &= D\epsilon^*\end{aligned}\tag{C-1}$$

The elastic strain energy density can now be written as^{*},

$$\bar{U} = \int_{\epsilon_0}^{\epsilon} \sigma^* d\epsilon = \int_{\epsilon_0}^{\epsilon} D\epsilon d\epsilon - \int_{\epsilon_0}^{\epsilon} D\epsilon_0 d\epsilon\tag{C-2}$$

^{*}See Reference [7], Section 3, Eq. (17).

$$\begin{aligned} \text{Let } \epsilon &= \epsilon_0 + \lambda(\epsilon - \epsilon_0) \\ \text{and } d\epsilon &= (\epsilon - \epsilon_0) d\lambda \\ \text{where } \lambda &\text{ is some constant.} \end{aligned} \tag{C-3}$$

Substituting for ϵ in Eq. (C-2) the strain energy density can be written as,

$$\begin{aligned} \bar{U} &= \int_0^1 D [\epsilon_0 + \lambda(\epsilon - \epsilon_0)](\epsilon - \epsilon_0) d\lambda - \int_0^1 D \epsilon_0 (\epsilon - \epsilon_0) d\lambda \\ &= \frac{1}{2} \epsilon^t D \epsilon - \epsilon^t D \epsilon_0 + \frac{1}{2} \epsilon_0^t D \epsilon_0 \end{aligned} \tag{C-4}$$

In performing the integration of Eq. (C-4) the quantities concerned have been assumed to be matrices and vectors.

The first variation of an energy functional: A necessary condition for a functional to attain a stationary value is that the first variation of the functional vanishes identically.* The procedure in taking the first variation of a functional is illustrated here for the elastic strain energy, Eq. 3.12,

$$U_e = \frac{1}{2} \int_V \{q_e\}^t [B]^t [D] [B] \{q_e\} dV \tag{C-5}$$

If we let $[B]^t [D] [B] = [H]$, Eq. (C-5) may be written more concisely as,

$$U_e = \frac{1}{2} \int_V \{q_e\} [H] \{q_e\} dV \tag{C-6}$$

The partial derivative of U_e with respect to the displacements $\{q_e\}$ is,

$$\frac{\partial U_e}{\partial \{q_e\}} = \int_V [H] \{q_e\} dV \tag{C-7}$$

Hence, the first variation of the elastic strain energy is,

$$\delta U_e = \frac{\partial U_e}{\partial \{q_e\}} \cdot \delta \{q_e\} \tag{C-8}$$

$$= \left[\int_V [H] \{q_e\} dV \right] \delta \{q_e\} \tag{C-9}$$

The conditions under which U_e will attain a stationary value are given by taking

$$\delta U_e = 0$$

*The conditions under which a functional attains a stationary value is the fundamental problem of the calculus of variations. See Courant and Hilbert [8], p 164.

Since the variation of displacement $\delta \{q_e\}$ is arbitrary, this condition is satisfied only if the expression within the square brackets of Eq. (C-9) vanishes identically. The vanishing of this expression then provides us with a set of equations; if the total potential energy has been minimised they will be stiffness equations.

APPENDIX D

Numerical Integration Techniques

The two most common methods of numerical integration are Gauss quadrature and Newton-Cotes quadrature, the latter method embodying the elementary trapezoidal and Simpson's rules. The following is a brief summary of each method.*

Suppose we are required to evaluate the integral

$$I = \int_a^b f(x) dx \quad (D-1)$$

This integral may be written in the general form,

$$I = \sum_{j=1}^n H_j f(a_j) + E \quad (D-2)$$

where a_j are called the 'abscissae' and H_j the corresponding 'weights'. E is the error involved in the numerical approximation.

The Newton-Cotes quadrature formulae: In this method the abscissae, of which there are $n + 1$, are constrained to be equally spaced. If we further restrict the discussion to closed formulae (where the end points of the interval $[a, b]$ are abscissae), then equation (D-2) becomes,

$$I = \sum_{j=0}^n H_j f(a + h_j) + E \quad (D-3)$$

where $h = \frac{b - a}{n}$.

With the abscissae already chosen, we are left with $(n + 1)$ unknown values of H_j to find. We can expect then to make the integral I exact for polynomials of degree n or less; in fact when n is even, we get exact results for polynomials of degree $(n + 1)$ or less.

The actual values of H_j for a given value of n are found from Lagrangian interpolation formulae. For $n = 1$ we have the trapezoidal rule, which is exact for first-order polynomials. For $n = 2$ we have Simpson's rule which is, contrary to expectation, exact for third-order polynomials. [10]

*Reference [9], p 85.

Simpson's rule for the closed interval $[a,b]$ (Fig. D-1) is given by,

$$I = \frac{d_0}{3} [f(a) + 4f(0) + f(b)] \quad (D-4)$$

where $d_0 = \frac{(b-a)}{2}$

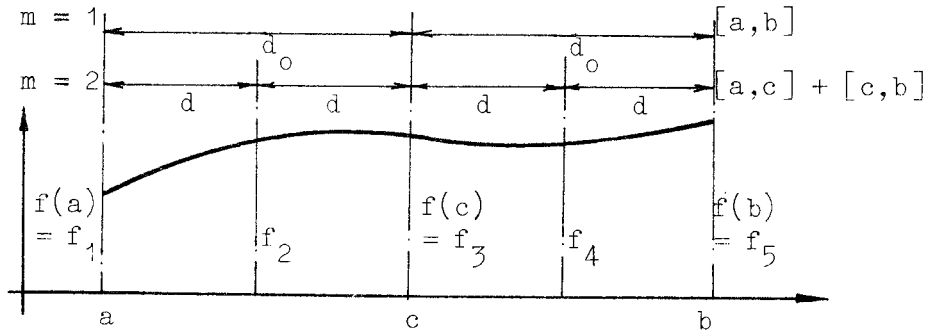


Fig. D-1

The accuracy of the formulae may however be improved by subdividing the original interval and applying the rule to each of the sub-intervals. By summing the results for each sub-interval a more accurate overall result is obtained. Such a procedure results in a composite quadrature formula. In general, if the interval $[a,b]$ is subdivided into m sub-intervals (m even) and each sub-interval has length $2d$, then Simpson's rule may be written as,

$$I = \frac{d}{3} [f_1 + 4f_2 + 2f_3 + 4f_4 + \dots + f_{2m+1}] \quad (D-5)$$

The Gaussian quadrature formulae: In deriving the Gaussian formulae no constraints are imposed on the abscissae or the weights, with the result that we have $2n$ unknown constants a_j and H_j to solve for. When the abscissae are chosen as the zeros of the Legendre polynomial of degree n , then the error term E in Eq. (D-2) is zero if $f(x)$ is a polynomial of degree $(2n - 1)$ or less.

To find the values of the constants a_j and H_j for a general closed interval $[a,b]$ involves the solution of higher order simultaneous equations in a and b . Most texts simplify the problem by giving values of a_j and H_j only for integration over the interval $[-1,1]$. However, the lack of a general formula incorporating arbitrary end points a and b makes it impossible to derive composite formulae involving further sub-intervals of $[a,b]$. The derivation of the necessary general formula was considered to be beyond the scope of the present work.

We are thus limited essentially to integration over the interval $[-1,1]$, using the same number of abscissae as the order n of the particular Gaussian formula being used. For example, the formula for $n = 4$ is, (Fig. D-2),

$$\int_{-1}^1 f(x) dx = 0,347[f(0,861) + f(-0,861)] + 0,652[f(0,339) + f(-0,339)] \quad (\text{D-6})$$

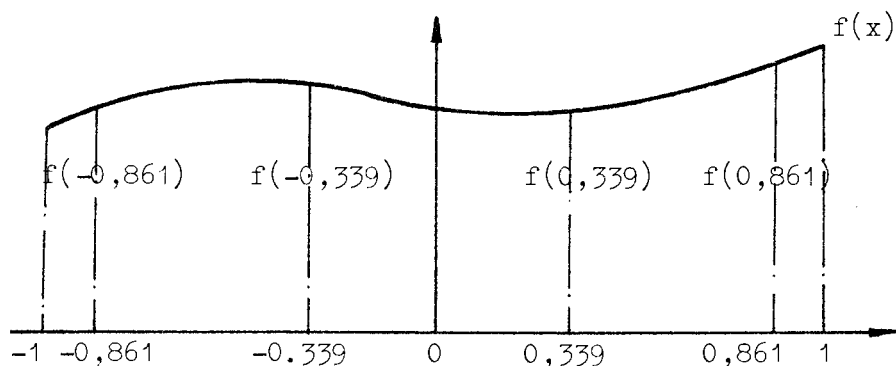


Fig. D-2

However, for intervals having arbitrary end points we can always make a suitable substitution whereby the integral over the original interval is converted to an equivalent integral over the interval $[-1, 1]$. For example, the integral

$$I = \int_1^3 x dx$$

is equivalent to the integral

$$I' = \int_{-1}^1 (y + 2) dy$$

when the substitution $x = y + 2$ is made. Such a procedure is, however, only practical in the case of reasonably simple integrals.

Alternatively, in the case of integration over the interval $[0,1]$ or $[-1,0]$ we can make use of the symmetry of the even Gaussian formulae in the following manner. For $n = 4$ the formula for the interval $[0,1]$ is,

$$\int_0^1 f(x) dx = 0,347 \times f(0,861) + 0,652 \times f(0,339) \quad (\text{D-7})$$

i.e., the terms in Eq. (D-6) corresponding to the abscissae within the interval $[0,1]$. Similar half-interval formulae can be written for $n = 6, 8$ and 10 . The actual values of the abscissae and weights for these formulae are given in the description of subroutine GELSTF in Appendix A.

APPENDIX E

Explicit Expressions for the Equivalent Nodal Surface and Body Forces

The derivation of the element load vector has been discussed in Section 3.1.3, where the interpretation of the equivalent nodal loads and their sign convention has been given. The following expression may be used directly to calculate the equivalent nodal loads for the types of loading mentioned.

The equivalent nodal surface forces: The integration of Eq. (3.22) yields the following expressions for the equivalent nodal surface forces:

$$U_1 = 2\pi L \left[\frac{-r_1 p_1 \sin \phi}{2} - \frac{3}{20}(r_1 p' \sin \phi + p_1 L \sin^2 \phi) - \frac{p' L \sin^2 \phi}{15} \right] \quad (E-1a)$$

$$W_1 = 2\pi L \left[\frac{r_1 p_1 \cos \phi}{2} + \frac{3}{20}(r_1 p' \cos \phi + p_1 L \sin \phi \cos \phi) + \frac{p' L \sin \phi \cos \phi}{15} \right] \quad (E-1b)$$

$$M_1 = 2\pi L \left[\frac{r_1 p_1 L}{12} + \frac{1}{30}(r_1 p' L + p_1 L^2 \sin \phi) + \frac{p' L^2 \sin \phi}{60} \right] \quad (E-1c)$$

$$U_2 = 2\pi L \left[\frac{-r_1 p_1 \sin \phi}{2} - \frac{7}{20}(r_1 p' \sin \phi + p_1 L \sin^2 \phi) - \frac{4p' L \sin^2 \phi}{15} \right] \quad (E-2a)$$

$$W_2 = 2\pi L \left[\frac{r_1 p_1 \cos \phi}{2} + \frac{7}{20}(r_1 p' \cos \phi + p_1 L \sin \phi \cos \phi) + \frac{4p' L \sin \phi \cos \phi}{15} \right] \quad (E-2b)$$

$$M_2 = 2\pi L \left[\frac{-r_1 p_1 L}{12} - \frac{1}{20}(r_1 p' L + p_1 L^2 \sin \phi) - \frac{p' L^2 \sin \phi}{30} \right] \quad (E-2c)$$

The equivalent nodal body forces: The integration of Eq. (3.24) yields the following expressions for the equivalent nodal body forces:

$$U_1 = 2\pi t L \gamma \left[\frac{r_1}{2} + L \sin \phi \left(\frac{\cos^2 \phi}{6} + \frac{3 \sin^2 \phi}{20} \right) \right] \quad (E-3a)$$

$$W_1 = 2\pi t L \gamma \left[\frac{L \sin^2 \phi \cos \phi}{60} \right] \quad (E-3b)$$

$$M_1 = 2\pi t L^2 \gamma \left[\frac{-r_1 \sin \phi}{12} - \frac{L \sin^2 \phi}{30} \right] \quad (\text{E-3c})$$

$$U_2 = 2\pi t L \gamma \left[\frac{r_1}{2} + L \sin \phi \left(\frac{\cos^2 \phi}{3} + \frac{7 \sin^2 \phi}{20} \right) \right] \quad (\text{E-4a})$$

$$W_2 = 2\pi t L \gamma \left[\frac{-L \sin^2 \phi \cos \phi}{60} \right] \quad (\text{E-4b})$$

$$M_2 = 2\pi t L^2 \gamma \left[\frac{r_1 \sin \phi}{12} + \frac{L \sin^2 \phi}{20} \right] \quad (\text{E-4c})$$

APPENDIX F

Circular Plate Theory

The circular plate is clearly a special case of the conical frustrum when $\phi = 90^\circ$ (Fig. 2.1). As such the strain-displacement and curvature-displacement relationships for a circular plate* can be obtained directly from Eqs. (2.14) by substituting $\sin \phi = 1$ and $\cos \phi = 0$.

Of specific interest here are the differential equations of equilibrium for a circular plate in pure bending, and in a state of plane stress. The solutions of these equations will be used to derive the bending and in-plane stiffnesses of a circular plate.

The bending stiffness of a circular plate: Consider a circular plate of radius a subject to a uniformly distributed moment M per unit of circumference (Fig. F-1).

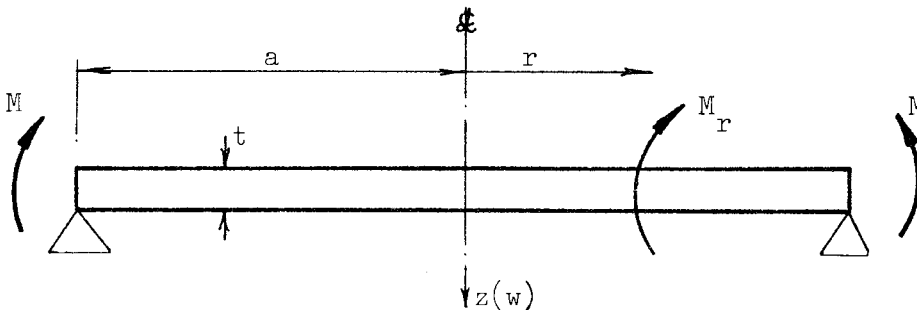


Fig. F-1

When there is no distributed loading on the plate the governing differential equation of equilibrium is,**

$$\frac{d}{dr} \left[\frac{1}{r} \frac{d}{dr} \left(r \frac{dw}{dr} \right) \right] = 0 \quad (F-1)$$

Integrating this equation three times we obtain,

$$\frac{1}{r} \frac{d}{dr} \left(r \frac{dw}{dr} \right) = C_1 \quad (a)$$

$$\frac{dw}{dr} = C_1 \frac{r}{2} + \frac{C_2}{r} \quad (b)$$

$$w = C_1 \frac{r^2}{4} + C_2 \log \left(\frac{r}{a} \right) + C_3 \quad (c)$$

* The expressions for the in-plane strains in a circular plate are given by Timoshenko and Goodier [2], p 76, and those for the curvatures by Timoshenko and Woinowsky-Krieger [3], p 51.

** Timoshenko and Woinowsky-Krieger [3], p 53.

Differentiating Eq. (b) with respect to r we have

$$\frac{d^2 w}{dr^2} = \frac{C_1}{2} - \frac{C_2}{r^2} \quad (d)$$

The expression for the meridional moment M_r is then,

$$\begin{aligned} M_r &= \frac{-Et^3}{12(1-\nu^2)} \left[\frac{d^2 w}{dr^2} + \frac{\nu}{r} \frac{dw}{dr} \right] \\ &= \frac{-Et^3}{12(1-\nu^2)} \left[\left(\frac{C_1}{2} - \frac{C_2}{r^2} \right) + \frac{\nu}{r} \left(\frac{C_1 r}{2} + \frac{C_2}{r} \right) \right] \end{aligned} \quad (e)$$

The three arbitrary constants C_1 , C_2 and C_3 are found by applying the following boundary conditions:

$$\text{at } r = 0, \quad \frac{dw}{dr} = 0$$

$$\text{at } r = a, \quad M_r = M$$

$$\text{at } r = a, \quad w = 0.$$

Solving for the arbitrary constants, and substituting back into equations (b) and (c) we find the following expressions for the displacement w and slope θ :

$$w = \frac{M}{2D(1+\nu)} (a^2 - r^2) \quad (F-2)$$

$$\theta = \frac{dw}{dr} = -\frac{Mr}{D(1+\nu)} \quad (F-3)$$

$$\text{where } D = \frac{Et^3}{12(1-\nu^2)}$$

If we let M^* be the total moment at the edge $r = a$, such that

$$M^* = 2\pi r M$$

then the bending stiffness of the plate at this edge is,

$$\begin{aligned} k_b &= \frac{M^*}{\theta} \\ &= 2\pi D (1+\nu) \\ &= \frac{2\pi Et^3}{12(1-\nu)} \end{aligned} \quad (F-4)$$

The radial stiffness of a circular plate: Consider a circular plate of radius a subject to a uniform axial force P per unit of the circumference (Fig. F-2).

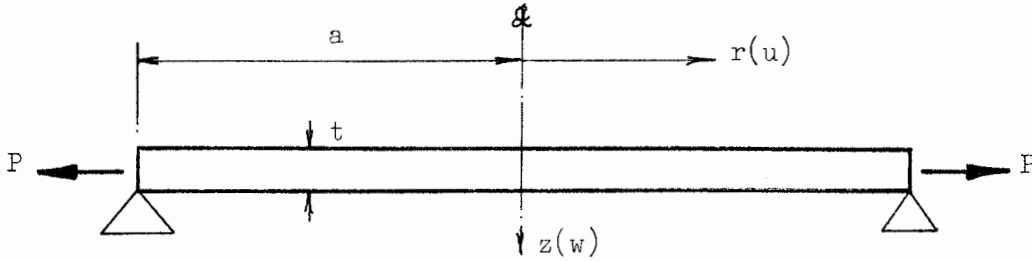


Fig. F-2

The plate is in a state of plane stress for which two equations of equilibrium may be written.* If we neglect shear stresses and body forces, the equation for equilibrium in the radial direction is,

$$\frac{\partial \sigma_r}{\partial r} + \frac{\sigma_r - \sigma_\theta}{r} = 0 \quad (\text{F-5})$$

Substituting for σ_r and σ_θ in Eq. (F-5),

$$\sigma_r = \frac{E}{1 - \nu^2} \left[\frac{du}{dr} + \nu \frac{u}{r} \right] \quad (\text{F-6})$$

$$\text{and } \sigma_\theta = \frac{E}{1 - \nu^2} \left[\frac{u}{r} + \nu \frac{du}{dr} \right]$$

and differentiating with respect to r , Eq. (F-5) can be written in the form,

$$\frac{d^2 u}{dr^2} + \frac{1}{r} \frac{du}{dr} - \frac{1}{r^2} u = 0 \quad (\text{F-7})$$

The second equation for equilibrium in the tangential direction is trivial when the shear stresses are neglected.

Integrating Eq. (F-7) twice with respect to r we obtain,

$$\frac{du}{dr} + \frac{u}{r} = C_1 \quad (\text{a})$$

$$\text{and } ur = C_1 \frac{r^2}{2} + C_2 \quad (\text{b})$$

The constants C_1 and C_2 are found by applying the following boundary

*See Timoshenko and Goodier [2], p 66, Eqs. (37).

conditions:

$$\text{at } r = 0, \quad u = 0$$

$$\text{at } r = a, \quad \sigma_r t = P$$

Solving for C_1 and C_2 and substituting back into Eq. (b) we have,

$$u = \frac{Pr(1-\nu)}{Et} \quad (\text{F-8})$$

If we let P^* be the total axial force at the edge $r = a$, such that

$$P^* = 2\pi a P$$

then the axial stiffness of the plate at this edge is,

$$\begin{aligned} k_a &= \frac{P^*}{u} \\ &= \frac{2\pi Et}{1-\nu} \end{aligned} \quad (\text{F-9})$$

Fixed-end moments and forces for a circular plate under a U.D.L.: Consider a circular plate of radius a , clamped at the outer edge and carrying a U.D.L. p (Fig. F-3).

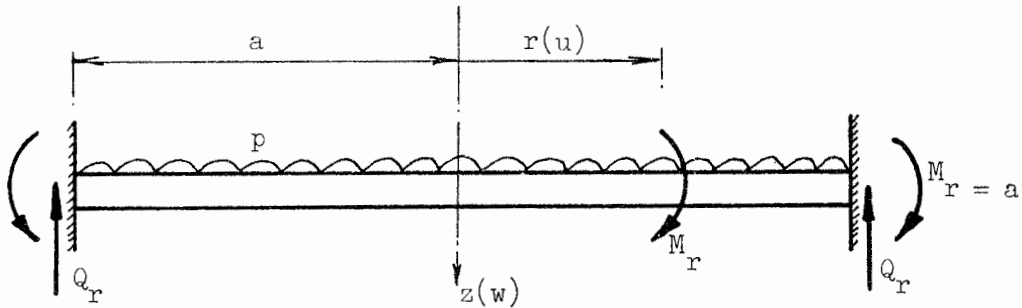


Fig. F-3

The meridional moment M_r per unit of circumference at a section of radius r is given by,*

$$M_r = \frac{p}{16} [-a^2(1+\nu) + r^2(3+\nu)]$$

from which the fixed-end moment per unit of circumference at the edge $r = a$ is,

*Ref. [3], p 55.

$$M_{r=a} = \frac{pa^2}{8} \quad (\text{F-10})$$

The total load on the circular plate is $\pi a^2 p$. Hence the fixed-end force per unit of circumference is,

$$Q_r = \frac{\pi a^2 p}{2\pi a} = \frac{pa}{2} \quad (\text{F-11})$$

APPENDIX G

The Theory of Cylindrical Water Tanks

The circular cylinder is a special case of the conical frustrum. Hence by taking $\phi = 0$ in Eqs. (2.13) we may immediately write down the equations for the stress resultants in a cylindrical water tank.* These are,

$$\begin{aligned} N_{\theta} &= D \left[\frac{w}{a} + \nu \frac{du}{dx} \right] \\ N_x &= D \left[\frac{du}{dx} + \nu \frac{w}{a} \right] \\ M_{\theta} &= K \nu \frac{d^2 w}{dx^2} \\ M_x &= K \frac{d^2 w}{dx^2} \end{aligned} \tag{G-1}$$

In the above expressions a is the radius of the tank and x denotes meridional distance along the tank.

In the case of water tanks we take the axial stress resultant N_x to be zero. Hence

$$\frac{du}{dx} = -\nu \frac{w}{a}$$

Substituting this result into the expression for N_{θ} , the hoop stress in a cylindrical water tank is

$$N_{\theta} = D (1 - \nu^2) \frac{w}{a} \tag{G-2}$$

The circumferential moment M_{θ} is usually ignored and in the following sections expressions for the meridional moment M_x in open and closed tanks are derived.

The open cylindrical water tank: The governing differential equation of a water filled, uniform thickness cylindrical tank of radius a is,

$$K \frac{d^4 w}{dx^4} + D (1 - \nu^2) \frac{w}{a^2} = p \tag{G-3}$$

where w is the radial displacement and $p = f(x)$ is the hydrostatic water

*Flügge [1], pp 269-276.

pressure in the tank (Fig. G-1). The complete solution of Eq. (G-3) is made up of the sum of the complementary function (when $p = 0$),

$$w_1 = e^{-\beta x}(A_1 \cos \beta x + A_2 \sin \beta x) + e^{-\beta(h-x)}(B_1 \cos \beta(h-x) + B_2 \sin \beta(h-x)) \quad (G-4)$$

and any particular integral of the governing differential equation. We choose the particular integral

$$w_2 = \frac{\gamma a^2}{D(1 - \nu^2)} (h - x) \quad (G-5)$$

where γ is the unit weight of the water in the tank.

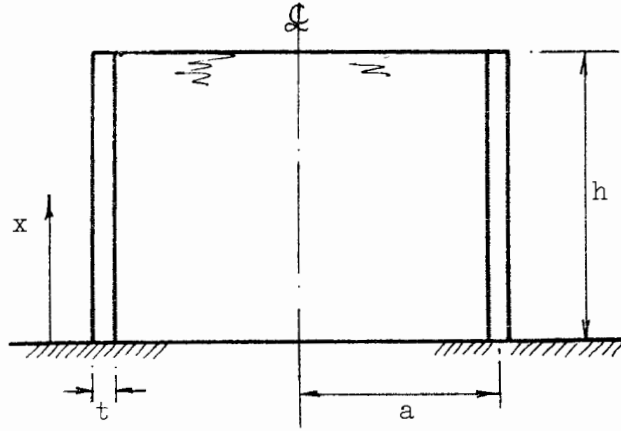


Fig. G-1

The constants A_1 , A_2 , B_1 and B_2 are found from the boundary conditions at the top ($x = h$) and bottom ($x = 0$) of the tank. If h is sufficiently large, the terms containing B_1 and B_2 have negligible affect at the base of the tank. Since in an open tank we are concerned more with the boundary conditions at the base of the tank we may drop the terms containing B_1 and B_2 . The complete expression for the displacement w then becomes

$$w = \frac{\gamma a^2}{D(1 - \nu^2)} (h - x) + e^{-\beta x} (A_1 \cos \beta x + A_2 \sin \beta x) \quad (G-6)$$

Differentiating with respect to x we have for the slope,

$$\frac{dw}{dx} = \frac{-\gamma a^2}{D(1 - \nu^2)} - \beta e^{-\beta x} [(A_1 - A_2) \cos \beta x + (A_1 + A_2) \sin \beta x] \quad (G-7)$$

The boundary conditions at the base ($x = 0$) are

$$w = 0 \quad \text{and} \quad \frac{dw}{dx} = 0$$

from which expressions for the constants A_1 and A_2 are derived. These are

$$A_1 = \frac{-\gamma a^2 h}{D(1 - \nu^2)}$$

$$\text{and } A_2 = \frac{\gamma a^2}{\chi D(1 - \nu^2)} (a - \chi h)$$

Substituting for A_1 and A_2 in Eq. (G-6) we have,

$$w = \frac{\gamma a^2}{Et} \left[(h - x) - h e^{-\beta x} \cos \beta x + \left(\frac{1}{\beta} - h \right) e^{-\beta x} \sin \beta x \right] \quad (G-8)$$

Differentiating Eq. (G-8) twice with respect to x yields the expression for the curvature, which when multiplied by the elastic constant K yields the equation for the meridional moment M_x , i.e.,

$$\begin{aligned} M_x &= K \frac{d^2 w}{dx^2} \\ &= K \beta^2 e^{-\beta x} \left[-\frac{2\gamma a^2}{Et} \left(\frac{a}{\chi} - h \right) \cos \beta x - \frac{2\gamma a^2 h}{Et} \sin \beta x \right] \\ &= \frac{Et^3}{12(1 - \nu^2)} \cdot \frac{\chi^2}{a^2} \left[-\frac{2\gamma a^2}{Et} \left(\frac{a}{\chi} - h \right) e^{-\beta x} \cos \beta x - \frac{2\gamma a^2 h}{Et} e^{-\beta x} \sin \beta x \right] \end{aligned}$$

Finally substituting $\chi^2 = \frac{\sqrt{Et} a}{2\sqrt{K}}$ we have

$$M_x = \frac{-\gamma a t}{\sqrt{12(1 - \nu^2)}} \left[\left(\frac{a}{\chi} - h \right) e^{-\beta x} \cos \beta x + h e^{-\beta x} \sin \beta x \right] \quad (G-9)$$

Notice that if the height h of the tank is large, both the displacement w and the moment M_x are effectively zero at the top of the tank.

The closed cylindrical water tank: When the water tank is monolithically joined to a circular disc (which acts as a roof to the tank), it is important to determine the effect which the disc has on the stress distribution in the tank. We therefore replace the disc by equivalent forces and moments acting at the upper edge of the tank (Fig. G-2).

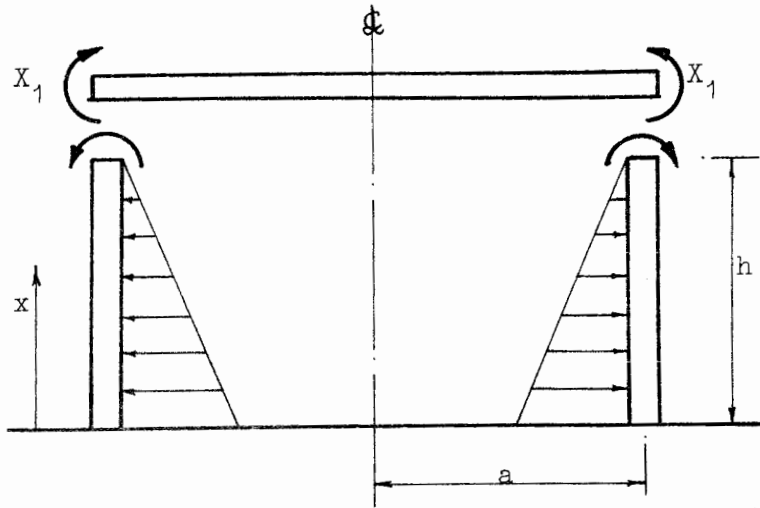


Fig. G-2

Transverse forces from the disc give rise to a state of plane stress in the tank which is not of significance in the present discussion. The basic problem is therefore essentially that of an open tank with an unknown applied moment X_1 at its upper edge. In this case however we have two additional boundary conditions at the edge $x = h$, viz.,

$$w = 0$$

$$M_x = X_1$$

If h is sufficiently large the terms in A_1 and A_2 (Eq. G-4) have negligible affect at the edge $x = h$. We may thus drop these terms and apply the above boundary conditions to find B_1 and B_2 . The equation for the radial displacement is then,

$$w = \frac{\gamma a^2}{D(1 - \nu^2)} (h - x) + e^{-\beta(h-x)} [B_1 \cos \beta(h - x) + B_2 \sin \beta(h - x)] \quad (G-10)$$

From the first boundary condition at the edge $x = h$ we have,

$$w = 0 = B_1$$

The equation for the moment M_x is then,

$$M_x = K \frac{d^2 w}{dx^2}$$

$$= K \beta^2 e^{-\beta(h-x)} [-2B_2 \cos \beta(h - x) + 2B_1 \sin \beta(h - x)] \quad (G-11)$$

The second boundary condition at this edge is,

$$M_x = X_1 = -2K\beta^2 \cdot B_2$$

$$\therefore B_2 = \frac{-X_1}{2K\beta^2}$$

Substituting the expression for B_1 and B_2 back into the original equations yields the following expression for the slope of the tank at the edge $x = h$:

$$\frac{dw}{dx} = \frac{-\gamma a^2}{Et} + \frac{X_1 a}{2K\chi} \quad (G-12)$$

Clearly the slopes of the tank and the circular disc must be compatible at the edge $x = h$. The slope of the disc at this edge is given by*,

$$\left(\frac{dw}{dx}\right)_d = \frac{a X_1}{K_d(1+\nu)} \quad (G-13)$$

$$\text{where } K_d = \frac{Et_d^3}{12(1-\nu^2)}$$

is the flexural rigidity of the circular disc. Hence, for compatibility of the slopes we have

$$\frac{a X_1}{2K\chi} - \frac{\gamma a^2}{Et} = -\frac{a X_1}{K_d(1+\nu)}$$

from which the value of redundant moment is

$$X_1 = \frac{\gamma a^2}{Et} \left[\frac{1}{\frac{a}{1K\chi} + \frac{a}{K_d(1+\nu)}} \right] \quad (G-14)$$

The complete expression for the curvature of the closed tank is then obtained by summing the curvature of the open tank and the curvature due to redundant moment X_1 . The expression for the moment M_x at any point in the closed tank is then,

$$M_x = \frac{-\gamma at}{\sqrt{12(1-\nu^2)}} \left[\left(\frac{a}{\chi} - h \right) e^{-\beta x} \cos \beta x + h e^{-\beta x} \sin \beta x \right]$$

$$+ X_1 e^{-\beta(h-x)} \cos \beta(h-x) \quad (G-15)$$

*Timoshenko and Woinowsky-Krieger [3], p 58.

It will be noticed that the first part of Eq. (G-15) is identical to Eq. (G-9) for the moment in an open tank. The solution of the closed tank problem is thus made up of the open tank solution plus a term expressing the clamping effect of the circular disc. The approximate method used to derive these equations is apparent from the fact that for sufficiently large h , the clamping moment X_1 is effective only near the top of the tank and the water pressure only near the base.

The preceding solution may be modified to take account of a U.D.L. on the tank roof. In this case the same procedure as before is followed except that Eq. (G-13) is replaced by the expression for the slope of a circular disc under a uniformly distributed load* p , viz.,

$$\frac{dw}{dx} = \frac{pa^3}{8 K_d(1 + \nu)} \quad (G-16)$$

By equating the expressions for the slope in the tank (Eq. G-12) and the slope in the disc (Eq. G-16) a new expression for X_1 is obtained in terms of the load p , viz.,

$$X_1 = \frac{pa^2 K \chi}{4[2K \chi + K_d(1 + \nu)]} \quad (G-17)$$

This expression may then be used directly in Eq. (G-15) for the moment M_x . Since the water pressure is no longer included, the equation for M_x reduces to,

$$M_x = X_1 e^{-\beta(h-x)} \cos \beta(h - x) \quad (G-18)$$

*Ibid., p 56.